0048215

BHI-00608
Rev. 1

Hanford Sitewide Groundwater Flow and Transport Model Calibration Report

Prepared for the U.S. Department of Energy
Office of Environmental Restoration and
Waste Management

Bechtel Hanford, Inc.
Richland, Washington

TRADEMARK DISCLAIMER

Reference herein to any specific commercial product, process, or service by trade name, trademark, manufacturer, or otherwise, does not necessarily constitute or imply its endorsement, recommendation, or favoring by the United States Government or any agency thereof or its contractors or subcontractors.

BHI-00608
REV: 1
OU: 200-PO-1
TSD: N/A
ERA: N/A

APPROVAL PAGE

Title of Document: HANFORD SITEWIDE GROUNDWATER FLOW AND TRANSPORT MODEL CALIBRATION REPORT

Author(s): A. Law
S. Panday
C. Denslow
K. Fecht
A. Knepp

Approval: A. J. Knepp, Groundwater Task Lead

BHI for A.J. Knepp — 9/29/97
Signature — Date

J. D. Isaacs, Groundwater Project Engineer

JDI per telecon — 9/29/97
Signature — Date

The approval signatures on this page indicate that this document has been authorized for information release to the public through appropriate channels. No other forms or signatures are required to document this information release.

BHI-DIS SEP 29 1997

THIS PAGE INTENTIONALLY
LEFT BLANK

BHI-00608
Rev. 1

Hanford Sitewide Groundwater Flow and Transport Model Calibration Report

Authors
A. Law
S. Panday
C. Denslow
K. Fecht
A. Knepp

Date Published
September 1996

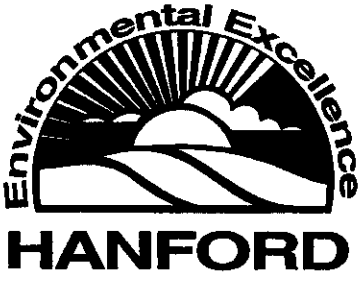

Prepared for the U.S. Department of Energy
Office of Environmental Restoration and
Waste Management

Bechtel Hanford, Inc.
Richland, Washington

THIS PAGE INTENTIONALLY
LEFT BLANK

CONTENTS

APPENDICES

FIGURES

TABLES

ACRONYMS

BWIP	Basalt Waste Isolation Project
CERCLA	*Comprehensive Environmental Response, Compensation, and Liability Act of 1980*
DOE	U.S. Department of Energy
DOE-RL	U.S. Department of Energy, Richland Operations Office
ERC	Environmental Restoration Contractor
HGIS	Hanford Geographic Information System
RCRA	*Resource Conservation and Recovery Act of 1976*
Tri-Party Agreement	*Hanford Federal Facility Agreement and Consent Order*
USGS	U.S. Geological Survey

1.0 INTRODUCTION

This report presents the results of the development and calibration of a three-dimensional, finite element model (VAM3DCG) for the unconfined groundwater flow system at the Hanford Site. This flow system is the largest radioactively contaminated groundwater system in the United States. Eleven groundwater plumes have been identified that contain organics, inorganics, and radionuclides. Because groundwater from the unconfined groundwater system flows into the Columbia River, the development of a groundwater flow model is essential to the long-term management of these plumes.

The Hanford Site is a U.S. Department of Energy (DOE) installation located in south-central Washington State (Figure 1-1) and has been in operation since 1943. Since 1987, the mission of the Hanford Site has been environmental restoration with the goals of controlling the spread of groundwater contamination and protection of the Columbia River.

Cost-effective decision making requires the capability to predict the effectiveness of various remediation approaches. Some of the alternatives available to remediate groundwater include: pumping contaminated water from the ground for treatment with reinjection or to other disposal facilities; containment of plumes by means of impermeable walls, physical barriers, and hydraulic control measures; and, in some cases, management of groundwater via planned recharge and withdrawals. Implementation of these methods requires a knowledge of the groundwater flow system and how it responds to remedial actions.

1.1 BACKGROUND

The DOE Richland Operations Office (DOE-RL) first recognized the need for a new sitewide groundwater model of the unconfined system in 1991, approximately 2 years after signing the *Hanford Federal Facility Agreement and Consent Order* (Tri-Party Agreement) (Ecology et al. 1989). Groundwater contamination was found in more than 518 km^2 (200 mi^2) of the unconfined aquifer on the Hanford Site. Initial estimates indicated that tens of years would be needed to remediate the known plumes. The overall effectiveness of the remediation efforts contained considerable uncertainty. It was recognized that groundwater cleanup would require the capability to estimate the effectiveness of alternative groundwater cleanup approaches. In addition, the reduction of liquid effluent being discharged to the soil has caused profound changes to the groundwater flow system that needed to be incorporated into groundwater remediation planning and implementation. Fifty years of study has yielded voluminous quantities of data describing the aquifer and soil matrix that make up the unconfined flow system. These data have required new interpretations to support the cleanup mission of the Hanford Site.

Implementation of this work lead to the development of two milestones (DOE-RL 1991a, 1991b) contained in the Tri-Party Agreement. Under Milestone M-29-01, "Description of Codes and Models to be Used in Risk Assessment," a combined DOE, contractor, and regulator committee was formed to exchange opinions and experiences relating to the use of various numerical codes.

A total of 12 numerical codes covering both saturated and unsaturated flow and transport phenomena were identified and evaluated.

The second milestone, M-29-02, stated "submit a plan for development of area-wide groundwater models to support risk assessment and to evaluate impacts of changing groundwater flow fields" (DOE-RL 1991b). As a result of this milestone, the VAM3DCG numerical code[1] was selected and an implementation plan proposed to guide model development (DOE-RL 1991b). The implementation plan called for an evaluation of the existing database, incorporating new data, model calibration and testing, and simulating future scenarios. This report documents model calibration and testing.

1.2 PURPOSE AND REPORT ORGANIZATION

This report presents the model development, calibration, and testing process for the new sitewide groundwater model of the unconfined aquifer using VAM3DCG. It provides the foundation for the model's use to assess groundwater remediation alternatives and other sitewide issues related to groundwater. The report is separated into five sections as follows.

Section 1.0 provides an introduction, the background of the project, and the purpose of the report.

Section 2.0 documents the geologic and hydrogeologic conceptual model of the unconfined flow system, which provides the basis for the development of the numerical model of the Hanford Site. The conceptual models are the result of the efforts of many professional scientists and engineers who have made contributions in defining these natural systems. These sections are extensively referenced.

Section 3.0 describes the model setup, site-specific information (facility effluents) assumptions, calibration process, and initial calibration results. Every numerical model is a simplification of the technical understanding and knowledge of what is important to solve a problem. The major assumptions made to simplify the conceptual models and allow them to be quantified within the VAM3DCG code are documented along with Hanford site-specific information needed for flow and transport calibration.

---

[1]The Variably Saturated Analysis Model in 3-Dimensions with Preconditioned Conjugate Gradient Matrix Solvers (VAM3DCG) code (developed by HydroGeoLogic, Inc. of Herndon, Virginia) was selected for the following reasons: (1) the solution algorithms were robust and the original developer, an internationally known expert, was available; (2) the VAM3DCG code efficiently simulates a fluctuating free-water surface, which makes it especially attractive for Hanford Site applications; (3) the code has the ability to deal with transitional elements, which permits the grid to be refined in regions of interest or steep gradients; and (4) it has the capability for dealing with partially saturated flow, a feature that enables it to be used for vadose zone analyses. Support for use of this proprietary code is available from HydroGeoLogic, Inc.

Section 4.0 presents a summary of conclusions and recommendations for future work.

Appendix A provides a technical description of the VAM3DCG model for the specific numerical approach and solution algorithms incorporated into this work.

Appendix B presents a sensitivity analysis quantifying the major factors affecting predictions of the movement of groundwater plumes.

Appendix C presents summary statistics comparing model predictions to observed water table values.

Figure 1-1. Location Map of the Hanford Site.

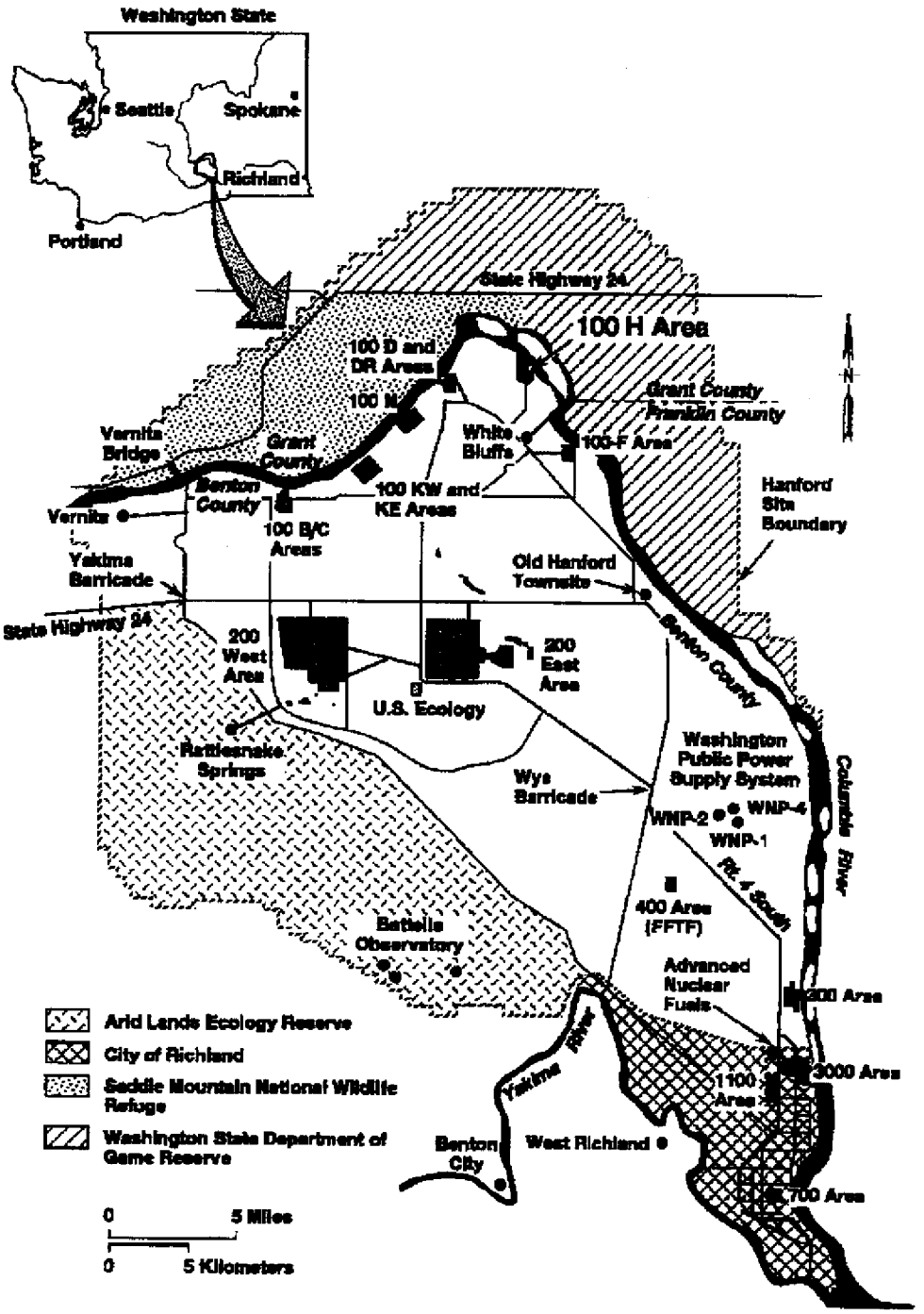

2.0 CONCEPTUAL MODEL

The conceptual geologic and hydrogeologic models provide the basis for the inputs to the numerical groundwater flow model. The descriptions of the conceptual models are based on numerous technical reports that describe the Hanford Site subsurface environment. This section discusses the salient features of the subsurface environment as they relate to the sitewide groundwater model.

The subsurface geologic conceptual model is a synthesis of data collected from the analyses of many samples from boreholes over the life of the Hanford Project. Interpretation of these data sets the stage for the conceptualized geohydrologic system, which defines the presence and movement of groundwater beneath the Hanford Site and the geohydrologic properties controlling the movement. This section provides: the geologic model development, stratigraphic descriptions, hydrogeologic system description, hydrogeologic properties, and liquid waste disposal facilities affecting the groundwater flow system.

2.1 GEOLOGIC MODEL DEVELOPMENT

Extensive geohydrologic investigations have been conducted at the Hanford Site since initial site construction in 1943. These investigations supported siting and construction of nuclear facilities, operating waste management storage and disposal facilities, monitoring and assessing environmental impacts, environmental remediation, and site restoration. Geohydrologic investigations were designed to support specific projects and often were conducted independently of other investigations. Thus, geohydrologic units were not uniformly defined and described. As a result, stratigraphic nomenclature was consistent only at the geologic formational level. Geologic descriptions at the formational level do not provide sufficient detail to develop a sitewide conceptual geologic or hydrogeologic model to support remedial action decisions. Therefore, a uniform stratigraphic nomenclature along with consistent geologic unit descriptions and distributions needed to be developed that were applicable to all areas of the Hanford Site.

An integrated plan was formulated to develop the information necessary for a site geologic model. The primary emphasis was to define the major geologic units beneath the Hanford Site with emphasis on the saturated suprabasalt sediments. The plan included the following tasks.

- Define the stratigraphy of major geologic units including unit subdivisions, descriptions, and distributions (Section 2.1.1).

- Create a surface geologic map of the Hanford Site for use in constraining the surface distribution of geologic units and to identify potential exposures/outcrops for measuring detailed geologic sections (Section 2.1.2).

- Define the base of the suprabasalt sediments and determine the structural fabric that may trend upward into the overlying sediments (Section 2.1.3).

- Create a geologic conceptual model consisting of geologic cross sections and structural contour maps that depict unit elevations and lateral continuities. The characteristics of each geologic unit are described in Section 2.2.

The plan included an evaluation of the extensive existing information base as well as collecting new field information.

2.1.1 Development of Site Suprabasalt Stratigraphy

The initial step in developing a site stratigraphic nomenclature was to define and document the major geohydrologic units of the suprabasalt sediments below the formational level with emphasis on the uppermost part of the suprabasalt groundwater flow system. A coordinated effort was established among several on-going projects to collect the information necessary to define and describe the major geologic units beneath the Hanford Site. These major geologic units would provide the framework for establishing geohydrologic units to be used in the sitewide groundwater model. The coordinated effort consisted of two tasks: (1) subdivide the Hanford formation and Ringold Formation/pre-Missoula gravels into major geologic units and describe each, and (2) determine the spacial distribution of the major geologic units across the Hanford Site.

The Ringold Formation is the oldest of the suprabasalt geologic units beneath the Hanford Site. The Ringold Formation traditionally has been divided into several informal units, including (1) basal gravel and sand unit with associated silty paleosols; (2) lower silt and clay unit; (3) middle gravel unit; (4) upper sand, silt, and clay unit; and (5) basaltic fanglomerate unit (Newcomb 1958; Brown 1959, 1962; Newcomb et al. 1972; Myers et al. 1979; Tallman et al. 1979; Bjornstad 1984, 1985; and DOE 1988). The Ringold Formation has also been subdivided into facies (Tallman et al. 1979) and fining upward sequences (PSPL 1982).

In 1989, a project was initiated to develop a sitewide stratigraphic framework for the Ringold Formation for use in waste management and environmental restoration projects. The project included an evaluation of borehole logs, core samples, and geologic exposures. Borehole geophysics, age dates, volcanic ash analyses, remnant magnetism, and surface geologic mapping were included in the evaluation. The results of the evaluation indicated that the Ringold Formation is best subdivided on the basis of sediment facies associations (Lindsey and Gaylord 1990; Lindsey 1991a, 1991b) (see Section 2.2).

Since 1991, additional geologic studies were conducted to confirm and refine sediment facies associations and descriptions in the Ringold Formation. Sitewide and site-specific geologic studies were integrated among waste management and environmental restoration projects to ensure a consistent approach in stratigraphic nomenclature and geologic unit descriptions (Lindsey 1991a, 1991b, 1992; Lindsey et al. 1994a). The sitewide studies focused on a Hanford Site geologic conceptual model that forms the geohydrologic framework for the site groundwater model (Connelly et al. 1992a, 1992b). The site-specific studies supported development of geohydrologic conceptual models for *Resource Conservation and Recovery Act of 1976* (RCRA) storage and disposal facilities (Lindsey et al. 1994b); remedial investigations of *Comprehensive Environmental Response, Compensation, and Liability Act of 1980* (CERCLA) operable units

(DOE-RL 1994; Lindsey et al. 1991, 1992; Lindsey and Jaeger 1993; Raidl 1994; Rohay 1994; Weekes et al. 1995); groundwater impact assessments of operating disposal facilities (WHC 1992; Alexander 1993; Alexander and Johnson 1993; Alexander et al. 1993, 1995; Johnson 1993a, 1995; Johnson et al. 1995; Singleton and Lindsey 1994; and Sweeney et al. 1995) and environmental monitoring programs (Johnson 1993b, 1995; Weekes et al. 1995).

Lindsey (1995) summarized Ringold Formation investigations conducted since 1989. The primary data used to define the sediment facies associations and their distribution include the following:

- Twenty-nine measured sections from exposures along the White Bluffs
- Lithologic logs of core samples from 28 coreholes on the Hanford Site
- Driller and geologist logs from hundreds of boreholes on the Hanford Site
- Thousands of grab samples from hundreds of boreholes on the Hanford Site.

Measured sections and core samples were used as control points for subdividing the Ringold Formation into sediment facies associations and to define analogues for use with borehole log and borehole sample data sets. Analogues were used as a basis of comparison with borehole grab samples and borehole logs to be evaluated against in order to determine probable subsurface geologic conditions. The use of analogues is critical to making interpretations of subsurface physical properties of the sediment facies associations. Drilling generates desegregated, disrupted, and/or abraded samples that are not representative of the geologic conditions. The analogues were used as aids (Lindsey 1995) to interpret the following:

- Facies type
- Probable mud content
- Extent of interstratified lithologies
- Cementation and compaction
- Grain-size range.

Lindsey (1995) divided the Ringold Formation into five sediment facies associations based on work by Miall (1977, 1978, 1985) and Rust (1978) (see Section 2.2). The Ringold Formation is divided into three informal members (Figure 2-1). The informal Ringold members are subdivided into units on the basis of the dominant sediment facies associations. A discussion of the Ringold Formation stratigraphy is presented in Section 2.2.

The pre-Missoula gravels originally were recognized as the upper uncemented gravels of the Ringold Formation that contained a higher content of "felsic" clasts giving the unit a "bleached" appearance. The pre-Missoula gravels were defined as a separate and distinct geologic unit by PSPL (1981) based on an extensive coring and drilling program used to site a nuclear power plant in the east-central Hanford Site. These gravels were further described and mapped in the subsurface by Lindsey (1995) (see Section 2.2).

The Hanford formation is the youngest formation underlying the Hanford Site (Figure 2-1). The Hanford formation consists of glaciofluvial gravel, fine- to coarse-grained sand, and silt derived from cataclysmic flooding. Surface mapping (Reidel and Fecht 1994a, 1994b) and subsurface

investigations (Price and Fecht 1976; Last and Marratt 1978a, 1978b; Smith 1988; WPPSS 1981, 1986) indicate that the Hanford formation can be described on the basis of three glaciofluvial textured facies: (1) gravel-dominated, (2) sand-dominated, and (3) silt/sand-dominated (Figure 2-2). The Hanford formation also can be subdivided based on age using pedogenitic alteration, ash chronology, and remnant magnetism (Fecht et al. 1987; Baker et al. 1991; Reidel and Fecht 1994a, 1994b). However, these subdivisions have proven only to be useful in surface mapping (Reidel and Fecht 1994a, 1994b) and mapping walls of large excavations (Baker et al. 1991). Many geologic descriptions and unit interpretations must be based solely on grab samples from drill cuttings in which the characteristics necessary to determine age relationships are destroyed during drilling. Therefore, the three textural facies are the only consistently reliable criteria that can be used to define major stratigraphic subdivisions of the Hanford formation beneath the site.

2.1.2 Surface Geologic Map of Hanford Environs

The surface geology of the Hanford environs was mapped to describe and determine the distribution of geologic units at the land surface and to identify potential exposures/outcrops for measuring detailed geologic sections. A secondary purpose of the mapping was to coordinate the geologic studies on the Hanford Site with the Washington Division Geology and Earth Resources state mapping project.

The geologic mapping was conducted at a variety of scales with the most common 1:24,000 U.S. Geological Survey (USGS) topographic maps. The mapping was compiled on 1:100,000-scale Priest Rapids and Richland quadrangles (Reidel and Fecht 1994a, 1994b). The geologic maps incorporated new geologic mapping since the publication of Myers et al. (1979). The mapping by Reidel and Fecht (1994a, 1994b) has been incorporated into the Hanford Geographic Information System (HGIS).

The geologic maps were used to constrain the distribution of major geologic units/facies of the Ringold Formation, pre-Missoula gravels, and Hanford formation.

2.1.3 Definition of Base of Suprabasalt Sediment Sequence

The base of the suprabasalt sequence is defined as the top of the bedrock (basalt) sequence. Basalt of the Columbia River Basalt Group is an extensive rock unit throughout the Columbia Basin (Waters 1961; Swanson et al. 1979a; Reidel and Hooper 1989). Maps depicting the top of the basalt sequence beneath Hanford were published earlier (ARHCO 1976; Brown 1959, 1962, 1971; Myers et al. 1979; Myers 1981). Each subsequent top-of-basalt map was built on the interpretations and data from earlier maps. A new top-of-basalt map was developed for the sitewide groundwater project. The map was developed by integrating an extensive base of geological and geophysical data including the following:

- New surface geologic maps of the Hanford Site (Reidel and Fecht 1994a, 1994b) (see Section 2.1.2)

- Corehole data (core samples and geologic/geophysical logs) (including Bjornstad 1984; PSPL 1982; WPPSS 1974, 1981, 1986; and various onsite well files/geological sample library)

- Borehole data (chip/grab samples and drillers, geologic/geophysical logs) (including Bjornstad 1984; Blume 1971; Crowley and Ledgerwood 1987; Fecht and Lillie 1982; Graham et al. 1984; Jackson et al. 1984; Ledgerwood 1986; PSPL 1982; Summers and Schwab 1977; Summers and Weber 1978; WPPSS 1974, 1981, and 1986; and various onsite well files/geological sample library)

- Surface-based geophysics (seismic reflection, gravity, magnetics) (including Ault 1981; Berkman 1984, 1986; Donaldson 1963; Holmes and Mitchell 1981; Kunk 1981, 1986; Odegard and Mitchell 1987; PSPL 1982; Raymond and Ratcliffe 1959; SSC 1978, 1979, 1980; WPPSS 1974, 1981,1986; and various onsite geophysical files)

- Single- and multiple-layer aeromagnetic surveys (including AERO 1980; Swanson et al. 1979b)

- Structural trends, features, and characteristics of Yakima folds based on structural investigations on Umtanum Ridge (Price 1982; Price and Watkinson 1989), Saddle Mountains (Reidel 1984), Rattlesnake Mountain (Fecht et al. 1984, Reidel et al. 1992) and the Columbia Basin (Reidel et al. 1984, 1989, 1994; WCC 1980) and remote sensing studies (including Glass 1977; Glass and Simmons 1977)

- Regional paleodrainage patterns of the ancestral Columbia, Palouse, Snake/Clearwater-Salmon, and Yakima Rivers (Fecht et al. 1985, 1987; Reidel et al. 1994)

- X-ray fluorescence analysis of core and chip samples from various Hanford Site geochemical databases.

Surface exposures based on geologic mapping compiled on 1:24,000 scale USGS topographic maps (published at a scale of 1:100,000) and subsurface corehole data were used to establish control points in developing a contour map on the basalt surface. Borehole data and geophysical data were used to extrapolate between control points and to refine structural trends. X-ray fluorescence data were used to identify the basalt flow exposed at the top of the basalt sequence, which was necessary to use the top-of-basalt map to assess structural trends in the upper part of the basalt sequence and the suprabasalt sediments.

Figure 2-3 shows the top-of-basalt map and depicts the results of analyzing and interpreting the aforementioned data sets. Only the contours on the basalt surface are presented on the map. The map is in the HGIS database and is available from the Environmental Restoration Contractor (ERC).

2.1.4 Geologic Model

The geologic conceptual model for the Hanford Site is presented in Lindsey (1995) as a series of geologic cross sections and structure contour maps. The conceptual model was developed using the methods and data discussed in Section 2.1. Figures 2-4 and 2-5 are example cross sections traversing through the Hanford Site south to north and west to east, respectively. The data from the cross sections and other borehole information were tabulated to generate a summary chart of unit contact elevations and thickness for each major suprabasalt sedimentary geologic unit and is included in this report as Table 2-1. In addition, Lindsey (1995) developed six structure contour maps of the five facies groups of the Ringold Formation and the Plio-Pleistocene Unit.

2.2 STRATIGRAPHIC DESCRIPTION

Major stratigraphic units at the Hanford Site are the Columbia River Basalt Group and intercalated Ellensburg Formation, Ringold Formation, pre-Missoula gravels, and Hanford formation. The stratigraphic relationships and ages are presented in Figure 2-1.

The Columbia River Basalt Group is composed of a thick sequence (>5,000 m) of tholeiite basalts that form the bedrock in the Columbia Basin. Intercalated between flows in the upper part of the basalt sequence are volcaniclastic and epiclastic sediments of the Ellensburg Formation.

The Ringold Formation consists of variably indurated clay, silt, pedogenically altered mud and sand, fine- to coarse-grained sand, and multi-lithologic gravels (Myers et al. 1979; Lindsey 1991a, 1995; Goodwin 1993). Ringold sediments are best described on the basis of sediment facies associations, which are defined on the basis of lithology, stratification, and pedogenic alteration (Lindsey and Gaylord 1990). These facies associations forms the basis for Ringold stratigraphic subdivisions. The Ringold facies associations are (1) fluvial gravel, (2) fluvial sand, (3) overbank deposits and paleosols, (4) lacustrine deposits, and (5) alluvial-fan deposits (Lindsey 1991a, 1995; Goodwin 1993). Detailed descriptions of these facies can be found in Lindsey (1991a, 1995) and Goodwin (1993).

Sediments comprising the Ringold Formation are divided into three informal members (Figure 2-1). The lowest member, the member of Wooded Island, contains five separate stratigraphic intervals, designated units A, B, C, D, and E, dominated by fluvial gravel (facies 1). These units are separated by intervals containing deposits typical of overbank-paleosol and lucustrine facies associations (facies 3 and 4). The lowermost of the fine-grained sequences, overlying unit A, is designated the lower mud unit. The member of the Wooded Island is overlain by the member of Taylor Flat, which is dominated by interbedded fluvial sands and overbank-paleosol deposits (facies 2 and 3). On the edges of the Pasco Basin and in the northern Hanford Site, the member of Wooded Island pinches out, interfingering with the member of Taylor Flat. The third member of the Ringold Formation, the member of Savage Island, consists dominantly of lacustrine deposits (facies 4) that are basin-wide in extent (Lindsey 1995).

The pre-Missoula gravels are composed of quartzose to gneissic clast-supported pebble to cobble gravel with a quartzo-feldspathic sand matrix. These gravels, called the pre-Missoula gravels (PSPL 1982), are up to 25 m thick, contain less basalt than the underlying Ringold gravels and the overlying Hanford deposits, have a distinctive white or bleached color, and sharply truncate underlying strata. The pre-Missoula gravels are approximately time equivalent to the early "Palouse" soil and the Plio-Pleistocene alluvium. The gravels are interpreted as mainstream deposits of the Columbia River.

The Hanford formation consists of gravel, fine- to coarse-grained sand, and silt. These deposits are divided into three facies: (1) gravel-dominated, (2) sand-dominated, and (3) silt/sand-dominated. The Hanford formation was deposited as a result of cataclysmic flooding of the Pasco Basin during three different episodes of Pleistocene glaciation (Fecht et al. 1987). The Hanford formation is commonly divided into two informal members: Pasco gravels and the Touchet Beds (Myers et al. 1979; Tallman et al. 1981; Fecht et al. 1987; DOE 1988). The Pasco gravels generally correspond to the gravel-dominated facies and the Touchet Beds to the sand-dominated and silt/sand-dominated facies. The Hanford formation is absent on the ridges more than 385 m above sea level, the highest level of cataclysmic flooding in the Pasco Basin (Baker et al. 1991).

Stratigraphic relationships (Figure 2-1) across the Hanford Site have been based on observations in intact core and outcrops. Sediment facies and basalt flows were identified from more than 40 measured sections (Myers et al. 1979; Baker et al. 1991; Lindsey 1995). Sedimentary and basalt data also were collected from more than 60 coreholes and from drilling cuttings and borehole logs from several thousand wells. The stratigraphic relationships were used to construct geologic structure contour maps of various stratigraphic horizons (Myers et al. 1979; Lindsey 1995). Key geologic maps to the geologic model are found in Figure 2-3 (top of basalt).

The top of basalt is based on surface geologic maps of the Pasco Basin (Reidel and Fecht 1994a, 1994b) and over 300 boreholes spudded in or drilled into the basalt sequence.

2.3 HYDROGEOLOGIC SYSTEM

2.3.1 Aquifers

Over 220 km^2 (85 mi^2) of unconfined aquifer on the Hanford Site is contaminated by hazardous and radioactive waste to levels above the federal drinking water standards (40 Code of Federal Regulations 141) and the State of Washington's ground water quality criteria (WAC-173-200). Beneath this unconfined aquifer is a series of confined aquifers that may interact with the unconfined aquifer to limited but unknown degree (Spane and Webber 1995).

The confined aquifers consist of sedimentary interbeds and basalt intraflow zones of the Ellensburg Formation within the Grande Ronde, Wanapum, and Saddle Mountain basalts. These aquifers are aerially extensive, covering much of the Columbia River plateau in Washington State and Idaho. When the potentiometric surfaces of one of the aquifers is above or below that of the adjoining aquifer, the potential exists for water to move from one aquifer to the other

(termed "aquifer intercommunication") depending on the vertical hydraulic conductivity of the confining basalt unit. Figure 2-6 illustrates this upward flow potential by comparing head valves for the upper basalt aquifer with those of the unconfined aquifer (Spane and Webber 1995). The direction of any leakage is determined by the relative position of the potentiometric surfaces. The confined aquifer systems were the focus of the Basalt Waste Isolation Project (BWIP) conducted during the period 1977 to 1987, and a detailed discussion of these aquifers is contained in DOE (1988).

The unconfined aquifer is contained within the Ringold Formation and the Hanford formation of the Pasco Basin. This basin is bounded by Umtanum Ridge, Yakima Ridge, and the Rattlesnake Hills on the west; Rattlesnake Mountain on the southwest; Saddle Mountains to the north; and Palouse Slope on the east. The Columbia River traverses through the basin and forms the northern and eastern boundary of the unconfined aquifer for the Hanford Site. The top of the Columbia River basalts generally is considered to form the bottom of the unconfined aquifer. However, for the purpose of the sitewide groundwater model, the bottom of the aquifer is taken to be the top of the lower mud unit of the Ringold Formation where it exists; otherwise, it is the top of the basalt. This is because the lower mud acts as an impermeable layer above the basalt (Figure 2-7). This portion of the aquifer is minimally contaminated by Hanford operations. Therefore, the saturated portion of the Ringold Formation and Hanford formation above the top of basalt/top of lower mud is most appropriate for dealing with the Hanford unconfined aquifer system.

Figure 2-8 shows that the saturated thickness of the unconfined aquifer varies, based on the 1979 water table configuration, from more than 150 m (500 ft) to less than 3 m (10 ft). Of particular interest is the portion of the aquifer where the pre-Missoula/Hanford formation exists in the uppermost portion of the aquifer (Figure 2-9). The portion of the aquifer is of high conductivity and permits contaminants to travel faster than the portions of the aquifer in the Ringold Formation.

2.3.2 Unconfined Aquifer Recharge and Discharge

Groundwater flows from regions of recharge to regions of discharge. The geohydrologic properties of the aquifer materials within the system control the magnitude of flow and determine the configuration of the water table, or upper limit of the saturated zone. Direction of flow is controlled by the aquifer properties along with the locations of recharge and discharge. Recharge may be either natural (e.g., streams, precipitation) or artificial (e.g., wastewater disposal) irrigation.

Migration of contaminants in a groundwater system depend on the flow of the groundwater, and also on the properties of the aquifer materials, the chemistry of the contaminant and aquifer material, and the natural degradation of some contaminants.

A first step in the development of a conceptual model of a groundwater system is the identification and evaluation or quantification of recharge and discharge to the system.

2.3.2.1 Groundwater Recharge. The primary recharge source for the unconfined aquifer system at the Hanford Site is the higher lands west of the Site: the Cold Creek and Dry Creek drainage basins. These streams are ephemeral on the Hanford Site. The drainage basins receive an annual average precipitation of about 40.6 cm (16 in.) compared to 16.5 cm (6.5 in.) of precipitation at the Hanford Site. Much of this precipitation falls as snow in the upper elevations. Other potential sources of recharge are precipitation and leakage from the underlying confined aquifers.

During a geology and hydrology investigation of the Hanford Site, Newcomb et al. (1972) estimated that subsequent to the cessation of irrigation in the Cold Creek and Dry Creek valleys in 1954, about 500 acre-ft/yr or 0.02 m^3/sec (0.7 ft^3/sec) recharged the unconfined aquifer at Hanford from the two valleys. The investigation also indicated an unknown amount of recharge to the unconfined aquifer by leakage of unconfined aquifer water at what has become known as the Cold Creek barrier. Newcomb et al. (1972) suggested that this leakage could contribute several hundred acre-feet of water per year (100 acre-ft/yr is equivalent to 0.004 m^3/sec [0.14 ft^3/sec]).

As part of a recharge evaluation to the confined aquifer system, Livesay (1986) estimated the surface runoff from the Cold Creek valley on the basis of a regression analysis of small watersheds in eastern Washington. For the Cold Creek watershed, an estimate of 0.23 m^3/sec (8 ft^3/sec) was obtained, with an area of 174 km^2 (67 mi^2), with an average annual precipitation of 25.4 cm (10 in.). For a combined Cold Creek/Dry Creek drainage area of approximately 259 km^2 (100 mi^2), this would be approximately 0.34 m^3/sec (12 ft^3/sec). However, Livesay correctly pointed out that the regression study was based on watersheds having a perennial base flow component and, therefore, may overestimate runoff from Cold Creek and Dry Creek.

Using a Darcian approach, Graham et al. (1981) estimated the groundwater recharge to Hanford from the Cold Creek valley as 0.06 m^3/sec (2 ft^3/sec). The parameter estimates used in this analysis were: hydraulic conductivity = 12.2 m/day (40 ft/day); saturated thickness = 61 m (200 ft); length of 3,049 m (10,000 ft); and hydraulic gradient = 0.002. No estimate was given for the Dry Creek valley. Graham et al. (1981) also noted that irrigation in the Cold Creek valley resumed in approximately 1969.

Other estimates of recharge are based on model calibrations. Jacobson and Freshley (1990), in performing an inverse calibration of the CFEST model, arrived at a boundary flux of 0.102 m^3/sec (3.6 ft^3/sec) from Cold Creek valley, which they noted was in agreement with the estimated flux of 0.105 m^3/sec (3.7 ft^3/sec) in the previous calibration of the VTT model. The VTT calibration indicated a boundary flux of 1.4×10^{-2} m^3/sec (0.5 ft^3/sec) for the Dry Creek valley.

Bennett (1992) approximated the runoff from the two valleys, based on limited information, as slightly over 0.23 m^3/sec (8 ft^3/sec). His estimate was based on an approximate water balance and was factored in an increase in irrigation from 1954 quantities.

Two additional potential sources of recharge to the unconfined aquifer are (1) recharge from the confined aquifer systems beneath the unconfined aquifer, and (2) recharge from precipitation on the Hanford Site that percolates to the water table.

During the BWIP, considerable emphasis was focused on the confined aquifer system at Hanford. Attention was also given to springs in the Cold Creek and Dry Creek basins that might provide recharge to one or more of the confined aquifer systems. In turn, the confined systems may provide recharge to the unconfined system, either as widespread upwelling over a broad area or at specific locations, such as the Cold Creek barrier noted by Newcomb et al. (1972). Although limited data are available to determine or quantify if leakage exists between the confined aquifer systems and the unconfined aquifer, the potential is recognized to exist. However, for the sitewide model, it is assumed that there is no recharge or discharge from the confined aquifer to the unconfined aquifer due to insufficient data.

Newcomb et al. (1972) also considered recharge to the unconfined aquifer via the precipitation route. Their review of well hydrographs suggested that annual recharge was zero or at least negligible. Graham et al. (1981) also suggested little, if any, recharge to groundwater from precipitation due to the high rate of evapotranspiration. Review of other pertinent Hanford literature indicates that there is general agreement that the recharge from precipitation is negligible when soils are fine-grained with a vegetative cover, especially if it is deep-rooted vegetation. When soils are coarse-grained and there is no vegetative cover, recharge can occur during years of high precipitation, especially when it occurs as snow with rapid melting and heavy rainfall (Rockhold et al. 1990, 1995; Routson and Johnson 1988; Gee et al. 1992; Prych 1995; Fayer and Walters 1995). For the purpose of the sitewide model, the recharge from precipitation is assumed to be negligible because almost all of the non-operating areas are vegetated and, in the operational areas. the quantity of any natural recharge is quite small compared to the artificial recharge resulting from waste disposal operations that is input to the model.

Along the southeast portion of the Hanford Site, the Yakima River contributes some flow into the unconfined aquifer.

2.3.2.2 Aquifer Discharge. Estimates of groundwater discharge to the Columbia River, from the unconfined aquifer have been made in previous studies (Luttrell et al 1992) estimated 6.6×10^6 m^3/yr (7.4 ft^3/s) of groundwater discharged to the river along a 1 km (0.6 mi) section near the old Hanford Townsite. Prater et al (1984) estimated groundwater discharge to the river at 2.7×10^6 m^3/yr (3.0 ft^3/s) along the same section as Luttrell (1992) using a groundwater flow model.

2.3.2.3 Aquifer Intercommunication. The Cold Creek fault (Johnson 1993b) has been interpreted to allow water from lower confined aquifers to move up into the upper confined aquifer. However, it is thought that no water moves up into the unconfined aquifer. Intercommunication exists between the uppermost confined aquifer and the unconfined aquifer in the area south of Gable Gap, which is the gap between Gable Mountain and Gable Butte. This intercommunication has been investigated by Ledgerwood and Deju (1976), Strait and Moore (1982), and Graham et al. (1984). The studies show that water from the unconfined aquifer

migrates down into the uppermost confined aquifer, but within the constraints of the area of the study, water from the confined aquifer then flows back into the unconfined aquifer. No quantification or estimate of such aquifer intercommunication has been made. The sitewide model does not attempt to take this intercommunication into account.

2.4 HYDROGEOLOGIC PROPERTIES

The movement and storage of groundwater in an aquifer is controlled by the hydrogeologic properties of the aquifer. The hydraulic conductivity (or transmissivity, which is the product of the hydraulic conductivity and the saturated thickness) is a measure of how the water moves in the aquifer. The storativity and specific yield are measures of the aquifer's ability to store water. Estimates of these parameters are obtained from aquifer tests conducted in one or preferably several wells. These tests can provide good estimates for near-well aquifer characteristics. The success of the model simulation depends on the representation of these tests to provide a numerical description of the model domain.

Table 2-2 is a listing of the wells for which aquifer test data are available. Figure 2-10 shows the locations of these wells. Hydraulic conductivities for the 200 East and 200 West Areas were obtained from Connelly et al. (1992a, 1992b). Hydraulic conductivities for the 600 Area were obtained from Thorne and Newcomer (1992). Data obtained from slug tests were discarded as they represent only very near well characteristics. For each well, the test results were reviewed for reasonableness with respect to the hydrogeologic unit tested.

Almost all the aquifer tests were single-well tests (i.e., there was no observation well for measuring drawdown). This results in hydraulic conductivity and transmissivity only being estimated and no estimate for storage properties of the formation. In addition, water-level measurements in the pumped well due to energy losses at the well-formation interface were not assessed.

The aquifer test results then were extended from the point measurements to areal values with the application of Earth Vision, a software program of Dynamic Graphics, Inc.

2.5 HANFORD OPERATIONS AND EFFLUENT DISPOSAL

Since operations started in 1943, large quantities of wastewater were disposed of to the soil column at Hanford, some of which was contaminated with radioactive and/or hazardous waste. Low-level radioactive waste, primarily cooling water, was disposed to surface ponds for infiltration into the soil. Intermediate-level radioactive waste, such as process condensates and steam condensates, was disposed to subsurface facilities termed cribs. These facilities isolated contaminants from animals and plants while allowing the water to percolate through the soil. Figure 2-11 shows the volumes of wastewater disposed to the ground from the processing facilities in the 200 Area plateau. Disposal of this wastewater raised the water table as much as 24.4 m (80 ft) in the 200 West Area and 9.1 m (30 ft) near the 200 East Area.

Process discharges from each facility are tabulated in annual waste volume reports for all cribs, ditches, and ponds. The sitewide model incorporated the major liquid waste disposal facilities located in the 200 East and 200 West Areas. Table 2-3 identifies each facility and provides the volume of liquids discharged over the period between 1980 and 1993. Locations of these facilities are shown in Figure 2-12. Discharges from these facilities account for over 90% of the total facility discharge. Total discharge over this period from all facilities was 2.39×10^{11} L (6.3×10^{10} gal). Only one of the liquid waste disposal facilities currently are is operating (B Pond).

Similarly, tritium was introduced into the groundwater from a number of liquid waste disposal facilities found in both the 200 East and 200 West Areas. Table 2-4 identifies those facilities and the quantity of tritium discharged from each over the period 1980 to 1993, which are included in the model. No significant discharges of tritium during this period are found in the 200 West Area. Total tritium discharged in the 200 East and 200 West Areas was 31,700 and 323 Ci, respectively.

The sitewide model assumes flow from sanitary systems is minimal. Approximately 86 individual septic systems are known to exist on the Hanford Site. The estimated flow from each is highly variable and aerially distributed (Luke 1995).

Figure 2-1. Idealized Suprabasalt Stratigraphy of the Hanford Site and Stratigraphic Nomenclature.

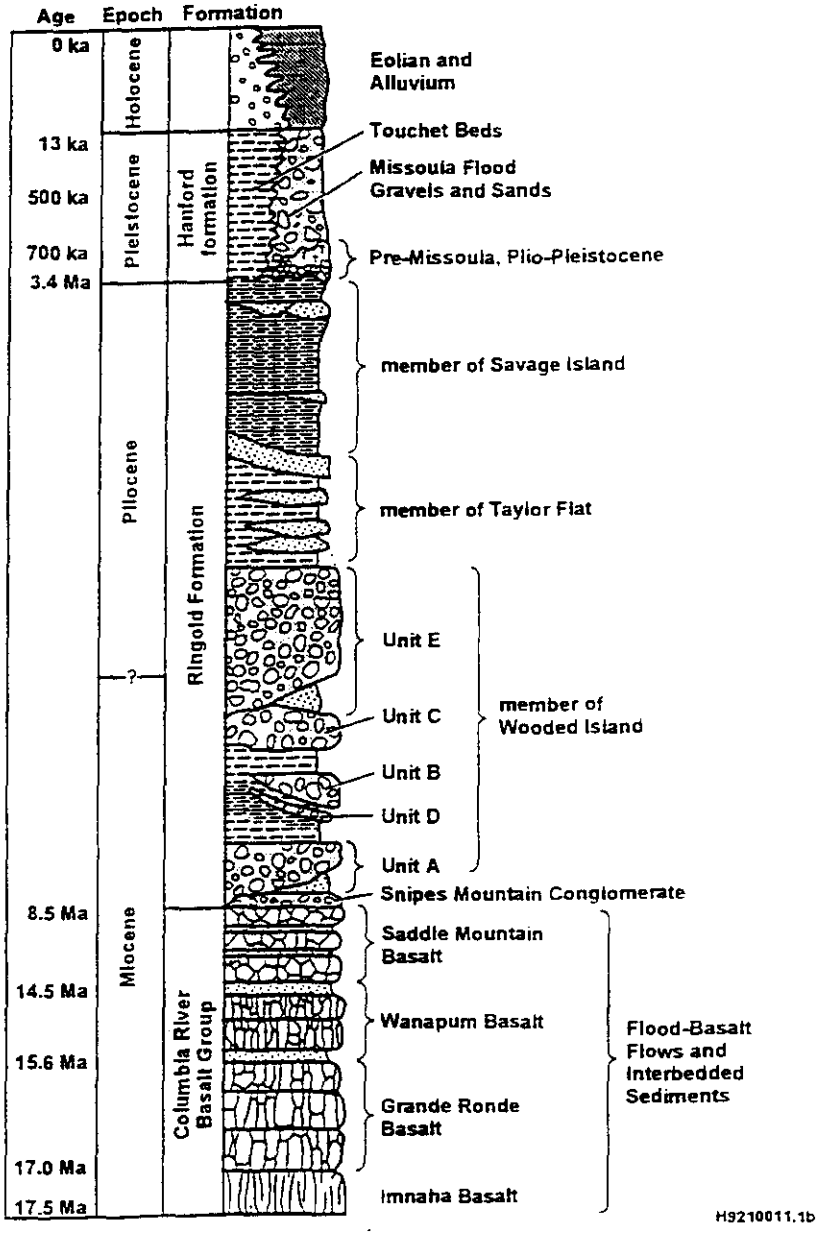

Figure 2-2. Distribution of Glaciofluvial Facies of Hanford Formation on the Hanford Site.

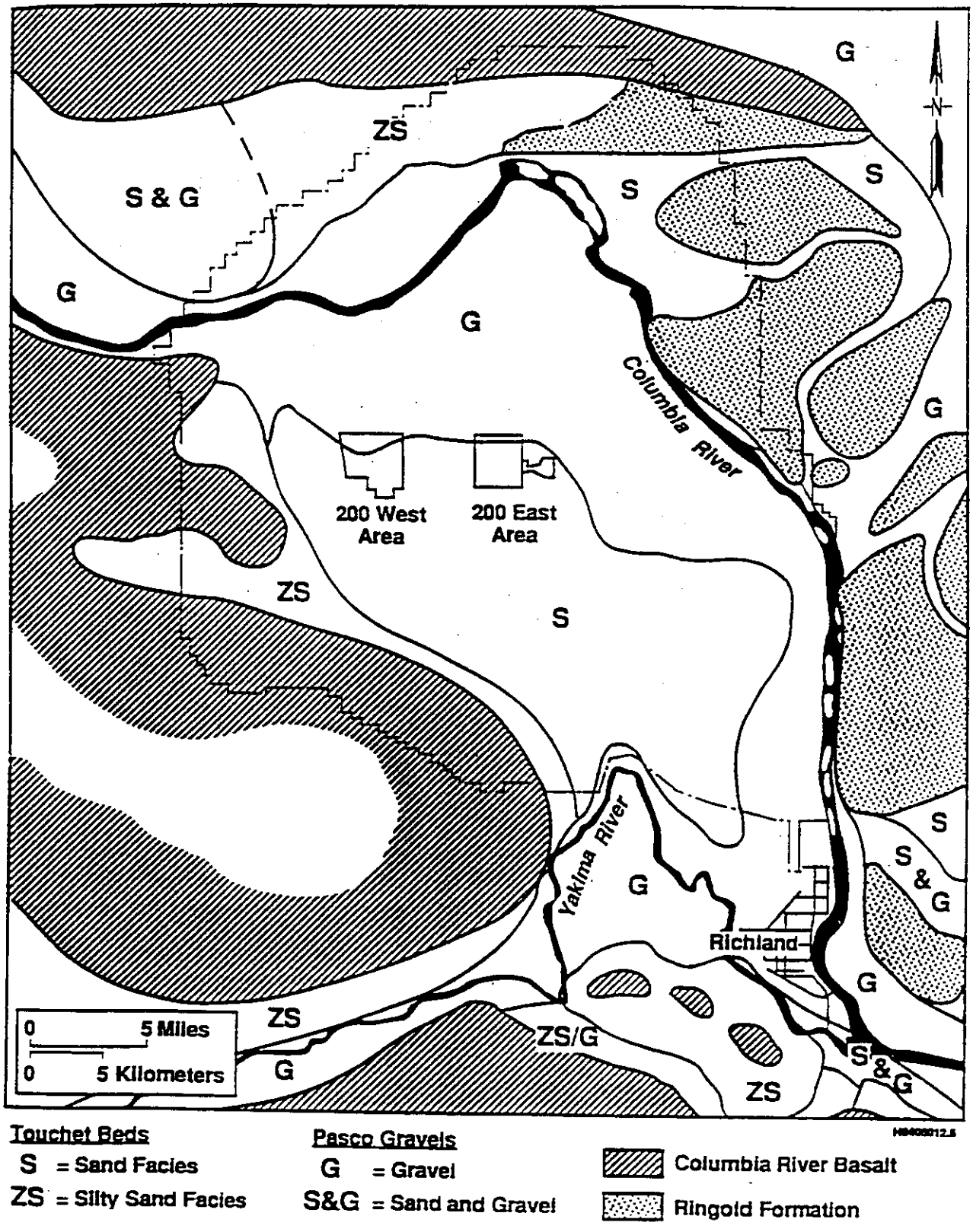

Figure 2-3. Top-of-Basalt Map.

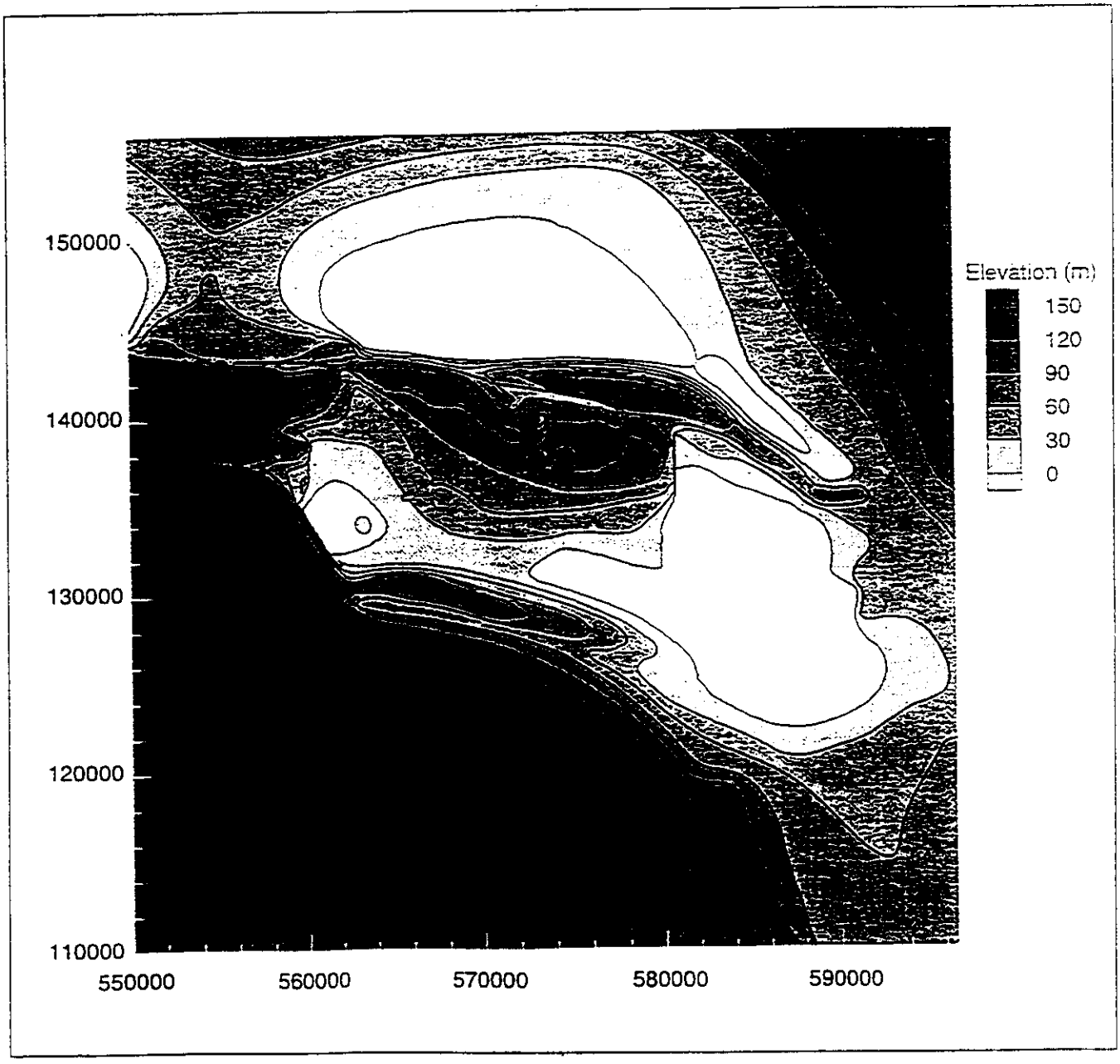

Figure 2-4. Miocene to Pliocene-Aged Suprabasalt Sediments of the Hanford Site - Cross Section H (from Lindsey 1995).

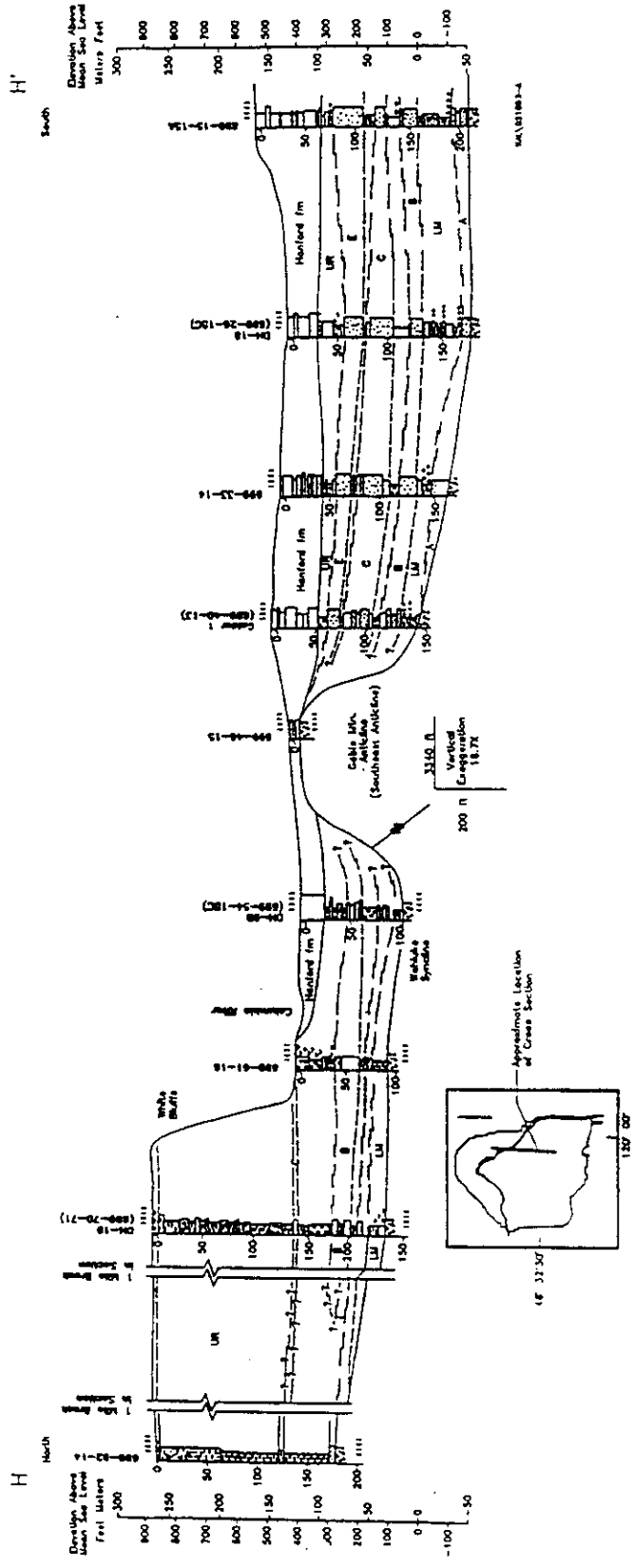

Figure 2-5. Miocene to Pliocene-Aged Suprabasalt Sediments of the Hanford Site - Cross Section N (from Lindsey 1995).

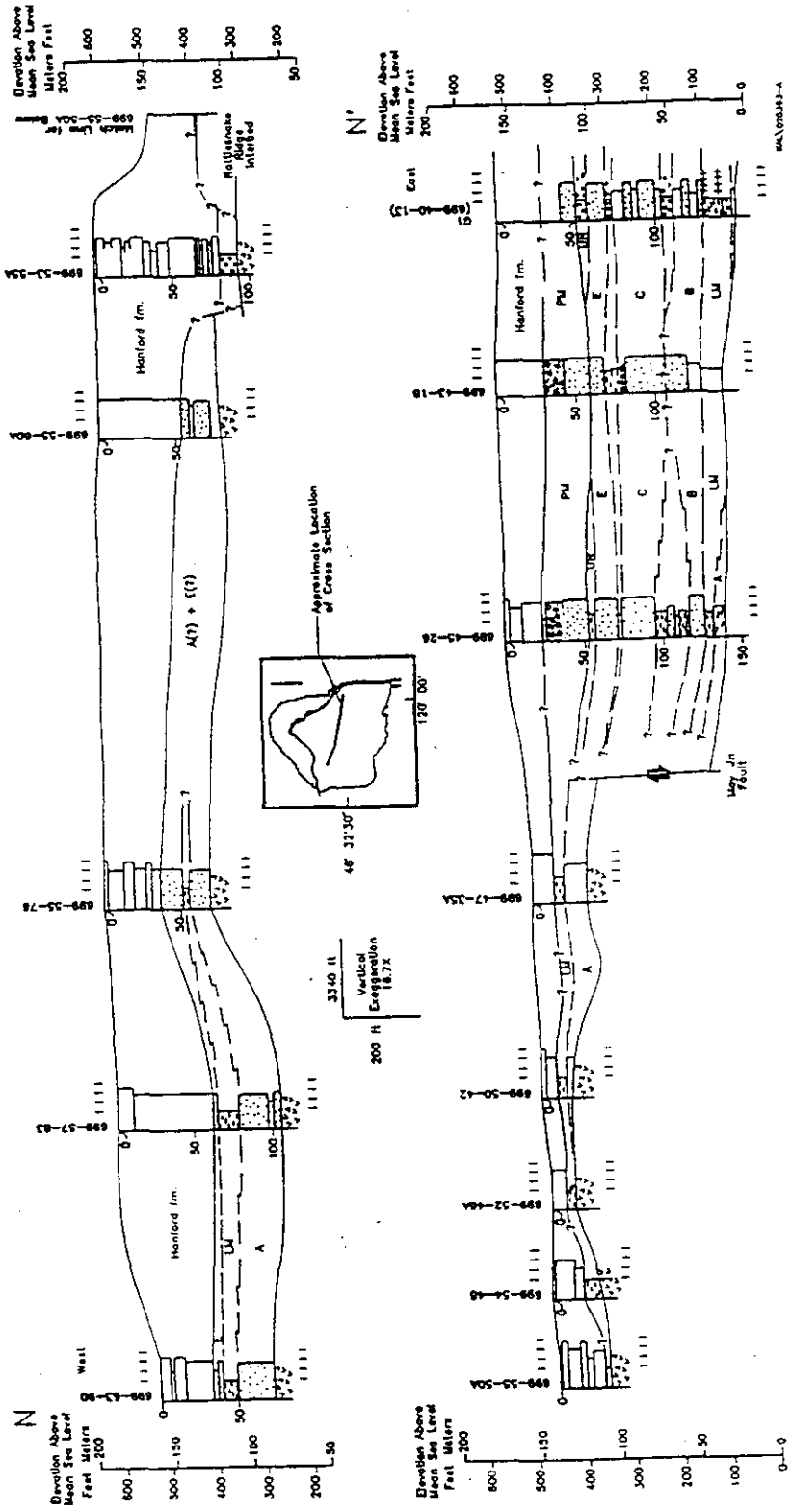

Figure 2-6. Comparison of Observed Hydraulic Heads for the Upper Basalt and Overlying Unconfined Aquifer Systems (from Spane and Webber 1995).

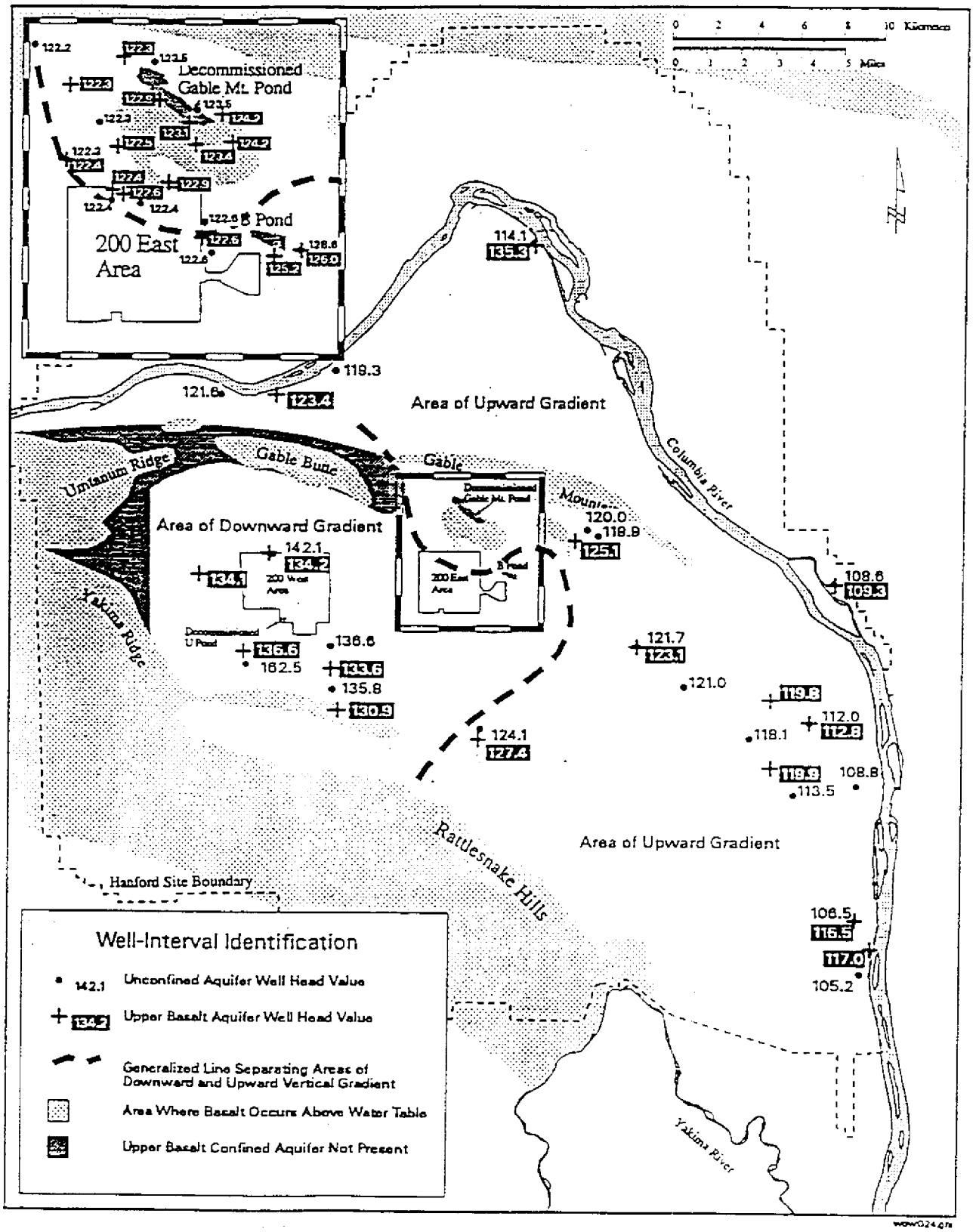

Figure 2-7. Bottom of the Modeled Aquifer.

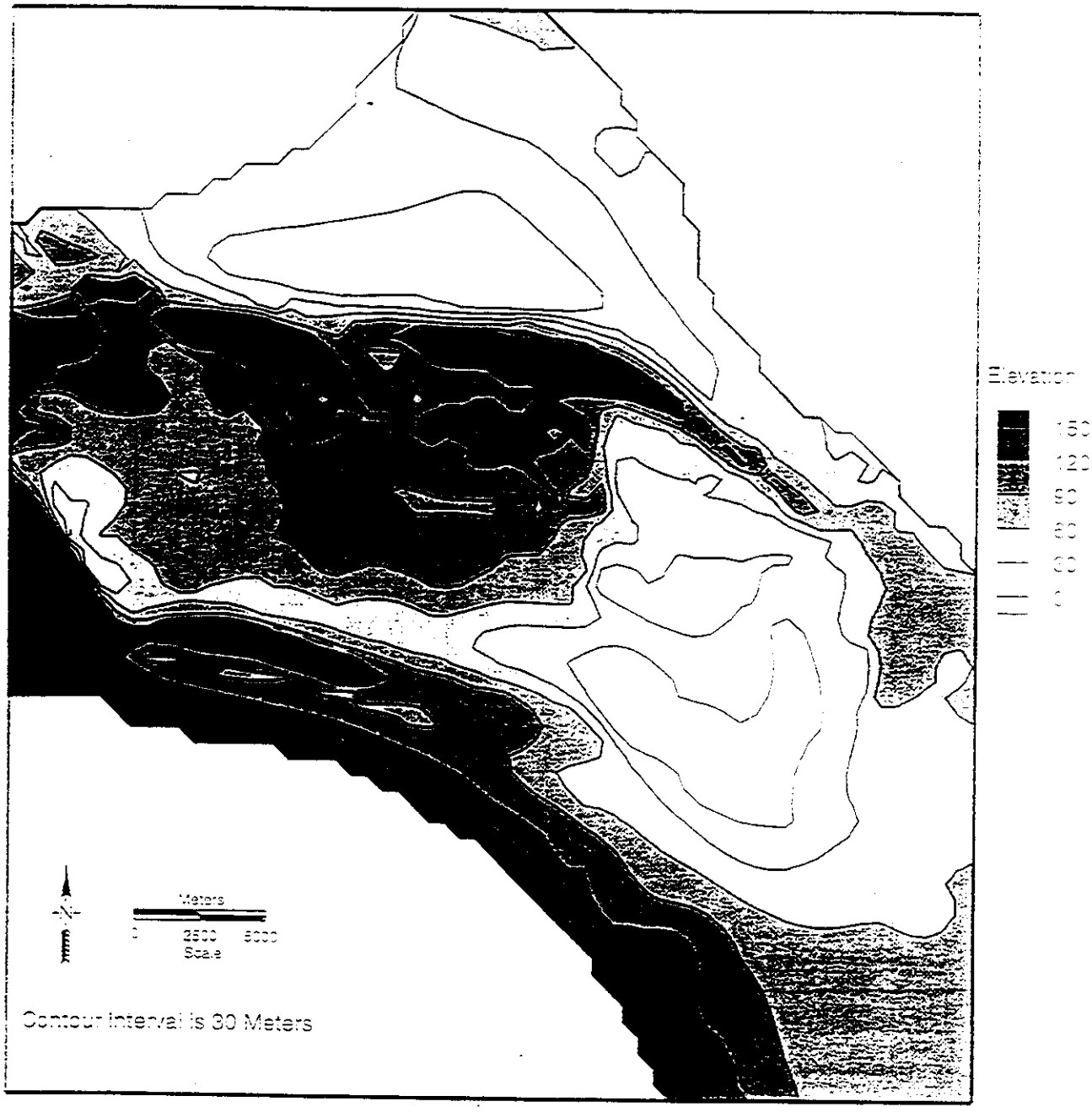

Figure 2-8. Saturated Thickness of the Unconfined Aquifer.

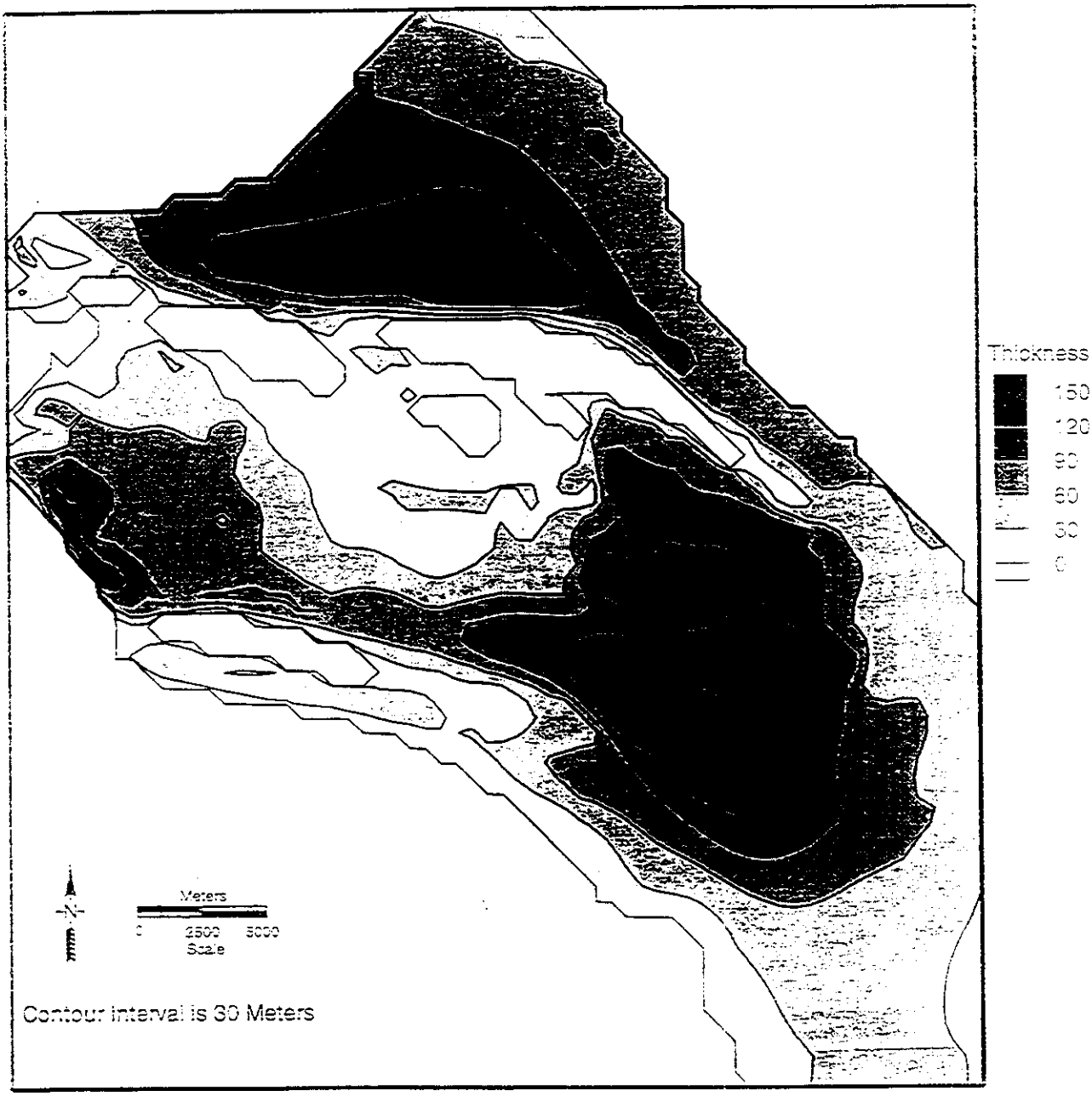

Figure 2-9. Saturated Thickness of the Pre-Missoula/Hanford Formation.

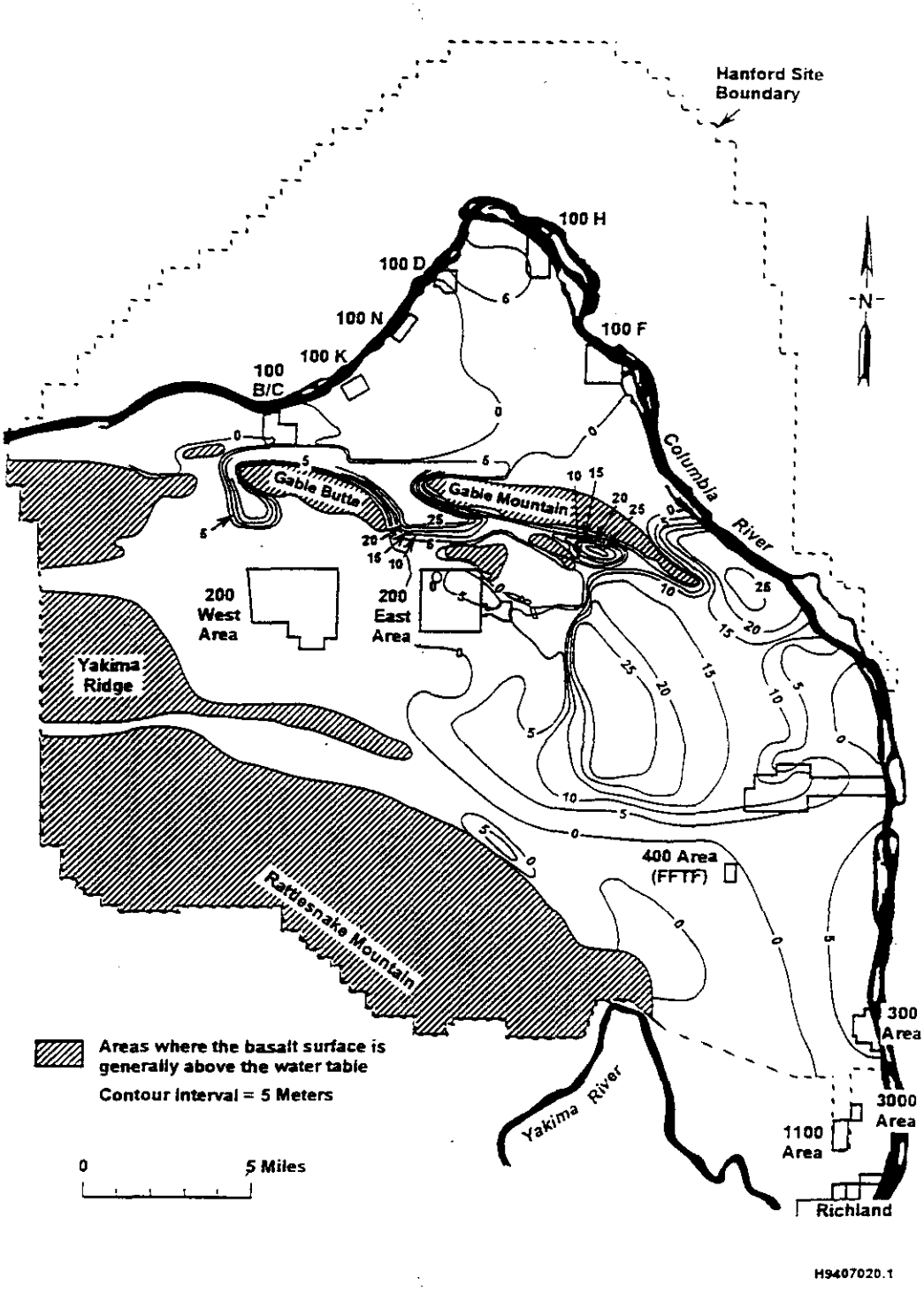

Figure 2-10. Location Map for Wells Used in Estimating Model Hydraulic Conductivities.

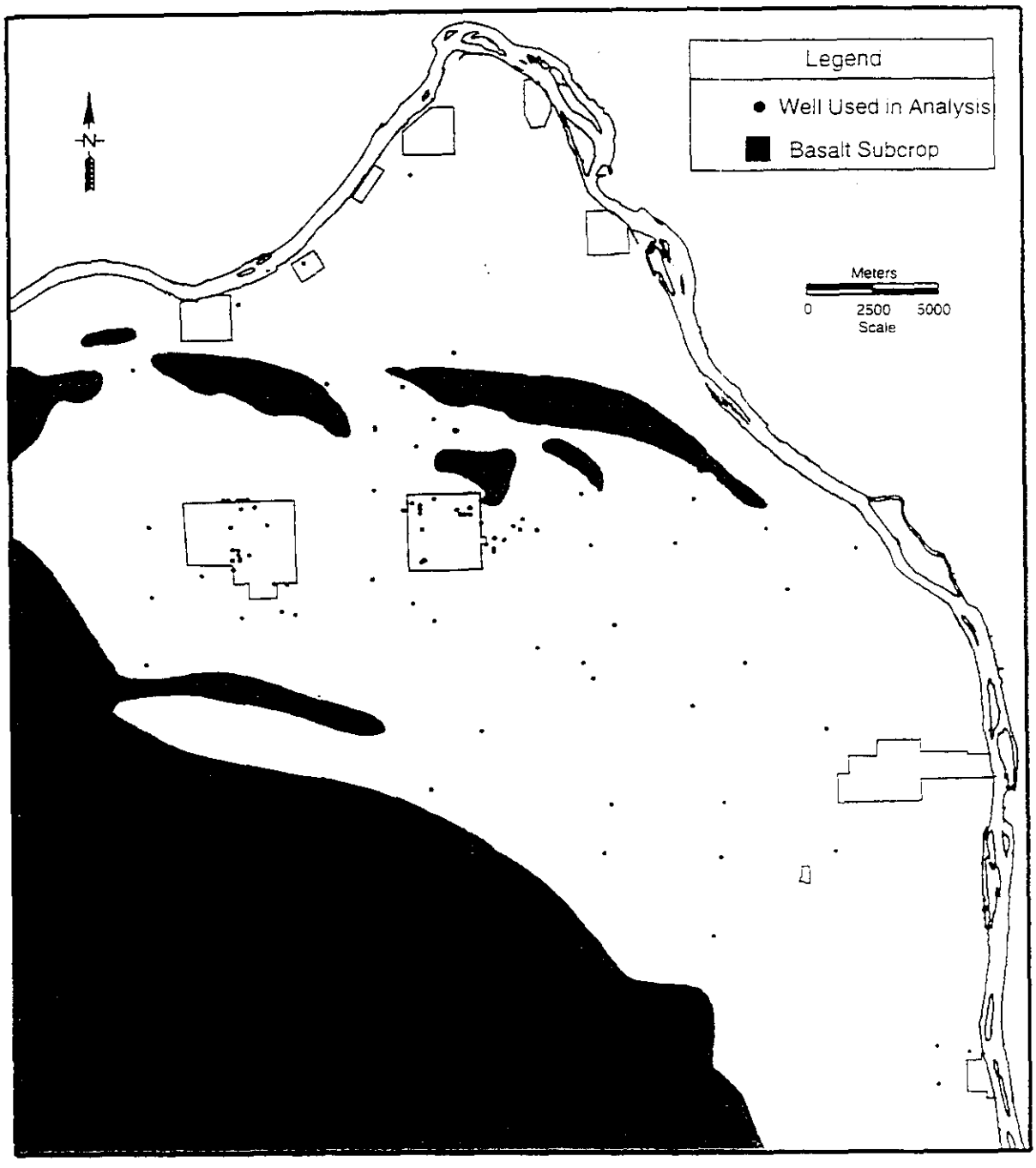

Figure 2-11. Liquid Effluents Discharged to the Soil Column.

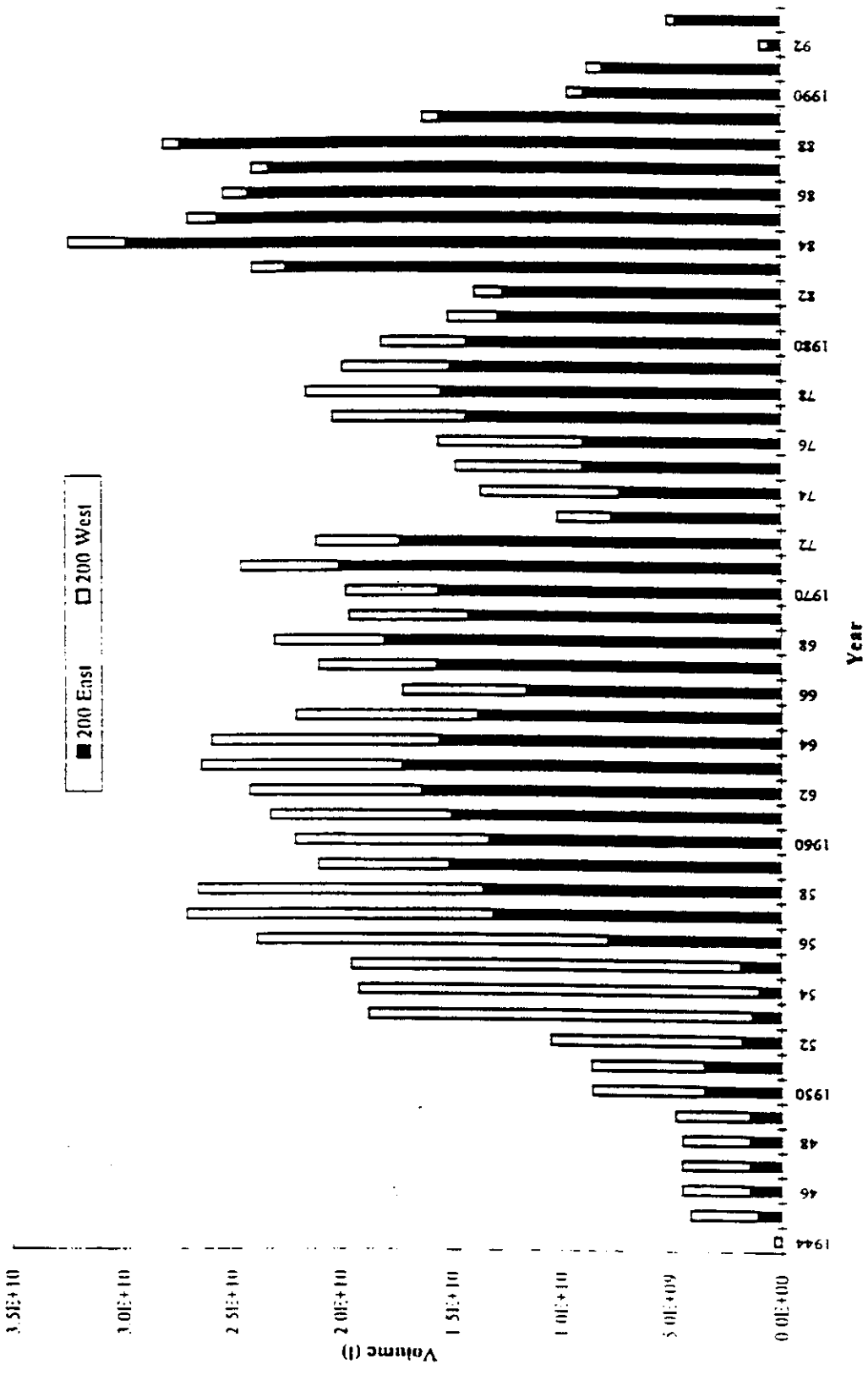

Figure 2-12. Location Map of Major Liquid Waste Disposal Facilities in the 200 East and 200 West Areas.

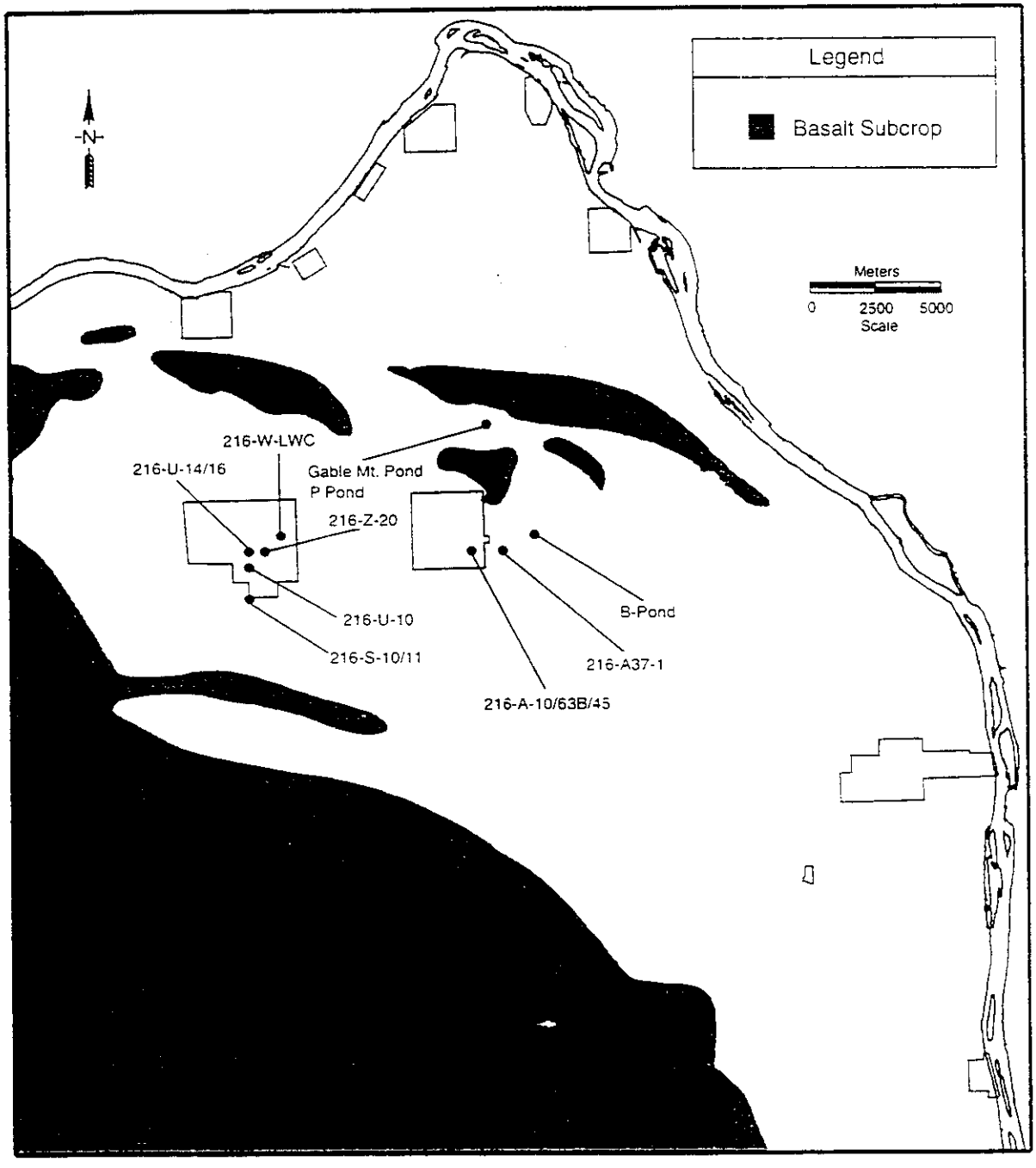

Table 2-1. Structure Contour and Isopach Data for the Ringold Formation at Selected Boreholes at the Hanford Site (from Lindsey 1995). (Page 1 of 7)

Borehole #	Easting	Northing	Top Bar	Top Sub A	Iso Sub A	Top A	Iso A	Top LM	Iso LM	Top DD	Iso DD	Top Sub C	Iso Sub C	Top C	Iso C	Top Sub E	Iso Sub E	Top E	Iso E	Iso C+E	Top UR	Iso UR	Top PMPP	Iso PMPP	Top HF	Iso HF	Iso Eo	Elev
101-48C	575722.89	154411.01																			338	>28	338	0	387	49	0	387
103-25	582315.60	155095.00	312																									
107-79	565779.00	156071.00	305																									
107-83	564464.70	156306.90	340																									
109-80	565525.40	156928.30	430																									
10-3	588880.00	126580.00	-84																									
10-30	580747.30	126573.40	43																									
10-54A	573597.40	126572.00	360													343	>27	420	77	77	420	0	420	0	507	87	9	518
10-E12	593575.00	126577.00	72		0	90	19	170	80	205	35	220	15	260	40	295	35	330	35	75	350	20	350	0	426	76	4	430
111-24	582526.00	157331.00	490																									
112-37	578693.00	157549.00	453																									
113-38	578388.40	158105.20	457																									
114-60	571642.00	158340.00	552																									
115-81	571379.00	158413.00	494																									
115-7	587830.00	158698.00	860																									
115-77	566261.00	158642.00	590																									
117-11	586518.50	159113.00	892																									
119-11	586463.80	159859.20	981																									
11-29	581154.00	126938.00	-184																									
11-45	576279.00	126808.00	203		0	268	65	353	85	353	0	353	0	353	0	353	0	408	55	55	408	0	408	0	578	170	0	578
11-E4E	590984.65	126738.23	-25	-25	0	25	50	115	90	145	30	145	0	145	0	205	60	330	125	125	330	0	330	0	440	110	0	440
11-E8B	592319.31	120746.12		84	0	89	25	129	40	212	83	212	0	249	37	259	10	344	85	122	344	0	344	0	449	105	0	449
122-11	586430.20	160085.60	1191																									
12-1	589981.80	127038.30	-81																									
12-18	584514.50	127197.50	-188																									
13-28	581994.10	127391.70	-235																									
13-28	589353.85	127336.18		-82	0	-28	36	29	55	149	120	149	0	149	0	179	30	319	140	140	349	30	349	0	439	90	0	439
13-64	570416.00	127309.00		390	0	390	0	390	0	390	0	390	0	390	0	390	0	443	53	53	443	0	443	0	552	109	0	552
14-36	578411.00	127782.00	92																									
14-E3E	590678.18	127837.60	8	8	0	55	47	125	70	165	40	165	0	165	0	218	53	325	109	109	345	20	345	0	450	105	0	450
14-E6P	591593.89	127703.47			0	88	43	153	65	178	25	178	0	178	0	203	25	323	120	120	323	0	323	0	458	135	0	458
15-15A	585353.58	128023.99		-160	2	-105	55	5	110	60	55	120	60	160	40	190	30	290	100	140	330	40	395	65	545	150	0	545
15-26	581875.98	128254.88																243			297	54	398	101	508	110	15	523
15-E13	593789.00	128200.00		104	7	170	56	204	34	243	39	245	2	293	48	341	8	341	48	104	341	0	341	0	404	63	8	410
16-23	582942.00	128372.00	-168																									
16-30A	580620.00	128449.00	-306																									
16-E4A	591005.01	128299.37		155	0	174	19	248	72	290	50	290	0	332	36	342	10	370	28	64	370	0	370	0	459	89	0	459
17-15	585418.60	128546.80	-137																									
17-26	581930.00	128750.00		-178	22	-132	46	-23	109	26	49	94	68	148	54	184	16	255	91	145	320	65	393	73	523	130	0	523
17-47	575490.00	128765.00		243	0	250	7	276	26	295	19	295	0	295	0	358	63	398	40	40	398	0	398	0	571	173	5	578
17-70	568578.00	128647.00		313	18	333	20	353	20	353	0	353	0	353	0	443	90	524	81	81	524	0	524	0	563	39	0	563
17-93	561565.00	128629.00			0	736	0	736	0	736	0	736	0	736	0	736	0	736	0	0	736	0	736	0	765	29	0	765
18-21	583735.70	128785.20	-149																									
18-25	582427.10	128901.40	-244																									
19-23	582995.40	129315.00	-141																									
19-27	581050.80	129220.40	-184																									
19-34	580100.10	129085.10	-172																									
19-58	572153.00	129252.00		368	0	388	0	383	15	383	0	383	0	383	0	383	0	424	41	41	424	0	424	0	573	149	0	573
19-88	583183.30	129255.20	293																									
1-18	584528.90	123948.86														217	>30	412	195	195	412	0	412	0	532	120	5	537
20-18	584484.00	129419.30	-75																									
20-25	582486.40	129660.60	-145																									
20-39	577999.00	129729.00			0	-54	15	56	110	70	14	148	78	155	9	210	55	380	170	179	380	0	430	50	525	95	15	540
20-69	568642.60	129485.80	493																									
20-82	564812.00	129506.00		269	0	269	0	309	40	309	0	309	0	309	0	308	0	546	237	237	546	0	546	0	608	62	6	614
20-E12	593573.00	129718.00		112	15	112	0	182	70	246	64	246	0	287	41	287	0	352	65	106	357	5	372	15	437	65	0	437
20-E2	590665.00	129722.00		-13	0	11	24	91	80	153	62	161	8	201	40	224	23	311	87	127	334	23	398	64	466	68	8	466
20-E5	591381.00	129611.00	147																									
21-17	584792.00	129855.00	-92																									
21-30B	580818.00	129982.00	-168																									
22-23	582992.00	130342.00	-131																									
22-70	568800.00	129504.00		482	0	492	0	492	0	492	0	492	0	492	0	492	0	492	0	0	492	0	492	0	614	122	0	614
23-33	578924.00	130029.00		-77	0	13	90	58	45	113	55	168	55	168	20	203	15	318	115	135	353	35	403	50	553	150	0	553
24-19	589494.53	130705.15		39	10	39	0	114	75	149	35	193	44	234	41	254	20	324	70	111	333	9	404	71	474	70	0	474
24-33	579752.75	130750.99		0	0													390	>30		390	0	454	64	507	53	17	524
24-48	575888.00	130790.00		-79	0	-14	65	96	110	106	10	106		106		106	90	381	165	185	381	0	431	50	597	166	0	597
25-20	583892.00	130998.00	-191																									
25-26	582044.00	131082.00		95	0	20	75	40	60	95	55	125	30	100	65	100	0	300	110	175	320	20	405	85	515	110	0	515
25-31	580460.00	131178.00		-54	0	11	65	81	70	126	45	106	70	261	65	268	5	351	65	150	351	0	391	40	511	120	0	511
25-55	573083.35	131206.00																406	>45		406	0	456	50	657	201	19	676
25-70	568544.00	131172.00						184	>15	184	0	184	0	184	0	184	0	442	258	258	474	32	499	25	599	100	30	629

Table 2-1. Structure Contour and Isopach Data for the Ringold Formation at Selected Boreholes at the Hanford Site (from Lindsey 1995). (Page 2 of 7)

Borehole #	Easting	Northing	Top Bat	Top Sub A	Iso Sub A	Top A	Iso A	Top LM	Iso LM	Top BD	Iso BD	Top Sub C	Iso Sub C	Top C	Iso C	Top Sub E	Iso Sub E	Top E	Iso E	Iso C+E	Top UR	Iso UR	Top PMPP	Iso PMPP	Top Hf	Iso Hf	Iso Ea	Elev
25-10	565875.00	131106.00		503	0	515	10	515	0	515	0	515	0	515	0	515	0	575	60	60	575	0	582	7	600	18	15	615
26-15C	565472.44	131330.29	-160	-160	0	-138	22	-35	103	37	72	95	58	182	87	195	13	258	63	163	330	70	330	0	442	112	2	444
20-29D	581083.00	131528.00	-193																									
26-83A	564532.00	131300.00	209																									
20-89	567778.60	131375.20		102	0	197	35	233	36	303	70	303	0	303	0	343	40	513	170	170	544	31	544	0	643	99	10	653
27-8	567499.70	131742.30	-101																									
28-23	562807.00	132004.00		-172	0	-107	65	-32	75	18	50	58	40	133	75	153	20	263	110	185	308	45	418	110	528	110	0	528
28-30	560816.00	131991.00			0	-48	135	32	80	32	0	32	0	32	0	32	0	282	230	230	322	60	437	115	532	95	0	532
28-40	577821.40	131932.13				192 >22		182	70	182	0	182	0	209	27	247	38	379	132	159	379	0	449	70	559	110	0	559
26-52A	574188.00	132111.00			0	99	100	274	175	274	0	274	0	274	0	274	0	420	146	146	420	0	439	19	684	245	0	684
29-76	566212.00	132414.00	58	81	23	153	72	208	55	228	20	237	0	237	0	299	71	458	159	159	483	25	483	0	647	164	0	647
29-83	564510.00	132373.60	67	67	0	183	116	250	67	298	48		0		0	311	13	490	179	179	503	13	557	54	60	623		623
2-3	588910.91	124098.21																382 >57		0	382	0	382	0	469	87	8	477
2-33A	579919.00	124047.00		84	0	118	32	101	75	231	40	345	114	371	26	381	10	412	31	57	412	0	412	0	531	119	5	536
2-E13-16	573119.10	134218.00				273 >15		328	55	328	0	328	0	328	0	328	0	388	60	60	388	0	388	0	728	340		728
2-E13-20	573609.60	134312.80	156	156	0	271	115	331	60	331	0	331	0	331	0	331	0	426	95	95	426	0	426	0	736	310	5	741
2-E14	594001.00	124029.00	68	68	0	108	40	158	50	213	55	213	0	213	0	248	35	323	75	75	323	0	323	0	388	65	0	388
2-E17-4	575118.20	135370.30																410 >05		>05	410	0	410	0	715	305	0	715
2-E19	595692.00	124133.00		104	0	139	35	199	60	234	35	234	0	234	0	274	40	324	50	50	324	0	324	0	369	45	15	384
2-E19-1	572870.20	135085.20	215																									
2-E24-7	574406.60	135560.90	271	271	0	381	110	381	0	381	0	381	0	381	0	381	0	381	0	0	381	0	381	0	716	335	0	716
2-E24-8	574547.00	136271.70	306	306	0	408	102	408	0	408	0	408	0	408	0	408	0	408	0	0	408	0	408	0	668	260	20	688
2-E25-1	575338.10	136031.30				408 >40		418	10	418	0	418	0	418	0	418	0	418	0	0	418	0	418	0	663	245	25	688
2-E25-12	575978.80	136491.30				357 >25		362	5	362	0	362	0	362	0	362	0	362	0	0	362	0	362	0	673	311	5	678
2-E25-13	575362.90	136139.90				399 >34		427	28	427	0	427	0	427	0	427	0	427	0	0	427	0	427	0	677	250	5	681
2-E25-17	575899.40	135703.20						407 >18		407	0	407	0	407	0	407	0	407	0	0	407	0	407	0	687	280	0	687
2-E25-18	575818.10	135698.70				386 >10		391	5	391	0	391	0	391	0	391	0	391	0	0	391	0	391	0	678	285	0	678
2-E25-19	575855.00	135657.60				399 >25		399	0	399	0	399	0	399	0	399	0	399	0	0	399	0	399	0	670	271	4	674
2-E25-2	575514.00	136062.00	319	319	0	405	86	420	15	420	0	420	0	420	0	420	0	420	0	0	420	0	420	0	663	243	12	675
2-E25-28	576011.80	136111.90	319	319	0	407	88	413	5	413	0	413	0	413	0	413	0	413	0	0	413	0	413	0	655	242	5	660
2-E25-32P	576382.30	136044.70	323	323	0	375	52	375	0	375	0	375	0	375	0	375	0	375	0	0	375	0	375	0	663	288	5	668
2-E25-33	575982.20	135713.20	291	291	0	384	93	403	19	403	0	403	0	403	0	403	0	403	0	0	403	0	403	0	672	269	0	672
2-E26-1	575251.90	137130.70	394	394	0	394	0	394	0	394	0	394	0	394	0	394	0	394	0	0	394	0	394	0	616	222	0	616
2-E26-10	575589.30	137023.80	394	394	0	394	0	394	0	394	0	394	0	394	0	394	0	394	0	0	394	0	394	0	598	204	0	598
2-E26-11	576180.20	137134.90	399	399	0	399	0	399	0	399	0	399	0	399	0	399	0	399	0	0	399	0	399	0	590	191	0	590
2-E26-9	575584.10	137133.40	399	399	0	399	0	399	0	399	0	399	0	399	0	399	0	399	0	0	399	0	399	0	599	200	0	599
2-E27-1	574515.80	136537.10				428 >70		428	0	428	0	428	0	428	0	428	0	428	0	0	428	0	428	0	681	253	0	681
2-E27-10	575100.60	137052.90	382	382	0	382	0	382	0	382	0	382	0	382	0	382	0	382	0	0	382	0	382	0	622	240	0	622
2-E27-11	574853.20	137063.20	378	378	0	378	0	378	0	378	0	378	0	378	0	378	0	378	0	0	378	0	378	0	643	262	0	643
2-E27-5	574688.80	136306.50				435 >70		440	5	440	0	440	0	440	0	440	0	440	0	0	440	0	440	0	685	245	0	685
2-E28-17	573492.00	136331.80				415 >50		415	0	415	0	415	0	415	0	415	0	415	0	0	415	0	415	0	708	293	0	708
2-E28-18	573095.20	136787.70				438 >50		438	0	438	0	438	0	438	0	438	0	438	0	0	438	0	438	0	692	254	0	692
2-E28-3	573708.80	136607.30				371 >5		371	0	371	0	371	0	371	0	371	0	371	0	0	371	0	371	0	692	321	0	692
2-E28-5	574033.90	136858.90	365	365		365	0	382	17	382	0	382	0	382	0	382	0	382	0	0	382	0	382	0	672	290	0	672
2-E33-10	573788.30	137385.60	395	395	0	402	7	441	39	441	0	441	0	441	0	441	0	441	0	0	441	0	441	0	843	202	0	843
2-E33-37	574091.50	137185.60	382	382	0	382	0	382	0	382	0	382	0	382	0	382	0	382	0	0	382	0	382	0	853	271	0	853
2-E33-4	573817.00	137693.00	399	399	0	399	0	399	0	399	0	399	0	399	0	399	0	399	0	0	399	0	399	0	629	230	0	629
2-E33-41	573707.30	137370.00	389	389	0	411	22	433	22	433	0	433	0	433	0	433	0	433	0	0	433	0	433	0	818	385	34	852
2-E34-2	574635.10	137221.00	388	388	0	388	0	388	0	388	0	388	0	388	0	388	0	388	0	0	388	0	388	0	629	241	0	629
2-E34-8	574206.50	137250.00	383	383	0	383	0	383	0	383	0	383	0	383	0	383	0	383	0	0	383	0	383	0	640	257	0	640
2-E35-1	575460.00	137485.20	402	402	0	402	0	402	0	402	0	402	0	402	0	402	0	402	0	0	402	0	402	0	595	193	0	595
2-E35-2	575578.50	137255.30	399	399	0	399	0	399	0	399	0	399	0	399	0	399	0	399	0	0	399	0	399	0	599	200	0	599
30-25C	582358.41	132593.51	-147	-135	12	-92	43	3	95	23	20	80	57	129	49	129	0	250	121	170	304	54	398	94	543	145	0	543
31-31	580550.00	132974.00						-71 >50		36	35	104	140	154	50	159	5	274	115	165	329	55	400	80	519	110	10	529
31-53A	573754.50	132962.41														281 >57		423	142		423	0	423	0	706	283	0	706
31-85	569981.00	132777.00				258 >15		291	35	291		291		291		291		471	180	180	471	0	471	0	676	205	5	681
31-8	587398.00	132828.00	-84	-84	0	-34	30	11	45	81	70	116	35	216	100	226	10	276	50	150	321	45	401	80	466	65	10	476
31-84A	584381.00	132999.00	21																									
32-22	583198.71	133257.40																358 >10			358	0	358	0	518	160	0	518
32-26	581891.00	133144.00	-140	-115	25	-90	25	25	115	55	30	90	35	185	75	185	0	285	100	175	315	50	460	145	510	50	10	520
32-32	580297.00	133208.00	-200	-200	0	-80	140	15	75	15	0	15	0	140	125	140	0	285	145	270	285	0	440	155	505	65	15	520
32-42	576961.37	133365.38																397			397	0	397	0	492	95	25	
32-62	571009.41	133217.69						302 >97		302	0	302	0	302	0	302	0	482	180	180	482	0	505	23	705	200	0	705
32-72	567943.00	133383.00	96	96	0	217	121	257	40	257	0	257	0	257	0	257	0	427	170	170	472	0	469	43	668	200	0	667
33-14	585534.00	133607.00	-77	-77	0	-27	50	3	30	83	60	113	30	228	115	238	10	298	60	175	338	40	423	85	483	40	10	473
33-21A	583372.00	133474.00	-115	-115	0	-65	50	-25	40	60	85	80	20	115	35	145	30	285	140	175	330	45	435	105	485	50	15	500
33-42	577020.24	133484.78																401 >10			401	0	401	0	490	95	20	510
33-56	572831.80	133535.50						316 >40		316	0	316	0	316	0	316	0	431	115	135	431	0	431	0	711	280	5	716
33-8	586013.00	133420.00	41																									
34-20	583053.00	133722.00	-118	-118	0	-65	53	0	65	75	75	75	0	155	80	175	20	275	100	180	300	25	355	55	475	120	25	500
34-41B	577338.20	133913.63																400 >10			400	0	400	0	570	170	0	

Table 2-1. Structure Contour and Isopach Data for the Ringold Formation at Selected Boreholes at the Hanford Site (from Lindsey 1995). (Page 3 of 7)

Borehole #	Easting	Northing	Top Bas	Top Sub A	Iso Sub A	Top A	Iso A	Top LM	Iso LM	Top BD	Iso BD	Top Sub C	Iso Sub C	Top C	Iso C	Top Sub E	Iso Sub E	Top E	Iso E	Iso C+E	Top UR	Iso UR	Top PMPP	Iso PMPP	Top Hf	Iso Hf	Iso Eo	Elev
34-8	587504.00	133960.00	-31																									
34-88	583035.20	133974.10	-18	-18	0	105	123	228	122	270	0	226	0	220	0	226	0	506	280	280	541	35	541	0	619	78	12	631
34-89D	582825.00	133663.00	-8																									
34-98	580789.70	134103.00	-22																									
35-16	585109.00	134124.00	-66																									
35-19A	584085.00	134090.00	-77																									
35-21	583514.00	134322.30	-59	-59	0	11	70	91	80	120	35	198	70	278	80	278	0	354	78	158	354	0	456	102	511	55	0	511
35-27	581859.80	134093.30	-84	-84	0	11	95	106	95	126	20	148	20	148	0	148	0	281	135	135	301	20	301	0	531	230	0	
35-28	581287.00	134019.00	-87	-87	0	8	95	73	65	78	5	133	55	108	65	108	0	283	65	150	318	35	483	165	528	45	5	533
35-3	588963.00	134190.00	26	26	0	26	0	131	105	131	0	131	0	226	95	256	30	316	60	155	331	15	431	100	466	35	20	486
35-5	588028.00	134321.00	5																									
35-66	569858.10	134094.00				273 >1		325	52	325	0	325	0	325	0	325	0	423	98	98	423	0	423	0	713	290	10	
35-70	568568.46	133987.75																422 >55			444	22	474	30	687	213	5	692
35-78D	566087.00	134273.00	78	83	5	168	85	240	72	240	0	240	0	240	0	240	0	498	258	258	498	0	553	55	658	105	0	658
35-9	587102.03	134089.57																	0	0	323 >111		334	49	495	112	5	500
36-1	589486.00	134610.00	218																									
36-10	586773.00	134605.00	-22																									
36-17	584706.00	134613.00																										
36-2	589225.00	134401.00	184																									
36-27	581805.00	134446.00	-64	-64	0	6	70	100	100	116	10	149	33	216	67	216	0	286	70	137	321	35	466	145	531	65	0	531
36-48P	575994.70	134518.20	182	182	0	266	84	341	75	341	0	341	0	341	0	341	0	410	69	69	410	0	410	0	701	291	0	701
36-61D	571400.80	134586.90	201	201	0	251	50	346	95	346	0	346	0	346	0	346	0	436	90	90	436	0	436	0	736	300	10	746
36-92	581850.00	134400.00																			586 >1		616	30	786	170	0	
36-93	581551.00	134420.00	-38	-32	6	101	133	198	97	230	32	230	0	230	0	258	28	408	240	240	508	10	508	0	643	135	5	842
36-E3	590777.00	134348.00	140	140	0	140	0	220	80	250	30	250	0	295	45	345	50	345	0	45	345	0	375	30	465	90	0	465
37-36	578973.00	134722.00	1223																									
37-4	588550.00	134741.00	258																									
37-43	576628.40	134785.10	180	180	0	264	84	289	25	289	0	289	0	304	15	350	46	203	44	58	404	10	404	0	689	285	0	689
37-87D	564903.71	134733.44	30	30	0	135	105	240	105	240	0	240	0	240	0	240	0	525	285	285	525	0	540	15	625	85	10	638
37-84	584247.00	134788.00	14	14	0	129	115	216	87	216	0	216	0	216	0	216	0	526	310	310	531	5	565	34	634	69	0	634
37-92	581921.00	134597.00	-29																									
37-E1	590283.00	134788.00																										
38-19	584256.00	135160.00	-29	-29	0	-29	0	91	115	101	10	139	38	206	67	206	0	301	95	162	331	30	461	80	451	40	10	461
38-3	589025.00	135121.00																										
38-34A	579490.79	135148.73	174	174	0	254	80	264	10	304	40	304	0	304	0	354	50	379	25	25	409	30	479	70	519	40	10	529
38-65	570091.10	135041.00	225	225	0	302	77	360	58	360	0	360	0	360	0	360	0	470	110	110	470	0	470	0	751	281	0	751
38-70	568500.94	135089.20						314 >20		314	0	314	0	314	0	314	0	464	150	150	509	45	524	15	704	180	5	709
38-8	587567.00	135241.00	75																									
38-9	587292.00	135022.00	41																									
38-E0	590153.10	135068.90	257																									
399-1-16C	594312.00	116410.00	205	205	0	205	0	270	65	270	0	270	0	270	0	270	0	325	55	55	325	0	325	0	380	55	0	
399-1-17C	594104.00	116409.00	206	206	0	206	0	261	55	261	0	261	0	261	20	281	0	326	45	65	326	0	326	0	371	45	5	
399-1-20	594257.00	116339.00	207																									
399-4-5	594128.00	115638.00	202	202	0	208	6	220	12	231	11	231	0	231	0	257	26	345	88	88	345	0	345	0	400	55	0	
39-103	558481.00	135431.00	752																									
39-23	582963.40	135347.20	-19	-19	0	26	45	81	55	151	70	166	15	256	90	256	0	321	65	155	351	30	431	80	476	45		475
39-2A	589372.00	135401.00	213																	8								
39-79	585890.92	135411.87																			522 >140		532	10	652	120	20	672
39-7A	587815.53	135440.73	339	339	0	339	0	352	13	352	0	352	0	352	0	352	0	352	0	0	352	0	352	0	492	140	0	
39-840	584238.00	135440.00	29																									
39-E2	590532.00	135451.00	219	219	0	219	0	239	20	249	10	249	0	249	0	279	30	279	0	0	279	0	364	85	404	40	0	404
3-45	578205.00	124401.00	373	373	0	373	0	373	0	373	0	373	0	373	0	373	0	373	0	0	373	0	373	0	504	131	0	504
3-8-5C	593388.00	116574.00	202	202	0	206	0	234	32	263	29	263	0	301	38	325	24	333	8	70	333	0	333	0	391	58	7	398
40-12B	586325.30	135837.23	52	52	0	52	0	108	56	137	29	189	52	253	64	290	37	327	37	190	352	25	407	55	512	105	5	515
40-13	585939.00	135850.00	26	26	0	26	0	90	64	50	60	184	34	276	92	283	7	328	45	137	348	20	391	43	508	117	0	507
40-2	589132.00	135806.00	106																									
40-20	583830.00	135878.00	-14	-14	0	16	30	101	85	146	45	156	10	216	60	226	10	321	95	165	336	15	425	89	476	51	0	532
40-32	580007.00	135578.00	199	199	0	273	74	388	115	388	0	388	0	388	0	388	0	388	0	0	388	0	388	0	518	130	5	523
40-33A	579704.81	135811.88	240	240	0	310	70	403	93	403	0	403	0	403	0	403	0	403	0	0	403	0	403	0	518	115	0	
40-36	578789.30	135833.80	252	252	0	328	76	413	85	413	0	413	0	413	0	413	0	413	0	0	413	0	413	0	522	109	4	526
40-39	577838.30	135648.20				338 >10		418	80	418	0	418	0	418	0	418	0	418	0	0	418	0	418	0	533	115	5	538
40-6	588101.00	135870.00	255																									
40-62	571149.10	135755.80						374 >10		374	0	374	0	374	0	374	0	435	61	61	435	0	435	0	744	309	4	
40-80	565517.00	135548.00	107	107	0	164	57	216	52	216	0	216	0	216	0	216	0	504	288	288	504	0	542	38	654	112	0	654
40-84	564248.00	135751.00	40	40	0	156	116	237	81	237	0	237	0	237	0	237	0	528	291	291	546	18	553	7	638	85	0	638
41-10	586962.00	136133.00	225																									
41-11	586650.00	136024.40	129																									
41-20	583878.00	136150.00	15	15	0	35	20	115	80	160	45	160	0	245	85	255	10	315	60	145	315	0	385	70	470	85	15	485
41-23	582923.00	135905.92																371			371	0	371	0	466	95	0	
41-31	580525.00	136007.00	194	194	0	283	71	369	105	369	0	369	0	369	0	369	0	369	30	30	393	0	424	25	499	75	5	504
41-35	579079.60	135947.40	270	270	0	352	82	417	65	417	0	417	0	417	0	417	0	417	0	0	417	0	417	0	517	100	0	517

Table 2-1. Structure Contour and Isopach Data for the Ringold Formation at Selected Boreholes at the Hanford Site (from Lindsey 1995). (Page 4 of 7)

Borehole #	Easting	Northing	Top Bas	Top Sub A	Iso Sub A	Top A	Iso A	Top LM	Iso LM	Top BD	Iso BD	Top Sub C	Iso Sub C	Top C	Iso C	Top Sub E	Iso Sub E	Top E	Iso E	Iso C+E	Top UR	Iso UR	Top PMPP	Iso PMPP	Top Hf	Iso Hf	Iso Eo	Elev
41-4	588047.00	136109.00	141																									
41-40	577614.00	135996.30				380	>12	421	41	421	0	421	0	421	0	421	0	421	0	0	421	0	421	0	543	122	0	543
41-42	577122.20	136068.20	305	305	0	386	81	414	28	414	0	414	0	414	0	414	0	414	0	0	414	0	414	0	634	220	0	640
41-5	588387.00	135900.00	262																									
42-10	586951.00	136269.00	291																									
42-12A	586318.00	136457.00	188	188	0	186	0	239	53	304	65	304	0	372	68	372	0	384	12	80	384	0	465	81	504	39	10	514
42-21	583404.00	136195.00			0	74	70	89	15	174	85	189	15	224	35	249	25	346	97	132	348	0	393	47	456	65	5	463
42-29	581045.00	136427.00			0	65	40	80	15	165	85	210	45	260	50	300	40	335	35	85	345	10	375	30	450	75	5	455
42-3	588908.00	136319.00	49	49	0	49	0	155	100	209	54	254	45	279	25	279	0	279	0	25	329	50	354	25	434	80	10	444
42-30	580786.00	136213.00	63	63	0	125	62	155	30	183	28	223	40	291	68	300	15	351	45	113	351	0	406	55	400	60	15	481
42-37	578476.30	136218.40	272	272	0	392	120	427	35	427	0	427	0	427	0	427	0	427	0	0	427	0	427	0	522	95	0	522
42-40C	577644.50	136410.20	328	328	0	403	75	418	15	416	0	416	0	416	0	416	0	416	0	0	416	0	416	0	546	130	0	546
42-42A	577068.60	136290.00	311	311	0	394	83	413	19	413	0	413	0	413	0	413	0	413	0	0	413	0	413	0	596	183	5	601
42-42B	576998.30	136434.40				402	>70	424	22	424	0	424	0	424	0	424	0	424	0	0	424	0	424	0	583	159	0	583
42-88	582931.00	136346.00	17	17	45	132	70	217	85	217	0	217	0	217	0	217	0	442	225	225	467	25	467	0	637	170	5	642
43-16	584394.00	136578.00	62	62	0	62	0	127	65	212	85	212	0	212	0	212	0	297	85	85	327	30	417	90	517	100	0	517
43-2	589431.00	136740.00	70																									
43-23	582978.00	136714.00	49	49	0	59	10	89	30	144	55	154	10	184	30	194	10	324	130	160	334	10	419	85	519	100	0	519
43-41E	577479.10	136594.40						425	>28			425	0	425	0	425	0	425	0	0	425	0	425	0	547	122	0	
43-41F	577480.00	136579.00				400	>38	428	20	428	0	428	0	428	0	428	0	428	0	0	428	0	428	0	548	122	0	
43-42	577145.30	136630.70	364	364	0	410	46	410	0	410	0	410	0	410	0	410	0	410	0	0	410	0	410	0	564	154	0	564
43-42J	577008.60	136452.19						423	>22			423	0	423	0	423	0	423	0	0	423	0	423	0	581	158	0	
43-43	576728.80	136576.50				406	>13	406	0	406	0	406	0	406	0	406	0	406	0	0	406	0	406	0	579	173	0	579
43-45	576283.90	136585.90																							595	>202	0	595
43-8	587597.00	136704.00	215																									
43-81	585083.00	136640.00	99																									
43-84	584184.00	136656.00			0	153	83	197	44	197	0	197	0	197	0	197	0	525	328	328	536	11	556	20	634	78	0	634
43-89	582917.14	136818.49																501			529	28	544	15	629	85	13	
43-9	587245.00	136507.00			0	325	0	325	0	325	0	325	0	325	0	325	0	325	0	0	325	0	325	0	490	165	0	490
43-91A	582223.00	136687.00	8																									
43-91B	582185.00	136892.00	18																									
44-116	553878.30	136907.60	900																									
44-16	584912.00	137002.00	98																									
44-42	577099.60	136833.90				416	>10	416	0	416	0	416	0	416	0	416	0	416	0	0	416	0	416	0	579	163	0	579
44-43D	576873.40	136897.80				420	>20	420	0	420	0	420	0	420	0	420	0	420	0	0	420	0	420	0	577	157	0	577
44-64	570459.80	136897.40	284	284	0	340	56	357	17	357	0	357	0	357	0	357	0	357	0	0	460	103	460	0	720	260	0	720
44-7	587838.00	136934.00	12																									
44-70	568508.00	136816.00	212																									
45-24	582552.00	137231.00	75	75	0	80	0	155	85	190	35	235	45	275	40	285	10	345	60	100	350	5	425	75	510	85	0	510
45-26	582081.00	137280.00	88	88	0	88	0	113	45	138	25	213	75	223	80	278	5	333	55	115	348	15	443	95	518	75	0	518
45-42	577057.50	137288.20	402	402	0	402	0	402	0	402	0	402	0	402	0	402	0	402	0	0	402	0	402	0	577	175	0	577
45-6A	588183.00	137185.00	40																									
45-78	586027.00	137045.00	181	181	203	218	22	247	44	247	0	247	0	247	0	247	0	553	306	306	568	15	598	30	688	90	0	688
46-15	585430.00	137428.00			0	415	0	415	0	415	0	415	0	415	0	415	0	415	0	0	415	0	415	0	444	29	0	444
46-3	588821.00	137692.00	78																									
46-5	586469.00	137488.00	59																									
46-85D	584038.40	137389.04	87	87	0	187	100	224	37	224	0	224	0	224	0	224	0	517	293	293	567	50	579	12	792	213	0	792
47-116	553814.30	137829.70	370																									
47-24	582598.00	137703.00	123																									
47-25	582128.00	137749.00	105																									
47-35B	579313.48	137793.68	370	370	0	420	50	440	20	440	0	440	0	440	0	440	0	440	0	0	440	0	440	0	470	30	5	475
47-42	577356.60	137840.60	401																									
47-48A	575869.00	137822.70			0	406	0	406	0	406	0	406	0	406	0	406	0	406	0	0	406	0	406	0	580	174	0	580
47-50	574797.80	137888.90	367	367	0	367	0	367	0	367	0	367	0	367	0	367	0	367	0	0	367	0	367	0	582	215	0	582
47-60	571474.00	137968.00	366	366	0	366	0	366	0	366	0	366	0	366	0	366	0	424	58	58	424	0	424	0	644	0	5	649
47-80A	585562.00	137693.00	180																									
47-80B	585556.00	137758.00	178																									
47-80C	585530.00	137713.00	180																									
47-80D	585494.00	137779.00	179																									
47-92	581959.00	137899.00	67																									
48-22	583118.00	138130.00	142	142	0	142	0	207	65	252	45	252	0	297	45	297	0	357	60	105	357	0	397	40	517	120	0	517
48-27	581722.00	138265.00	128																									
48-50	574817.90	138227.20	373																									
48-71	568351.00	138045.00																517			517	0	517	0	682	165	5	
48-77B	586414.00	137970.00	218	218	0	347	129	347	0	347	0	347	0	347	0	347	0	590	243	243	607	17	650	43	870	20	2	872
49-100C	559305.17	138504.54	390	390	0	390	0	398	8	398	0	398	0	398	0	398	0	585	187	187	585	0	590	25	773	183	17	790
49-21	583634.00	138555.00	364	364	0	364	0	364	0	364	0	364	0	364	0	364	0	364	0	0	364	0	364	0	494	130	0	494
49-31	580537.00	138317.00	131																									
49-32B	580174.00	138299.00	360																									
49-33	579776.00	138287.00	427																									
49-48	575103.40	138570.30			0	431	0	431	0	431	0	431	0	431	0	431	0	431	0	0	431	0	431	0	552	121	0	552

Table 2-1. Structure Contour and Isopach Data for the Ringold Formation at Selected Boreholes at the Hanford Site (from Lindsey 1995). (Page 5 of 7)

Borehole #	Easting	Northing	Top Bas	Top Sub A	Iso Sub A	Top A	Iso A	Top LM	Iso LM	Top BO	Iso BO	Top Sub C	Iso Sub C	Top C	Iso C	Top Sub E	Iso Sub E	Top E	Iso E	Iso C+E	Top UR	Iso UR	Top PMPP	Iso PMPP	Top Hf	Iso Hf	Iso Eo	Elev
49-55A	573146.30	138351.78	393	393	0	393	0	393	0	393	0	393	0	393	0	393	0	393	0	0	393	0	393	0	528	135	0	528
49-55B	573139.00	138351.00	394																									
49-57B	572536.60	138381.40			0	389	0	389	0	389	0	389	0	389	0	389	0	389	0	0	389	0	389	0	547	158	4	551
49-85B	563917.00	138506.00	122																									
49-95	560900.59	138503.03				296	>28	316	20	316	0	316	0	316	0	316	0	557	241	241	557	0	557	0	802	245	5	807
50-30	580792.00	138827.00	159	159	0	159	0	214	55	234	20	249	15	299	50	309	10	419	110	160	440	21	440	0	529	89	0	529
50-42	577111.10	138781.40	400	400	0	409	9	428	19	428	0	428	0	428	0	428	0	428	0	0	428	0	428	0	466	38	0	466
50-45	576172.00	138772.00	412	412	0	412	0	412	0	412	0	412	0	412	0	412	0	412	0	0	412	0	412	0	448	36	2	450
50-48A	575155.00	138685.60	438	438	0	438	0	438	0	438	0	438	0	438	0	438	0	438	0	0	438	0	438	0	549	111	0	549
50-53B	573855.50	138659.80	399																									
50-85	564130.00	138670.00	154	154	0	219	65	267	48	267	0	267	0	267	0	267	0	534	267	267	619	85	674	55	739	65	0	739
50-99	559790.00	138598.00	322																									
51-36D	578926.41	139066.17	479	479	0	479	0	479	0	479	0	479	0	479	0	479	0	479	0	0	479	0	479	0	515	36	0	515
51-46	575738.00	139004.00			0	430	0	430	0	430	0	430	0	430	0	430	0	430	0	0	430	0	430	0	443	13	0	443
51-63	570664.00	139152.00	388	388	0	388	0	388	0	388	0	388	0	388	0	388	0	388	0	0	388	0	388	0	570	182	0	570
51-75	568980.00	138904.00			0	305	41	309	4	309	0	309	0	309	0	309	0	429	120	120	429	0	429	0	641	212	0	641
52-117	554223.00	139278.00	933																									
52-118	553932.00	139355.00	1110																									
52-46A	575952.30	139394.60	403	403	0	403	0	419	16	419	0	419	0	419	0	419	0	419	0	0	419	0	419	0	454	35	0	454
52-54	573254.00	139194.00	395																									
52-57	572782.00	139115.00	487																									
53-103	558364.00	139513.00	259																									
53-111	555929.00	139585.00	752																									
53-114	555122.00	139478.00	845																									
53-55A	573114.80	139632.00	279	316	0	316	0	316	0	316	0	316	0	316	0	316	0	316	0	0	316	0	316	0	574	258	0	474
54-15	585187.00	139833.00			0	57	0	150	93	155	5	210	55	265	55	265	0	265	0	55	305	40	305	0	395	90	10	405
54-18C	584471.84	139998.88	63	63	0	63	0	108	45	134	26	200	66	247	47	247	0	247	0	47	327	80	327	0	402	75	0	404
54-34	579497.10	140008.00	400																									
54-37A	578871.00	139981.00	397																									
54-42	578950.00	140068.00			0	370	0	370	0	370	0	370	0	370	0	370	0	370	0	0	370	0	370	0	510	140	0	510
54-45A	578317.00	140008.00						389	>5			389	0	389	0	389	0	389	0	0	389	0	389	0	494	105	0	494
54-48	575357.00	139823.00			0	359	0	391	32	391	0	391	0	391	0	391	0	391	0	0	391	0	391	0	449	58	5	454
55-44	576588.00	140392.00			0	378	>20	418	40	418	0	418	0	418	0	418	0	418	0	0	418	0	418	0	513	95	5	518
55-50A	574842.00	140247.30	343	343	0	343	0	343	0	343	0	343	0	343	0	343	0	343	0	0	343	0	343	0	438	95	5	443
55-55	573227.10	140150.00	270																									
55-57	572445.00	140119.80	384	384	0	384	0	384	0	384	0	384	0	384	0	384	0	384	0	0	384	0	384	0	552	168	2	554
55-60A	571562.95	140267.37																							568	>230	4	
55-60B	571550.48	140366.40																							572	>289	0	572
55-65B	569953.60	140323.70	440	440	0	440	0	440	0	440	0	440	0	440	0	440	0	445	5	5	445	0	445	0	578	133	2	580
55-70	568561.00	140328.00	388	388	0	387	19	403	16	403	0	403	0	403	0	403	0	518	115	115	518	0	518	0	568	50	0	568
55-78	568750.00	140227.00	360	360	0	403	43	416	13	416	0	416	0	416	0	416	0	463	47	47	463	0	463	0	583	120	0	583
55-95	560942.00	140210.00			0	305	43	400	95	400	0	400	0	400	0	400	0	640	240	240	640	0	665	25	775	110	0	775
56-26A	582038.00	140508.00	406																									
56-40A	577581.31	140465.18	505	505	0	505	0	505	0	505	0	505	0	505	0	505	0	505	0	0	505	0	505	0	566	61	0	566
56-42	577286.60	140580.60	547																									
56-43	576756.00	140628.00	487																									
56-53	573793.10	140652.40	332	332	0	332	0	332	0	332	0	332	0	332	0	332	0	332	0	0	332	0	332	0	432	100	0	432
57-41	577550.90	141098.40	661																									
57-42	577175.10	141046.20	641																									
57-83A	564583.00	140825.00	233	233	0	321	88	367	46	367	0	367	0	367	0	367	0	372	5	5	372	0	372	0	577	205	0	577
58-40	577774.30	141190.70	742																									
58-41A	577531.00	141153.00	689																									
59-101	559189.00	141400.00	465	465	0	465	0	465	0	465	0	465	0	465	0	465	0	465	0	0	465	0	465	0	580	115	0	580
59-44	576818.00	141538.00	643																									
59-55	573048.00	141544.20																							405	>135	0	405
59-80B	565637.87	141574.98	416	416	0	436	20	436	0	436	0	436	0	436	0	436	0	505	69	69	505	0	505	0	581	76	0	581
60-32	580115.00	141902.00	348																									
60-57	572824.00	141871.00	325	325	0	325	0	325	0	325	0	325	0	325	0	325	0	325	0	0	325	0	325	0	470	145	0	470
60-60	571589.00	141764.00	381																									
61-16A	585101.00	142243.00	112	112	0	112	0	170	58	186	16	205	19	269	64	269	0	269	0	64	412	143	412	0	412	0	0	412
61-53	573714.00	141978.00	684																									
61-62	570915.00	141922.00	316	316	0	316	0	316	0	316	0	316	0	316	0	316	0	316	0	0	364	48	364	0	495	131	2	497
61-66	569788.00	142008.00	307	307	0	307	0	307	0	307	0	307	0	307	0	307	0	307	0	0	307	0	307	0	522	215	0	522
62-58	572684.90	142452.90	442																									
63-55	573094.00	142582.00	314	314	0	314	0	314	0	314	0	314	0	314	0	314	0	314	0	0	314	0	314	0	425	111	1	426
63-58	572283.00	142583.00	372																									
63-90	562367.00	142812.00	274	274	0	347	73	375	28	375	0	375	0	375	0	375	0	393	18	18	393	0	393	0	510	117	0	510
63-95	560915.00	142651.00	407	407	0	407	0	407	0	407	0	407	0	407	0	407	0	407	0	0	407	0	407	0	485	78	0	485
65-50	574591.00	143188.00	-108	-108	0	-87	21	22	109	97	75	217	120	287	70	287	0	287	0	70	365	78	365	0	467	102	0	467
65-95	560815.00	143193.00	398	398	0	432	34	433	1	433	0	433	0	433	0	433	0	433	0	0	433	0	433	0	452	19	0	452
66-36	578294.02	143607.67																			409	>127	409	0	436	27	0	436

Table 2-1. Structure Contour and Isopach Data for the Ringold Formation at Selected Boreholes at the Hanford Site (from Lindsey 1995). (Page 6 of 7)

Borehole #	Easting	Northing	Top Bas	Top Sub A	Iso Sub A	Top A	Iso A	Top LM	Iso LM	Top HD	Iso HD	Top Sub C	Iso Sub C	Top C	Iso C	Top Sub E	Iso Sub E	Top E	Iso E	Iso C+E	Top UH	Iso UR	Top PMPP	Iso PMPP	Top Hf	Iso Hf	Iso Eo	Elev
66-61	562175.00	145478.00	308	308	0	410	43	411	1	411	0	411	0	411	0	411	0	411	0	0	411	0	411	0	467	56	0	467
67-51	574178.93	143933.22												324 >50		324	0	324	0		309	45	369	0	524	155	0	
67-98	559944.00	143715.00	285																									
69-45	576157.41	144556.31								105 >9		236	41	265	29	265	0	265	0	29	395	130	395	0	484	89	2	486
8-2A	589311.74	125194.36	-78	-78	0	-2	76	67	69	117	50	175	58	235	60	235	0	388	153	213	388	0	388	0	457	69	4	461
70-17	584592.00	144961.00	110											278 >25		278	0	278	0		368	90	366	0	401	35	0	401
71-30	580603.35	145226.91														308 >55		398	30		398	0	398	0	520	122	3	
71-52	573907.74	145215.10												197 >25		207	100	387	70		387	0	387	0	472	105	0	472
71-77	566401.95	145098.81																										
71-78	565418.00	145348.00	-213	-213	0	-153	60	-26	127	13	39	83	50	183	120	292	109	387	95	215	387	0	387	0	442	55	0	442
72-73	567551.54	145418.78														318 >35		398	80		398	0	398	0	483	85	0	
72-92	581839.42	145359.75																300 >50			300	0	300	0	450	150	0	450
74-44	576393.09	146098.78														375 >80		400	25		400	0	400	0	443	43	2	
74-48	575237.72	146037.71														362 >25		420	58		420	0	420	0	487	67	0	487
77-38	578847.55	146868.58												277 >15		277	0	277	0		367	90	367	0	410	43	2	
77-54	573385.87	146854.80																390 >60			390	0	390	0	480	90	0	480
78-62	570877.30	147166.22														344 >25		425	81		425	0	425	0	488	63	1	
80-43P	576703.83	147729.91						38 >30		88	30	203	135	308	105	308	0	308	0	105	373	65	373	0	412	39	1	413
81-58	572165.84	148173.68												294 >5		349	55	374	25		374	0	374	0	439	65	0	
81-62	570943.00	148103.00	-88	-88	0	-65	23	40	105	110	70	235	125	245	10	341	96	406	65	75	406	0	406	0	440	34	0	440
83-1	589517.50	148735.80	390																									
83-47	575492.04	148705.25																			355 >70		355	0	435	80	0	435
83-60	571548.00	148674.00	-66																									
84-35A	579193.10	149093.73	45	45	0	45	0	119	74	155	36	155	0	155	0	155	0	155	0		365	210	365	0	400	35	0	400
84-59	571731.00	149176.00			0	-52	12	58	110	124	66	265	141	280	15	353	73	403	50	65	403	0	403	0	456	53	4	460
86-60	571825.00	149601.00	-70																									
86-64	570334.00	149616.00	-53																									
87-55	572969.75	149903.87																418 >50			418	0	418	0	459	41	0	459
89-35	579121.74	150543.51																			342 >21		342	0	396	54	0	
8-17	584699.84	126000.11																		0	332 >10		396	64	509	113	13	522
8-25	582298.26	125937.78																404			404	0	404	0	484	80	25	
92-14	585588.00	151545.00	274	274	0																							
93-48	575094.32	151795.52																			368 >15		368	0	429	83	9	
93-93	581024.00	151800.10	120																									
96-43	576781.65	152805.54																			377 >8		377	0	421	44	1	
96-49	574851.58	152858.31																			359 >40		359	0	418	60	0	419
97-43	576872.03	153090.52																			377 >55		377	0	422	45	0	
9-E2	590028.00	126138.00	-4																									
9 E5A	591479.51	126312.20	-23	-23	0	7	30	153	146	218	65	218	0	218	0	248	30	353	105	105	353	0	388	33	453	67	0	453
B3-2	565848.00	145328.00	-208	-208	0	-152	54	-8	143	15	24	63	48	183	120	243	60	364	141	201	384	0	384	0	440	56	0	440
D2-5	573812.47	151148.41														368 >7		408	40		408	0	408	0	458	50	0	
D5-12	573839.81	151557.51														379 >3		418	39		418	0	418	0	468	50	0	468
D5-20	573239.97	152030.15														363 >2		412	49		412	0	412	0	460	48	0	
E13-1	573684.21	134391.22																390 >10			390	0	390	0	740	350	0	740
E13-13	573409.07	134085.72																390 >20			390	0	390	0	724	334	0	
E13-18	573119.18	134215.87				273 >15		328	55	328	0	328	0	328	0	328	0	443	115	115	443	0	443	0	727	284	0	727
E13-20	573609.57	134312.73	156	156	0	270	114	331	61	331	0	331	0	331	0	331	0	426	95	95	426	0	426	0	741	315	0	
E17-4	575118.14	135370.33						330 >15		330	0	330	0	330	0	330	0	410	80	80	410	0	410	0	717	307	0	717
E18-1	573298.80	135200.37																396			396	0	396	0	716	320	0	
E19-1	572819.87	135085.89	215	215	0	309	94	360	51	360	0	360	0	360	0	360	0	385	25	25	385	0	385	0	734	349	0	734
E24-7	574406.78	135560.73	271	271	0	381	110	381	0	381	0	381	0	381	0	381	0	381	0	0	381	0	381	0	714	333	0	
E24-8	574547.00	136271.68	306	306	0	408	102	408	0	408	0	408	0	408	0	408	0	408	0	0	408	0	408	0	668	260	0	668
E25-2	575513.88	136032.15	319	319	0	405	86	419	14	419	0	419	0	419	0	419	0	419	0	0	419	0	419	0	675	256	0	
E26-1	575251.84	137130.71	393	393	0	393	0	393	0	393	0	393	0	393	0	393	0	393	0	0	393	0	393	0	616	223	0	615
E26-9	575578.37	137133.40	397	397	0	397	0	397	0	397	0	397	0	397	0	397	0	397	0	0	397	0	397	0	600	203	0	
E27-10	575100.71	137052.80	382	382	0	382	0	382	0	382	0	382	0	382	0	382	0	382	0	0	382	0	382	0	622	240	0	622
E27-11	574653.20	137063.00	378	378	0	378	0	378	0	378	0	378	0	378	0	378	0	378	0	0	378	0	378	0	640	262	0	
E27-13	575065.10	136489.50																							666 >276		0	666
E27-8	575245.06	138332.47	336	336	0	404	68	414	10	414	0	414	0	414	0	414	0	414	0	0	414	0	414	0	671	257	0	
E28-2	573704.48	136863.69	373	373	0	402	29	402	0	402	0	402	0	402	0	402	0	402	0	0	402	0	402	0	679	277	0	679
E28-22	574041.35	136320.83	337	337	0	430	93	430	0	430	0	430	0	430	0	430	0	430	0	0	430	0	430	0	700	270	0	
E28-3	573708.86	136607.30				366 >5		366	0	366	0	366	0	366	0	366	0	366	0	0	366	0	366	0	693	327	0	693
E28-5	574034.10	136856.90	383	383	0	380	17	380	0	380	0	380	0	380	0	380	0	380	0	0	380	0	380	0	665	285	5	
E33-18	573779.39	137388.52	388	388	0	404	18	433	29	433	0	433	0	433	0	433	0	433	0	0	433	0	433	0	643	210	0	649
E33-29	573228.13	137231.47	385	385	0	433	48	433	0	433	0	433	0	433	0	433	0	433	0	0	433	0	433	0	671	238	0	
E33-37	574091.71	137185.70	385	385	0	385	0	385	0	385	0	385	0	385	0	385	0	385	0	0	385	0	385	0	653	268	0	653
E33-4	573618.97	137603.40	397	397	0	397	0	397	0	397	0	397	0	397	0	397	0	397	0	0	397	0	397	0	612	215	15	
E33-41	573707.19	137389.84	389	389	0	411	22	433	22	433	0	433	0	433	0	433	0	433	0	0	433	0	433	0	652	219	0	652
E34-2	574035.18	137220.92	388	388	0	388	0	388	0	388	0	388	0	388	0	388	0	388	0	0	388	0	388	0	629	241	0	
E34-4	574025.29	137744.20	409	409	0	409	0	409	0	409	0	409	0	409	0	409	0	409	0	0	409	0	409	0	585	176	0	585
E34-8	574208.66	137249.88	381	381	0	381	0	381	0	381	0	381	0	381	0	381	0	381	0	0	381	0	381	0	638	257	0	

Table 2-1. Structure Contour and Isopach Data for the Ringold Formation at Selected Boreholes at the Hanford Site (from Lindsey 1995). (Page 7 of 7)

Borehole #	Easting	Northing	Top Bat	Top Sub A	Iso Sub A	Top A	Iso A	Top LM	Iso LM	Top BD	Iso BD	Top Sub C	Iso Sub C	Top C	Iso C	Top Sub E	Iso Sub E	Top E	Iso E	Iso C+E	Top UR	Iso UR	Top PMPP	Iso PMPP	Top HF	Iso HF	Iso Eo	Elev
H3-2C	577632.23	152750.54																			350	>95	350	0	416	60	0	416
H4-12C	578011.97	152920.10																			352	>160	352	0	411	59	0	
H4-15C	577907.86	153060.27	92	92	0	92	0	194	102	200	6	200	0	200	0	200	0	200	0	0	357	157	357	0	406	49	0	406
H4-2	578094.00	152502.00	84	84	0	84	0	170	86	229	59	229	0	229	0	229	0	229	0	0	356	127	356	0	420	64	0	420
K-20	569520.52	147667.24																420			420	0	420	0	420	0	0	
K-24	568833.85	146934.33																445	>1		445	0	445	0	467	22	0	467
N-2	571478.21	149859.43														351	>27	386	35		386	0	386	0	451	65	0	
N-5	571405.70	149675.17														349	>15	399	50		399	0	399	0	454	55	0	454
N-69	571483.89	149804.60														358	>3	415	59		415	0	415	0	457	42	0	
N-80	571477.78	149951.09														357	>29	417	60		417	0	417	0	455	38	0	455
S11-E12A	593576.40	120173.85	129	129	0	160	31	195	35	225	30	225	0	225	0	255	30	310	55	55	310	0	310	0	385	55	0	385
S12-29	580953.00	119932.00	308	308	0	308	0	332	24	352	20	352	0	352	0	362	10	427	65	65	427	0	427	0	487	60	0	487
S12-3	589113.03	119761.79														326	>2	391	65		391	0	391	0	430	39	5	
S14-20A	583921.00	119087.00			0	347	15	357	10	357	0	357	0	357	0	357	0	392	35	35	392	0	392	0	472	80	20	492
S16-24	582765.00	118540.00	534																									
S18-E14A	594330.00	118797.00	204																									
S17-24	582523.60	118338.70	500																									
S17-25	582373.80	118332.50	450																									
S17-28	581487.90	118348.10	440																									
S17-30	580932.10	118311.90	430																									
S18-51	574395.00	117994.00	1169																									
S18-E2A	590549.00	117881.00	185	185	0	185	0	229	44	274	45	274	0	274	0	279	5	364	85	85	364	0	364	0	424	60	10	434
S19-11	586583.82	117799.80																388			388	0	388	0	483	95	0	
S19-E13	593835.39	117605.36																316	>5		316	0	316	0	376	60	15	391
S1-7	587776.50	123118.90	-72																									
S1-8H	587524.94	123302.58	-57	-57	0	0	57	70	70	120	50	120	0	120	0	145	25	410	265	265	410	0	410	0	550	140	5	555
S22-E9C	592589.00	116753.00	201	201	0	201	0	222	21	256	34	261	5	310	49	326	16	341	15	64	341	0	341	0	367	26	4	371
S24-19	584102.00	116200.00	381	381	0	381	0	381	0	381	0	381	0	381	0	381	0	403	22	22	403	0	403	0	428	23	1	427
S27-E9C	592721.00	115325.00	189	189	0	189	0	211	22	252	41	268	16	288	20	314	26	341	27	47	341	0	341	0	386	45	2	388
S28-E0	590205.30	114994.30	225																									
S29-E12	593828.16	114569.68																339	>35		339	0	339	0	384	45	0	384
S29-E16C	594742.00	114731.00	202	202	0	202	0	256	54	292	36	292	0	292	0	292	0	319	27	27	319	0	319	0	374	55	3	377
S30-E15C	594368.00	114270.00	201	201	0	201	0	241	40	271	30	271	0	271	0	281	10	331	50	50	331	0	331	0	399	68	2	401
S31-1	589749.00	114213.00	239	239	0	239	0	274	35	311	37	311	0	311	0	327	16	387	60	60	387	0	387	0	444	57	18	460
S3-25	582459.90	122587.80																398	>39		398	0	398	0	493	95	30	523
S3-87	589448.00	122507.00	1160																									
S3-E12	583586.00	122615.00			0	145	0	178	33	225	47	245	20	308	81	313	7	340	27	88	351	11	351	0	378	27	17	395
S4-E16	594988.00	122405.00	187	187	0	187	0	193	6	230	43	230	0	230	0	270	34	318	48	48	318	0	318	0	343	25	0	343
S6-E14A	594262.39	121508.74	181	181	0	181	0	202	21	280	78	280	0	280	0	288	8	342	54	54	342	0	342	0	378	36	0	378
S6-E4C	591083.17	121663.58	64	64	0	102	38	130	34	198	82	234	36	291	57	314	23	376	62	118	376	0	376	0	431	55	0	431
S7-34	579431.00	121503.00	384	384	0	401	17	435	34	435	0	435	0	435	0	435	0	435	0	0	435	0	435	0	523	88	4	527
S7-62	579034.00	121248.00	1250																									
S8-19	584228.54	120964.55																391	>36		391	0	391	0	484	93	19	503
S9-56	572988.00	120672.00	1112																									
S9-83D	570661.00	120745.00	1168																									
W10-14	586018.00	138809.00						248	>11	248	0	248	0	248	0	248	0	559	311	311	559	0	566	7	696	130	0	696
W11-2	567407.00	136671.00	199	199	0	272	73	289	17	289	0	289	0	289	0	289	0	564	275	275	564	0	601	37	707	106	5	712
W11-26	567045.00	136564.00	190	190	0	264	74	281	17	281	0	281	0	281	0	281	0	552	271	271	563	11	589	26	694	105	0	690
W14-7	567034.00	135654.00	159	159	0	214	55	253	39	253	0	253	0	253	0	253	0	547	294	294	547	0	558	11	672	114	5	677
W14-8	568073.30	135698.70	186	186	0	265	79	282	17	282	0	282	0	282	0	282	0	547	265	265	547	0	555	8	722	167	0	722
W15-14	566093.00	135648.00	134	134	0	199	65	240	41	240	0	240	0	240	0	240	0	517	277	277	528	11	540	12	693	153	5	698
W15-5	566735.00	135512.00	142	142	0	188	46	242	54	242	0	242	0	242	0	242	0	532	290	290	532	0	549	17	652	103	18	670
W18-22	566089.13	134990.30						281	>70	281	0	281	0	281	0	281	0	521	240	240	521	0	530	15	666	130	0	666
W19-10	566887.00	134925.00	125	125	0	195	70	221	26	221	0	221	0	221	0	221	0	509	288	288	509	0	540	31	680	140	0	680
W19-4	568003.00	135366.40	178	176	0	191	15	210	19	210	0	210	0	210	0	210	0	455	245	245	470	15	548	78	708	160	5	713
W19-8	567564.00	135220.00	140	140	0	235	95	267	32	267	0	267	0	267	0	267	0	490	223	223	490	0	525	35	700	175	0	700
W22-19	567818.44	133981.44																453	>223		453	0	487	34	678	191	2	680
W22-24	567848.00	134411.00	122	122	39	262	101	293	31	293	0	293	0	293	0	293	0	450	157	157	473	23	500	27	690	190	0	690
W22-27	567151.00	134497.00	120	120	8	174	45	228	52	228	0	228	0	228	0	228	0	469	241	263	524	35	544	20	679	135	0	679
W27-2	566908.55	133670.83						250	>12	250	0	250	0	250	0	250	0	449	199	109	474	25	501	27	672	171	2	
W8-1	587214.00	137510.00	232	232	0	267	35	277	10	277	0	277	0	277	0	277	0	602	325	325	642	40	662	20	697	35	5	702
W8-3	587118.18	137299.13				280	>10	290	10	290	0	290	0	290	0	290	0	607	317	317	617	10	644	27	705	61	0	705
W8-8	587319.00	137838.59				271	>31	285	14	285	0	285	0	285	0	285	0	602	317	317	650	48	681	31	710	29	0	710
W7-3	586292.00	137639.00	199	199	0	308	109	308	0	308	0	308	0	308	0	308	0	568	260	260	593	25	639	46	673	34	0	673
13-26	581844.00	127490.00	-228	-228	0	-148	80	-43	105	-5	40	32	35	67	32	97	30	247	150	215	307	60	397	90	492	95	20	512
18-30A	580620.00	128449.00	-305	-305	0	-215	90	-130	85	-90	40	-30	60	25	55	50	25	170	120	200	270	100	430	160	545	115	15	560

Table 2-2. Hydraulic Conductivity Used in Model Setup.
(Page 1 of 2)

Hanford Well Designation	Hydraulic Conductivity
199-K-10	110
299-E18-1	50
299-E18-3	210
299-E25-22	6,200
299-E25-34	19,000
299-E25-35	6,500
299-E27-8	6,800
299-E27-9	3,500
299-E28-27	4,800
299-E32-4	950
299-E33-28	5,300
299-E33-29	5,100
299-E33-30	5,600
299-E34-2	11,400
299-E34-3	1,400
299-W10-13	700
299-W10-14	350
299-W15-15	1,000
299-W15-16	1,200
299-W15-17	1,200
299-W15-18	1,400
299-W18-21	5,100
299-W18-22	42
299-W18-23	2,300
299-W18-24	4,400
299-W6-2	50
299-W7-1	140
299-W7-2	74
299-W7-4	95
299-W7-5	9
299-W7-6	4
299-W8-1	8
399-1-13	1,400
699-1-18	30
699-10-54A	346
699-17-47	50
699-17-5	9
699-2-3	333
699-2-33A	31
699-20-20	32
699-24-33	2,200

Table 2-2. Hydraulic Conductivity Used in Model Setup.
(Page 2 of 2)

699-26-15	167
699-26-35C	650
699-26-89	2
699-31-31	2,100
699-31-53B	117
699-32-77	21
699-33-56	115
699-35-9	195
699-36-61A	60
699-37-82A	9
699-40-1	582
699-40-33A	12,500
699-41-23	190
699-42-12A	480
699-43-43	13,400
699-43-88	10
699-46-21B	17
699-47-35C	19
699-47-60	80
699-55-50B	6,150
699-61-66	500
699-63-90	450
699-65-50	340
699-71-77	110
699-8-17	297
699-8-32	20
699-87-55	17
699-S22-E9C	150
699-S27-E9C	67
699-S8-19	130

Table 2-3. Total Discharges from 1980 to 1993 at Liquid Waste Disposal Facilities at and near the 200-East and 200-West Areas, Which Were Used in the Model Calibration.

200 East Area		200 West Area	
Facility	Total Discharge (L [gal])	Facility	Total Discharge (L [gal])
216-A-10	3.30×10^8 (8.71×10^7)	216-S-10	1.59×10^9 (4.20×10^8)
216-A-36B	2.20×10^8 (5.80×10^7)	216-U10	7.47×10^9 (1.97×10^9)
216-A37-1	3.09×10^8 (8.16×10^7)	216-U-14	3.08×10^9 (8.13×10^8)
216-A-45	1.03×10^8 (2.72×10^7)	216-U-16	4.09×10^8 (1.08×10^8)
Gable Mountain Pond	7.98×10^{10} (2.11×10^{10})	6-W-LWC	1.04×10^9 (2.75×10^8)
B Pond	1.41×10^{11} (3.72×10^{10})	216-Z-20	4.07×10^9 (1.07×10^9)

Table 2-4. Tritium Discharged from Liquid Waste Disposal Facilities (Ci/yr).

200 East Area	
216-A-10	2.37×10^4
216-A-36B	6.47×10^2
216-A-37	1.85×10^3
216-A-45	4.20×10^3
B Pond	3.08

3.0 VAM3DCG MODEL APPLICATION

3.1 MODEL SETUP

The modeled region covers approximately 971 km^2 (375 mi^2) and is bounded by Rattlesnake Mountain to the southwest, Cold and Dry Creeks to the west, and the Columbia River to the north and east. The domain consists of the unconfined aquifer system with the bottom of the Ringold Formation at the base and the pre-Missoula/Hanford formation on the top where it exists. The general trend for water in the unconfined modeled system is from west to east, with water entering the domain from Cold Creek and Dry Creek, and discharge occurring into the Columbia River. The system also receives artificial recharge of wastewater generated by the Hanford operations, primarily from surface ponds, ditches, and cribs located in the 200 West and 200 East Areas. Communication between the modeled unconfined aquifer and the underlying confined systems is assumed negligible, as is areal recharge over the site due to precipitation.

Water table levels across the simulation domain were observed to remain fairly constant from 1976 to 1979, and the model first was calibrated for steady-state conditions to these water levels. Transient simulations were performed for a 14-year period to represent model system behavior from January 1980 through December 1993. Recharge of water from the cribs and ponds was varied to reflect the changing wastewater disposal trends at the site. Wastewater disposal volumes have been declining since the mid- to late 1980's.

3.2 GRID

The model grid size is dependent on the domain area of interest and the problem to be solved. Small grid spacing provides for greater accuracy but requires increased computer time, and a larger grid spacing provides for less computer time but provides for less accuracy. Therefore, a compromise must be established. A horizontal finite element grid size of 600 m by 600 m (1,970 ft by 1,970 ft) (Figure 3-1) was selected because it provided the needed accuracy and with a reasonable amount of computer computational time. The Hanford Site unconfined groundwater flow system was simulated using a six-layer model with 2,474 elements and 2,611 nodes per layer. The vertical grid spacing was established considering the saturated thickness of the aquifer in total and the individual saturated thicknesses of the two geohydrologic units. Vertical discretization was performed using six elemental layers; the top three represent the pre-Missoula/Hanford formation and the bottom three the underlying Ringold Formation. Application of "pseudo-soil" model functions, used to deal with unconfined groundwater conditions, requires that the water table be located between two grid nodes (see Appendix A for a discussion of "pseudo-soil" model functions). Thus, at least two layers of elements are required. In addition, during contaminant transport modeling, it was determined that multiple layers were required for vertical segregation of contaminants, In consideration of the above modeling needs and requirements, a model using six layers was selected. A six-layer model represented an appropriate compromise between numerical issues and the project needs. The six layers are not intended to present individual geohydrologic layers, but are used to allow for model computational requirements. Thus, only geohydrologic units are represented in the model.

A vertically deformed grid was used to allow the model geometry to conform to the topography of the top and bottom of the modeled formation. Vertical discretization varied from 0.5 m (1.6 ft) to 20 m (65.6 ft) depending on formation thicknesses.

3.3 INITIAL ELEMENT PROPERTIES

The hydrogeologic units of interest consist of the Ringold Formation overlain (in eastern portions of the domain) by the highly conductive pre-Missoula/Hanford formation. The domain is separated into two distinct hydrogeologic units, the Ringold and the pre-Missoula/Hanford formations. Each of the units is represented by three elemental layers with material properties assigned to each model element. For groundwater flow, horizontal and vertical hydraulic conductivity, specific storage, storativity, and porosity values are assigned. Eighteen distinct elemental zones were identified, which covered the expected aquifer parameter range for the site. For initial conditions, these distinct material zones were assigned to each element of the finite-element grid such that the hydraulic conductivities approximated the observed value at each location. Material properties were distributed homogeneously in the vertical direction for each hydrogeologic unit.

Model calibration was conducted by adjusting the element or zone conductivity values such that the modeled behavior mimics the observed water levels and recharge/discharge values. The elemental zones and material properties for the final calibrated groundwater flow model are listed in Table 3-1. Figures 3-2 and 3-3 show the calibrated model material zone distribution across the modeled area for the Ringold and pre-Missoula/Hanford units. Specific storage values were varied to represent observed condition, and storativity was held constant. Porosity was varied in a few of the element zones to represent observed conditions.

3.4 BOUNDARY CONDITIONS

Boundary conditions were applied to the model as conceptualized in Chapter 2.0. Inflow boundaries along Cold Creek, Dry Creek, and the Yakima River initially were treated as prescribed head conditions, with the head values supplied from observed water table elevations in the region. Holding heads constant allows the model to calculate recharge into the system so that the reasonableness of model recharge can be assessed. After the model was calibrated to satisfactorily emulate field conditions, the upstream boundaries for Cold and Dry Creeks were changed to flux boundaries, using flux values obtained from the simulations using constant head. The change to flux boundaries was warranted due to the likelihood of declining water levels for simulations of future groundwater flow conditions. Boundary conditions for the Yakima River remained as constant head. Model boundaries are shown in Figure 3-4.

The southwest model boundary, along the front of Rattlesnake Ridge, is set at no flow as the recharge along Rattlesnake Ridge is assumed to be negligible. If recharge does occur along this boundary, the effects on the overall model would be minimal, as this portion of the model domain is separated from the main portion by the subsurface extension of Yakima Ridge.

The model boundary along the Columbia River is constant head with head values determined from the average annual stage from five river-stage gages. Because of river gradient, the head values are constant with time but variable in distance. The stage values were noted to be fairly stable through time, and therefore individual element values were not varied during the model simulation period. The Yakima River, on the southern boundary of the model, is treated as a constant head boundary.

Boundaries to flow also were set in the domain interior at Gable Mountain, Gable Butte, associated subcrops, and the subcrop associated with the subsurface extension of Yakima Ridge. For these features, the hydraulic properties were set to zero to establish no flow in these elements. The bottom model boundary is assumed to have a no-normal-flow condition.

Recharge to the model primarily is from natural sources Dry and Cold Creeks and from artificial sources resulting from Hanford Site operations. Recharge from precipitation generally is agreed to be negligible in areas with vegetation and fine-grained sediments (see discussion in Section 2.3.2.1) and was set to zero in the model domain.

The model assumes that there is no interchange of water between the underlying confined aquifer system and the unconfined system. Potentiometric data indicate the possibility for vertical leakage as discussed in Section 2.3.2.1. However, there is inadequate data on which to quantify leakage. In addition, the vertical conductivity of the underlying basalt is very low, which would indicate low leakage rates.

Artificial recharge resulting from Hanford operations, discussed in Section 2.5, was input at nodes coincident with the disposal site location. Table 2-3 provides a listing of the volumes disposed of to the various disposal facilities represented in the model. The estimated average fluxes from 1976 to 1979 were used to calibrate steady-state model flow conditions. Annual estimated fluxes for each disposal facility were input for the years 1980 through 1993. Recharge from facilities contributing only negligible volumes was not included. Artificial recharge volumes from included facilities representing approximately 90% of the total volume disposed of across the site.

3.5 INITIAL CONDITIONS AND PLAN FOR MODEL CALIBRATION

The groundwater flow portion of model was calibrated to both steady-state and transient groundwater flow conditions. The steady-state flow was calibrated to 1979 conditions, and the transient period was run for 14 years from 1980 through 1993. The transient calibration was evaluated for 1988 and 1993. 1979 was chosen for the steady-state calibration point because water levels and waste water discharges between 1976 and 1979 remained relatively constant. This assumption is confirmed by Jacobson and Freshley (1990) who reported: "A review of cooling water discharge information at major disposal facilities within the 200-East and 200-West Areas suggests that, compared with other periods of time, the discharges remained relatively constant from 1976 through 1979. In general, the water levels in wells monitoring the unconfined aquifer near the ponds reflect the relatively constant trend in discharge data from 1976 - 1979. Because discharges and water levels remain constant from 1976 through 1979,

1979 represents the closest approximation to steady state conditions within recent Hanford Operations."

Figure 3-5 is a west-to-east cross section through the central modeled domain. The figure shows the vertical distribution of the calibrated material properties. Figure 3-6 shows the contoured elevations of the pre-Missoula/Hanford formation - Ringold Formation Contact.

The calibration of groundwater flow was confirmed by simulating tritium transport. Tritium was selected because it has been discharged to the ground in large quantities at numerous locations across the site and is the most aerially distributed contaminant onsite, as other radioisotopes and hazardous chemicals are not as widespread in the groundwater. Tritium also is ideal for confirming groundwater movement because it is a chemically unretarded contaminant moving at the same rate as the groundwater.

Groundwater flow calibration confirmation using tritium transport began by including the observed 1979 tritium distribution with the calibrated steady-state flow model. Transient simulations were run for the period 1979 through 1993, and actual versus simulated plumes checks were made for 1988 and 1993.

3.6 FLOW CALIBRATION AND VALIDATION

Several groundwater flow simulations were first performed to calibrate the model to where it reasonably emulates observed water levels. Each simulation series was composed of a steady-state flow simulation followed by a transient simulation. The steady-state simulation was calibrated to water levels observed in December 1979, and the transient simulations were run for 14 years to December 1993. During the steady-state calibration process, the various material properties are adjusted to better simulate groundwater levels during December 1979. The final material values for the calibrated model are listed in Table 3-1. The distribution of these values throughout the modeled domain are shown in Figures 3-2 and 3-3. Figure 3-7 shows a comparison between observed water table elevations and the calibrated model results for the steady-state conditions of December 1979. In general, observed water table and modeled elevations are in agreement when observed from a sitewide perspective. Water levels throughout most of the modeled domain are within a few feet of observed values. There are. however, local areas where modeled values are different than observed values. These areas are associated with groundwater flow gaps where groundwater flows between no-flow zones near basalt ridges and immediately north of the ridges. Summary statistics comparing model predictions to observed water table values are presented in Appendix C. Groundwater flux through the water gaps is uncertain as well as hydraulic properties of the units, which results in a poorer match between actual and simulated water levels. In addition, there is an approximately 3-m (10-ft) difference between observed and simulated water levels along the Columbia River Boundary.

Recharge to the system from Cold Creek was 0.12 m^3/sec (4.3 ft^3/sec) and Dry Creek was 0.51 m^3/sec (18.1 ft^3/sec), which is in agreement with field estimates of 0.028 to 0.28 m^3/sec (1 to 10 ft^3/sec) discussed in Section 2.3.2. The model simulated that an average of 1.47 m^3/sec (51.9 ft^3/sec) was discharged to the Columbia River during the modeled year 1979. This results in

approximately 0.022 m^3/sec (0.80 ft^3/sec) of groundwater discharged per kilometer of river. This value is within an order of magnitude of the discharge estimates of Luttrell et al (1992) and Prater et al. (1984) who estimated 0.21 m^3/sec (7.4 ft^3/sec) and 0.085 m^3/sec (3.0 ft^3/sec), is reasonable when considering the uncertainty of these estimates.

The calibrated steady-state simulation next was used as the starting point for a transient simulation of 14 years. Flux boundary conditions over the ponds and cribs were varied annually in a stepwise fashion to represent the annual recharge at the respective locations. Figures 3-8 and 3-9 compare observed water table conditions with those modeled for 1988 and 1993. Figure 3-10 is a contour plot showing the difference between the observed and simulated model values (residuals) for the 1993 data. These modeled water levels are reasonably in agreement with observed water levels. However, as with the steady-state simulation flow, there are differences near the water gaps associated with basalt ridges and along the boundary of the Columbia River. Features to note in these figures are: (1) the groundwater mound in 200 West Area declines during the 14-yr modeled period; and (2) the groundwater mound associated with 200 East Area and B Pond can be seen to increase between December 1979 and 1988, due to increased recharge to B Pond, and then decline with decreased discharge through 1993. Both of these are in agreement with observed water levels.

Figures 3-11, 3-12, and 3-13 illustrate the groundwater flow directions for the Hanford Site by using steady-state velocity streamlines for 1979, 1988, and 1993. Each streamline represents the path that a single non-retarded, non-degraded particle would take if the groundwater flow was at steady state. Each solid dot represents 5 years of travel time. Comparison of the three plots illustrates the following:

- The decline of the groundwater mound in the 200 West Area, which results in changing the groundwater flow from being split between flowing north through Gable Gap and easterly south of the 200 East Area towards the 300 Area, to all flow being directed through Gable Gap

- Flow in the central portion of the 200 East Area from flow south out of the 200 East Area then east towards the 300 Area to flowing north through Gable Gap and due east to the Columbia River just south of Gable Mountain.

These flow directions are consistent with observed tritium concentrations in and near Gable Gap between 1979, 1988, and 1993 (tritium concentrations are low in the Gable Gap area in 1979, then increase in 1988). The increased tritium concentrations in Gable Gap area are due to increased discharges of tritium contaminated water in 200 East Area and due to the change in flow directions with time.

3.7 TRANSPORT MODEL FOR FATE OF TRITIUM

The objective of the transport simulations is to start with the tritium plume identified for 1979 conditions, and model the fate of tritium for 14 years, through 1993. Transport of tritium is subject to the calibrated transient flow field obtained for the same time period in earlier sections.

Mechanisms that govern the fate of the tritium plume include advection, dispersion, and decay with adsorption being assumed negligible.

3.7.1 Tritium Numerical Model Development

The fate of tritium at the Hanford Site from January 1980 to January 1994 is examined under the flow field generated by the transient calibrated flow model over the same time period. The same material zones that were used for the flow model are provided to the transport model. Uniform transport properties are provided to all material zones in the Ringold and the pre-Missoula/Hanford formations. Transport properties of the material zones are provided in Table 3-2. The dispersivities and porosities are representative of the soil at the site, and diffusion and decay constants are typical for tritium. The decay constant of 0.0564 yr^{-1} is based on the 12.3 year half-life of tritium. The tritium plume configuration shown in Figure 3-13 is the observed averaged 1979-1981 conditions and provides initial conditions for the simulation. It should be noted that tritium concentrations along the 100 Areas were not input as part of the calibration process. The plume is known to not penetrate the Ringold Formation in the east, and modeled contaminant distributions were provided only on the top four layers of nodes, as initial conditions representative of January 1980. Boundary conditions for transport include a zero concentration for inflow at Cold and Dry Creeks and the Yakima River, and a zero normal concentration gradient condition at the discharge nodes along the Columbia River, which allows advective flux out to the river. Transient mass flux conditions are provided at inflow locations in the cribs and ponds. Observed annual average tritium mass inflows are supplied to the model as stepped annual variations in accordance with the flux conditions for the flow model.

Figures 3-15 and 3-16 provide 1979 simulated tritium concentrations and a comparison of simulations and measured initial conditions.

3.7.2 Simulation Results

The transport model was simulated through 14 years (through December 1993) with the groundwater flow velocities supplied from the corresponding flow simulation. This ensures that the water table levels of the flow simulation are honored so that the combined flow and transport behavior of the model emulates site conditions. The transport simulation is performed and tritium distributions through the fifth nodal plane (second layer from the top) are presented. Figures 3-17, 3-18, and 3-19 present measured, simulated, and comparative plots 1988 conditions, respectively. Similarly, Figures 3-20, 3-21, and 3-22 present measured, simulated, and comparative plots for 1993 conditions, respectively. During the simulation period, 1.75×10^{13} pCi of tritium were discharged along the Columbia River boundary, whereas 2.09×10^{14} pCi were lost to decay. This illustrates that the greatest tritium loss is from radioactive decay. Including tritium input from B-Pond operations, the domain lost a net 2.16×10^{14} pCi of tritium during the 14 year simulation. These numbers include the continual operation of B Pond tritium releases.

The transport calibration process requires a recalibration of the flow field under which advection occurs. The entire model, for flow and transport, is noted to emulate field conditions fairly well

from all parameters known, including Cold and Dry Creek recharge, water-table levels, and tritium plume distribution for 1979 and through 1988 and 1994.

Figure 3-1. VAM3DCG Finite Element Grid.

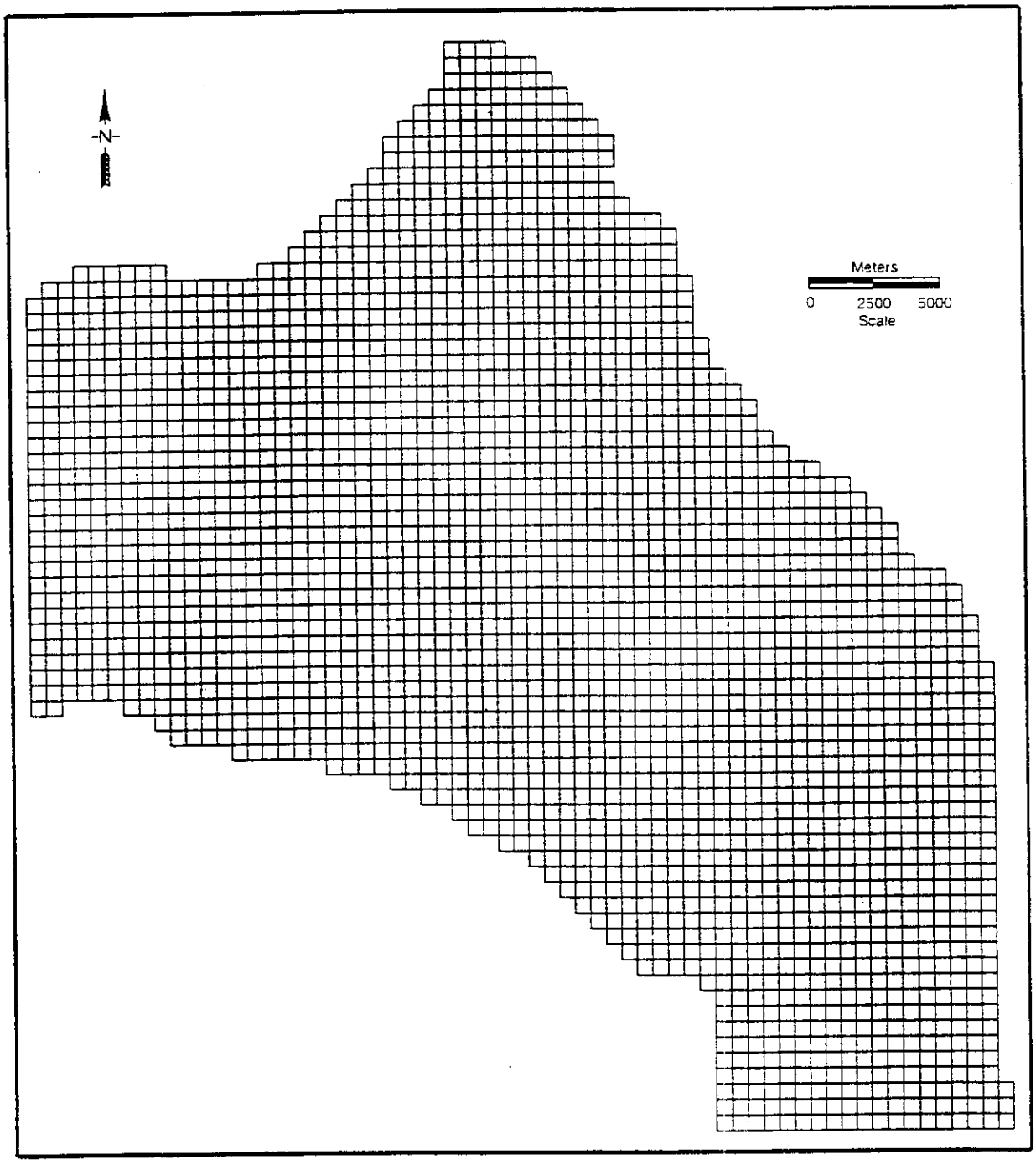

Figure 3-2. Material Property Distribution for the Lower Three Elemental Layers Within the Domain. (See Table 3-1 or key to material properties)

Figure 3-3. Material Property Distribution for the Upper Three Elemental Layers Within the Domain. (See Table 3-1 for key to material properties)

Figure 3-4. Model Boundary Conditions.

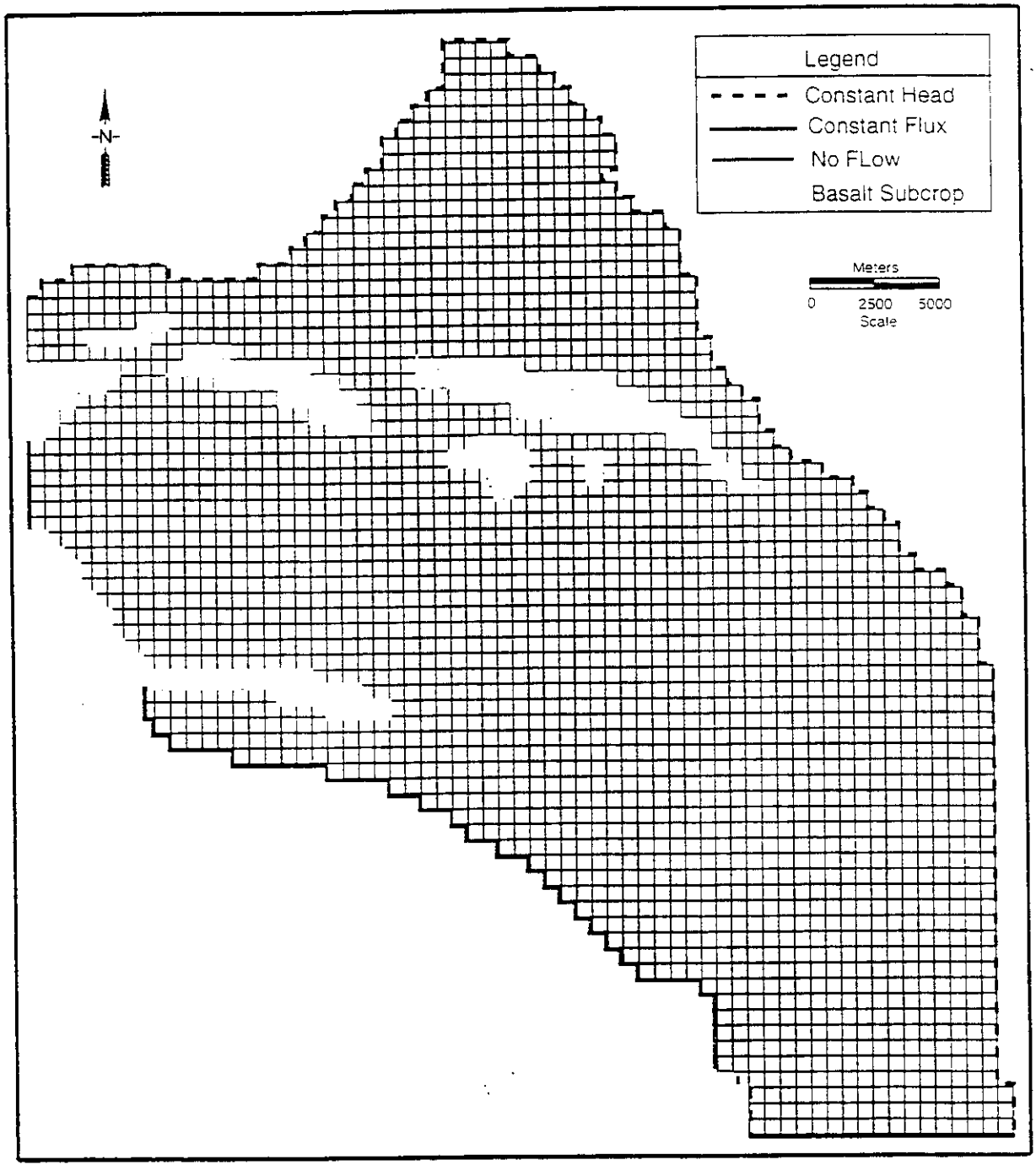

Figure 3-5. West-East Material Property Cross Section Through Center of Modeled Domain.

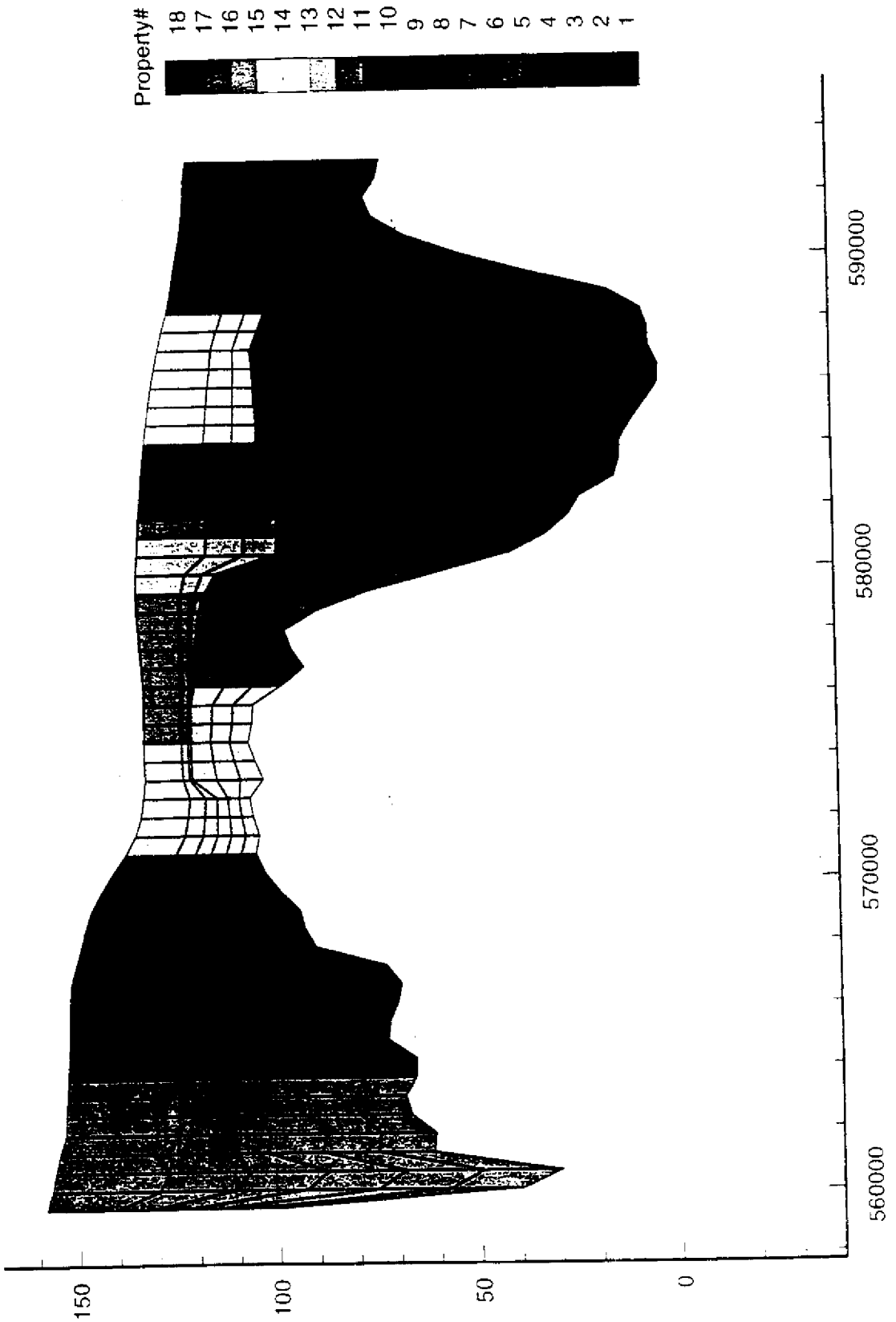

Figure 3-6. Elevation of Pre-Missoula/Hanford Formation - Ringold Formation Contact.

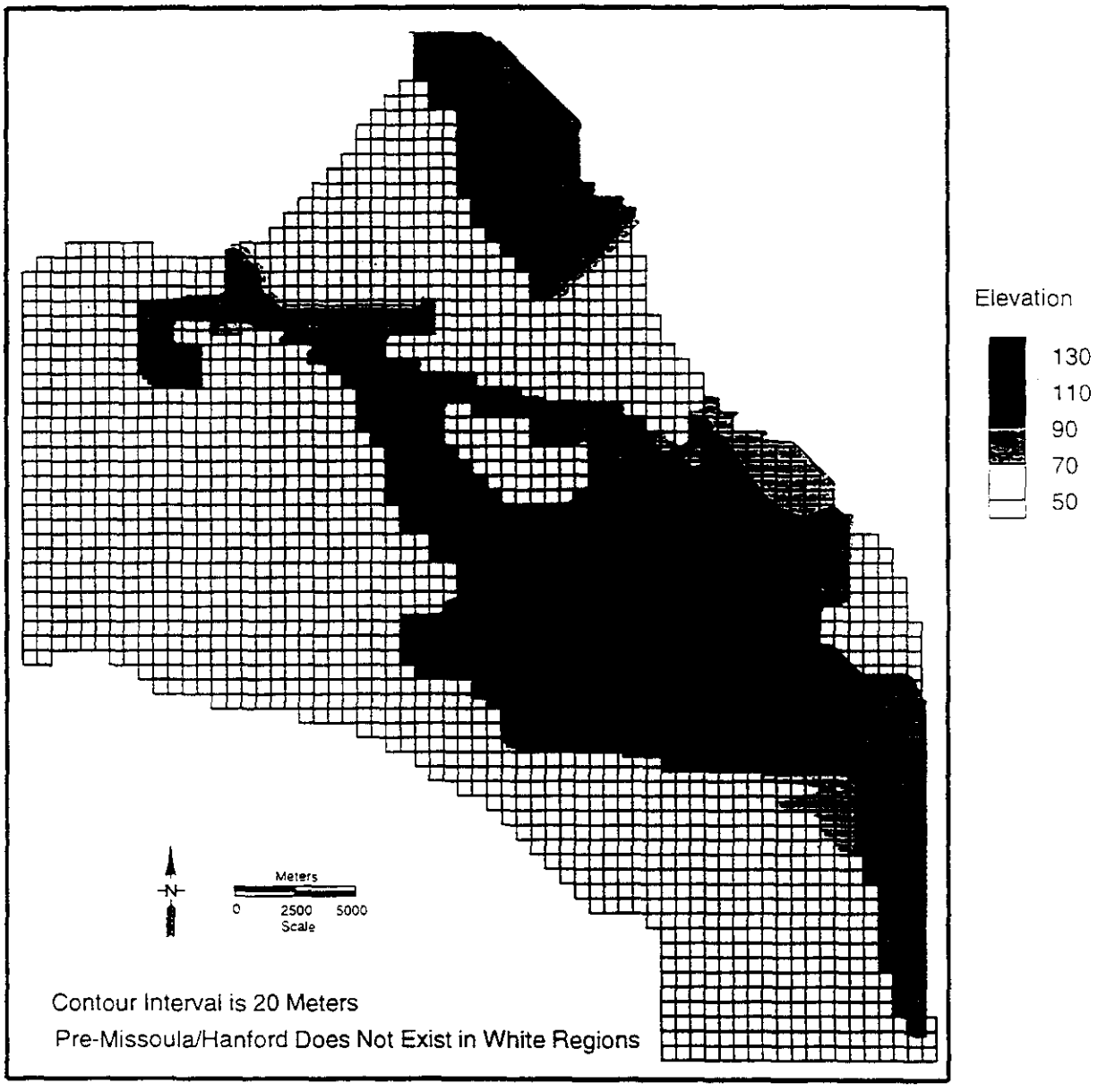

Figure 3-7. Comparison of Steady-State Simulated Water Table Elevations Representing December 1979 Conditions.

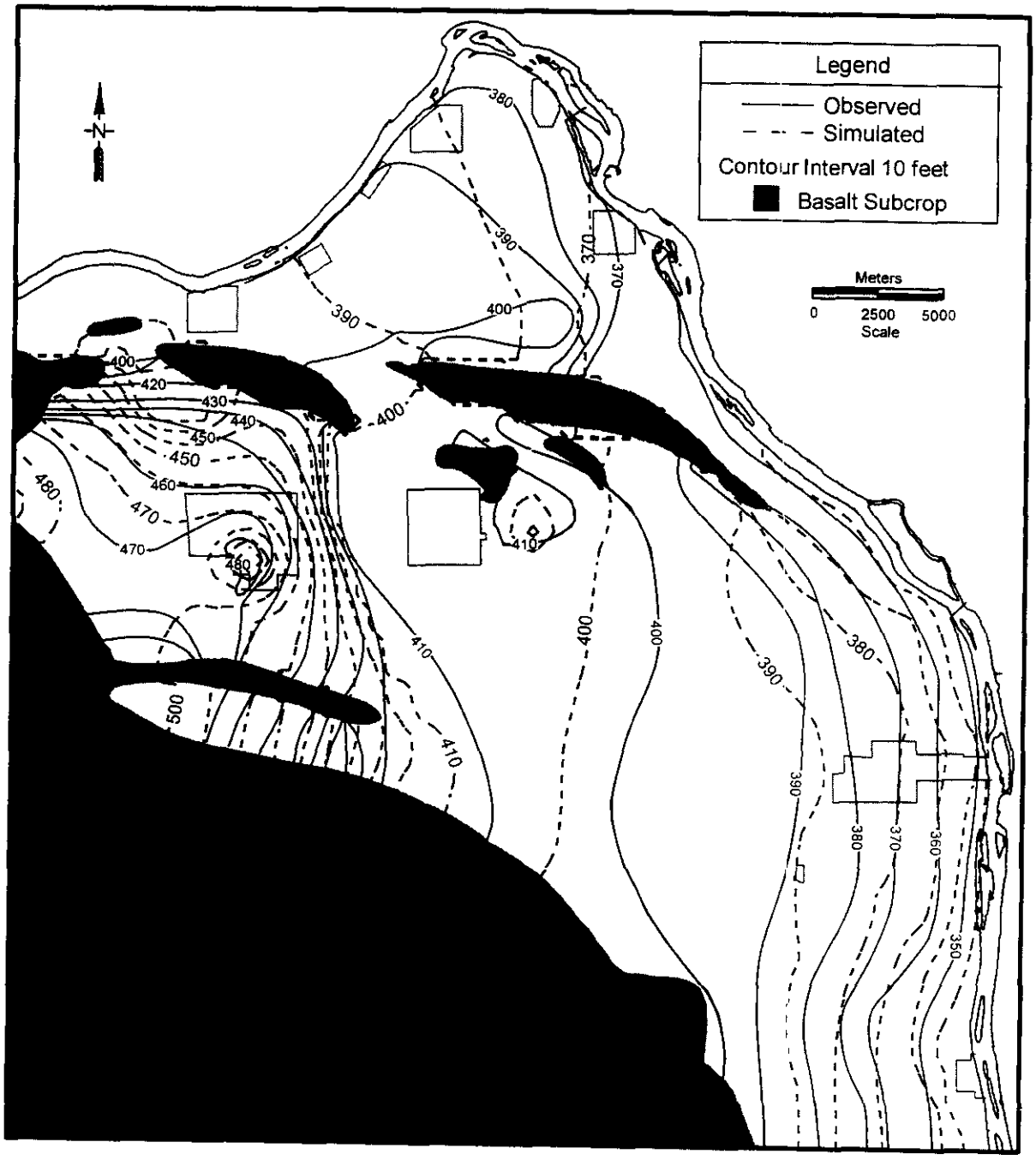

Figure 3-8. Water Table Comparison After 9 Years of Transient Simulation Representing 1988 Conditions.

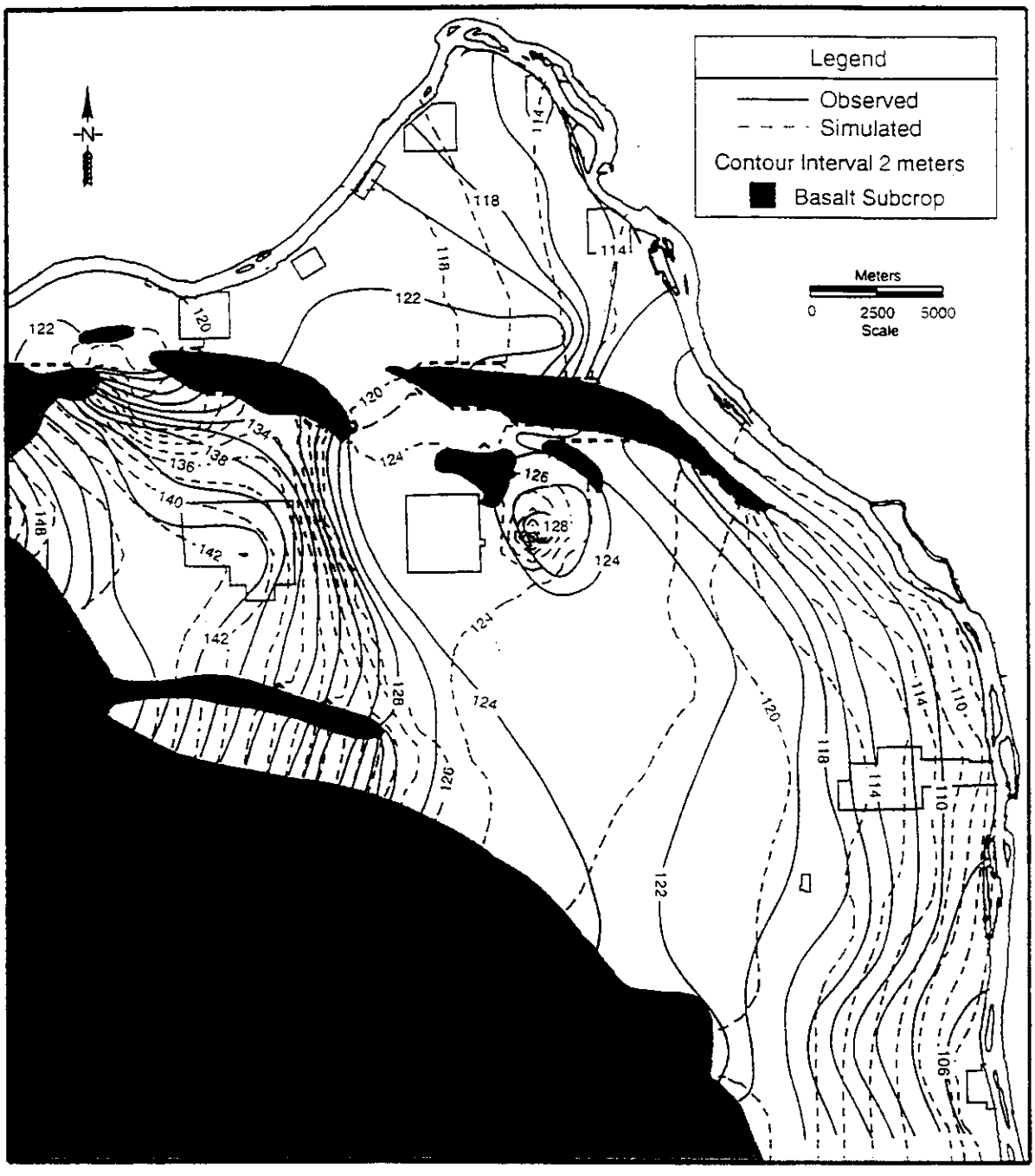

Figure 3-9. Water Table Comparison After 14 Years of Transient Simulation Representing 1993 Conditions.

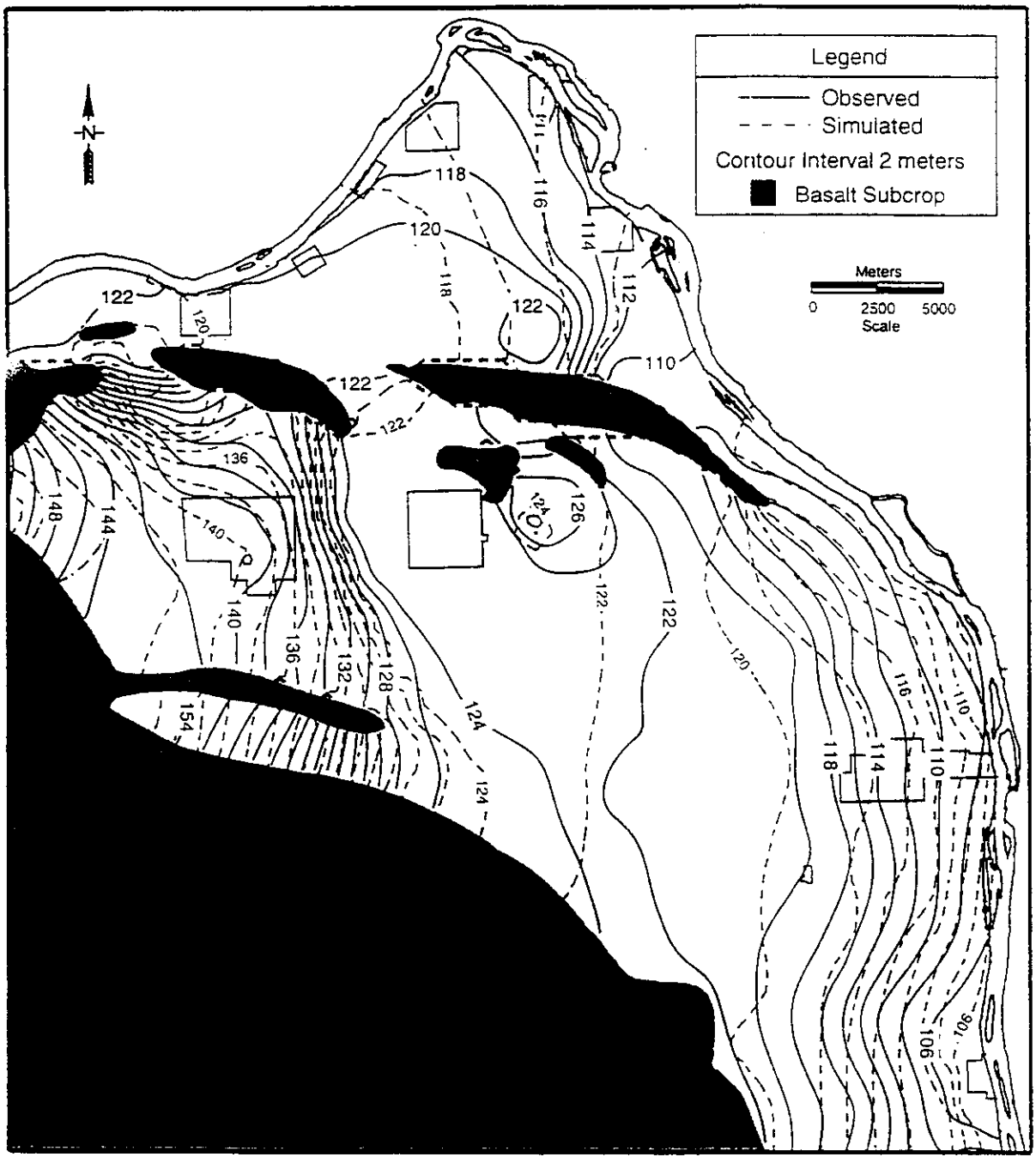

Figure 3-10. Contoured Residual Data Showing the Difference Between the Observed and Simulated Water Levels for 1993.

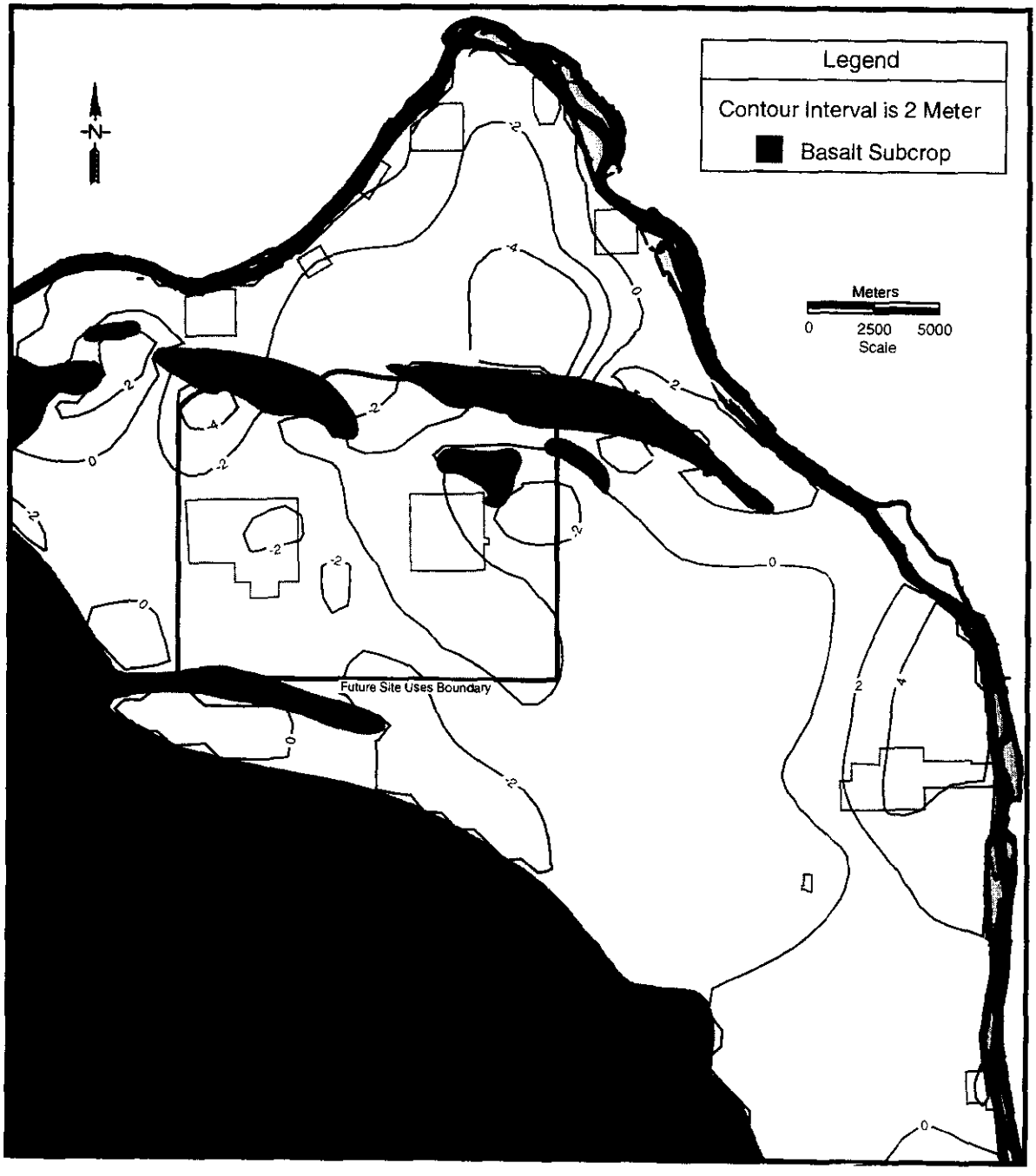

Figure 3-11. Simulated Steady-State Pore Velocity Streamlines - 1979.

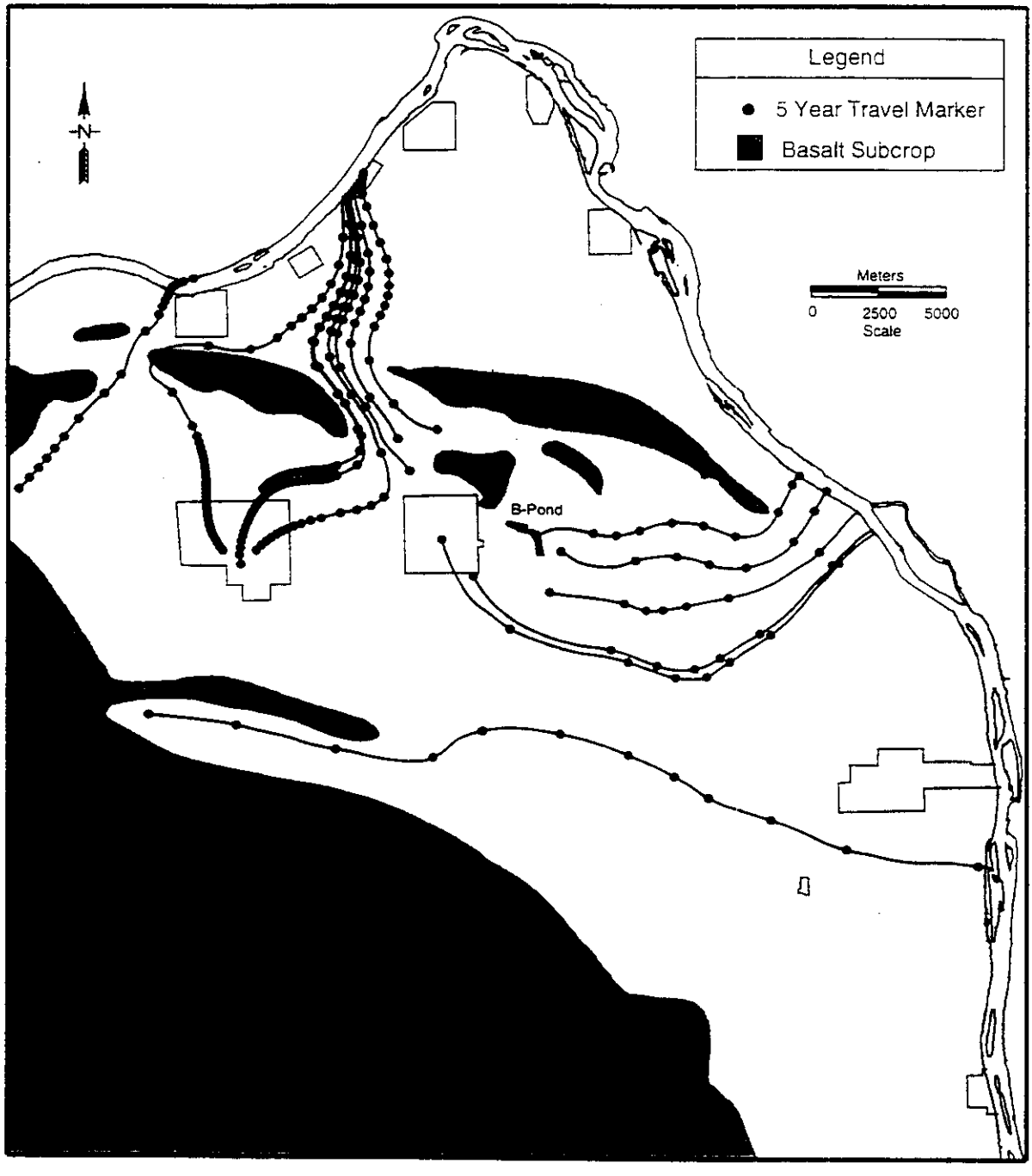

Figure 3-12. Simulated Steady-State Velocity Streamlines - 1988.

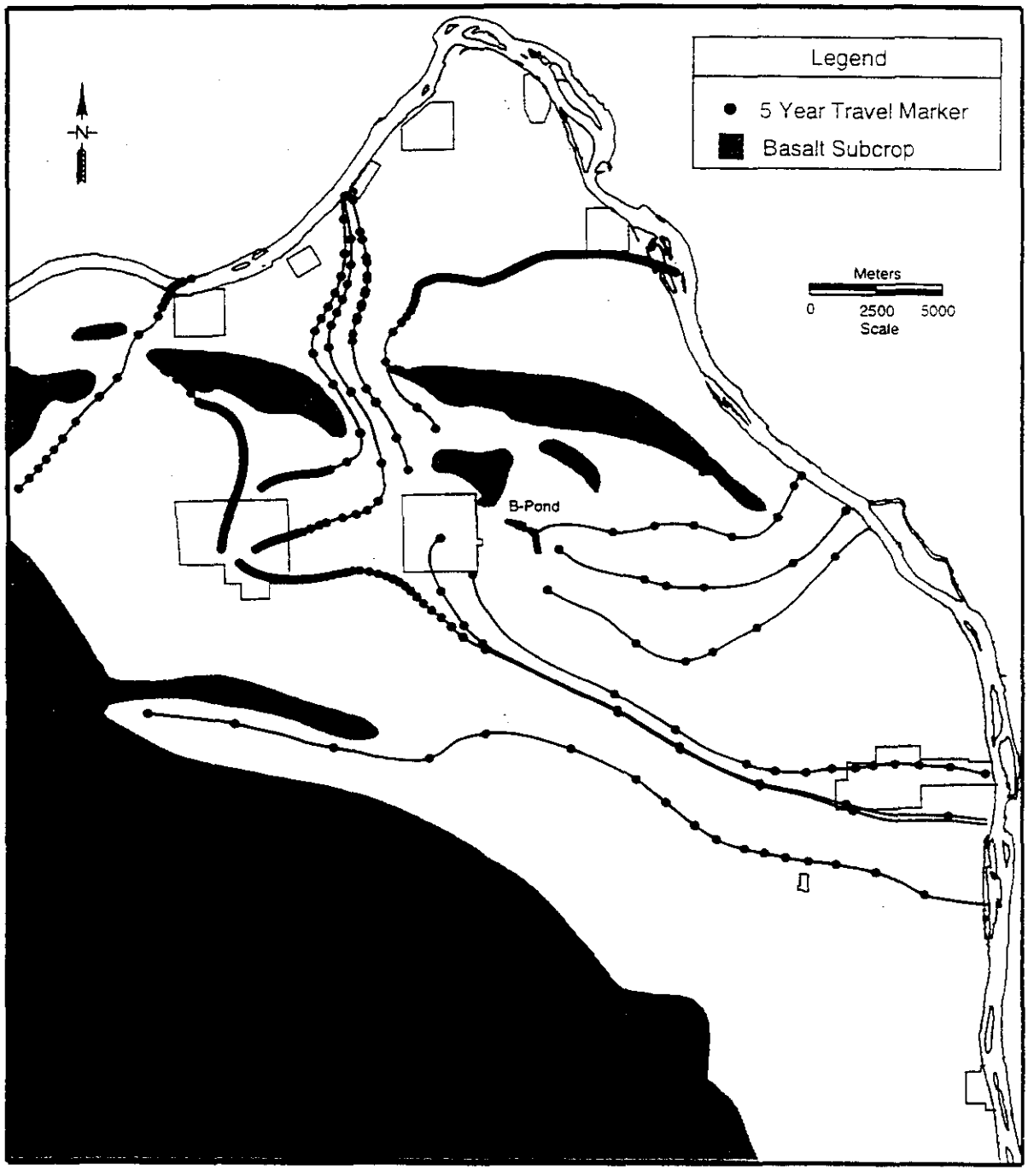

Figure 3-13. Simulated Steady-State Velocity Streamlines - 1993.

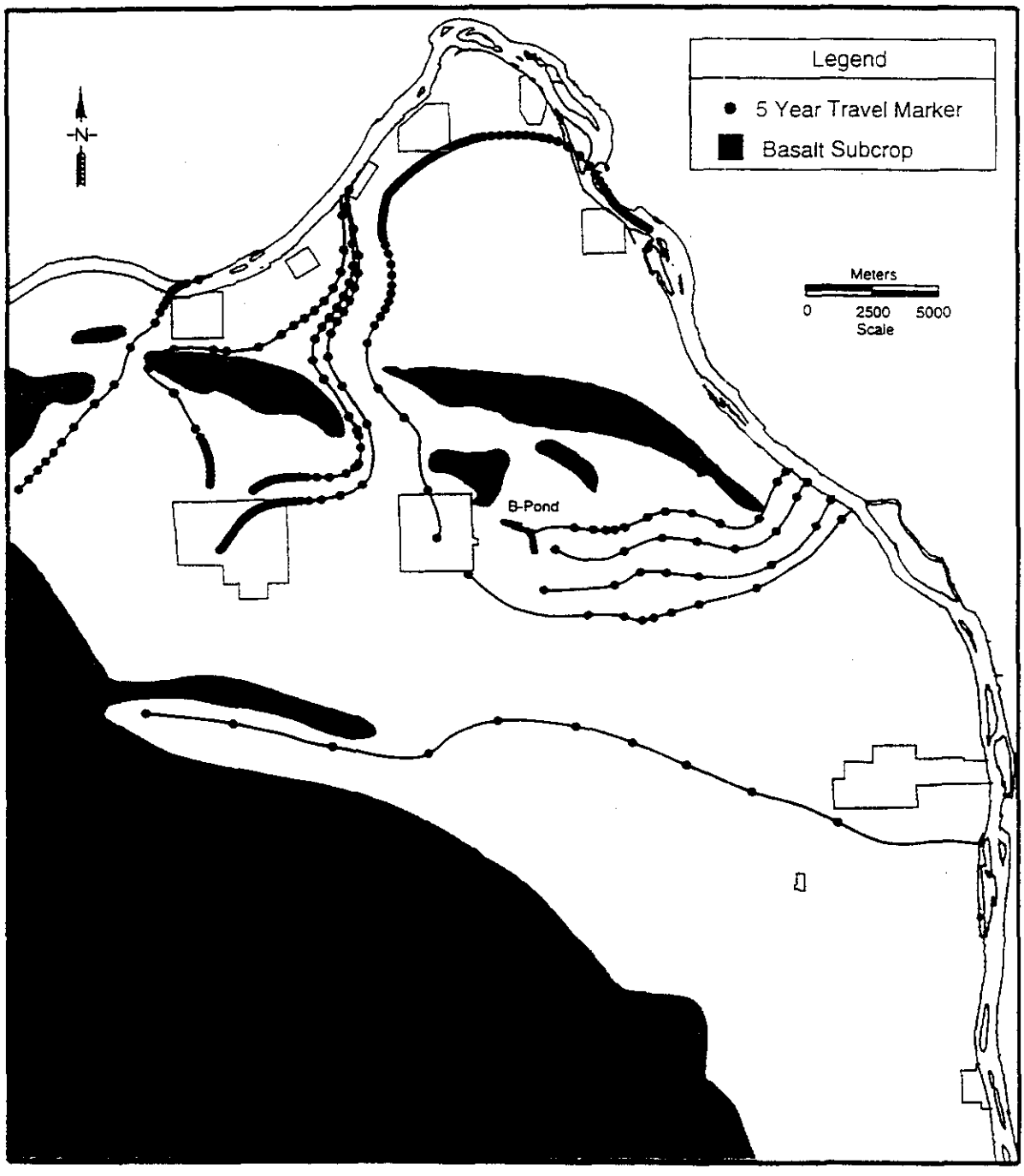

Figure 3-14. Averaged 1979-1981 Distribution of Tritium Under the Hanford Site.

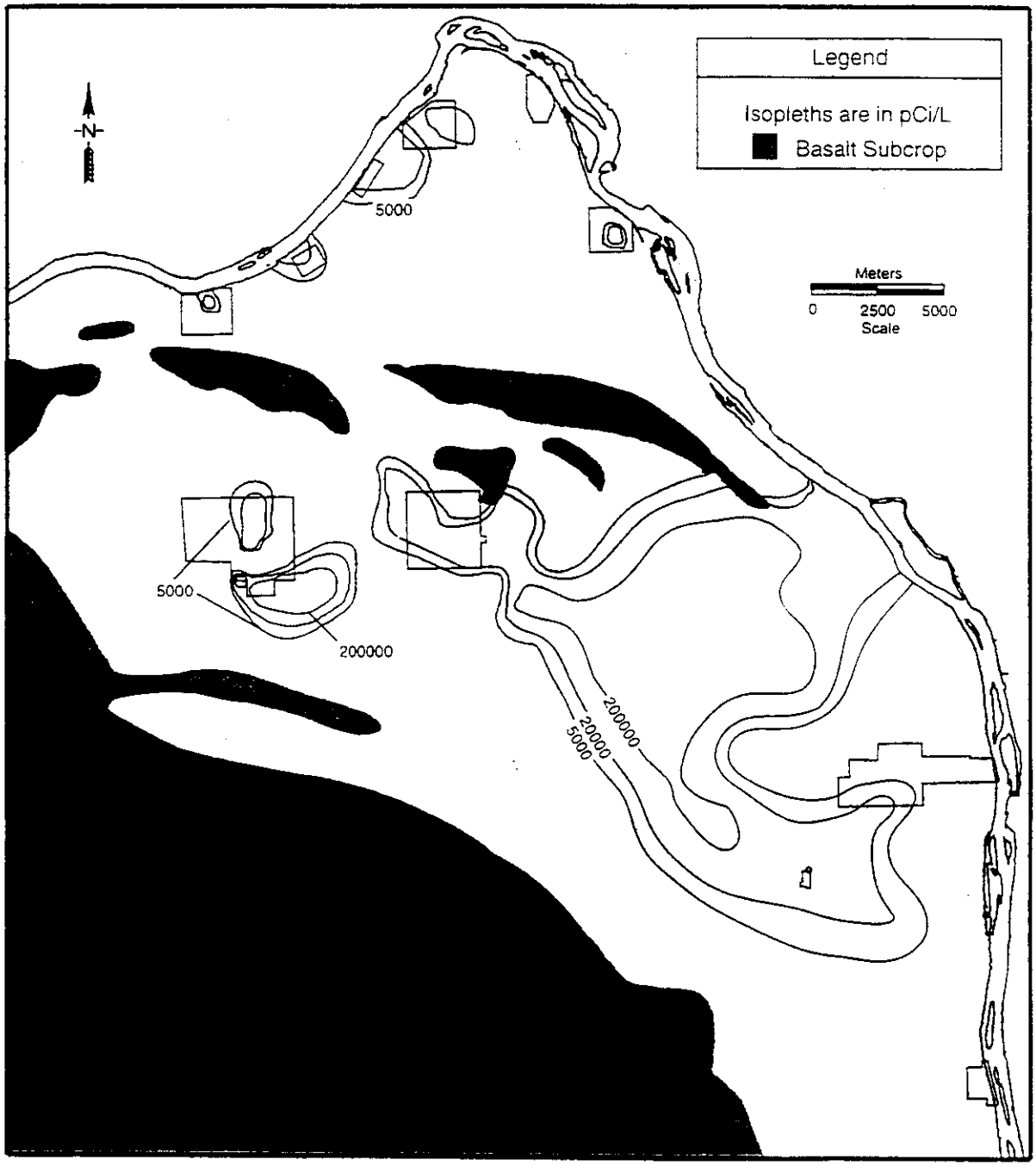

Figure 3-15. Simulated Tritium Plume - 1979.

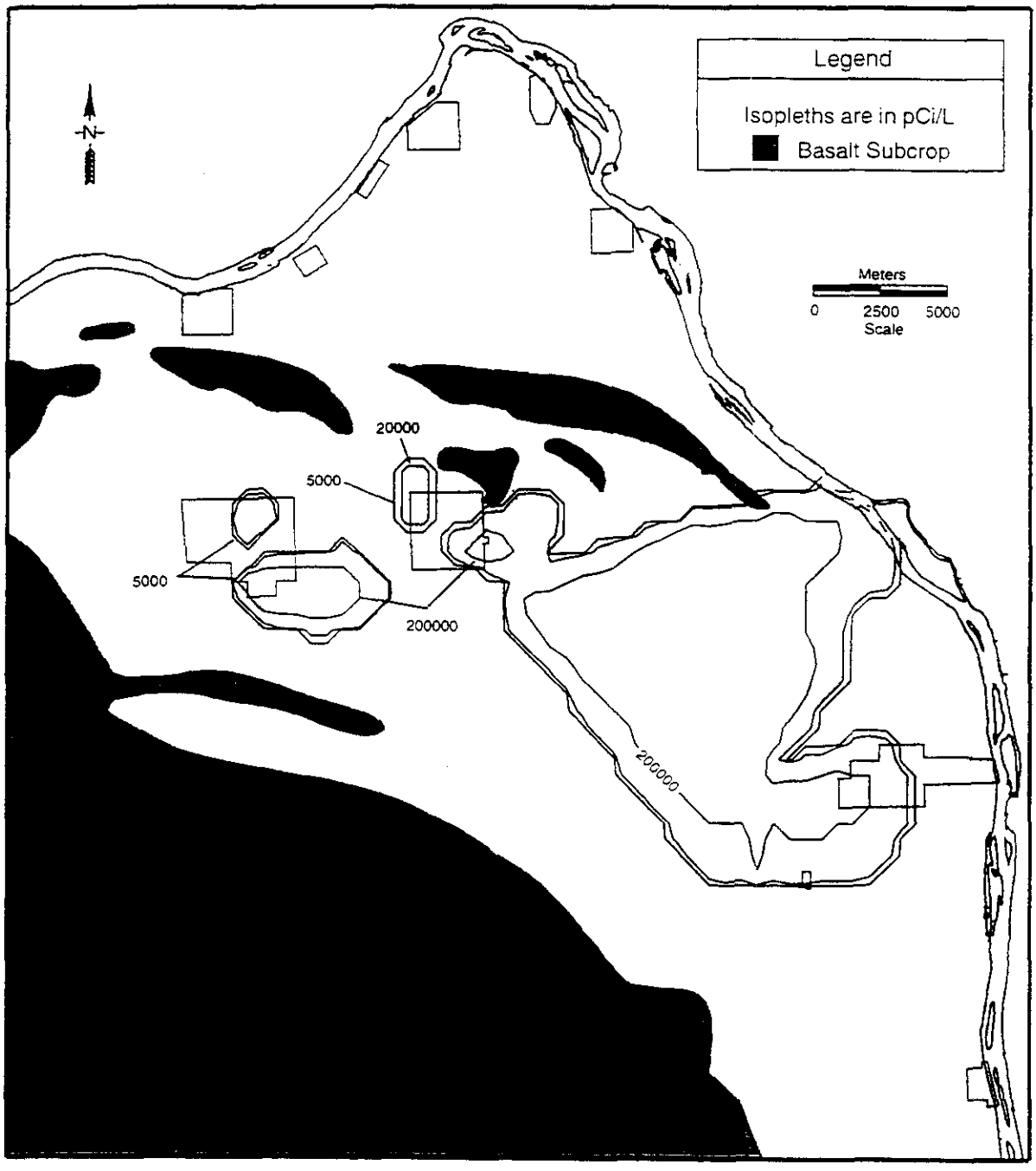

Figure 3-16. Comparison of Initial Conditions Versus Simulated Results - 1979.

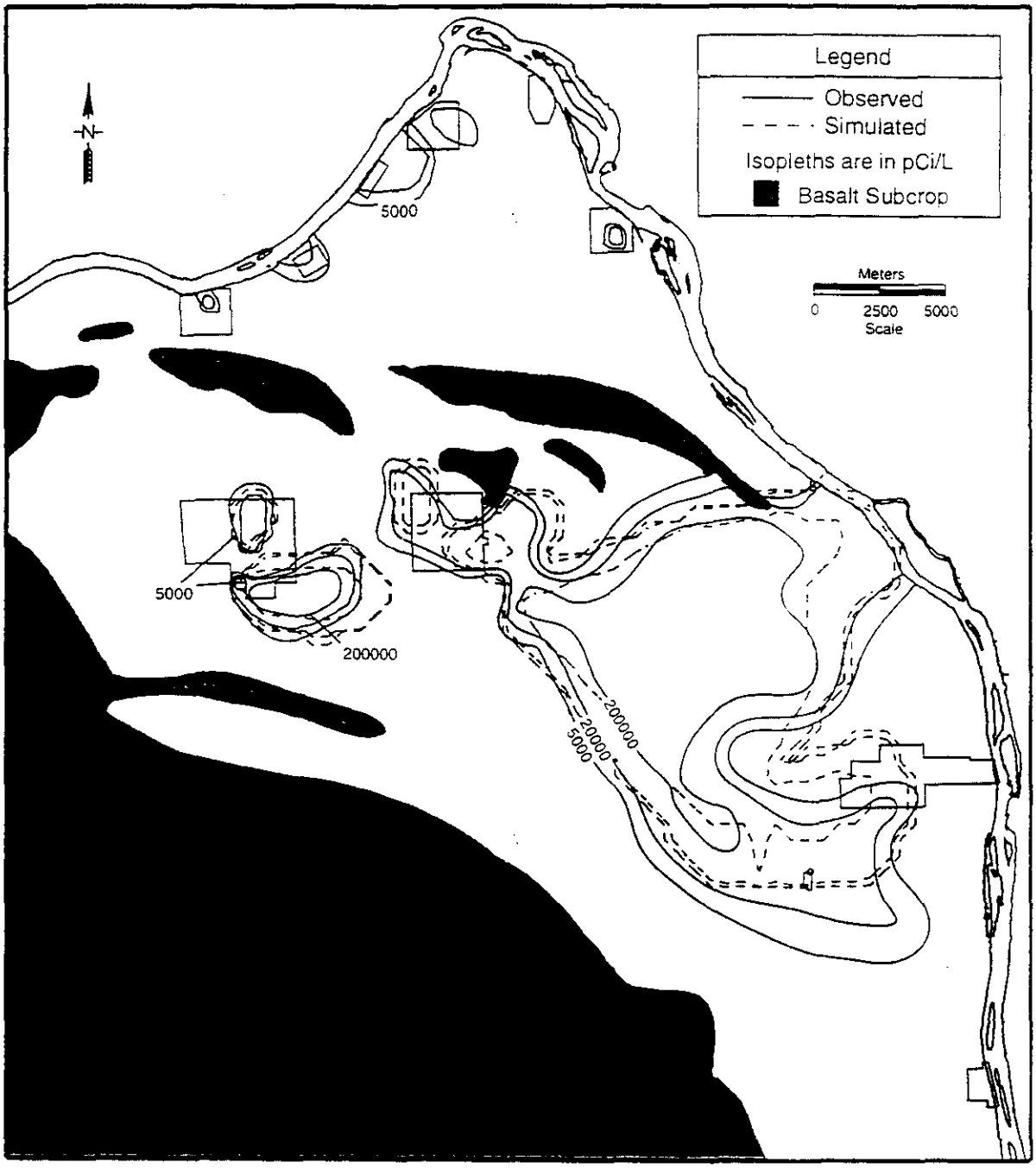

Figure 3-17. Observed Tritium Plume - 1988.

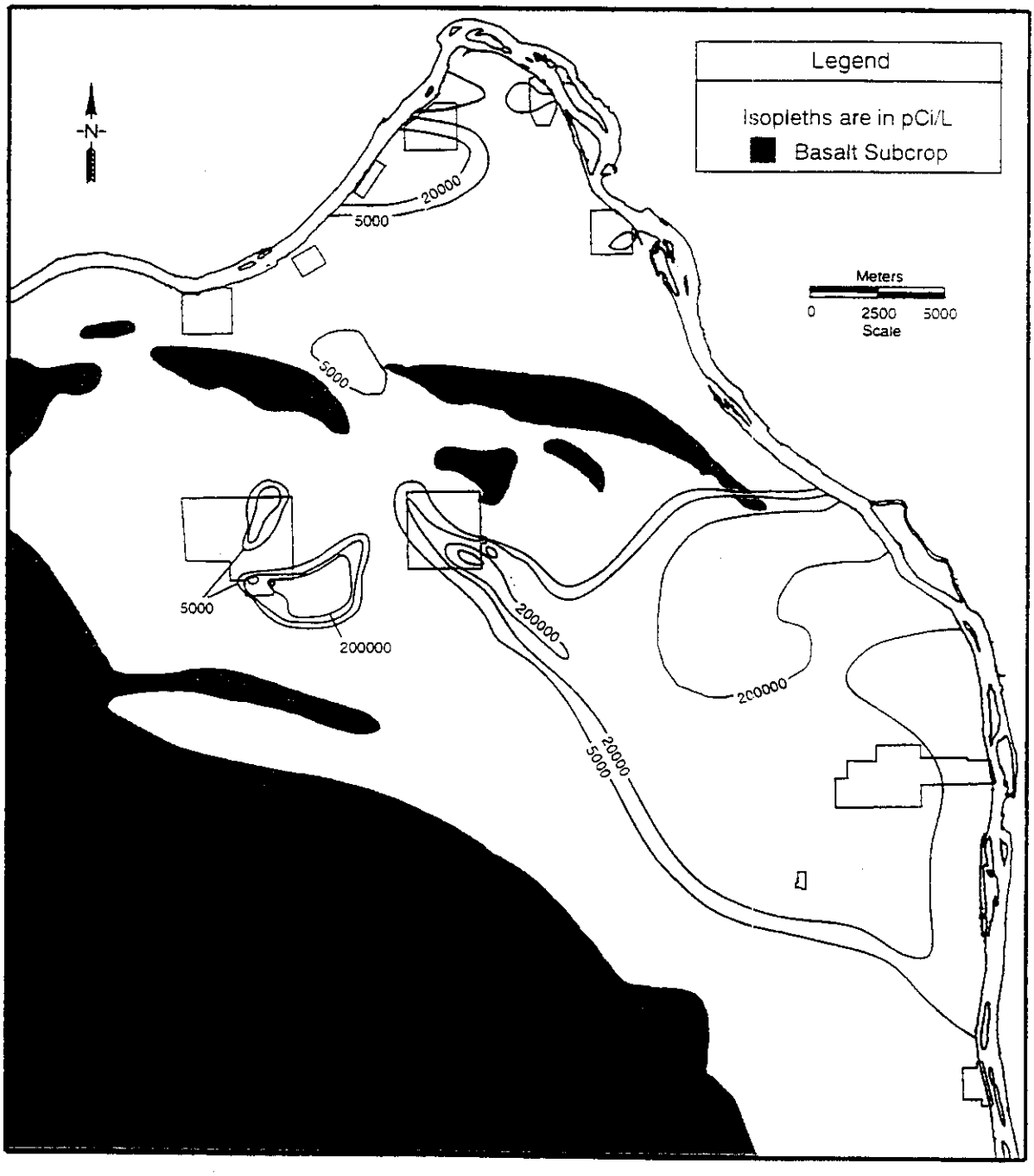

Figure 3-18. Simulated Tritium Plume - 1988.

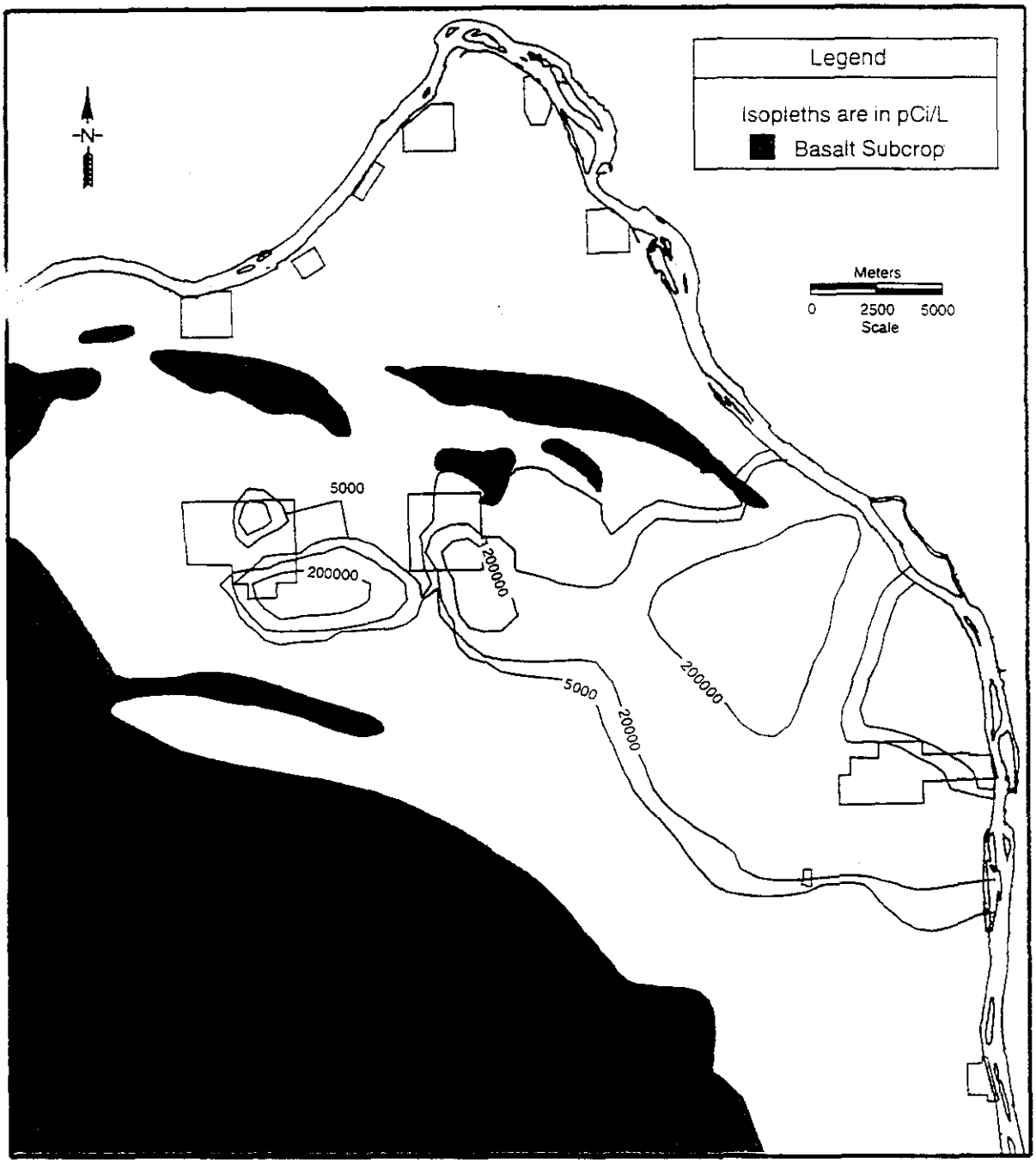

Figure 3-19. Observed Versus Simulated Tritium Results - 1988.

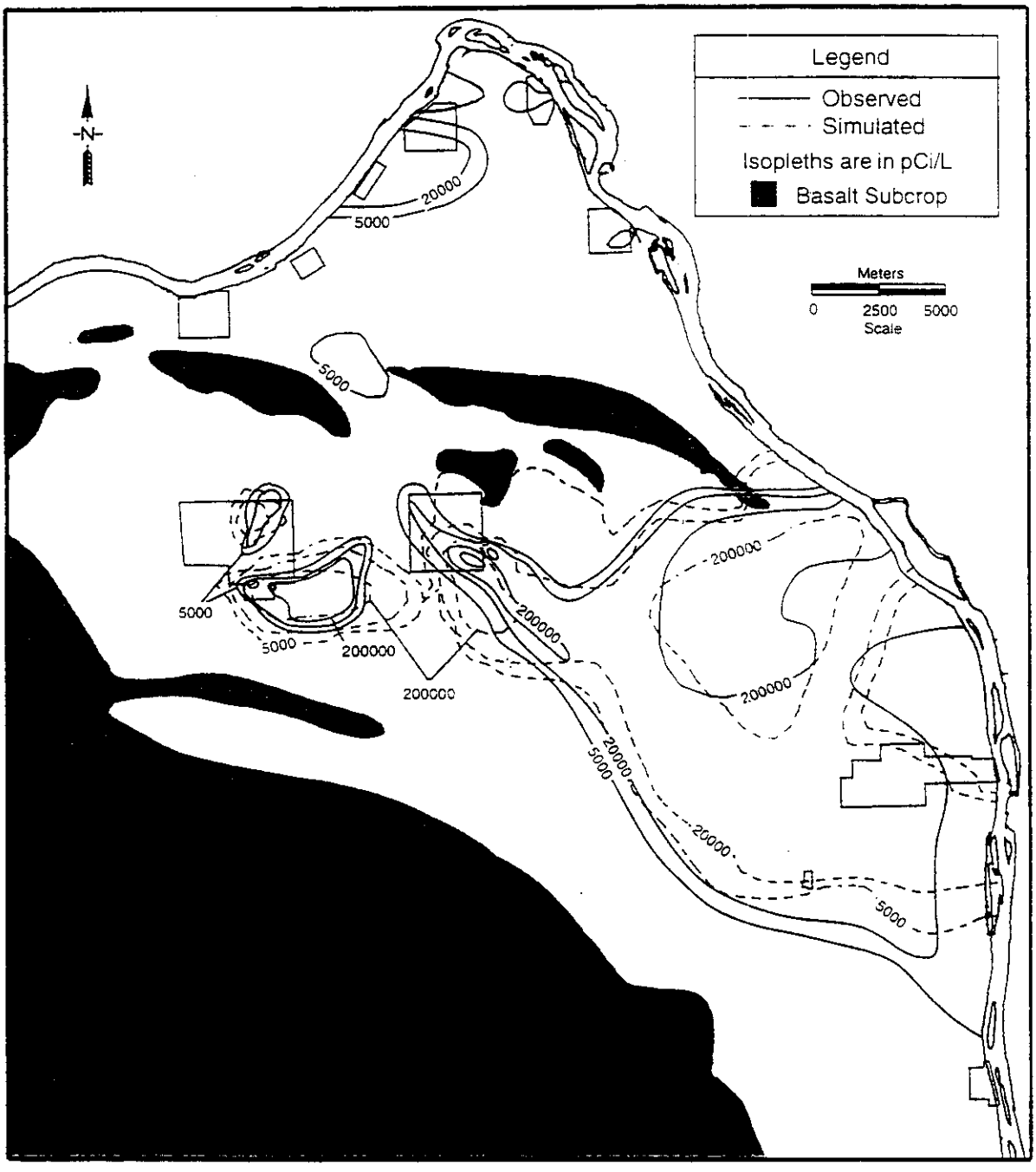

Figure 3-20. Observed Tritium Plume - 1993.

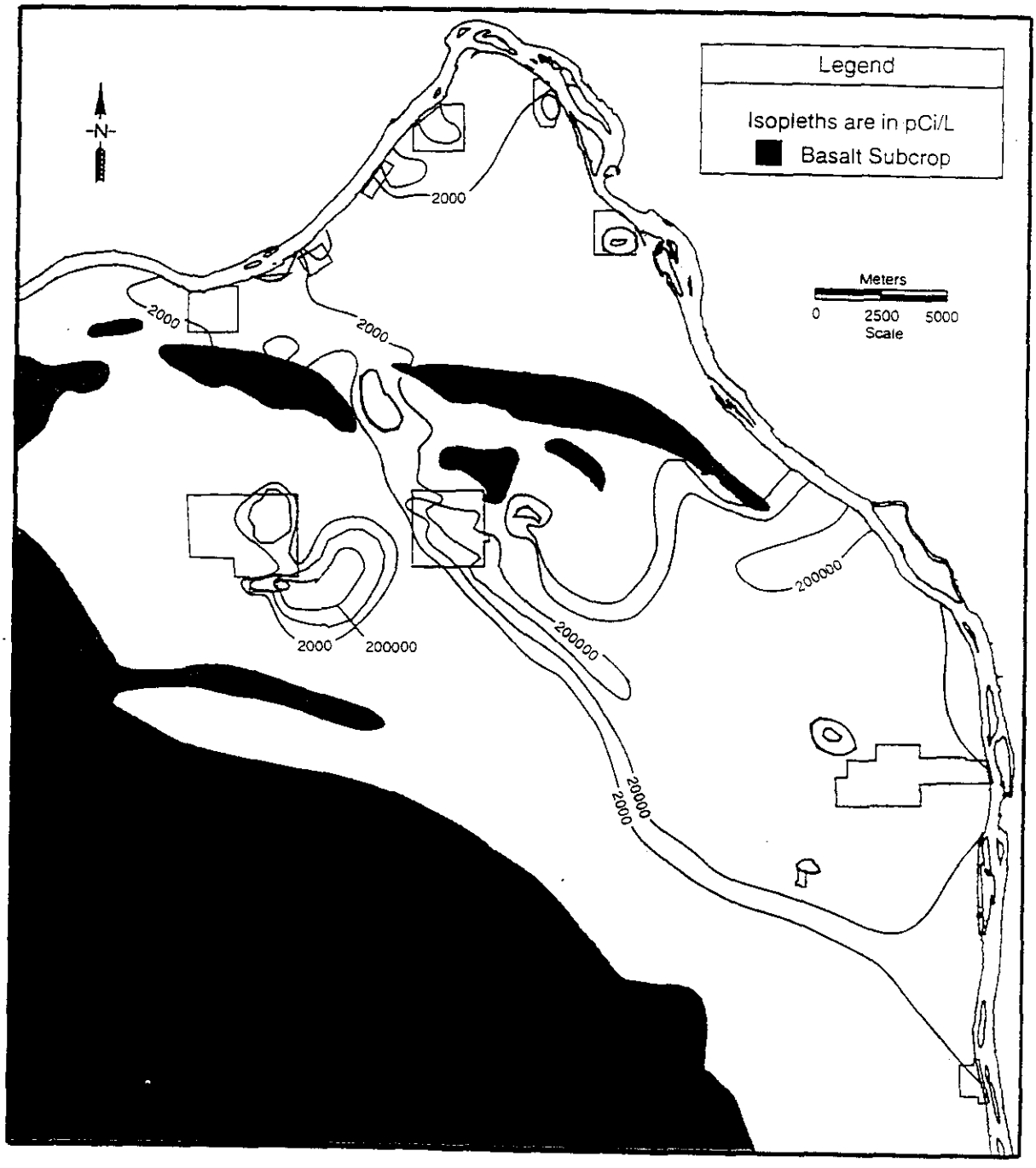

Figure 3-21. Simulated Tritium Plume - 1993.

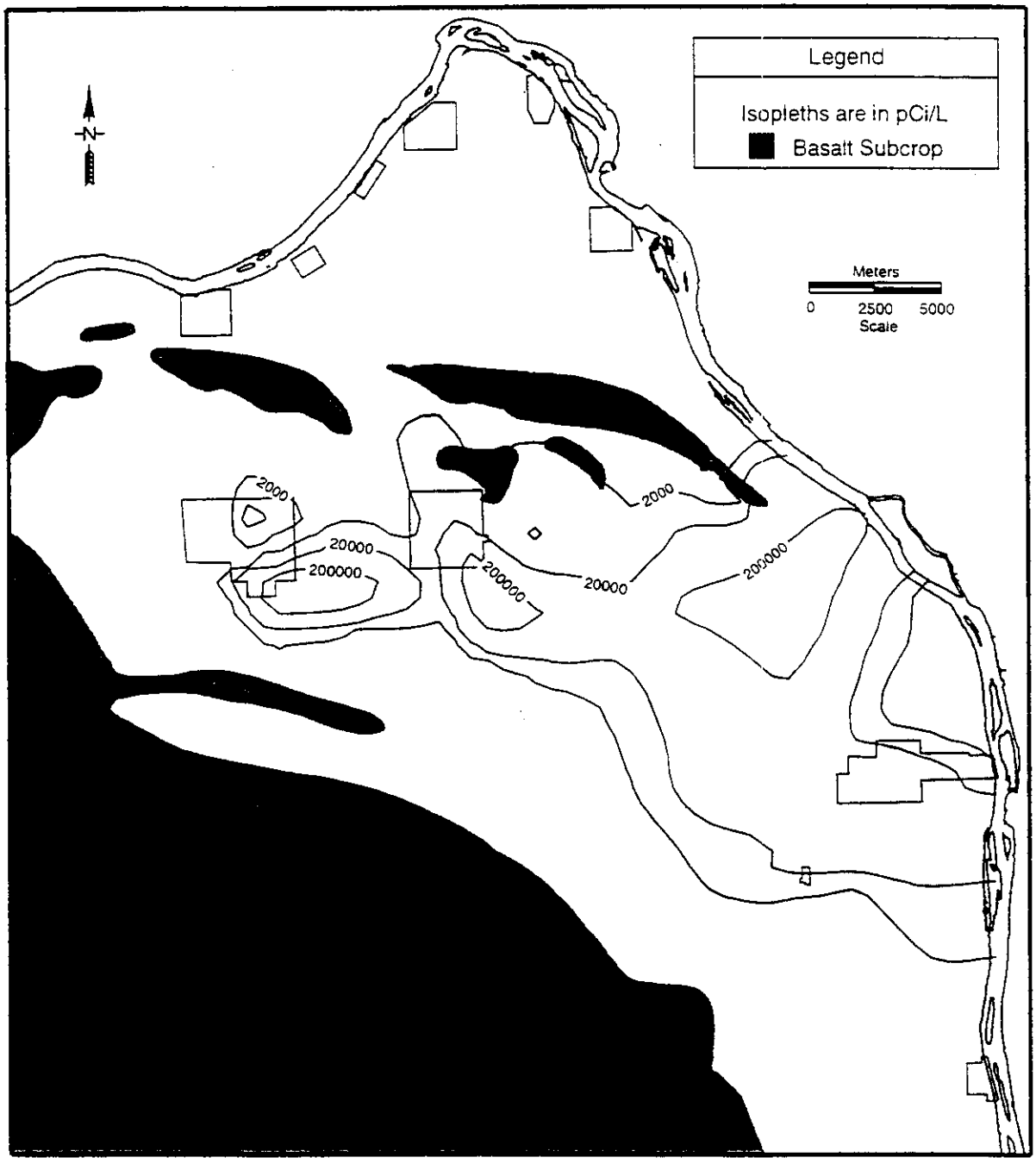

Figure 3-22. Observed Versus Simulated Tritium Results - 1993.

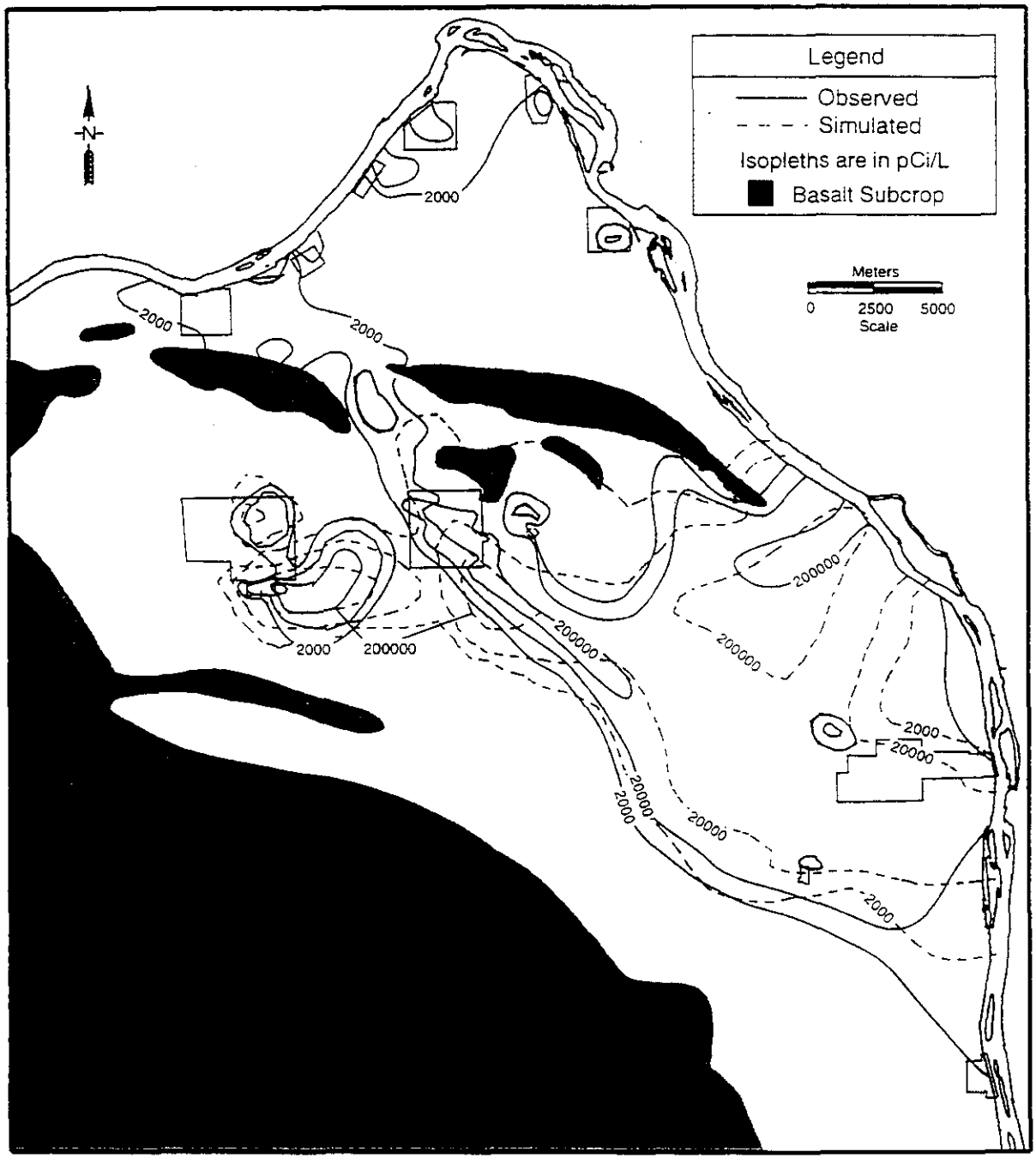

Table 3-1. Element Material-Zone Flow Properties.

Zone	K_{xx} (m/yr)	K_{yy} (m/yr)	K_{zz} (m/yr)	S_s (1/m)	Porosity (%)
1	.800E+03	.800E+03	.800E+02	.100E-05	10
2	.190E+04	.190E+04	.190E+03	.100E-05	25
3	.500E+04	.500E+04	.500E+03	.100E-05	10
4	.650E+04	.650E+04	.650E+03	.100E-05	10
5	.140E+05	.140E+05	.140E+04	.100E-05	25
6	.720E+05	.720E+05	.720E+04	.100E-05	25
7	.260E+05	.260E+05	.260E+04	.100E-05	10
8	.300E+05	.300E+05	.300E+04	.100E-05	25
9	.430E+05	.430E+05	.430E+04	.100E-05	25
10	.055E+06	.055E+06	.055E+05	.100E-05	25
11	.770E+05	.770E+05	.770E+04	.100E-05	25
12	.899E+05	.899E+05	.899E+04	.100E-05	25
13	.140E+06	.140E+06	.140E+05	.100E-05	25
14	.300E+06	.300E+06	.300E+05	.100E-05	25
15	.750E+06	.750E+06	.750E+05	.100E-05	25
16	.113E+07	.113E+07	.113E+06	.100E-05	25
17	.183E+07	.183E+07	.183E+06	.100E-05	25
18	.213E+07	.213E+07	.213E+06	.100E-05	25

K_{xx} = Hydraulic conductivity in the north-south direction.
K_{yy} = Hydraulic conductivity in the east-west direction.
K_{zz} = Hydraulic conductivity in the vertical direction.
S_s = Specific storage
1/m = 1 per meter

Table 3-2. Transport Properties for Tritium.

Longitudinal dispersivity	α_L	=	30.5 m
Transverse dispersivity	α_T	=	3 m
Decay coefficient	λ	=	0.0564 year $^{-1}$
Adsorption coefficient	κ_d	=	0

Note: Porosities of the material zones are the same as for the flow run shown in Table 3-1.

4.0 SUMMARY OF CONCLUSIONS

The development of a new model of groundwater flow in the unconfined aquifer represents an important step in remediating Hanford groundwater contamination. This model allows large-scale groundwater remediation alternatives to be evaluated and allows their impacts to be visualized on a sitewide basis. This calibrated model also offers many opportunities for programs outside of the remediation program to estimate the impacts they may have on groundwater flow conditions and thus the cleanup program. Conclusions of the model calibration are as follows:

- The VAM3DCG model has the capability and flexibility to simulate the major features needed to evaluate the effectiveness of alternative groundwater remediation approaches currently under consideration.

- Input to the VAM3DCG model effectively incorporates the most updated geologic and hydrogeologic conceptualization of the groundwater flow and transport system available on the Hanford Site.

- The reduction in liquid effluent discharges to the soil column is causing significant alterations to the groundwater flow system that can best be considered on a sitewide basis using a sitewide model.

- The combined steady-state and transient simulations used in the calibration approach provide an evaluation that indicates the model is calibrated.

- Quantification of the ability of the model to predict groundwater travel time is a significant feature needed for effective use by the groundwater remediation program.

- Comparison of simulated and measured tritium plume concentrations indicates local geologic/lithologic control of transport is not currently incorporated into the model; in particular, the May Junction Fault to the east is not well delineated.

- Sensitivity of modeled results to input assumptions varies throughout the modeled domain. Interpretations of results must incorporate information gained under the sensitivity studies performed.

5.0 REFERENCES

AERO, 1980, *Final Report Multilevel Aeromagnetic Survey of the Hanford Site*, 8035469, AERO Report to Rockwell Hanford Operations, Richland, Washington.

Alexander, D. J., 1993, *Groundwater Impact Assessment Report for the 100-D Ponds*, WHC-EP-0666, Westinghouse Hanford Company, Richland, Washington.

Alexander, D. J. and V. G. Johnson, 1993, *Groundwater Impact Assessment Report for the 1325-N Liquid Waste Disposal Facility*, WHC-EP-0675, Westinghouse Hanford Company, Richland, Washington.

Alexander, D. J., V. G. Johnson, and K. A. Lindsey, 1993, *Groundwater Impact Assessment Report for the 284-WB Powerplant Ponds*, WHC-EP-0679, Westinghouse Hanford Company, Richland, Washington.

Alexander, D. J., S. D. Evelo, V. G. Johnson, and M. D. Sweeney, 1995, *Groundwater Impact Assessment Report for the 216-T-4-2 Ditch*, WHC-EP-0815, Westinghouse Hanford Company, Richland, Washington.

ARHCO, 1976, *Preliminary Feasibility Study on Storage of Radioactive Wastes in Columbia River Basalts*, ARH-ST-137, Vol. 1, p. 57, Atlantic Richfield Hanford Company, Richland, Washington.

Ault, T. D., 1981, "Geophysical Investigations of the Gable Mountain-Gable Butte Area," in C. W. Myers and S. M. Price (eds.), *Subsurface Geology of the Cold Creek Syncline*, RHO-BWI-ST-14, Rockwell Hanford Operations, Richland, Washington.

Baker, V. R., B. N. Bjornstad, A. J. Busacca, K. R. Fecht, E. P. Kiver, U. L. Moody, J. G. Rigby, O. F. Stradling, and A. M. Tallman, 1991, "Quaternary Geology of the Columbia Plateau," in *Quaternary Nonglacial Geology; Conterminous United States: The Geology of North America*, R. B. Morrison (ed.), Geological Society of America, Vol. K-2.

Bennett, G. B., 1992, Letter to Heather Duncan of A. J. Kerny, Inc., *Draft Report, Ground-Water Aspects of the Macroengineering Approach at the Hanford Reservation*.

Berkman, E., 1984, *Reprocessing and Interpretation-Seismic Reflection Data - Hanford Site, Pasco Basin, South-Central Washington*, RHO-SD-BWI-TI-177, Rockwell Hanford Operations, Richland, Washington.

Berkman, E., 1986, *Reprocessing of Two Mile Seismic Test Line, Hanford Site*, Emerald Exploration, Austin, Texas.

Bierschenk, W. H., 1959, *Aquifer Characteristics and Ground-Water Movement at Hanford*, HW-60601, General Electric, Richland, Washington.

Bjornstad, B. N., 1984, *Suprabasalt Stratigraphy within and Adjacent to the Reference Repository Location*, RHO-SD-BWI-DP-039, Rockwell Hanford Operations, Richland, Washington.

Bjornstad, B. N., 1985, *Late Cenozoic Sediments and Tectonic Evolution within a Subsiding Basin, South-Central Washington [Abstract]*, Geological Society of America Abstracts with Programs, Vol. 17, No. 7, p. 524.

Blume, J. A., 1971, *Subsurface Investigations for the FFTF Project in the Pasco Basin*, JABE-WADCO-07, J. A. Blume and Associates, San Francisco, California.

Brown, D. J., 1959, *Subsurface Geology of the Hanford Separation Areas*, HW-61780, General Electric Company, Richland, Washington.

Brown, D. J., 1962, *Geology Underlying the Reactor Areas*, HW-69571, General Electric Company, Richland, Washington.

Brown, D. J., 1971, *The Preliminary Hanford Stratigraphic Framework - Interim Report*, ARH-2170, Atlantic Richfield Hanford Company, Richland, Washington.

Comprehensive Environmental Response, Compensation, and Liability Act of 1980, 42 USC 9601 et seq.

Connelly, M. P., J. V. Borghese, C. D. Delaney, B. H. Ford, J. W. Lindberg, and S. J. Trent, 1992a, *Hydrogeologic Model for the 200 East Groundwater Aggregate Area*, WHC-SD-EN-TI-019, Westinghouse Hanford Company, Richland, Washington.

Connelly, M. P., J. V. Borghese, C. D. Delaney, B. H. Ford, J. W. Lindberg, and S. J. Trent, 1992b, *Hydrogeologic Model for the 200 West Groundwater Aggregate Area*, WHC-SD-EN-TI-014, Westinghouse Hanford Company, Richland, Washington.

Crowley, W. H. and R. K. Ledgerwood, 1987, *Borehole Status Chart and Location Map*, RHO-SD-BWI-DP-044, Rockwell Hanford Operations, Richland, Washington.

Deju, R. A., 1974, *The Hanford Field Testing Program*, CA-168-RAD-3, Atlantic Richfield Hanford Company, Richland, Washington.

DOE, 1988, *Consultation Draft Site Characterization Plan*, DOE/RW-0164, Vols. 1-9, Office of Civilian Radioactive Waste Management, U.S. Department of Energy, Washington, D.C.

DOE-RL, 1991a, *Description of Codes and Models to be Used in Risk Assessment*, DOE/RL-91-44, U.S. Department of Energy, Richland Operations Office, Richland, Washington.

DOE-RL, 1991b, *Ground-Water Model Development Plan in Support of Risk Assessment*, DOE/RL-91-62, U.S. Department of Energy, Richland Operations Office, Richland, Washington.

DOE-RL, 1994, *Phase 1 Remedial Investigation Report for the 300-FF-5 Operable Unit*, DOE/RL-93-21, U.S. Department of Energy, Richland Operations Office, Richland, Washington.

Donaldson, J. A. 1963, *Seismic Survey, Hanford Atomic Products Operations, Richland, Benton County, Washington*, GEH-26275, General Electric Company, Richland, Washington.

Ecology, EPA, and DOE, 1989, *Hanford Federal Facility Agreement and Consent Order*, as amended, Washington State Department of Ecology, U.S. Environmental Protection Agency, and U.S. Department of Energy, Richland Operations Office, Olympia, Washington.

Fayer, M. J. and T. B. Walters, 1995, *Estimated Recharge Rates at the Hanford Site*, PNL-10285, Pacific Northwest Laboratory, Richland, Washington.

Fecht, K. R. and J. T. Lillie, 1982, *A Catalog of Borehole Lithologic Logs from the 600 Area, Hanford Site*, RHO-LD-158, Rockwell Hanford Operations, Richland, Washington.

Fecht, K. R., R. E. Gephart, D. L. Graham, S. P. Reidel, and A. C. Rohay, 1984, *Summary of Geotechnical Information in the Rattlesnake Mountain Area*, RHO-SD-BWI-TI-247, Rockwell Hanford Operations, Richland, Washington.

Fecht, K. R., S. P. Reidel, and A. M. Tallman, 1985, *Evolution of the Columbia River System in the Central Columbia Plateau of Washington from Miocene to the Present [Abstract]*, Geological Society of America Abstracts with Programs, Vol. 14, No. 4, p. 163.

Fecht, K. R., S. P. Reidel, and A. M. Tallman, 1987, "Paleodrainage of the Columbia River System on the Columbia Plateau of Washington State -- A Summary," in J. E. Schuster (ed.), *Selected Papers on the Geology of Washington, Washington State Division of Geology and Earth Resources*," Bulletin 77, p. 219-248.

Gee, G. W., M. J. Fayer, M. L. Rockhold, and M. D. Campbell, 1992, "Variations in Recharge at the Hanford Site," *Northwest Science* 66:237-250.

Gilmore, T. J., D. R. Newcomer, S. K. Wurstner, and F. A. Spane, Jr., 1992, *Calculation of Groundwater Discharge to the Columbia River in the 100-N Area*, PNL-8057 Pacific Northwest Laboratory, Richland, Washington.

Glass, C. E., 1977, "Remote Sensing Analysis of the Columbia Plateau," in WPPSS, *Preliminary Safety Analysis Report*, Amendment 23, Appendix 2RK, Washington Public Power Supply System, Richland, Washington.

Glass, C. E. and D. B. Simmons, 1977, "Imagery and Topographic Interpretation of Geologic Structures in Central Washington," in WPPSS, *Preliminary Safety Analysis Report*, Amendment 23, Appendix 2RF, Washington Public Power Supply System, Richland, Washington.

Goodwin, S. M., 1993, "Petrography of the Coarse-Grained Facies of the Miocene-Pliocene Ringold Formation, South-Central Washington State," M.S. thesis, Western Washington University, Bellingham, Washington.

Graham, M. J., M. D. Hall, S. R. Strait, and W. R. Brown, 1981, *Hydrology of the Separations Area*, RHO-ST-42, Rockwell Hanford Operations, Richland, Washington.

Graham, M. J., G. V. Last, and K. R. Fecht, 1984, *An Assessment of Aquifer Intercommunication in the B Pond-Gable Mountain Pond Area of the Hanford Site*, RHO-RE-ST-12P, Rockwell Hanford Operations, Richland, Washington.

Holmes, G. E. and T. H. Mitchell, 1981, "Seismic Reflection and Multi-level Aeromagnetic Surveys in the Cold Creek Syncline Area," in C. W. Myers and S. M. Price (eds.), *Subsurface Geology of the Cold Creek Syncline*, RHO-BWI-ST-14, Rockwell Hanford Operations, Richland, Washington.

Huyakorn, P. S. and S. M. Panday, 1994, *VAM3DCG: Variably Saturated Analysis Model in Three Dimensions with Preconditioned Conjugate Gradient Matrix Solvers*, Documentation and User's Guide, Version 3.1, HydroGeoLogic, Inc., Herndon, Virginia.

Jackson, R. L., L. D. Diediker, R. K. Ledgerwood, and M. D. Veatch, 1984, *Piezometer Completion Report for Borehole Cluster Sites DC-19, DC-20 and DC-22*, RHO-SD-BWI-TI-226, Rockwell Hanford Operations, Richland, Washington.

Jacobson, E. A. and M. D. Freshley, 1990, *An Initial Inverse Calibration of the Ground-Water Flow Model for the Hanford Unconfined Aquifer*, PNL-7144, Pacific Northwest Laboratory, Richland, Washington.

Johnson, V. G., 1993a, *Groundwater Impact Assessment Report for the 216-Z-20 Crib, 200 West Area*, WHC-EP-0674, Westinghouse Hanford Company, Richland, Washington.

Johnson, V. G., 1993b, *Westinghouse Hanford Company Operational Groundwater Status Report, 1990-1992*, WHC-EP-595, Westinghouse Hanford Company, Richland, Washington.

Johnson, V. G., 1995, *Groundwater Monitoring and Assessment Plan for the 100-K Area Fuel Storage Basins*, WHC-SD-EN-AP-174, Westinghouse Hanford Company, Richland, Washington.

Johnson, V. G., A. G. Law, S. P. Reidel, S. D. Evelo, D. B. Barnett, and M. D. Sweeney, 1995, *Groundwater Impact Assessment Report for the 216-B-3 Pond System*, WHC-EP-0813, Westinghouse Hanford Company, Richland, Washington.

Kipp, K. L. and R. D. Mudd, 1973, *Collection and Analysis of Pump Test Data for Transmissivity Values*, BNWL-1709, Battelle Northwest Laboratory, Richland, Washington.

Kipp, K. L, and R. P. Mudd, 1974, *Selected Water Table Contour Maps and Well Hydrographs for the Hanford Reservation, 1944-1973*, BNWL-B-360.

Kunk, J. R., 1981, "Geophysical Investigations in the Southwestern Cold Creek Syncline," in C. W. Myers and S. M. Price (eds.), *Subsurface Geology of the Cold Creek Syncline*, RHO-BWI-ST-14, Rockwell Hanford Operations, Richland, Washington.

Kunk, J. R., 1986, *Seismic Reflection Data, BO62650, DAP No*, 03-00035, Walker Geophysical Company for Rockwell Hanford Operations, Richland, Washington.

Last, G. V. and M. J. Marratt, 1978a, *Generalized Geology of the 241-AW Tank Farm*, RHO-LD-31, Rockwell Hanford Company, Richland, Washington.

Last, G. V. and M. J. Marratt, 1978b, *Generalized Geology of the 241-AN Tank Farm*, RHO-LD-32, Rockwell Hanford Company, Richland, Washington.

Ledgerwood, R. K. and R. A. Deju, 1976, *Hydrogeology of the Uppermost Confined Aquifers Underlying the Hanford Reservation*, ARH-SA-253, Atlantic Richfield Hanford Company, Richland, Washington.

Ledgerwood, R. K., 1986, *Borehole Depths and Thicknesses for Saddle Mountains and Wanapum Basalts*, RHO-SD-BWI-DP-068, Rockwell Hanford Operations, Richland, Washington.

Lindsey, K. A., 1991a, *Revised Stratigraphic Nomenclature for the Ringold Formation, Hanford Site, South-Central Washington*, WHC-SD-EN-EE-004, Westinghouse Hanford Company, Richland, Washington.

Lindsey, K. A., 1991b, *Sedimentation and Basin Evolution of the Late Neogene Ringold Formation, Central Columbia Plateau, South-Central Washington*, Geological Society of America Abstracts with Programs, Vol. 23, No. 5, p. A285.

Lindsey, K. A., 1992, *Geology of the Northern Part of the Hanford Site: An Outline of Data Sources and the Geologic Setting of the 100 Areas*, WHC-SD-EN-TI-011, Westinghouse Hanford Company, Richland, Washington.

Lindsey, K. A., 1995, *Miocene- to Pliocene-Aged Suprabasalt Sediments of the Hanford Site, South-Central Washington*, BHI-00184, Rev. 0, Bechtel Hanford, Inc., Richland, Washington.

Lindsey, K. A. and D. R. Gaylord, 1990, "Sedimentology and Stratigraphy of the Miocene-Pliocene Ringold Formation, Hanford Site, South-Central Washington," *Northwest Science*, Vol. 64, No. 3, pp. 165-180.

Lindsey, K. A. and G. K. Jaeger, 1993, *Geologic Setting of the 100-HR-3 Operable Unit, Hanford Site, South-Central Washington*, WHC-SD-EN-TI-132, Westinghouse Hanford Company, Richland, Washington.

Lindsey, K. A., B. N. Bjornstad, and M. P. Connelly, 1991, *Geologic Setting of the 200 West Area: An Update*, WHC-SD-EN-TI-008, Westinghouse Hanford Company, Richland, Washington.

Lindsey, K. A., B. N. Bjornstad, J. W. Lindberg, and K. M. Hoffman, 1992, *Geologic Setting of the 200 East Area: An Update*, WHC-SD-EN-TI-012, Westinghouse Hanford Company, Richland, Washington.

Lindsey, K. A., S. P. Reidel, K. R. Fecht, J. L. Slate, A. G. Law, and A. M. Tallman, 1994a, "Geohydrologic Setting of the Hanford Site, South-Central Washington," in D. A. Swanson and R. A. Haugerud (eds.), *Geologic Field Trips of the Pacific Northwest, 1994 Geological Society of America Annual Meeting*, Department of Geological Sciences, University of Washington, Seattle, Washington, pp. K1-K16.

Lindsey, K. A., J. L. Slate, G. K. Jaeger, K. J. Swett, and R. B. Mercer, 1994b, *Geologic Setting of the Low-Level Burial Grounds*, WHC-SD-EN-TI-290, Westinghouse Hanford Company, Richland, Washington.

Livesay, D. M., 1986, *The Hydrogeology of the Upper Wanapum Basalt, Upper Cold Creek Valley, Washington*, M. S. Thesis, Department of Geologic Engineering, Washington State University, Pullman, Washington.

Luke, J. J., Westinghouse Hanford Company, to J. E. Rasmussen, U.S. Department of Energy, Correspondence, December 19, 1995, Correspondence Control No. 9504951BR1.

Luttrell, S. P., D. R. Newcomer, S. S. Teel, and V. R. Vermeul, 1992, *Hydrogeologic Controls on Ground-Water and Contaminant Discharge to the Columbia River Near the Hanford Townsite*, PNL-8167, Pacific Northwest Laboratory, Richland, Washington.

Miall, A. D., 1977, "A Review of Braided River Depositional Environment," *Earth Science Reviews*, Vol. 13, p. 1-62.

Miall A. D. (ed.), 1978, *Lithofacies types and Vertical Profile Models in Braided River Deposits, A Summary, Fluvial Sedimentology*, Canadian Society of Petroleum Geologists Memoir 5, pp. 597-604.

Miall, A. D., 1985, "Architectural-Analysis: A New Method of Facies Analysis Applied to Fluvial Deposits," *Earth Science Reviews*, Vol. 22, pp. 261-308.

Myers, C. W., 1981, "Bedrock Structure of the Cold Creek Syncline Area," in C. W. Myers and S. M. Price (eds.), *Subsurface Geology of the Cold Creek Syncline*, RHO-BWI-ST-14, Rockwell Hanford Operations, Richland, Washington.

Myers, C. W., S. M. Price, J. A. Caggiano, M. P. Cochran, W. H. Czimer, N. J. Davidson, R. C. Edwards, K. R. Fecht, G. E. Holmes, M. G. Jones, J. R. Kunk, R. D. Landon, R. K. Ledgerwood, J. T. Lillie, P. E. Long, T. M. Mitchell, E. H. Price, S. P. Reidel, and A. M. Tallman, 1979, *Geologic Studies of the Columbia Plateau: A Status Report*, RHO-BWI-ST-4, Rockwell Hanford Operations, Richland, Washington.

Newcomb, R. C., 1958, "The Ringold Formation of the Pleistocene Age in the Type Locality, the White Bluffs, Washington," *American Journal of Science*, Vol. 33, No. 1, pp. 328-340.

Newcomb, R. C., J. R. Frank, and F. J. Frank, 1972, *Geology and Groundwater Characteristics of the Hanford Formation of the Hanford Reservation of the U.S. Atomic Energy Commission, Washington*, Professional Paper 717, U.S. Geological Survey, Washington, D.C.

Newcomer, D. R., M. A. Chamness, D. L. McAlister, R. J. Brockman, A. W. Pearson, and S. T. Teel, 1992a, *Unconfined Aquifer Hydrologic Test Data Package for the 200 East Area*, WHC-SD-EN-DP-030, Rev. 0, Westinghouse Hanford Company, Richland, Washington.

Newcomer, D. R., S. S. Teel, A. W. Person, K. R. Barton, B. N. Bjornsted, and T. J. Gilmore, 1992b, *Unconfined Aquifer Test Data Package for the 200-West Area*, WHC-SD-EN-DP-029, Rev. 0, Westinghouse Hanford Company, Richland, Washington.

Odegard, M. E. and T. H. Mitchell, 1987, *Seismic Velocity Structure in the BWIP Reference Repository Location from Seismic Refraction and Vertical Seismic Profiling Data*, RHO-SD-BWI-TI-359, Westinghouse Hanford Company, Richland, Washington.

Prater, L. S., J. T. Rieger, C. S. Cline, E. J. Janson, and T. L. Liikala, 1984, *Ground-Water Surveillance at the Hanford Site for CY-1983*, PNL-5041, Pacific Northwest Laboratory, Richland, Washington.

Price, E. H., 1982, *Structural Geometry, Strain Distribution, and Mechanical Evolution of Eastern Umtanum Ridge and a Comparison with other Selected Localities within Yakima Fold Structures, South-Central Washington*, RHO-BWI-SA-138, Rockwell Hanford Operations, Richland, Washington, and Washington State University Doctor of Philosophy Thesis.

Price, E. H. and A. J. Watkinson, 1989, "Structural Geometry and Strain Distribution within Eastern Umtanum Fold Ridge, South-Central Washington," in S. P. Reidel and P. R. Hooper (eds.), *Volcanism and Tectonism in the Columbia River Flood-Basalt Province*, Geological Society of America Special Paper 239, p. 265-281.

Price, W. H. and K. R. Fecht, 1976, *Generalized Geology of the 241-SY Tank Farm*, ARH-LD-139, Atlantic Richfield Hanford Company, Richland, Washington

Prych, E. A., 1995, *Using Chloride and Chlorme-36 Tracers to Estimate Deep Percolation at Selected Locations on the U.S. Department of Energy's Hanford Site, Washington*, Open File Report 94-514, U.S. Geological Survey, Denver, Colorado.

PSPL, 1981 and 1982, *Skagit/Hanford Nuclear Project, Preliminary Safety Analysis Report*, Puget Power and Light Company, Bellevue, Washington, 7 vols.

Raidl, R. F., 1994, *Geology of the 100-FR-3 Operable Unit, Hanford Site, South-Central Washington*, WHC-SD-EN-TI-221, Westinghouse Hanford Company, Richland, Washington.

Raymond, J. R. and C. A. Ratcliffe, 1959, *A Test of the Refraction Seismic Method on the Hanford Project*, HW-61796, General Electric Company, Richland, Washington.

Reidel, S. P., 1984, "The Saddle Mountains -- The Evolution of an Anticline on the Yakima Fold Belt," *American Journal of Science*, vol. 243-A, No. 5, p. 479-485.

Reidel, S. P. and K. R. Fecht, 1994a, *Geologic Map of the Priest Rapids 1:100,000 Quadrangle, Washington, Washington Division of Geology and Earth Sciences Resources Open-File Report 94-13*, 22 p; 1 plate.

Reidel, S. P. and K. R. Fecht, 1994b, *Geologic Map of the Richland 1:100,000 Quadrangle, Washington, Washington Division of Geology and Earth Sciences Resources Open-File Report 94-8*, 21 p; 1 plate.

Reidel, S. P. and P. R. Hooper (eds.), 1989, *Volcanism and Tectonism in the Columbia River Flood-Basalt Province*, Geological Society of America Special Paper 239, 386 p., 1 pl.

Reidel, S. P., G. R. Scott, D. R. Bazard, R. W. Cross, and B. Dick, 1984, *Post-12 Million Year Clockwise Rotation in the Central Columbia Plateau*, American Geophysical Union, Vol. 3, No. 2, pp. 251-273.

Reidel, S. P., K. A. Lindsey, and K. R. Fecht, 1992, *Field Trip Guide to the Hanford Site*, WHC-MR-0391, Westinghouse Hanford Company, Richland, Washington.

Reidel, S. P., N. P. Campbell, K. R. Fecht, and K. A. Lindsey, 1994, "Late Cenozoic Structure and Stratigraphy of South-Central Washington," in R. Lasmanis and E. S. Cheney

(conveners), *Regional Geology of Washington State, Washington Division of Geology and Earth Resources*, Bulletin 80, pp. 159-180.

Resource Conservation and Recovery Act of 1976, 42 USC 6901 et seq.

Rockhold, M. L., M. J. Fayer, G. W. Gee, and M. J. Kanyid, 1990, *Natural Ground-Water Recharge and Water Balance at the Hanford Site*, PNL-7215, Pacific Northwest Laboratory, Richland, Washington.

Rockhold, M. L., M. J. Fayer, C. T. Kincaid, and G. W. Gee, 1995, *Estimation of Natural Recharge for Performance Assessment of a Low-Level Waste Disposal Facility at the Hanford Site*, PNL-10508, Pacific Northwest Laboratory, Richland, Washington.

Rohay, V. J., 1994, *1994 Conceptual Model of the Carbon Tetrachloride Contamination in the 200 West Area at the Hanford Site*, WHC-SD-EN-TI-248, Westinghouse Hanford Company, Richland, Washington.

Rouston, R. C. and V. G. Johnson, 1988, *Recharge Estimates for the Hanford Site 200 Area Plateau*, WHC-SA-0393-FP, Westinghouse Hanford Company, Richland, Washington.

Rust, B. R., 1978, "A Classification of Alluvial Channel Systems, Fluvial Sedimentology," in A. D. Miall (ed.), *Lithofacies types and Vertical Profile Models in Braided River Deposits, A Summary, Fluvial Sedimentology*, Canadian Society of Petroleum Geologists Memoir 5, pp. 187-198.

Singleton, K. M. and K. A. Lindsey, 1994, *Groundwater Impact Assessment Report for the 216-U-14 Ditch*, WHC-EP-0698, Westinghouse Hanford Company, Richland, Washington.

Smith, G. A., 1988, *Neogene Synvolcanic and Syntectonic Sedimentation in Central Washington*, Geological Society of America Bulletin, Vol. 100, pp. 1479-1492.

Spane, F. A. Jr. and W. D. Webber, 1995, *Hydrochemistry and Hydrogeologic Conditions Within the Hanford Site Upper Basalt Confined Aquifer System*, PNL-10817, Pacific Northwest Laboratory, Richland, Washington.

SSC, 1978, *Final Report on a Seismic Reflection Field Testing Conducted in Benton County, Washington, Pasco Basin, Hanford Reservation, Basalt Waste Isolation Program*, Seismograph Service Corporation for Rockwell Hanford Operations, Richland, Washington.

SSC, 1979, *Final Report on a Seismic Reflection Survey Conducted in Benton and Grant Counties, Washington, Pasco Basin, Hanford Site, Basalt Waste Isolation Program*, B067305, Seismograph Service Corporation for Rockwell Hanford Operations, Richland, Washington.

SSC, 1980, *Final Report on a Seismic Reflection Survey Conducted in Benton County, Washington, FY-80 Program, Hanford Site, Basalt Waste Isolation Program*, B067306, Seismograph Service Corporation for Rockwell Hanford Operations, Richland, Washington.

Strait, S. R. and B. A. Moore, 1982, *Geohydrology of the Rattlesnake Ridge Interbed in the Gable Mountain Pond Area*, RHO-ST-38, Rockwell Hanford Operations, Richland, Washington.

Summers, W. K. and G. Schwab, 1977, *Drillers Logs of the Hanford Reservation*, ARH-C-16, Atlantic Richfield Hanford Company, Richland, Washington.

Summers, W. K. and P. A Weber, 1978, *Data for Wells Penetrating Basalt in the Pasco Basin Area, Washington*, RHO-BWI-C-19, Rockwell Hanford Operations, Richland, Washington.

Swanson, D. A, T. L. Wright, P. R. Hooper, and R. D. Bentley, 1979a, *Revisions in Stratigraphic Nomenclature of the Columbia River Basalt Group*, U.S. Geological Survey Bulletin 1457-G, 59 p.

Swanson, D. A, T. L. Wright, and I. Zietz, 1979b, *Aeromagnetic Map and Geologic Interpretation of the West-Central Columbia Plateau, Washington and Adjacent Oregon*, Open-File Report 76-51, Map GP-917, U.S. Geological Survey, Denver, Colorado.

Sweeney, M. D., D. J. Alexander, S. D. Evelo, K. A. Lindsey, V. M. Johnson, and K. M. Singleton, 1995, *Groundwater Impact Assessment Report for the 216-T1 Ditch*, WHC-EP-0814, Westinghouse Hanford Company, Richland, Washington.

Tallman, A. M., K. R. Fecht, M. C. Marratt, and G. V. Last, 1979, *Geology of the Separations Areas, Hanford Site, South-Central Washington*, RHO-ST-23, Rockwell Hanford Operations, Richland, Washington.

Tallman, A. M., J. T. Lillie, and K. R. Fecht, 1981, "Suprabasalt Sediments of the Cold Creek Syncline Area," in C. W. Myers and S. M. Price (eds.), *Subsurface Geology of the Cold Creek Syncline*, RHO-BWI-ST-14, Rockwell Hanford Operations, Richland, Washington.

Thorne, P. D. and D. R. Newcomer, 1992, *Summary and Evaluation of Available Hydraulic Property Data for the Hanford Site Unconfined Aquifer System*, PNL-8337, Pacific Northwest Laboratory, Richland, Washington.

Waters, A. C., 1961, "Stratigraphic and Lithologic Variations in the Columbia River Basalt," *American Journal of Science*, Vol. 259, No. 8, pp. 583-611.

Weekes, D. C., G. K. Jaeger, and B. H. Ford, 1995, *Preoperational Survey and Site Characterization Report for the Environmental Restoration Disposal Facility*, BHI-00270, Bechtel Hanford, Inc., Richland, Washington.

Weeks, D. C., S. P. Luttrell, and M. R. Fuchs, 1987, *Interim Hydrogeologic Characterization Report and Groundwater Monitoring System for the Nonradioactive Dangerous Waste Landfill, Hanford Site, Washington*, WHC-EP-0021, Westinghouse Hanford Company, Richland, Washington.

WCC, 1980, *Assessment of the Effects of Surfical Geologic Processes in the Pasco Basin, Final Report*, RHO-BW-CR-129P, Woodward-Clyde Consultants for Rockwell Hanford Operations, Richland, Washington.

WHC, 1990, *Interim Hydrologic Characterization Report for the 216-B-3 Pond*, WHC-SD-EU-002, Westinghouse Hanford Company, Richland, Washington.

WHC, 1992, *Groundwater Impact Assessment Report for the 400 Area Ponds*, WHC-EP-0587, Westinghouse Hanford Company, Richland, Washington.

WPPSS, 1974, *Preliminary Safety Analysis Report, Amendment 5, WPPSS Nuclear Project No. 2*, Washington Public Power Supply System, Richland, Washington.

WPPSS, 1981, *Final Safety Analysis Report, WPPSS Nuclear Project No. 2*, Washington Public Power Supply System, Richland, Washington.

WPPSS, 1986, *Final Safety Analysis Report, WPPSS Nuclear Project Nos. 1/4*, Washington Public Power Supply System, Richland, Washington.

APPENDIX A

DESCRIPTION OF VAM3DCG

A1.0 DESCRIPTION OF VAM3DCG

A1.1 INTRODUCTION

VAM3DCG is a three-dimensional, finite element code developed to simulate moisture movement and solute transport in variably saturated porous media. The code is capable of simulating a wide range of conditions commonly encountered in the field. Simulations can be performed efficiently for fully three-dimensional, two-dimensional, or axisymmetric problems. Both flow and transport simulations can be handled concurrently or sequentially. Material heterogeneities and anisotropy are handled by taking advantage of the finite element approach. Efficient matrix computational and solution schemes are employed in conjunction with simple rectangular prism elements or hexahedral orthogonal curvilinear elements, to analyze problems involving highly nonlinear, hysteretic/nonhysteretic soil moisture characteristics. Many types of boundary conditions can be accommodated:

- Water table conditions
- Atmospheric conditions associated with seepage faces (i.e., evaporation and nonponding infiltration)
- Water uptake by plant roots
- Vertical recharge of the water table
- Pumping and injection wells.

The model formulation used in VAM3DCG is a descendant of the formulation used in the FLAMINCO and VAM3DCG code presented by Huyakorn et al. (1986, 1987), and has been published by Panday et al. (1993). Where possible, the VAM3DCG code has been rigorously checked against available analytical or semianalytical solutions and similar numerical codes including UNSAT2, FEMWATER/FEMWASTE, SATURN, FLAMINCO, and VAM3DCG. A variety of field simulation problems described in the works of Huyakorn et al. (1984, 1985, 1987), Enfield et al. (1983), and Carsel et al. (1985) have been used to validate VAM3DCG and demonstrate its utility.

A1.2 OVERVIEW OF CODE CAPABILITIES AND SALIENT FEATURES

Multidimensional modeling of water flow and waste migration in variably saturated subsurface systems is a formidable task. Recognizing this point, VAM3DCG was developed to have not only essential modeling capabilities, but also salient features that facilitate practical use. The following is an overview of these code aspects.

- VAM3DCG can perform transient analyses or single-step, steady-state analyses of both variably saturated water flow and solute transport problems. If the flow and transport

problems are associated, a dual simulation can be performed by solving the problems concurrently or sequentially in a single computer run. (Feature used in model.)

- The finite element formulation and nonlinear solution procedures in VAM3DCG are based on the state-of-the-art technology designed to accommodate a wide range of field conditions, including highly nonlinear moisture characteristics, material heterogeneity and anisotropy, and rapidly fluctuating transient boundary conditions. (Feature used in model with the exception of transient boundary condition.)

- VAM3DCG uses highly efficient matrix computational and matrix solution techniques. The code is directly interfaced with iterative ORTHOMIN and Preconditioned Conjugate Gradient matrix solvers designed to efficiently handle large, sparse problems. (Feature used in model.)

- An orthogonal curvilinear mesh can be used with this version of VAM3DCG, which makes the code attractive for undulating layered systems, and is more capable of handling irregular boundaries, geometry, and material properties. (Feature used in model.)

- Transition elements have been provided with VAM3DCG for finer gradation of the grid in regions of interest with coarser gridding elsewhere. This allows for significant savings in grid points and the resulting computational memory and time. (Feature used in model.)

- Various matrix connectivity options are provided with this version of VAM3DCG which comprise the accuracy of the simulation for computational speed and storage. (Feature used in model.)

- The flow simulator of VAM3DCG can handle various boundary conditions and physical processes including infiltration, evaporation, plant root uptake, well pumping recharge, and varying water table conditions. Temporal variations of head and flux boundary conditions can be handled conveniently using either continuous piecewise linear representations or discontinuous (stepped) representations. Further, the pseudo-soil moisture relations are incorporated for use when the unsaturated zone moisture relations are unknown and moisture behavior above the water table is unimportant. (Pseudo-soil functions and changing head and flux boundary conditions used in model.)

- The transport simulator of VAM3DCG is designed to handle both conservative and nonconservative solutes. Its formulation is designed to have an upstream weighting capability as an option to circumvent numerical oscillations. Both steady and time-varying release of contaminants from each source can be simulated. (Feature used in model.)

A1.3 GOVERNING AND SUPPLEMENTARY EQUATIONS FOR VARIABLY SATURATED FLOW

To perform a variably saturated flow analysis, the VAM3DCG code uses the pressure head or the hydraulic head as the dependent variable if a rectangular grid is used. For an orthogonal curvilinear grid, the dependent variable is the hydraulic head. This is advantageous because it precludes the necessity of computing gradients in the elevation potential term. The governing mass balance for water flow in a variably saturated soil is calculated by Equation 1:

$$\frac{\partial}{\partial x_i}\left[\rho_w K_{ij} k_{rw} \left(\frac{\partial \psi}{\partial x_j} + e_j\right)\right] = \frac{\partial}{\partial t}\left(\rho_w \phi S_w\right) - \rho_w q \qquad (1)$$

where

P_w = density of water
ψ = pressure head
K_{ij} = saturated hydraulic conductivity tensor
k_{rw} = relative permeability with respect to the water phase
x_i (I = 1, 2, 3) are a set of orthogonal spatial coordinates
t = time
e_j = unit vector assumed to be vertically upward
S_w = water phase saturation
ϕ = effective porosity
q = volumetric flow rate via sources (or sinks) per unit volume of the porous medium.

The pressure head and hydraulic head h are related as $h = \psi + z$, where z is the vertically upward direction.

For a slightly compressible fluid, Equation 1 can be written in the form of Equations 2, 3, or 4 (Cooley 1971):

$$\frac{\partial}{\partial x_i}\left[K_{ij} k_{rw} \left(\frac{\partial \psi}{\partial x_j} + e_j\right)\right] = S_w S_s \frac{d\psi}{dt} + \frac{\phi dS_w}{dt} - q \qquad (2)$$

or

$$\frac{\partial}{\partial x_i}\left[K_{ij} k_{rw} \left(\frac{\partial \psi}{\partial x_j} + e_j\right)\right] = \eta \frac{\partial \psi}{\partial t} - q \qquad (3)$$

where η is a coefficient defined as

$$\eta = S_w S_s + \phi \frac{dS_w}{d\psi} \quad (4)$$

the coefficient S_s is defined as the specific storage in Equation 5 (Bear 1979)

$$S_s = \rho_w g (\phi\beta + \alpha) \quad (5)$$

where g is the gravitational constant, and α and β are coefficients of compressibility of the porous medium and water, respectively.

The off-diagonal components of the saturated conductivity tensor will be zero if the coordinate system coincides with the principal axes of anisotropy of the hydraulic conductivity (e.g., the x_1 and x_3 directions are parallel to the plane of stratification, and x_2 direction is normal to the plane of stratification). The initial and boundary conditions of the variably saturated flow problem are shown in Equations 6, 7, and 8:

$$\psi(x_i, 0) = \psi_o(x_i) \quad (6)$$

$$\psi(x_i, t) = \tilde{\psi} \quad on \ B_1 \quad (7)$$

and

$$V_i n_i = -V_n \ on \ B_2 \quad (8)$$

where

ψ_o = initial head value
B_1 = portion of the flow boundary where ψ is prescribed as $\tilde{\psi}$
V_i = Darcy velocity vector
B_2 = portion of the flow boundary where the outward normal velocity is prescribed as $-V_n$
n_i = outward unit normal vector.

The boundary and initial conditions are provided in terms of hydraulic head h instead of the pressure head ψ when the hydraulic head is the dependent variable.

The relationships of relative permeability versus water phase saturation are given by two alternative functional expressions in Equation 9 (Brooks and Corey 1966):

$$k_{rw} = S_e^{\,n} \tag{9}$$

and Equation 10 (van Genuchten 1976):

$$k_{rw} = S_e^{1/2}[1-(1-S_e^{1/\gamma})^{\gamma}]^2 \tag{10}$$

where n and γ are empirical parameters and S_e is effective water saturation defined as $S_e = (S_w - S_{wr})/(1-S_{wr})$ with S_{wr} being referred to as the residual water saturation.

The relationship of pressure head versus water saturation is described by Equation 11 (van Genuchten 1976; Mualem 1976):

$$\frac{S_w - S_{wr}}{1 - S_{wr}} = \begin{cases} \dfrac{1}{[1+(\alpha|\psi-\psi_a|)^{\beta}]^{\gamma}} & for \quad \psi < \psi_a \\ 1 & for \quad \psi \geq \psi_a \end{cases} \tag{11}$$

where

α and β = empirical parameters
ψ_a = air entry pressure head value
S_{wr} = residual water phase saturation.

The parameters β and γ are usually related by $\gamma = 1-1/\beta$.

Moisture retention and relative permeability characteristics for a given soil can be measured in the laboratory using Equations 9 and 10.

Equation 3 is solved numerically using the Galerkin finite element method subject to the initial and boundary conditions given in Equations 5 through 7. After the distributions of ψ (or h) and S_w have been determined, Darcy velocity components are calculated from Equation 12.

$$V_i = -K_{ij}k_{rw}\left(\frac{\partial\psi}{\partial x_j} + e_j\right) = -K_{ij}k_{rw}\frac{\partial h}{\partial x_j} \tag{12}$$

A1.4 TREATMENT OF HYSTERESIS AND ANISOTROPY

To simulate the effect of hysteresis in soil moisture properties in a variably saturated flow simulation, VAM3DCG incorporates the procedure described by Kool and Parker (1987). This procedure requires that the boundary wetting and drying curves in the $S_w(\psi)$ relation are known.

In VAM3DCG it is assumed that these boundary curves are described by expressions that have the same form as Equation 11 but with different parameter values for the wetting and drying boundary curves.

Using superscripts w and d to distinguish between wetting and drying, respectively, the boundary $S_w(\psi)$ curves are described by the following relationships in Equations 13 and 14:

$$\frac{S_w^w - S_{wr}}{S_{ws} - S_{wr}} = \begin{cases} \dfrac{1}{[1+(\alpha^w|\psi-\psi_a|)^{\beta^w}]^{\gamma^w}} & \psi < \psi_a \\ 1 & \psi \geq \psi_a \end{cases} \tag{13}$$

$$\frac{S_w^d - S_{wr}}{1 - S_{wr}} = \begin{cases} \dfrac{1}{[1+(\alpha^d|\psi-\psi_a|)^{\beta^d}]^{\gamma^d}} & \psi < \psi_a \\ 1 & \psi \geq \psi_a \end{cases} \tag{14}$$

In Equation 13, S_{ws} represents the maximum saturation value upon rewetting of an initially air-dry soil. If no air entrapment occurs, $S_{ws} = 1.0$. However, if air entrapment occurs, S_{ws} will be less than one. Parameters α, β, and γ are the van Genuchten curve shape parameters, with different values for wetting and drying. Note that α^w cannot be less than α^d:

$$\alpha^w \geq \alpha^d$$

Often, the following simplifications can be used (Kool and Parker 1987):

$$\beta^w = \beta^d = \beta$$
$$\gamma^w = \gamma^d = 1 - 1/\beta$$

With these simplifications, only four parameters are required to characterize the hysteretic saturation-pressure head relation. The parameters are the residual saturation, S_{wr}, and the shape parameters α^w, α^d, and β. If data are locking, $\alpha^w = 2\alpha^d$ may be used as a first approximation (Kool and Parker 1987). A typical hysteretic $S_w(\psi)$ relation is shown in Figure A-1. This figure illustrates the correspondence of the parameters in Equations 13 and 14 to the boundary wetting and drying curves.

In a hysteretic flow simulation, VAM3DCG automatically computes scanning curves in the $S_w(\psi)$ relation to determine the appropriate saturation path for every element in the modeled domain when reversals from wetting to drying, or vice versa occur. This is achieved by defining "pseudo" values of the residual and saturated values of S_w. In the simulation, these pseudo-values are substituted into Equations 13 and 14. This has the effect of scaling the boundary wetting and drying curves to make them pass through the reversal points. For a reversal from wetting to drying, the nominal value of 1.0 for S_w at saturation is replaced by Equation 15:

$$S_{ss}' = \frac{S_w^{rev} - S_{wr}\,[1 - S_e^{d}\,(\psi^{rev})]}{S_e^{d}\,(\psi^{rev})} \tag{15}$$

where S_w^{rev} and ψ^{rev} are saturation and pressure head at the reversal point, respectively, and $S_e^d\,(\psi^{rev})$ is effective drying saturation given by the left-hand side of Equation 14 for $\psi = \psi^{rev}$.

Analogously, for a reversal from drying to wetting, a pseudo-value for S_{wr} is used, which is given by Equation 16:

$$S_{wr}' = \frac{S_w^{rev} - S_e^{w}\,(\psi^{rev})}{1 - S_e^{w}\,(\psi^{rev})} \tag{16}$$

where S_e^w is effective wetting saturation corresponding to the left-hand side of Equation 13. The hysteresis subroutine in VAM3DCG checks whether each element is wetting or drying and computes the appropriate values of S_{ss}' and S_{wr}' for each element. This is achieved by means of an index variable, κ_i, which is set to $\kappa_i = +1$ if the I-th element is wetting and $\kappa_i = -1$ if the I-th element is drying. At the end of every time step, a check is made for every element to determine whether a reversal in the saturation path has occurred. A reversal occurs if

$$\frac{\bar{\psi}_i^{t-\Delta t} - \bar{\psi}_i^{t}}{\kappa_i} > \delta_\psi \tag{17}$$

where

δ_ψ = pressure head iteration convergence tolerance.
$\bar{\psi}_i$ = average nodal pressure head for the I-th element:

$$\bar{\psi}_i = \frac{1}{n_i} \sum_{j=1}^{n_i} \psi_{ij} \tag{18}$$

where n_i is the number of nodes for the element.

When a reversal occurs, the code determines the new scanning curve for the element that is subsequently used to calculate $S_w(\psi)$. An example of such scanning curves is shown in Figure A-2. In this example, the boundary hysteresis loop is closed at saturation; i.e., $S_{ws} = 1.0$. The figure shows a primary wetting scanning curve (1) and a secondary drying scanning curve (2). To completely specify the initial conditions for a hysteretic simulation, the user must specify

not only the initial nodal values of ψ, but also the initial saturation values for each element and whether the element is initially wetting or drying.

A1.5 TREATMENT OF VARIABLE UNSATURATED ANISOTROPY

Many natural soils and other geologic media exhibit some degree of stratification leading to anisotropy of hydraulic conductivity, with higher conductivity in the direction parallel to stratification than perpendicular to stratification. This anisotropy is usually expressed as a ratio (Equation 19a):

$$r = \frac{K_{11}}{K_{33}} = \frac{K_{22}}{K_{33}} \tag{19a}$$

where the indexes 1 and 2 indicate the directions parallel to stratification and 3 corresponds to the perpendicular direction. As expressed by Equation 19a, the anisotropy ratio is constant and independent of saturation. Recent research (e.g., Yeh et al. 1985; Mantoglou and Gelhar 1987; McCord et al. 1988) suggests that, in reality, the relative permeability k_{rw} may be subject to strong anisotropy. This research indicates that for unsaturated conditions, the hydraulic conductivity anisotropy is inversely related to the degree of water saturation. Assuming an exponential $k_{rw}(\psi)$ relation and using stochastic theory, Yeh et al. (1985) have developed the following expression (Equation 19b) for anisotropy as a function of pressure head for layered soils with a mean unit downward hydraulic gradient

$$r(\psi) = \frac{(Kk_{rw})_{11}}{(Kk_{rw})_{33}} = \frac{(Kk_{rw})_{22}}{(Kk_{rw})_{33}} = \exp\left[\frac{\sigma_f^2 + \sigma_a^2 \bar{\psi}^2}{1 + \mu\, \bar{a} \cos\omega}\right] \tag{19b}$$

where

σ_f^2 = variance of the log saturated conductivity
$(\ln K)\, a$ = slope of the $\ln(k_{rw})$ versus ψ curve
$\bar{a}$ = mean value of a
σ_a^2 = variance of $\bar{a}$
$\bar{\psi}$ = mean value of ψ
μ = spatial correlation length
ω = angle between the soil layer stratification and the horizontal.

Equation 19b indicates that anisotropy increases as an exponential function of the second power of pressure head. Following Equation 19b, anisotropy will also be more pronounced when the spatial variability of hydraulic conductivity increases and the correlation length, μ, decreases. The concept of variable anisotropy is based on mainly theoretical considerations; the predictive value of Equation 19b has not been extensively tested. Nevertheless, McCord et al. (1988) have experimentally observed patterns of water and solute plume migration in a hill slope infiltration

study that are similar to results obtained by computer simulation that incorporated Equation 19b to model variable anisotropy.

VAM3DCG has been modified to simulate the effect of saturation dependent anisotropy on unsaturated flow by using Equation 19b to evaluate anisotropy as a function of pressure head. This requires input values of the variables σ_f^2, σ_a^2, μ, and ω. The parameter $\bar{a}$ can be treated either as an input variable or be evaluated by VAM3DCG as the derivative of the $\ln[k_{rw}(\psi)]$ relation. When the latter option is used with Equations 9, 10, or pseudo-soil relative permeability functions to describe the $k_r(S_w)$ relation, the value of $\bar{a}$ will tend to decrease with decreasing saturation. This will magnify the predicted anisotropy compared to the case of a user-specified constant value for $\bar{a}$, up to a user-specified upper bound. A value of $r_{max} = 10^7$ has been found to give satisfactory results in many cases. Further, Equation 19b provides the conductivity ratio, but not the actual values of conductivities parallel and perpendicular to stratification. To obtain the desired monotonically decreasing $k_{rw}(\psi)$ relations, VAM3DCG uses an empirical logarithmic interpolation procedure to ensure that $(Kk_{rw})_{11}$, $(Kk_{rw})_{22}$, and $(Kk_{rw})_{33}$ decrease with decreasing pressure head and that the correct anisotropy ratio is maintained for any ψ value. An example anisotropic $k_{rw}(\psi)$ relation as modeled by VAM3DCG is shown in Figure A-3. This figure shows relative conductivity as a function of soil water pressure head. The solid curve represents the isotropic case in which conductivity is given by Equation 10. The dashed lines represent the anisotropic case with anisotropy ratio computed from Equation 19b. The following anisotropy parameters were used:

σ_f^2 = 0.82
σ_a^2 = 0.0005
μ = 40 cm
ω = 0.0.

Figure A-3 clearly illustrates the dramatic effect of tension (pressure head) variations on the magnitude of anisotropy.

A1.6 PSEUDO-SOIL FUNCTIONS FOR PREDICTING WATER-TABLE LEVELS

When the soil retention and relative permeability functions of a soil are unknown, and the unsaturated zone moisture behavior is unimportant to the simulated scenario, VAM3DCG uses pseudo-relations to predict the water-table levels. With this option, the code utilizes simple linear relations to account for changes in element saturated thickness and relative permeability as a result of the transient movement of the water table in the aquifer.

These linear pseudo-soil moisture relations are provided in Equation 20:

$$S_w = 1 - (|\bar{\psi} - \psi_s|)/b \geq 0.001 \quad (20)$$

and

$$k_{rw} = S_w$$

where

S_w = saturation of the element defined such that S_w=1 when the water table is above the top of the element
S_w ≈ 0 when the water table is below the bottom of the element
$\bar{\psi}$, = pressure head at the element centroid, which governs the pseudo-relation
b = average elemental thickness
ψ_s = b/2 is the pressure head scaling parameter.

The pseudo-relative permeability function ensures that the vertically integrated transmissivity of the element is adjusted to its saturated thickness as is done in the solution to the vertically integrated areal 2-D aquifer flow equations.

The following is a summary of the main advantages of the VSPS modeling approach:

- The VSPS approach is general, robust, and able to handle complex multilayer problems involving desaturation and resaturation of grid blocks (or drastic changes in the water table position).

- The VSPS approach is efficient and practical to use because of its fixed-grid formulation and linearized constitutive relations. No additional user input is required.

- The VSPS approach is a flexible modeling approach that can be simplified to that equivalent to the areal modeling approach by using a 3-D grid with two nodes on each vertical grid line or a single element covering the entire aquifer thickness. In such a case, vertical flow components are essentially neglected. On the other hand, the VSPS approach can be made rigorous by using a 3-D grid with multiple element subdivisions in the vertical direction, thus allowing proper account of vertical flow components, as well as accommodating the presence of seepage faces if desirable.

A1.7 ATMOSPHERIC BOUNDARY CONDITIONS

Atmospheric boundaries may correspond to soil-air interfaces where evaporation or infiltration occurs. They may also correspond to seepage faces through which water seeps from the saturated portion of the flow domain.

Along infiltration and evaporation boundaries, conditions may change from the Dirichlet (prescribed head) to the Neuman (prescribed flux) type.

In the absence of surface ponding, a numerical solution must be obtained by maximizing the absolute value of the flux (while maintaining the appropriate sign) subject to the following requirements in Equation 21 (Hanks et al. 1969; Neuman et al. 1974):

$$|v_i n_i| \leq |E_s^*|$$

and

$$\psi_L \leq \psi \leq 0 \tag{21}$$

where E_s^* is maximum potential surface flux under the prevailing atmospheric conditions and ψ_L is minimum pressure head allowed under the prevailing soil conditions.

For cases involving plant root uptake, the sink term in Equation 3 is represented by Equation 22 (Feddes et al. 1974):

$$q = K_{11} k_{rw} (\psi - \psi_r) b' \tag{22}$$

where ψ_r is root-pressure head, and b′ is the root-effectiveness function.

A1.8 GOVERNING EQUATIONS AND INITIAL AND BOUNDARY CONDITIONS FOR THE SOLUTE TRANSPORT MODEL

The governing equation for three-dimensional transport of a nonconservative component in a variably saturated soil takes the form in Equation 23 (Bear 1979).

$$\left(D_{ij} \frac{\partial c}{\partial x_j}\right) - \frac{\partial}{\partial x_i}(v_i c) = \frac{\partial}{\partial t}[\phi S_w c + \rho_s (1 - \phi) c_s] - q + \lambda [\phi S_w c + \rho_s (1 - \phi) c_s], \quad i \text{ or } j = 1, 2, 3 \tag{23}$$

where

D_{ij}	=	apparent hydrodynamic dispersion ensor
c	=	solute concentration in the fluid.
v_i	=	Darcy velocity
ρ_s	=	density of solid grains
c_s	=	adsorbed concentration

Assuming that the relation between adsorbed and solution concentration is described by a linear equilibrium isotherm, Equation 23 can be expressed as Equation 24:

$$(D_{ij}\frac{\partial c}{\partial x_j}) - \frac{\partial}{\partial x_i}(v_i c) = \frac{\partial}{\partial t}\left[\phi S_w\left(1 + \frac{\rho_s(1-\phi)k_d}{\phi S_w}\right) c\right] - q + \lambda\phi S_w\left[1 + \frac{\rho_s(1-\phi)k_d}{\phi S_w}\right] c \quad (24)$$

where k_d is the distribution coefficient.

Equation 24 reduces to

$$\frac{\partial}{\partial x_i}(D_{ij}\frac{\partial c}{\partial x_j}) - \frac{\partial}{\partial x_i}(v_i c) = \frac{\partial}{\partial t}(\phi S_w R c) + \lambda\phi S_w R c - q c^* \quad (25)$$

where R is the retardation factor defined as

$$R = 1 + \frac{\rho_s(1-\phi)k_d}{\phi S_w} = 1 + \frac{\rho_B k_d}{\phi S_w} \quad (26)$$

with the bulk density ρ_B being defined as $(1-\phi)\rho_s$. By expanding the convective and mass accumulation terms of Equation 25, using the continuity equation of fluid flow, and assuming that the time derivative of $(\rho_B k_d)$ is negligible, the equation reduces to the following:

$$\frac{\partial}{\partial x_i}(D_{ij}\frac{\partial c}{\partial x_j}) - v_i\frac{\partial c}{\partial x_i} = \phi S_w R\left(\frac{\partial c}{\partial t} + \lambda c\right) + q(c - c^*) \quad (28)$$

Note that the term q(c-c*) is zero for the case where q corresponds to the specific discharge of a pumped well because c ≡ c*. The hydrodynamic dispersion tensorial components are computed in Equation 29a using the following constitutive relations for homogeneous systems (Scheidegger 1961):

$$D_{ij} = \alpha_T |V| \delta_{ij} + (\alpha_L - \alpha_T)\frac{v_i v_j}{|V|} + \tau D^o \delta_{ij} \quad (29a)$$

$$D_{ij} = \alpha_T |V| \delta_{ij} + (\alpha_L - \alpha_T) \frac{v_i v_j}{|V|} + \tau D^o \delta_{ij} \quad (29a)$$

where

α_L and α_T	=	longitudinal and transverse dispersivities, respectively
δ_{ij}	=	Kronecker delta
D^o	=	bulk molecular diffusion coefficient
τ	=	tortuosity given by the Millington-Quirk (1961) equation as $\tau = S_w^{10/3} \phi^{4/3}$.

Alternatively, the hydrodynamic dispersion may be computed from the relations provided by Burnett and Frind (1987) for stratified porous media (the equation used for the predictions model):

$$D_{xx} = \alpha_L \frac{v_x^2}{|v|} + \alpha_T \frac{v_y^2}{|v|} + \alpha_v \frac{v_z^2}{|v|} + \tau D_o \quad (29b)$$

$$D_{yy} = \alpha_T \frac{v_x^2}{|v|} + \alpha_L \frac{v_y^2}{|v|} + \alpha_v \frac{v_z^2}{|v|} + \tau D_o \quad (29c)$$

$$D_{zz} = \alpha_T \frac{v_x^2}{|v|} + \alpha_v \frac{v_y^2}{|v|} + \alpha_L \frac{v_z^2}{|v|} + \tau D_o \quad (29d)$$

$$D_{xy} = D_{yx} = (\alpha_L - \alpha_T) v_x v_y / |v| \quad (29e)$$

$$D_{yz} = D_{zy} = (\alpha_L - \alpha_v) v_y v_z / |v| \quad (29f)$$

$$D_{zx} = D_{xz} = (\alpha_L - \alpha_v) v_z v_x / |v| \quad (29g)$$

where z is the index for the vertical direction.

Note that Equations 29b through 29g collapse to Equation 29a when $\alpha_v = \alpha_T$.

Equation 28 is the required form of the transport equation and will be approximated using the upstream weighted residual finite element technique of Huyakorn and Nilkuha (1979). The initial and boundary conditions associated with Equation 28 are as follows:

$$c(x_1, x_2, 0) = c_o \quad (30a)$$

$$D_{ij} \frac{\partial c}{\partial x_j} n_i = q_c^D \quad on \quad B_2' \tag{30c}$$

$$D_{ij} \frac{\partial c}{\partial x} n_i - v_i n_i c = q_c^I \quad on \quad B_3' \tag{30d}$$

where

B_1' = portion of the boundary where concentration is prescribed as
$\check{c}$, B_2' and B_3' = portions of the boundary where the dispersive and the total solute mass fluxes are prescribed as q_c^D and q_c^T, respectively.

A1.9 NUMERICAL TECHNIQUES FOR VARIABLY SATURATED FLOW

A1.9.1 Galerkin Formulation

Equation 3 is solved by the Galerkin finite element method. In the Galerkin procedure, the pressure head function is represented by a trial function of the form

$$\psi(x_i,t) = N_J(x_i)\ \psi_J(t), \qquad J = 1,2...,n \tag{31}$$

where

$N_J(x_i)$ and $\psi_J(t)$ = basis functions and nodal values of pressure head at time t, respectively
n = the number of nodes in the finite element network, and repeated indices imply nodal summation. Applying the Galerkin criterion to Equation 3 and transforming the second-order derivative term, the following can be obtained:

$$\int_R K_{ij}\, k_{rw} \frac{\partial N_I}{\partial x_i} \frac{\partial N_J}{\partial x_j} \psi_J\, dR + \int_R K_{ij}\, k_{rw} \frac{\partial N_I}{\partial x_i} e_j\, dR$$

$$+ \int_R \eta\, N_I\, N_J \frac{d\psi_J}{dt}\, dR - \int_B K_{ij}\, k_{rw} \left(\frac{\partial \psi}{\partial x_j} + e_j\right) N_I n_i\, dB$$

$$- \int_R N_I\, q\, dR = 0 \quad , \quad I = 1,2,...,n \tag{32}$$

where R is the solution domain with boundary B and n is the number of nodes in the finite element network.

Equation 32 can be written more concisely as

$$A_{IJ}\ \psi_J + B_{IJ}\ \frac{d\psi_J}{dt} = F_I \quad , \quad I = 1,2,...,n \tag{33a}$$

where

$$A_{IJ} = \sum_e \int_{R^e} k_{ij}\ k_{rw}\ \frac{\partial N_I}{\partial x_i}\ \frac{\partial N_J}{\partial x_j}\ dR \tag{33b}$$

$$B_{IJ} = \sum_e \int_{R^e} \eta\ N_I\ N_J\ dR \tag{33c}$$

$$F_I = \sum_e \left(\int_{R^e} - K_{ij}\ k_{rw}\ \frac{\partial N_I}{\partial x_i}\ e_j\ dR\right)$$

$$+ \int_R N_I\ q\ dR + \sum_e \left(\int_{B^e} V_n\ N_I\ dB\right) \tag{33d}$$

where R^e is the element subdomain with boundary B^e and V_n is the normal velocity at the boundary.

The sign convention for V_n is the same as for q. That is, V_n is positive for inward flow and negative for outward flow. A_{IJ} is the seepage influence matrix, B_{IJ} is the storage matrix and F_I represents all sources, sinks and other boundary conditions. The Galerkin approximation process is detailed in Huyakorn et al. (1984). The global coefficient matrices A_{IJ}, B_{IJ}, and F_{IJ} are assembled as a sum of the element matrices for a general eight-noded and 10-noded orthogonal curvilinear element shown in Figure A-4. The 10-noded element is the transition element that can be used to grade the grid within the domain. The nodes along the edges of the element (nodes 9 and 10 of Figure A-4) are the pinch nodes. Influence coefficient techniques presented by Huyakorn et al. (1984) and Huyakorn et al. (1986) for linear basis functions along the coordinate axis can be effectively used for assembling 8-noded prism elements to avoid integration of each of the elemental matrices. The seepage influence coefficients provide the appropriate connectivity for flow between the nodes of the element. The finite element structure of 27 points has a full nearest-neighbor connectivity, and the finite difference 7-point structure excludes all diagonal connectivity. The lattice structures for the various elemental connectivities are shown in Figure A-5. The influence coefficients for the 27-point lattice connectivity are

provided by Huyakorn et al. (1986, 1987), and the influence coefficients for the 7-point lattice structure are provided by Panday et al. (1992). Fully lumped or consistent mass matrix options are provided for the 27-point lattice connectivity. A fully lumped diagonalized mass matrix is used for the 7-point lattice. The finite difference connectivity of a 7-point lattice requires least computational effort for both matrix assembly and solution, and has the smallest global matrix structure. The finite element connectivity of 27 points requires maximum computational effort, with a global matrix structure almost four times larger.

The 10-noded curvilinear prism transition elements (see Figure A-4) are assembled into the matrix equation by considering two imaginary nodes 11 and 12 and developing the transition element influence coefficients as a combination of two 8-noded elements by static condensation. Due to the linear nature of the basis function between the nodes of an element along the local coordinate axis, the variables ψ_{11} and ψ_{12} at the imaginary nodes are eliminated from the two-element combination as

$$\psi_{11} = \frac{m_2}{m_T}\,\psi_2 + \frac{m_1}{m_T}\,\psi_3 = \alpha\,\psi_2 + \beta\,\psi_3 \tag{34a}$$

and

$$\psi_{12} = \frac{m_2}{m_T}\,\psi_6 + \frac{m_1}{m_T}\,\psi_7 = \alpha\,\psi_6 + \beta\,\psi_7 \tag{34b}$$

where

m_1, m_2 and m_T are length proportions of the transition element shown in Figure A-4, and the terms of the influence coefficient matrix for the 10-noded element are obtained by combining the influence coefficients of the two 8-noded subelements using Equations 34a and 34b to give

$$[a_{I,1},\ (a_{I,2} + \alpha\, a_{I,11}),\ (a_{I,3} + \beta\, a_{I,11}),\ a_{I,4},\ a_{I,5},$$

$$(a_{I,6} + \alpha\, a_{I,12}),\ (a_{I,7} + \beta\, a_{I,12}),\ a_{I,8},\ a_{I,9},\ a_{I,10}] = [A_{I,J}]^e \tag{34c}$$

$$for\ I = 1, \ldots 10.$$

Transition elements with pinch nodes on edges other than those shown in Figure A-4 are assembled by mapping their structure to that of Figure A-4, so that Equations 34a through 34c are applicable. It should be noted that when transition elements are present in a system, the lattice connectivity increases to 33, and 9 for the finite element and finite-difference lattices respectively.

A1.9.2 Picard and Newton-Raphson Schemes

Equations 33a through 33d represent a system of n nonlinear ordinary differential equations. Time integration of these equations is performed using implicit finite difference approximations. Two alternative nonlinear treatment procedures are provided in the code. The first scheme is a Picard scheme that leads to a system of algebraic equations with a symmetric coefficient matrix. The second scheme is a Newton-Raphson scheme that leads to a system of algebraic equations with an asymmetric coefficient matrix. Both schemes are discussed briefly in this section.

In the Picard scheme, Equations 33a through 33d are approximated by the following fully implicit equation:

$$A_{IJ}^{k+1}\ \psi_J^{k+1} + \frac{B_{IJ}^{k+1}}{\Delta t_k}\ (\psi_J^{k+1} - \psi_J^k) = F_I^{k+1} \quad , \quad I = 1,2,...,n \tag{35}$$

where ^{k} and $^{k+1}$ are previous and current time level, respectively, and Δt_k is t_{k+1}-t_k.

Equations 35 is now rearranged in the form

$$(A_{IJ}^{k+1} + \frac{B_{IJ}^{k+1}}{\Delta t_k})\ \psi_J^{k+1} = F_I^{k+1} + \frac{B_{IJ}^{k+1}}{\Delta t_k}\ \psi_j^k \tag{36}$$

which represents a symmetric matrix equation in view of the fact that both [A] and [B] are symmetric matrices. Nonlinear iterations are performed within each time step to achieve a stable numerical solution. For each iteration, the most recent nodal values ψ_I^{k+1} are used to calculate coefficient matrices and the right-hand side vector. The code uses backward difference time stepping combined with lumping (diagonalization) of storage matrix [B]. This proves to be advantageous for highly nonlinear situations where damping of oscillatory convergence behavior of the numerical solution is desirable. Central differencing of the temporal term and a consistent storage matrix assembly are also provided as options.

In the Newton-Raphson scheme, Equations 33a through 33d are replaced by the following integrated, fully implicit finite difference approximation:

$$G_I = A_{IJ}\ \psi_J^{k+1} + B'_{IJ}\ (\psi_J^{k+1} - \psi_J^k)/\Delta t_k$$

$$+ E_{IJ}\ (S_{wJ}^{k+1} - S_{wJ}^k)/\Delta t \quad = \quad 0,\ I=1,2...,n \tag{37}$$

where G_I = nonlinear (vector array) function of the nodal head values
B'_{IJ} and E_{IJ} =

$$B'_{IJ} = \int_R S_s\, S_w\, N_I\, N_J\, dR \tag{38a}$$

$$E_{II} = \int_R \phi N_I dR \quad and \quad E_{IJ\,(J\neq I)} = 0 \tag{38b}$$

Application of the Newton-Raphson procedure to Equation 37 yields the following (see Huyakorn and Pinder 1983):

$$G_I^{r+1} = G_I^r + \left(\frac{\partial G_I}{\partial \psi_J}\right)_r \Delta\psi_J^{r+1} = 0 \quad , \quad I=1,2,...,n \tag{39}$$

where r and r+1 denote previous and present iteration levels at the current time value, and $\Delta\psi_J^{r+1}$ is an iteration displacement vector defined as

$$\Delta\psi_J^{r+1} = \psi_J^{r+1} - \psi_J^r \tag{40}$$

and $(\partial G_I/\partial\psi_J)^r$ is the Jacobian of the Newton-Raphson iteration. Equations 38a through 38b can be written in the form

$$H_{IJ}^r\, \psi_J^{r+1} = H_{IJ}^r\, \psi_J^r - G_I^r \quad , \quad I=1,2,...,n \tag{41}$$

where H_{IJ} is $(\partial G_I/\partial\psi_J)^r$.

Because [H] is an asymmetric matrix, Equation 41 represents an asymmetric matrix equation. As in the Picard scheme, it is necessary to perform nonlinear iterations within the time step to achieve a converged numerical solution. Iterations are performed until the successive change in head values are within prescribed tolerance limits. VAM3DCG utilizes automatic time-step reduction and underrelaxation procedures to handle convergence difficulties.

A1.9.3 Matrix Solution Techniques

For a fully three-dimensional analysis, the system of algebraic equations resulting from the finite element approximation of the flow equation needs to be solved using an efficient matrix solver to obtain cost-effective simulations of realistic field problems.

The Preconditioned Conjugate Gradient (PCG) method (see Kershaw 1978) has emerged as one of the most promising iterative methods for solving large sparse matrix equations generated by finite element (or finite difference) approximations of multidimensional field problems. There have been a number of recent papers describing successful conjunctive applications of PCG and finite element or finite difference method to groundwater flow problems. These include the

publications by Gambolati (1980); Kuiper (1981, 1987); Gambolati et al. (1986); Kalf (1988); and Meyer et al. (1989).

The symmetric PCG solver implemented into VAM3DCG is based on a two-step procedure developed by Meijerink and van der Vorst (1977) and extended and implemented by Kershaw (1978) and Anderson (1983). It is used in VAM3DCG to solve the system of algebraic equations resulting from the Picard scheme of the finite element flow formulation. The first step of this PCG algorithm involves preconditioning of the finite element coefficient matrix A of a general symmetric matrix system Ax = y by computing an incomplete triangular Cholesky decomposition (LDL^T) of A. The second step involves conjugate gradient iterations on an initial guess x^o of the vector x. The CG recursive equations are as follows:

Let

$$K \equiv (LDL^T) \tag{42a}$$

$$r^o = y - Ax^o \tag{42b}$$

$$p^o = K^{-1} r^o \tag{42c}$$

$$q^o = Ap^o$$

Then

I = 0,1,2,...

$$\alpha_i = (r^i, K^{-1} r^i)/(p^i, q^i) \tag{43}$$

$$x^{i+1} = x^i + \alpha_i p^i \tag{44}$$

$$r^{i+1} = r^i - \alpha_i q^i \tag{45}$$

$$\beta_i = (r^{i+1}, K^{-1} r^{i+1})/(r^i, K^{-1} r^i) \tag{46}$$

$$p^{i+1} = K^{-1} r^{i-1} + \beta_i p^i \tag{47}$$

$$q^{i+1} = M p^{i+1} \tag{1.46}$$

This scheme is repeated until the L_2 norm of the head error is less than a prescribed tolerance criterion.

In a case where the nonlinear variably saturated flow problem is treated using the Newton-Raphson technique, the resulting finite element matrix system is asymmetric. For such a case,

VAM3DCG uses the asymmetric PCG/ORTHOMIN algorithms described later in Section 1.10.2. If VAM3DCG is implemented in a 2-D mode, a banded direct solver is used.

A1.10 NUMERICAL TECHNIQUE FOR SOLUTE TRANSPORT

A1.10.1 Upstream Weighted Residual Formulation

For the contaminant transport simulation, VAM3DCG solves Equation 25 for single-species transport using an upstream weighted residual finite element method.

To illustrate the application of the technique, consider Equation 25 and a trial solution for concentration be written in the following form:

$$c(x_i, t) = N_J(x_i) c_J(t) \tag{48}$$

where $N_J(x_i)$ and $c_J(t)$ are basis functions and nodal values of concentration at time t, respectively.

In the upstream weighted residual technique, the weighted residual integral equation is obtained using asymmetric (upstream) weighting functions (Huyakorn and Nilkuha 1979) to weight the spatial derivative terms of the transport equation, and the standard basis functions to weight the remaining mass accumulation term. Application of this procedure to Equation 25 yields

$$\int_R W_I \left[\frac{\partial}{\partial x_i} \left(D_{ij} \frac{\partial c}{\partial x_j} - v_i \frac{\partial c}{\partial x_i} \right) \right] - \int_R N_I \left[\phi s_w R \left(\frac{\partial c}{\partial t} + \lambda c \right) + q (c - c*) \right] dR = 0 \tag{49}$$

where W_I is upstream weighting functions.

Using Green's theorem to remove the second derivative and substituting for c, the following is obtained:

$$\int_R \left(D_{ij} \frac{\partial W_I}{\partial x_i} \frac{\partial N_J}{\partial x_j} + v_i W_I \frac{\partial N_J}{\partial x_i}\right) c_J \, dR$$

$$\int_R \phi S_w R N_I N_J \left(\frac{dc_J}{dt} + \lambda c_J\right) dR + \int N_I q (c^* - N_J c_J) \, dl \qquad (50)$$

$$- \int_B W_I \left(D_{ij} \frac{\partial c}{\partial x_j}\right) n_i \, dB = 0$$

Equation 25 can be expressed in the form

$$(E_{IJ} + B^*_{IJ}) c_J + \tilde{B}_{IJ} \frac{dc_J}{dt} = \tilde{F}_I \qquad (51)$$

where

$$\tilde{F}_I = - \int_R N_I q (c^* N_J c_J) \, dR + \int_B W_I \left(D_{ij} \frac{\partial c}{\partial x_j}\right) n_i \, dB$$

$$E_{ij} = \int_R \left(D_{ij} \frac{\partial W_I}{\partial x_i} \frac{\partial N_J}{\partial x_j} + v_i W_I \frac{\partial N_J}{\partial x_i}\right) dR$$

$$\tilde{B}_{IJ} = \int_R (\phi S_W R) N_I N_J \, dR$$

$$B^*_{IJ} = \int_R (\lambda \phi S_W R) N_I N_J \, dR$$

Once all of the element matrices have been computed and assembled into global matrices, the system of ordinary differential Equation 51 can be integrated with respect to time. This leads to the following system of algebraic equations

$$\left(E_{IJ} + B^*_{IJ}\right) + \frac{\tilde{B}_{IJ}}{\Delta t_k}\Bigg] c_J^{k+1} = (\omega - 1)\left(E_{IJ} + B^*_{IJ}\right) c_J^k + \frac{\tilde{B}_{IJ}}{\Delta t_k} c_j$$

$$+ \omega \tilde{F}_I^{k+1} + (1-\omega) \tilde{F}_I^k \qquad (52)$$

where ω is the time-weighting factor.

Equation 69 can be rearranged in the following form:

$$G_{IJ}\, c_J^{k-1} = R_I^{k+1} \tag{53}$$

where

$$R_I^{k+1} = (\omega-1)\,(E_{IJ} + B_{IJ}^{*})\, c_J^{k} + \frac{\tilde{B}_{IJ}}{\Delta t_k}\, c_J^{k} + \omega\, \tilde{F}_I^{k+1} + (1-\omega)\, \tilde{F}_I^{k} \tag{54a}$$

and

$$G_{IJ} = \omega(E_{IJ} + B_{IJ}^{*}) + \tilde{B}_{IJ} / \Delta t_k \tag{54b}$$

To obtain a second-order accuracy in time approximation, ω is chosen to be 0.5, thus yielding the Crank-Nicholson time-stepping scheme. Equation 53 represents a system of linear algebraic equations with an asymmetric-banded coefficient matrix; its solution is achieved by using either a direct solver (for two-dimensional simulations) or the ORTHOMIN solver.

The finite element and finite difference lattice connectivity options are provided for the transport equation as well. The 27-point lattice connectivity values for the various influence coefficient matrices are discussed in Huyakorn et al. (1985, 1986), and the influence coefficient formulas for the 7-point lattice connectivity are provided by Panday et al. (1992). Influence coefficient matrices for the 10-noded transition elements of the transport equation are assembled in an identical manner to the 10-noded transition elements of the flow equation, with c replacing ψ in Equations 34a through 34c. A consistent mass matrix is used for the 27-point lattice connectivity and a fully-lumped matrix is generated for the 7-point lattice. In addition, all cross terms of the dispersive matrix are incorporated into the right-hand side vector in an explicit manner for the 7-point connectivity. Fully implicit and Crank-Nicholson options for time discretization provide for the alternatives of higher stability or a higher order of accuracy.

A1.10.2 Matrix Solution Techniques

In a full three-dimensional analysis, the system of algebraic equations resulting from the finite element approximation of the transport equation is solved efficiently using an iterative solver for an asymmetric coefficient matrix. The ORTHOMIN scheme presented by Behie and Winsome (1982) is well suited for these matrices and is guaranteed to converge for an M matrix. The ORTHOMIN procedure may be considered as another variant of the standard preconditioned

conjugate gradient procedure described in Section 1.9.3; their formulations are similar. The full ORTHOMIN procedure is provided in the following.

Let M be approximated by K ≡ LU. Starting with n = 0, the residual vector r^o is first evaluated as

$$r^o = y - Mx^o \tag{55}$$

Then for n = 0,1,2..., the following computation is made:

$$v^{n+1} = K^{-1} r^n \tag{56a}$$

$$p^{n+1} = v^{n+1} - \sum_{i=1}^{n} a_i^{n+1} p^i \tag{56b}$$

$$q^{n+1} = Mp^{n+1} \tag{56c}$$

$$x^{n+1} = x^n + \omega^{n+1} p^{n+1} \tag{56d}$$

and

$$r^{n+1} = r^n - \omega^{n+1} q^{n+1} \tag{56e}$$

where

$$a_i^{n+1} = (q^i, Mv^{n+1}) / (q^i, q^i) \tag{56f}$$

and

$$\omega^{n+1} = (r^n, q^{n+1}) / (q^{n+1}, q^{n+1}) \tag{56g}$$

The orthogonalizations are restarted after NORTH times, where NORTH is prescribed by the user.

A2.0 REFERENCES

Anderson, D. V., 1983a, "Subprograms for the Solution of a Linear Asymmetric Matrix Equation Arising from a 7-, 15-, 19-, or 27-point 3D Discretization," in *Computer Physics Communications*, Vol. 30, pp. 43-49.

Anderson, D. V., 1983b, "Subprograms for the Solution of a Linear Symmetric Matrix Equation Arising from a 7-, 15-, 19-, or 27-point 3D Discretization," in *Computer Physics Communications*, Vol. 30, 51-57.

Brooks, R. H., and A. T. Corey, 1966, "Properties of Porous Media Affecting Fluid Flow," *American Society of Chemical Engineers Journal*, Vol. 92, pp. 61-88.

Burnett, R. D., and E. O. Frind, 1987, "Simulation of Contaminant Transport in Three Dimensions, "Two Dimensionality Effects," *Water Resources Research*, Vol. 23, No. 4, pp. 695-705.

Carsel, R. F., L. A. Mulkey, M. N. Lorber, and L. B. Baskin, 1985, "The Pesticide Root Zone Model (PRZM): A Procedure for Evaluating Pesticide Leaching Threats to Groundwater," *Ecological Modeling*, Vol. 30, pp. 49-69.

Cooley, R. L., 1971, "A Finite Difference Method for Unsteady Flow in Variably Saturated Porous Media: Application to a Single Pumping Well," *Water Resources Research*, Vol. 7, No. 6, pp. 1607-1625.

Feddes, R. A., E. Bresler, and S. P. Neuman, 1974, "Field Test of a Modified Numerical Model for Water Uptake by Root Systems," *Water Resources Research*, Vol. 10, No. 6, pp. 1199-1206.

Gambolati, G., 1980, "Fast Solution to Finite Element Flow Equations by Newton Iteration and Modified Conjugate Gradient Method," *Int. J. Numer. Meth. Engng.*, Vol. 15, pp. 661-675.

Gambolati, G., F. Sartoretto, and F. Uliana, 1986, "A Conjugate Gradient Finite Element Model of Flow for Large Multiaquifer Systems," *Water Resources Research*, Vol. 22, No. 7, pp. 1003-1015.

Hanks, R. J., A. Klute, and E. Bresler, 1969, "A Numeric Method for Estimating Infiltration, Redistribution, Drainage, and Evaporation of Water from Soil," *Water Resources Research*, Vol. 5, No. 5, pp. 1064-1069.

Huyakorn, P. S., and K. Nilkuha, 1979, "Solution of Transient Transport Equation Using an Upstream Finite Element Scheme," *Applied Mathematical Model*, Vol. 3, pp. 7-17.

Huyakorn, P. S., S. D. Thomas, and B. M. Thompson, 1984, "Techniques for Making Finite Elements Competitive in Modeling Flow in Variably Saturated Porous Media," *Water Resources Research*, Vol. 20, No. 8, pp. 1099-1115.

Huyakorn, P. S., J. W. Mercer, and D. S. Ward, 1985, "Finite Element Matrix and Mass Balance Computational Schemes for Transport in Variably Saturated Porous Media," *Water Resources Research*, Vol. 21, No. 3, pp. 346-358.

Huyakorn, P. S., E. P. Springer, V. Guvanasen, and T. D. Wadsworth, 1986, "A Three-Dimensional Finite Element Model for Simulating Water Flow in Variably Saturated Porous Media," *Water Resources Research*, Vol. 22, No. 12, pp. 1790-1808.

Huyakorn, P. S., P. F. Andersen, J. W. Mercer, and H. O. White, Jr., 1987, "Saltwater Intrusion in Aquifers: Development and Testing of a Three-Dimensional Finite Element Model," *Water Resources Research*, Vol. 23, No. 2, pp. 293-312.

Kershaw, D. S., 1978, "The Incomplete Cholesky-Conjugate Gradient Method for the Iterative Solution of Systems of Linear Equations," *J. Comp. Physics*, Vol. 26, pp. 43-65.

Kool, J. B., and J. C. Parker, 1987, "Development and Evaluation of Closed-Form Expressions for Hysteretic Soil Hydraulic Properties," *Water Resources Research*, Vol. 23, pp. 105-114.

Kuiper, L. K., 1981, "A Comparison of the Incomplete Cholesky-Conjugate Gradient Method with the Strongly Implicit Method as Applied to the Solution of Two-Dimensional Groundwater Flow Equations," *Water Resources Research*, Vol. 17, No. 4, pp. 1082-1086.

Kuiper, L. K., 1987, "A Comparison of Iterative Methods as Applied to the Solution of the Nonlinear Three-Dimensional Groundwater Flow Equation," *SIAM J. Sci. Stat. Comput.*, Vol. 8, No. 4, pp. 521-528.

McCord, J. T., D. B. Stephens, and J. L. Wilson, 1988, "Field Experiments and Numerical Simulations of Unsaturated Flow and Transport: The Roles of Hysteresis and State-Dependent Anisotropy," Proc. Nato Advanced Study Institute on Recent Advances in Modeling Hydrologic Systems, Sintra, Portugal, July 9-23.

Meijerink, J. A. and H. A. van der Vorst, 1977, "An Iterative Solution Method for Linear Systems of Which the Coefficient Matrix Is a Symmetric Matrix," *Math. of Comp.*, Vol. 31, No. 137, pp. 148-162.

Meyer, P. D., A. J. Valocchi, S. F. Ashby, and P. E. Saylor, 1989, "A Numerical Investigation of the Conjugate Gradient Method as Applied to Three-Dimensional Groundwater Flow Problems in Randomly Heterogeneous Porous Media," in press, *Water Resources Research*, Technical Note.

Montaglou, A., and L. W. Gelhar, 1987, Effective Hydraulic Conductivities of Transient Unsaturated Flow in Stratified Soils," *Water Resources Research*, Vol. 23, pp. 57-68.

Mualem, Y., 1976, "A New Model for Predicting the Hydraulic Conductivity of Unsaturated Porous Media," *Water Resources Research*, Vol. 12, No. 3, pp. 513-522.

Neuman, S. P., R. A. Feddes, and E. Bresler, 1974, "Finite Element Simulation of Flow in Saturated-Unsaturated Soils Considering Water Uptake by Plants," *Hydrodynamics and Hydraulic Engineering Laboratory Report for Project No. ALO-SWC-77*, Haifa, Israel.

Panday, S., P. S. Huyakorn, R. Therrien, and R. L. Nichols, 1993, "Improved Three-Dimensional Finite-Element Techniques for Field Simulation of Variably Saturated Flow and Transport," *Journal of Contaminant Hydrology*, Vol. 12, pp. 3-33.

Scheidegger, A. E., 1961, "General Theory of Dispersion in Porous Media," *J. Geophys.*, Res., v. 66, pp. 3273 - 3278.

van Genuchten, M. Th., 1980, "A Closed-Form Equation for Predicting the Hydraulic Conductivity of Unsaturated Soils," *Soil Science Society of American Journal*, Vol. 44, pp. 892-898.

Yeh, T. C. J., L. W. Gelhar, and A. L. Gutjahr, 1985, "Stochastic Analysis of Unsaturated Flow in Heterogeneous Soils 2. Statistically Anisotropic Media with Variable α," *Water Resources Research*, Vol. 21, pp. 457-464.

Figure A-1. Example of Hysteric S_w (Ψ) Relation Showing the Boundary Wetting and Drying Curves.

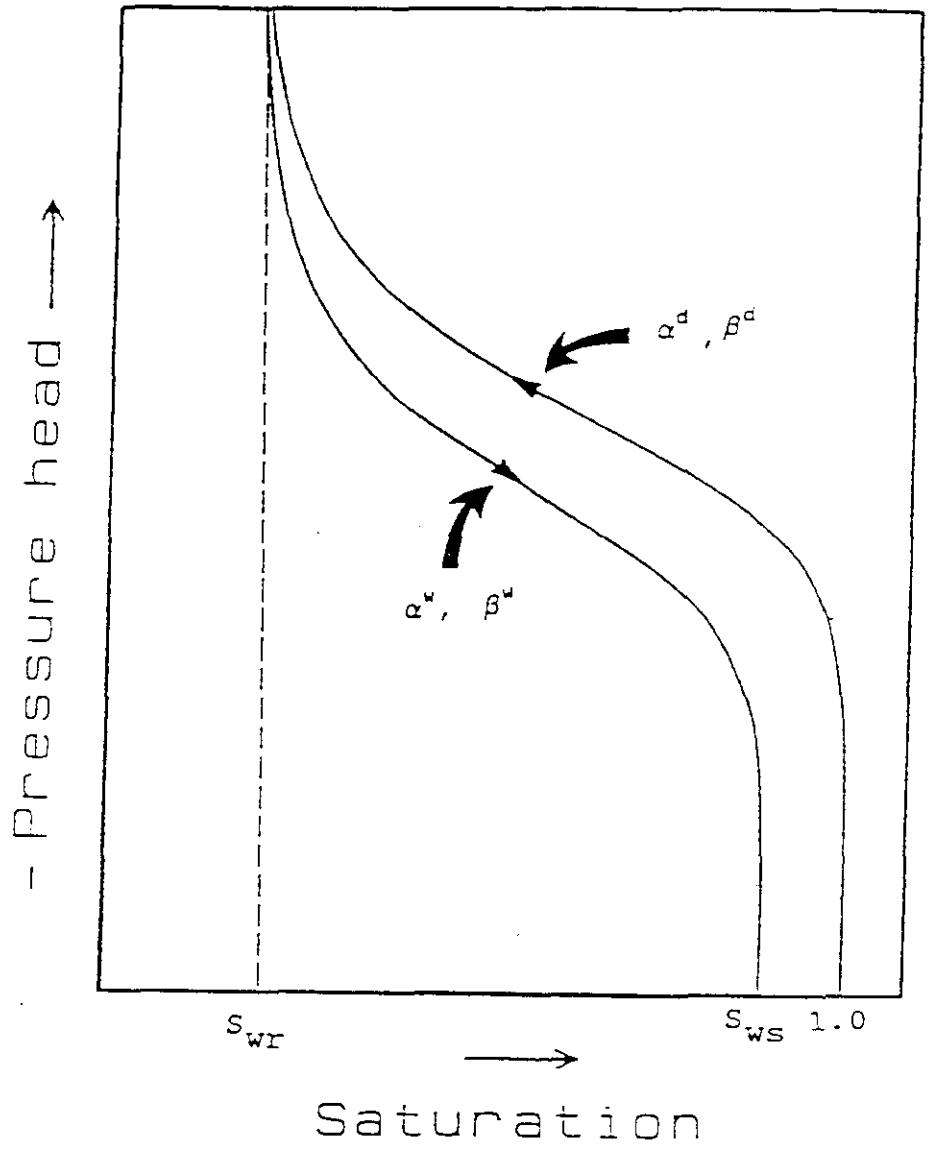

Figure A-2. Typical Scanning Curves Produces by the Hysteresis Model in VAM3DCG.

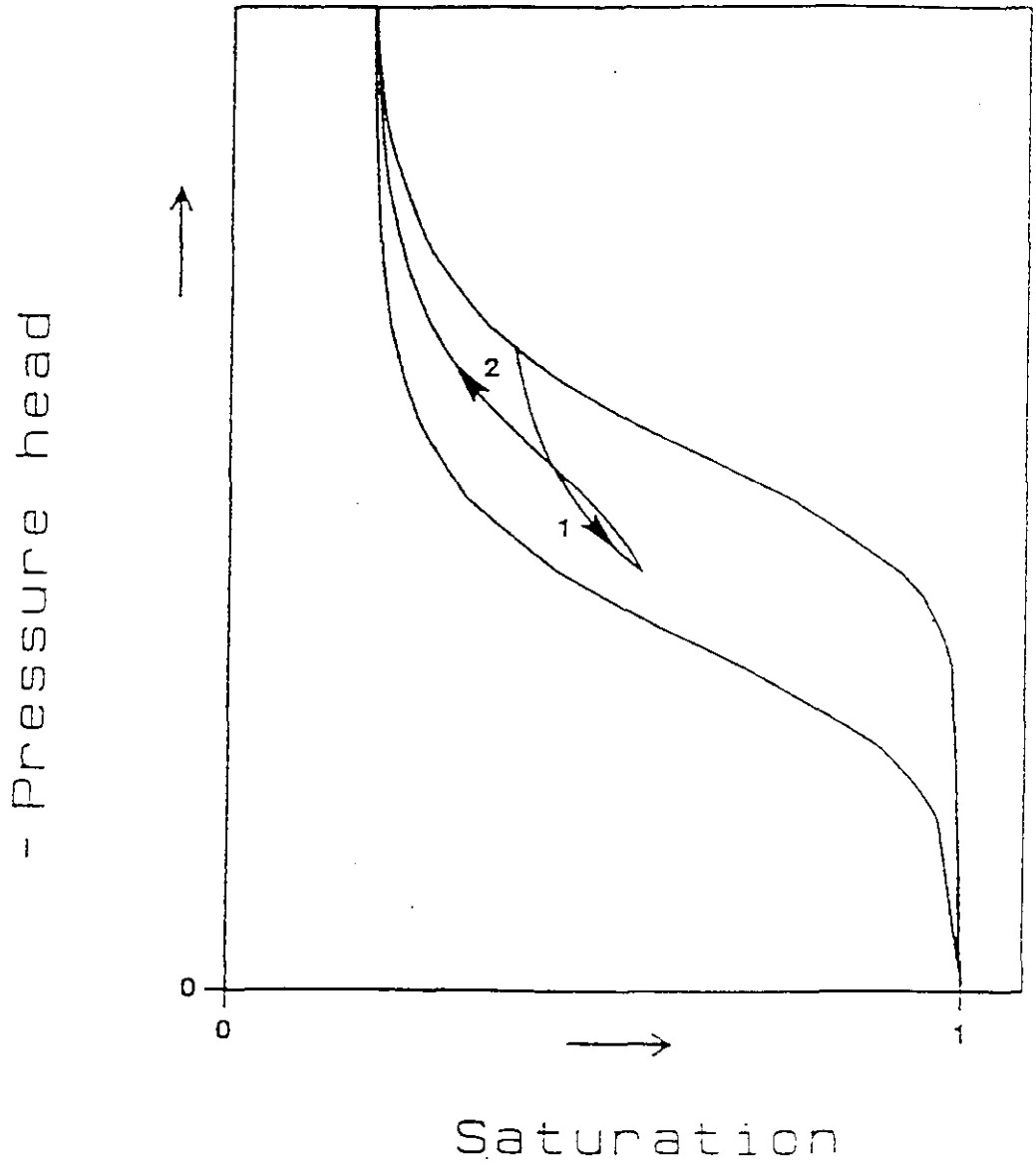

Note: Curve 1 denotes primary wetting scanning curve; and curve 2 denotes secondary drying scanning curve.

Note: Curve 1 denotes primary wetting scanning curve; and curve 2 denotes secondary drying scanning curve.

Figure A-3. Example of Anisotropic k_{rw} (Ψ) Relation as Modeled by VAM3DCG.

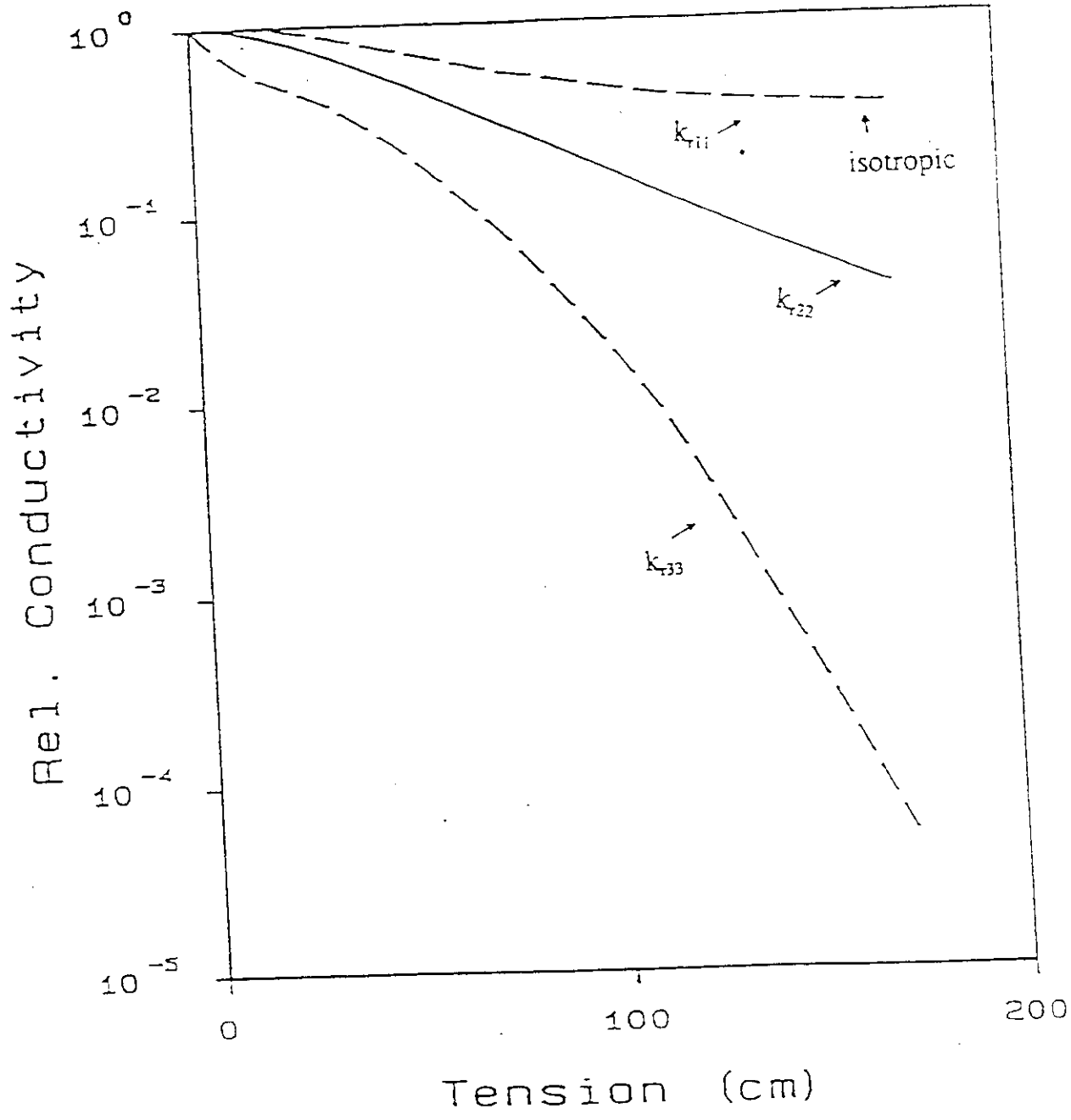

Figure A-4. Types of Elements Used by VAM3DCG.

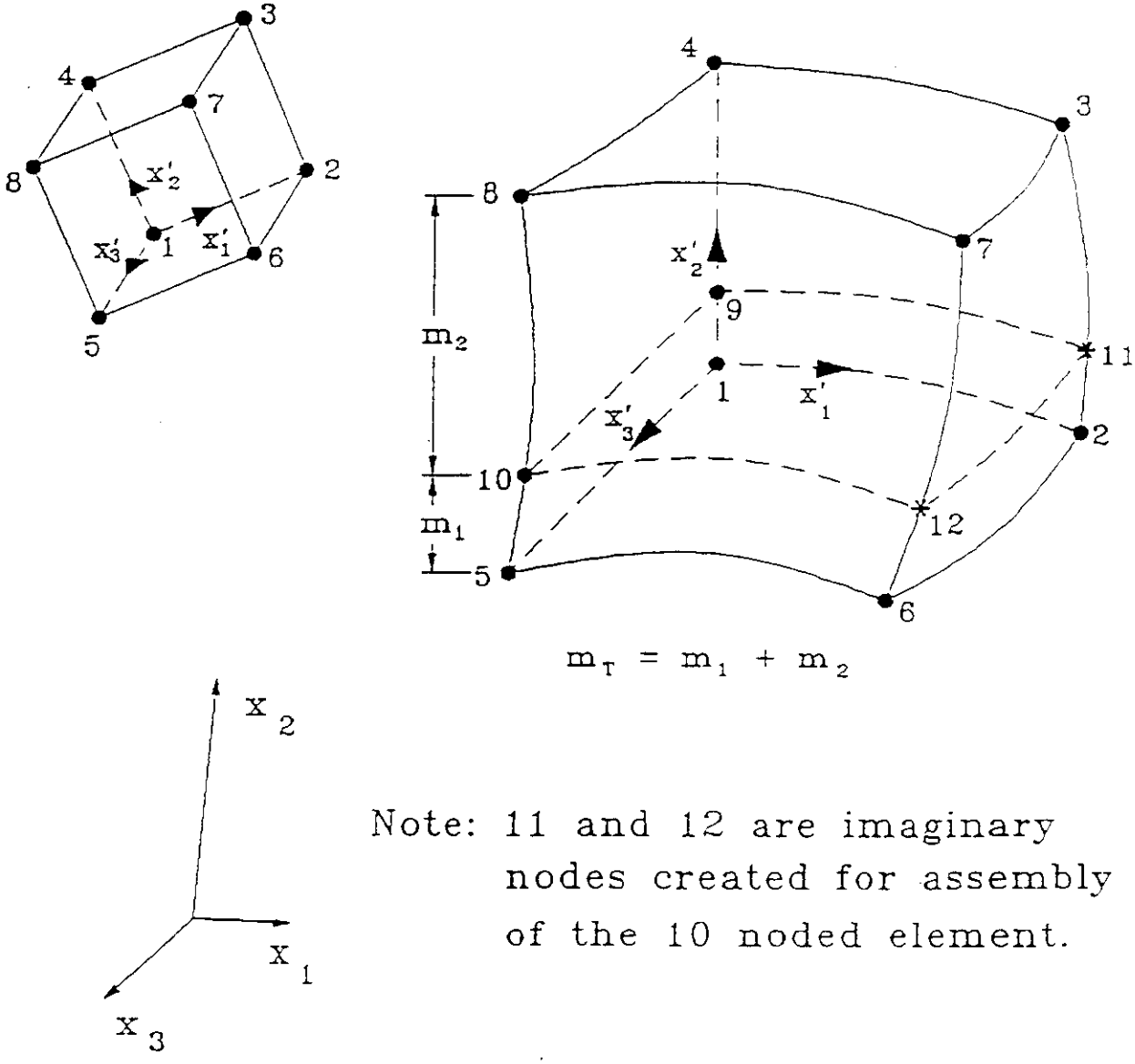

Note: 11 and 12 are imaginary nodes created for assembly of the 10 noded element.

Figure A-5. Elemental Lattice Connectivity Structures Used by VAM3DCG.

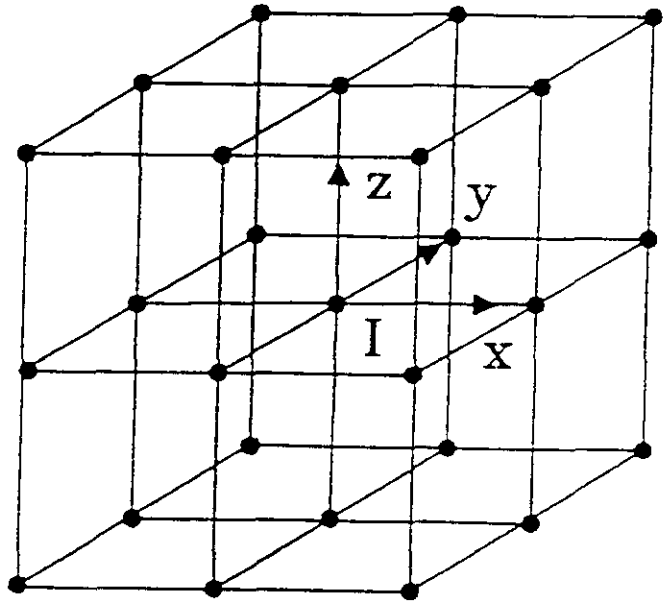

27 point lattice

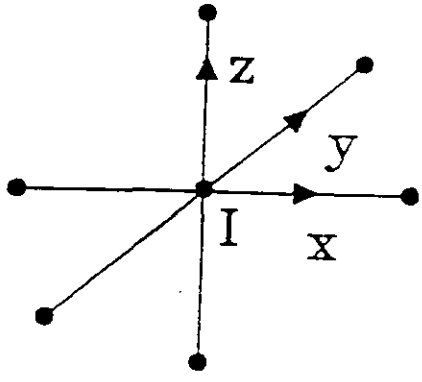

7 point lattice

APPENDIX B

MODEL SENSITIVITY ANALYSIS

B.0 SENSITIVITY ANALYSIS

Sensitivity analyses were performed by varying a parameter (or set of parameters) from the calibrated base case to observe the change in flow and transport behavior. The objective of the analysis is to determine the effects of several modeling assumptions and to identify critical parameters and mechanisms governing flow and transport under the site. Flow and transport parameters studied were as follows:

- Hydraulic conductivity
- Hydrostratigraphy
- Tritium decay
- Dispersivity.

The model sensitivity to different parameters is investigated for water levels and fluxes, as well as influences on the tritium plume.

B.1 HYDRAULIC CONDUCTIVITY SENSITIVITY

Two scenarios were evaluated to determine the model sensitivity to different hydraulic conductivity. The first scenario examines the effects of doubling the hydraulic conductivity for all material layers. The second evaluates the effects of doubling the hydraulic conductivity for the pre-Missoula/Hanford formation materials only.

B.1.1 Sensitivity to Higher Hydraulic Conductivity in All Materials

The model sensitivity to higher hydraulic conductivity was examined to determine the effects on groundwater flow and tritium transport. To perform this assessment, the hydraulic conductivity was doubled for all materials in the model domain. The effects of higher hydraulic conductivity were examined under both steady-state and transient flow conditions. All other material zone properties remained unchanged.

Water table levels for the steady-state flow simulation with doubled hydraulic conductivity are presented in Figure B-1. Evident from this plot is that the groundwater mound in the 200 West Area is not present and water levels in the eastern portion of the domain are slightly lower. There is no impact to the flux into or out of the model as the recharge boundaries along Cold and Dry Creeks are set to constant flux. However, if the sensitivity analysis is conducted on the pre-calibration simulation with the recharge boundaries set as constant head, the recharge to the system is changed from 0.12 m^3/sec (4.3 ft^3/sec) to 0.62 m^3/sec (22 ft^3/sec) for Cold Creek and from 0.47 m^3/sec to 0.96 m^3/sec (16.6 ft^3/sec to 34 ft^3/sec) for Dry Creek. Discharge to the Columbia River is changed from 1.47 m^3/sec to 2.72 m^3/sec (51.9 ft^3/sec to 96 ft^3/sec).

Water levels for transient simulation yr 9 and 14 (1988 and 1993) are shown in Figures B-2 and B-3. The water levels also are much lower than for the base case simulations and similar to the

'steady' state sensitivity simulation, except for the B Pond mound east of 200 East Area. No change in water levels north of Gable Mountain was observed.

Tritium concentration distributions after 9 and 14 yr of simulation are shown in Figures B-4 and B-5, respectively. The tritium plume lobes in both the eastern and eastern portion of the model have moved faster than for the base case. The 200,000-pCi/L contour has moved only slightly further eastward than for the base case, even with doubled conductivities, due to the dominant effect of decay (see Section B.3).

B.1.2 Sensitivity to Higher Hydraulic Conductivity in the Pre-Missoula/Hanford Unit

This sensitivity analysis case examines the effect of doubling only the hydraulic conductivity of the more conductive pre-Missoula/Hanford formation. All other base case model conditions were unchanged. Water levels for the 1979 steady-state simulation are shown in Figure B-6. Heads in the Cold Creak recharge area are about 3 m (10 ft) lower than for the base case. However, immediately to the east in 200 West Area, the water levels are similar to the base case simulation. This is because the Ringold Formation is the only saturated unit in this area, and changing the hydraulic conductivity in the pre-Missoula/Hanford formation has no effect on water levels. However, further east where the pre-Missoula/Hanford formation becomes saturated, water levels are significantly lower, and even lower than for the sensitivity case where the hydraulic conductivity for both units was increased. Figures B-7 and B-8 show water table levels after 9 and 14 yr of transient simulation. These water levels also are lower than base case values as well as those in the previous sensitivity study presented in Section 4.1.1.

Transient simulation results for tritium are shown in Figures B-9 and B-10. These figures show tritium concentrations after 9 and 14 yr of simulation. The tritium plume in the western portion of the modeled domain is similar to the base case. The plume in the central and eastern portions of the domain, in particular the 200,000-pCi/L concentration contour, has traveled farther than for the base case, although slightly less than for the sensitivity analysis where conductivity values were doubled for both units. This demonstrates that both groundwater flow and contaminant transport are sensitive to hydraulic conductivity.

B.2 SENSITIVITY TO HYDROGEOLOGIC UNIT CONTACT

The model sensitivity to the vertical position of the contact between the Ringold Formation and overlying pre-Missoula/Hanford formation is examined by rasing the contact by 1 m (3 ft). The initial contact elevation is shown in Figure 3-6. This analysis addresses the uncertainty in position of this contact. Simulation results show that for steady-state conditions, water levels in the eastern portions of the domain, where the pre-Missoula/Hanford formation is saturated, are up to 1.8 m (6 ft) higher than for the base case (Figure B-11). This is the result of raising the contact position and necessity of the model to saturate additional pre-Missoula/Hanford formation material. In the western portion of the domain, where the Ringold Formation is the only saturated unit, water levels fell approximately 1 m (3 ft). This drop in water level is the result of increasing the saturated thickness of the Ringold Formation in the eastern portion of the model domain, which requires that water from the west be moved to saturate the increased

Ringold Formation thickness. Figures B-12 and B-13 show the water table levels for the transient simulation at 9 and 14 yr. Similar changes in water levels are observed for the transient case as for the steady-state simulation discussed previously. The results of this sensitivity case demonstrate that water levels are sensitive to the contact position.

Figures B-14 and B-15 show the tritium distribution at 9 and 14 yr of transient simulation, respectively. These figures show that there is little difference between the this sensitivity case and the base case simulation for tritium transport. Therefore, it can be concluded that tritium transport is insensitive to the contact position.

B.3 SENSITIVITY TO TRITIUM DECAY

The base case simulation shows that the majority of tritium loss, approximately 80 percent, is due to decay. This sensitivity case examines the behavior of the tritium plume, through 14 yr of simulation, due to decay alone. Initial tritium distributions were set along the top four nodal layers; with no advective or dispersive flow through the domain. No recharge from the cribs or ponds is allowed. Thus, the only mechanisms for tritium attenuation is decay. Figures B-16 and B-17 show the tritium distribution through the fifth nodal plane (second layer from top) for 9 and 14 yr, respectively. Evident from these figures is that the 200,000-pCi/L contours are more centered and larger than for the base case simulation. However, the areal extent of the plume, with greater than 5,000 pCi/L concentration, is smaller that for the base case. The domain lost a net 2.05×10^{14} pCi in 14 yrs of simulation, which compares well with the activity 2.09×10^{14} pCi lost during the base case simulation. This demonstrates the dominant effect of decay on the tritium transport simulations.

B.4 TRITIUM PLUME SENSITIVITY TO ADVECTIVE AND DISPERSIVE FLOW

Due to the dominant effect of decay on the tritium plume as demonstrated for the base case simulation and in Section B.3, the impacts of advective and dispersive flow were assessed. To accomplish this, the decay of tritium is set to zero, and all other material and transport parameters held the same as for the base case. Figures B-18 and B-19 show the model results after 9 and 14 yr of transient simulation. The areal extent of the plume is slightly larger in areal extent, with the 200,000-pCi/L contour being much larger. In addition, the two plumes associated with the 200 West and 200 East Areas merge together, which was not seen in the base case simulation due to the dominant effect of decay. The movement of the eastern end of the 200,000-pCi/L contour near the Columbia River also is seen have a greater impact on the river. The model results calculate that 1.14×10^{12} pCi are left the domain during the 14-yr simulation period. This is approximately two orders of magnitude less than for the base case. This demonstrates that advection and dispersion have an impact on the tritium plume movement, however the plume concentrations are dominantly controlled by tritium decay.

Figure B-1. Comparison of Water Table for Doubled Hydraulic Conductivity Sensitivity Case with Base Case - 1979.

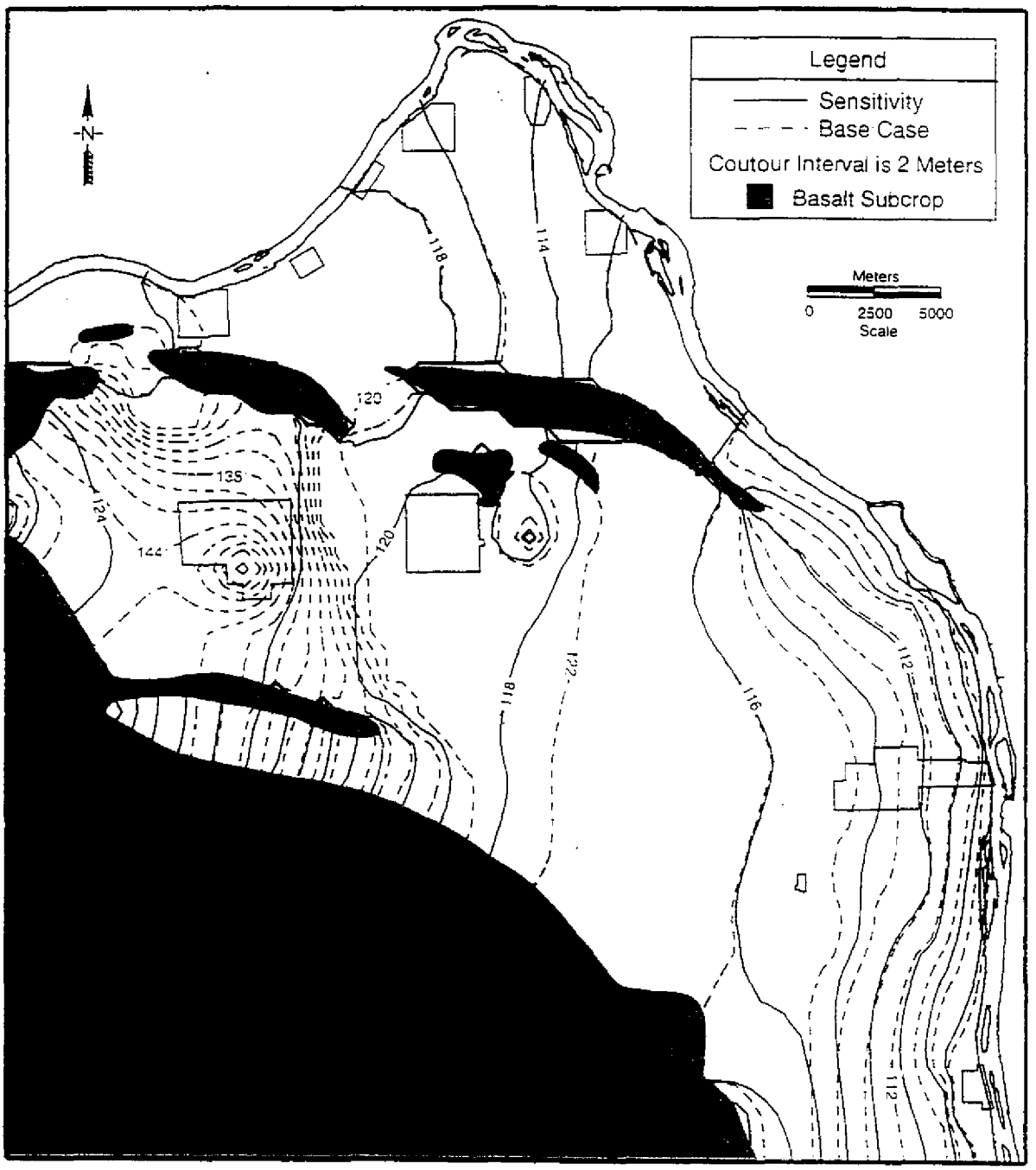

Figure B-2. Comparison of Water Table for Doubled Hydraulic Conductivity Sensitivity Case with Base Case - 1988.

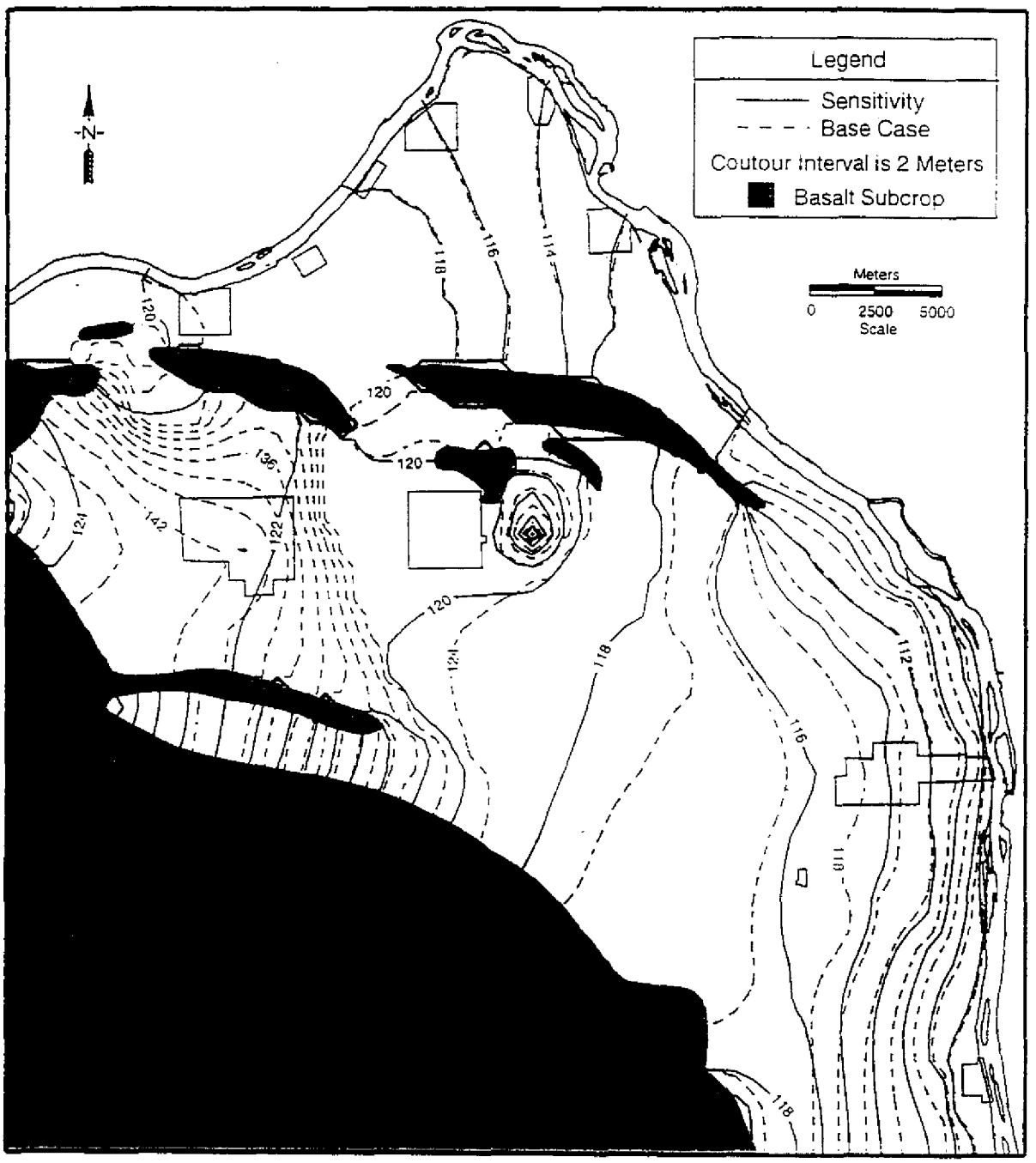

Figure B-3. Comparison of Water Table for Doubled Hydraulic Conductivity Sensitivity Case with Base Case - 1993.

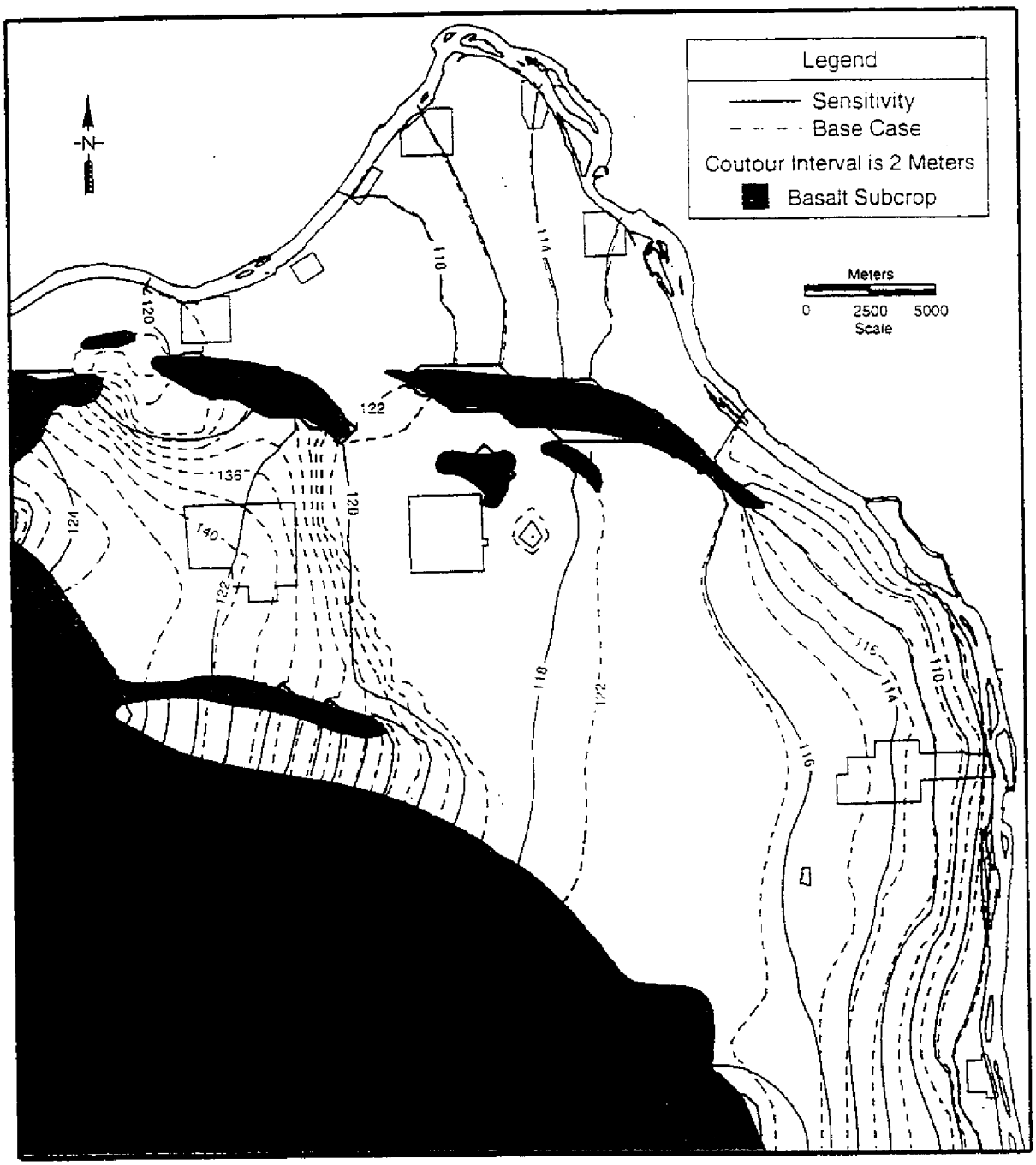

Figure B-4. Comparison of Tritium Concentrations for Doubled Hydraulic Conductivity Sensitivity Case with Base Case - 1988.

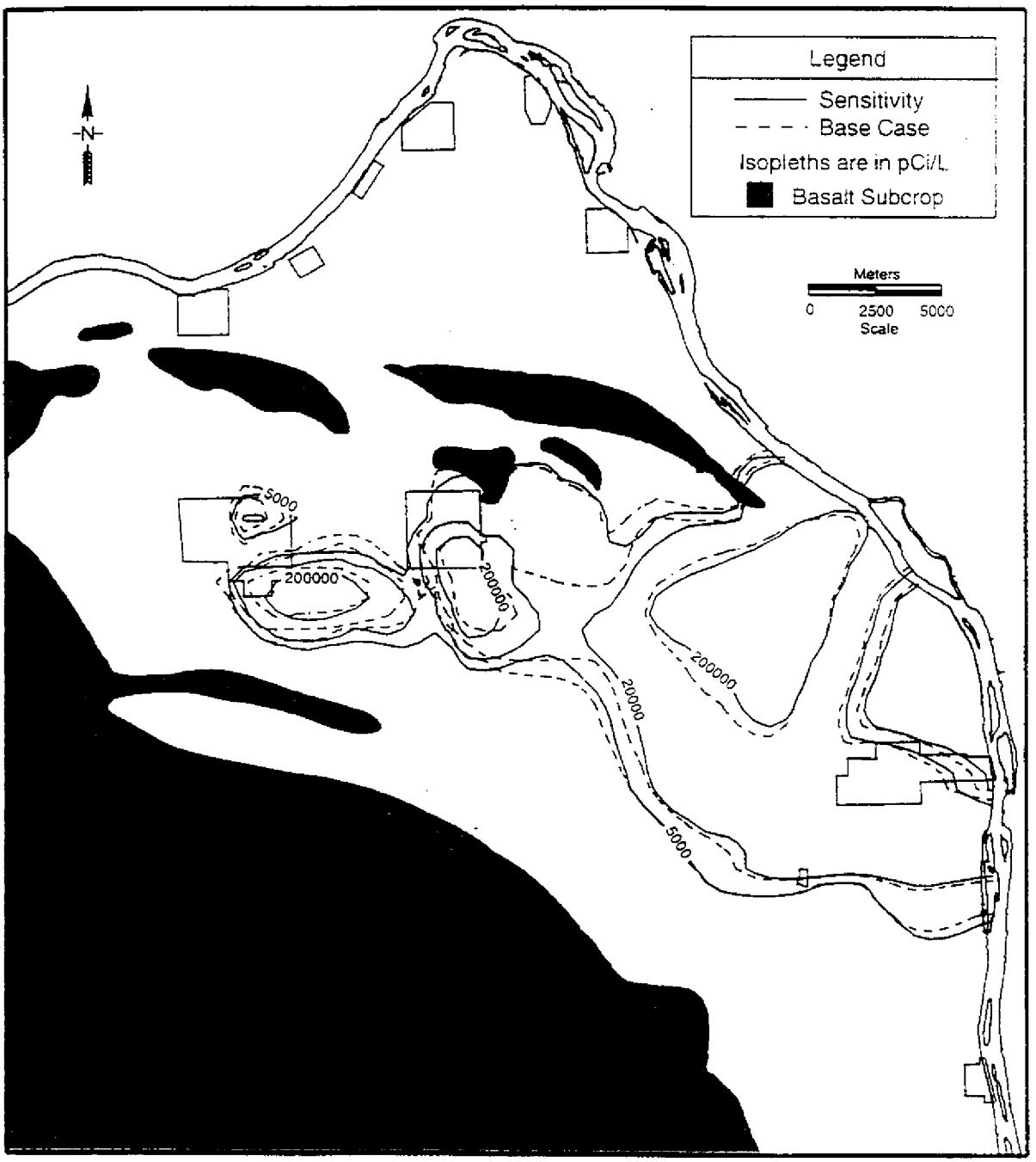

Figure B-5. Comparison of Tritium Concentrations for Doubled Hydraulic Conductivity Sensitivity Case with Base Case - 1993.

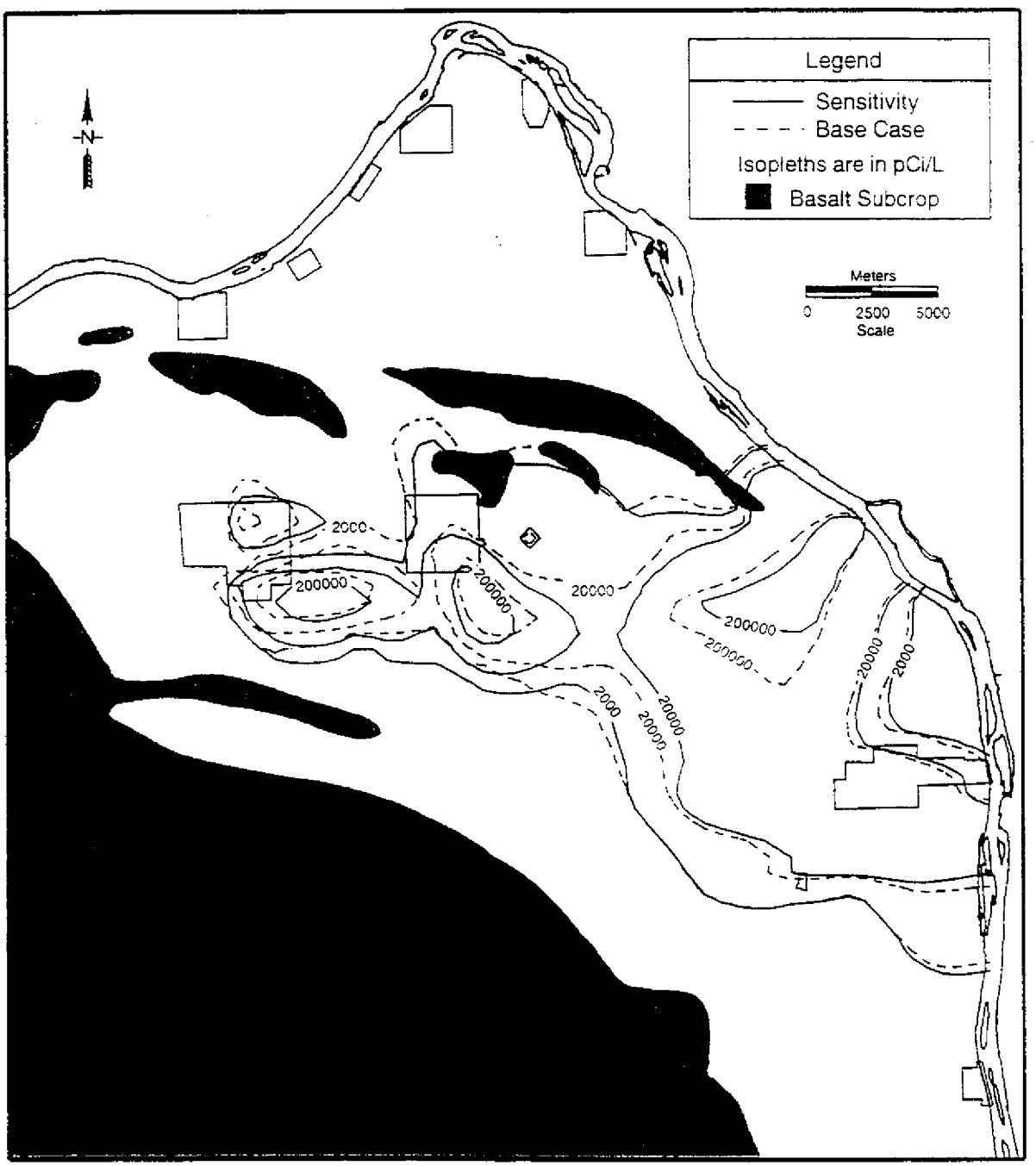

Figure B-6. Comparison of Water Tables for Doubled Hydraulic Conductivity for the Pre-Missoula/Hanford Unit Sensitivity Case with Base Case - 1979.

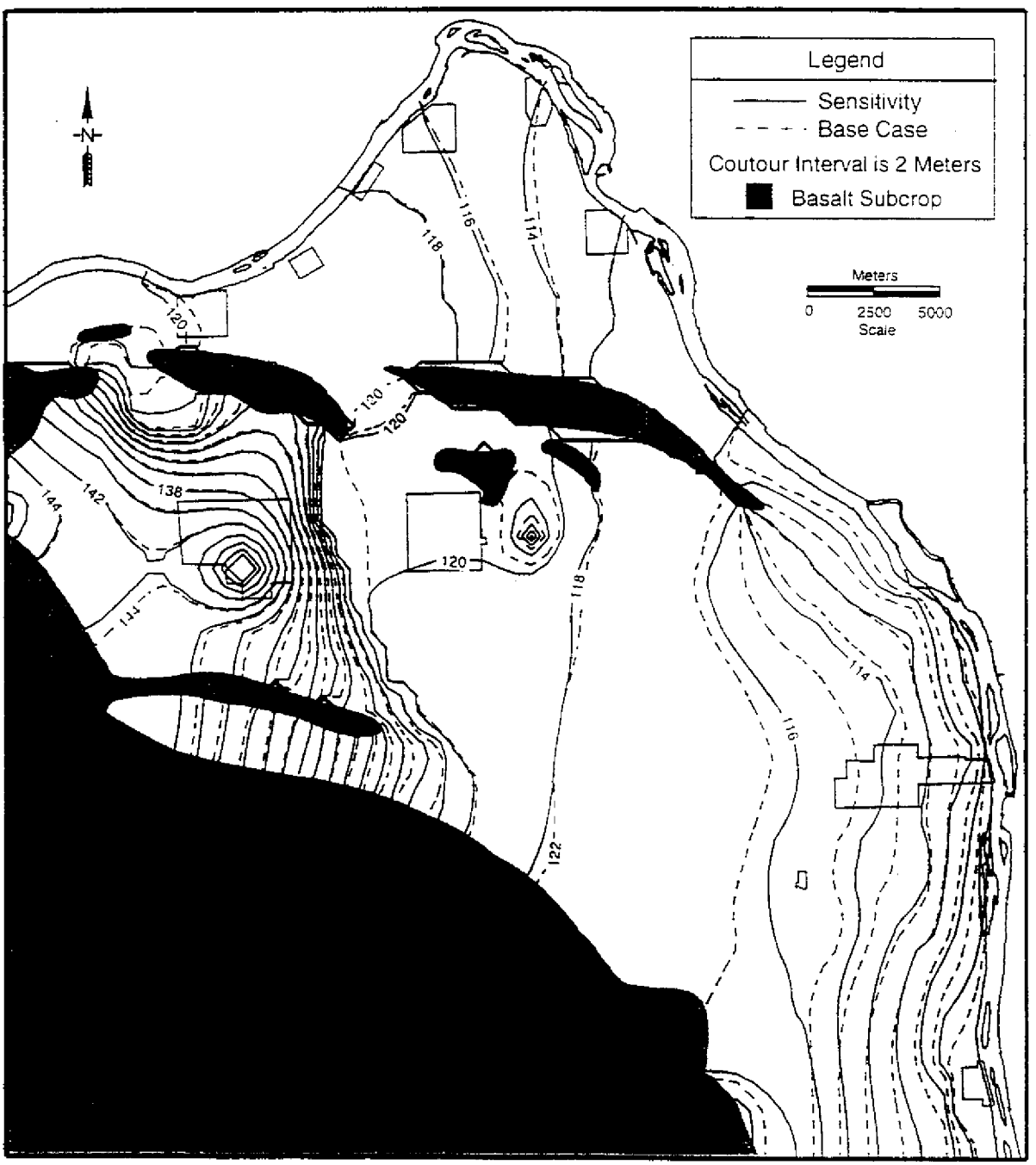

Figure B-7. Comparison of Water Tables for Doubled Hydraulic Conductivity for the Pre-Missoula/Hanford Unit Sensitivity Case with Base Case - 1988.

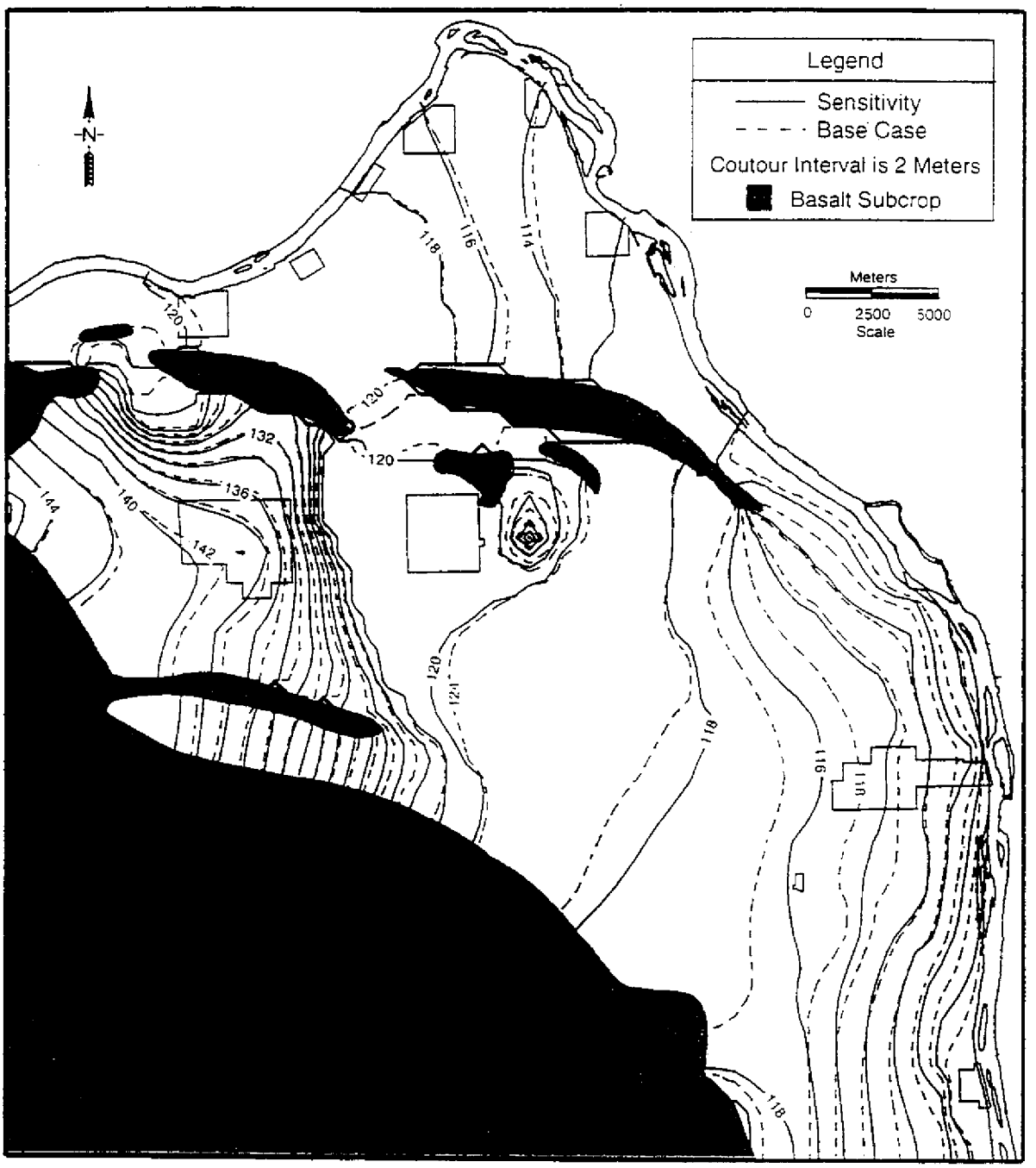

Figure B-8. Comparison of Water Tables for Doubled Hydraulic Conductivity for the Pre-Missoula/Hanford Unit Sensitivity Case with Base Case - 1993.

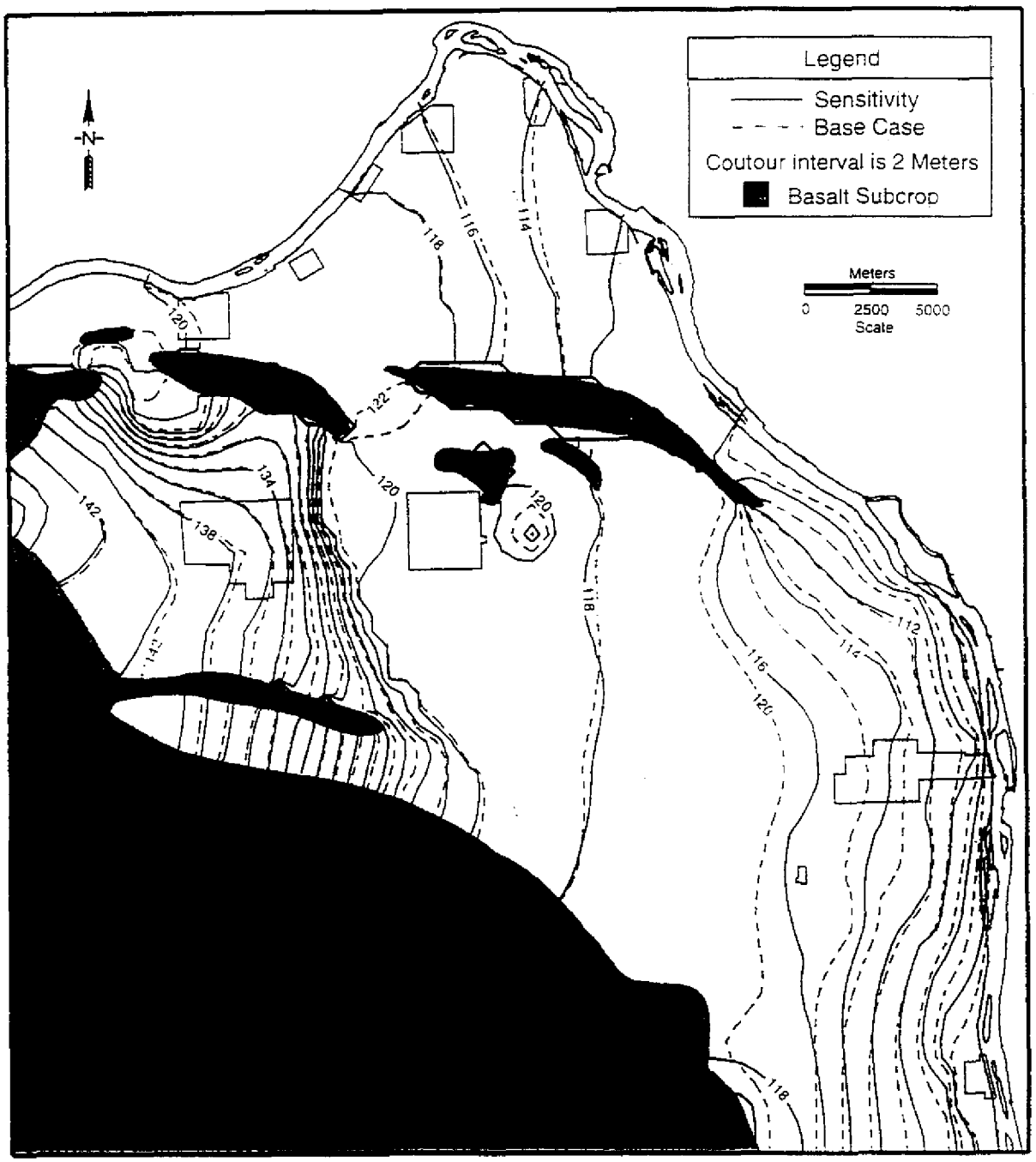

Figure B-9. Comparison of Tritium Concentrations for Doubled Hydraulic Conductivity for the Pre-Missoula/Hanford Unit Sensitivity Case with Base Case - 1988.

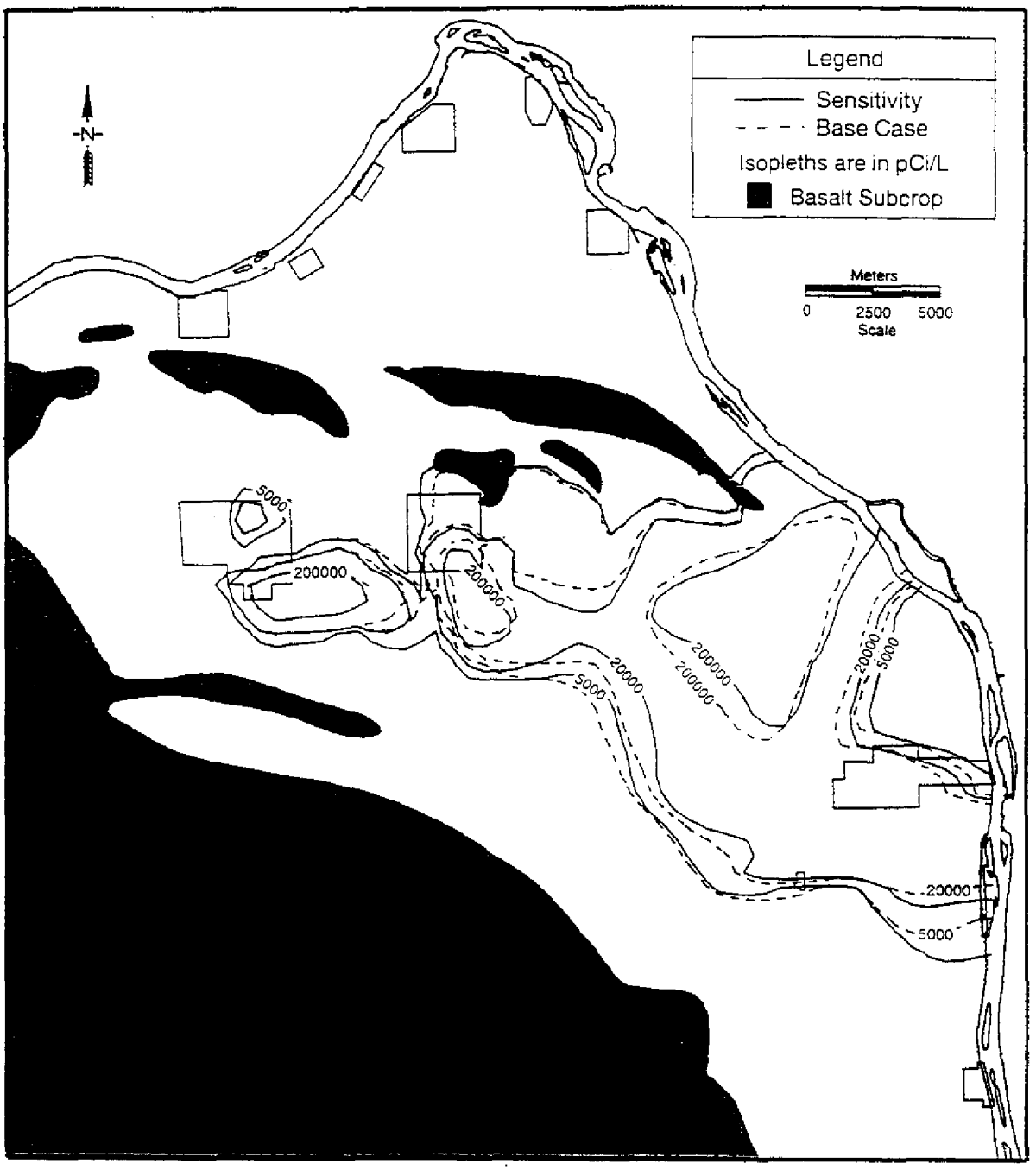

Figure B-10. Comparison of Tritium Concentrations for Doubled Hydraulic Conductivity for the Pre-Missoula/Hanford Unit Sensitivity Case with Base Case - 1993.

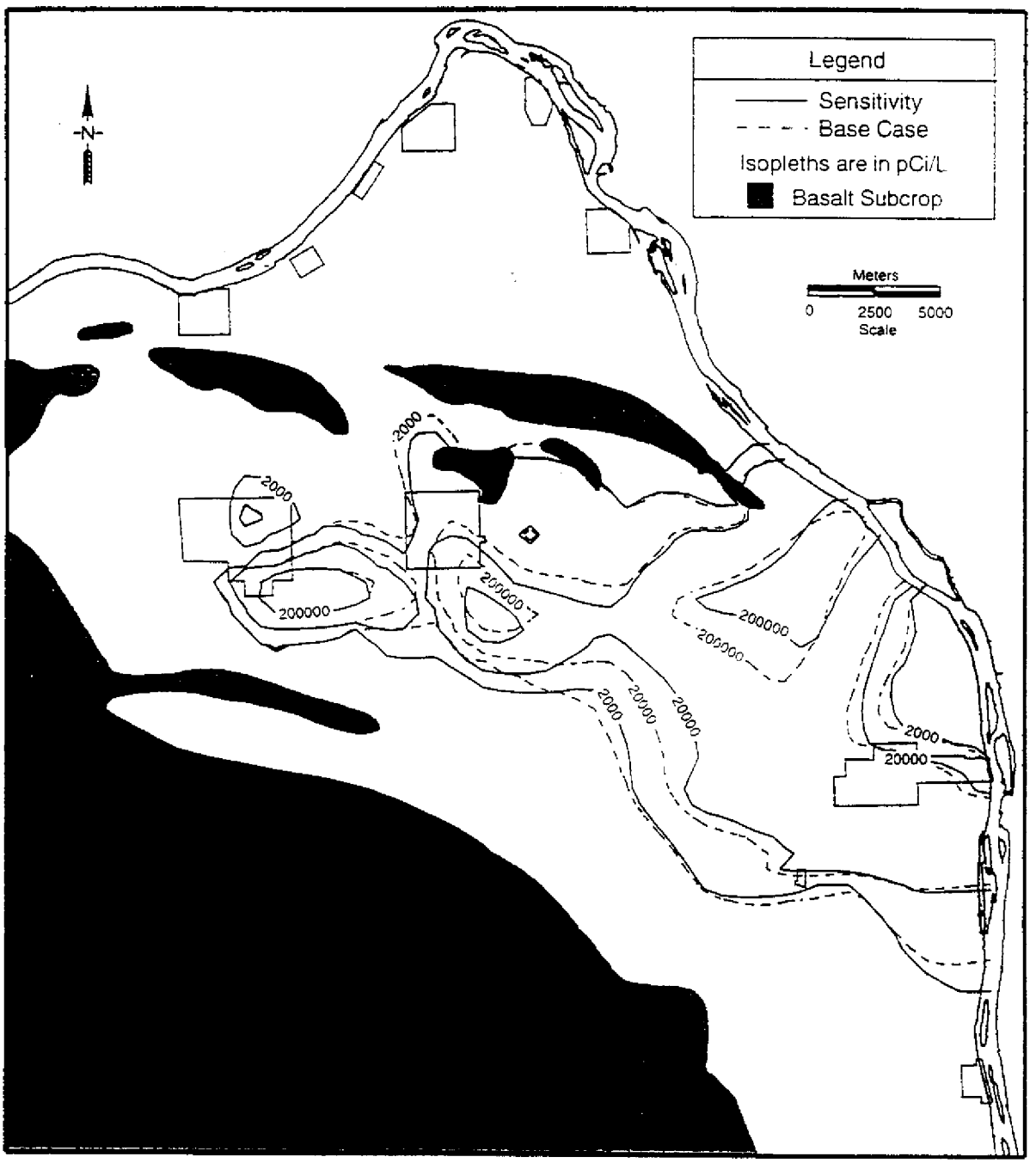

Figure B-11. Comparison of Water Table for Hydrogeologic Unit Contact Position Sensitivity Case with Base Case - 1979.

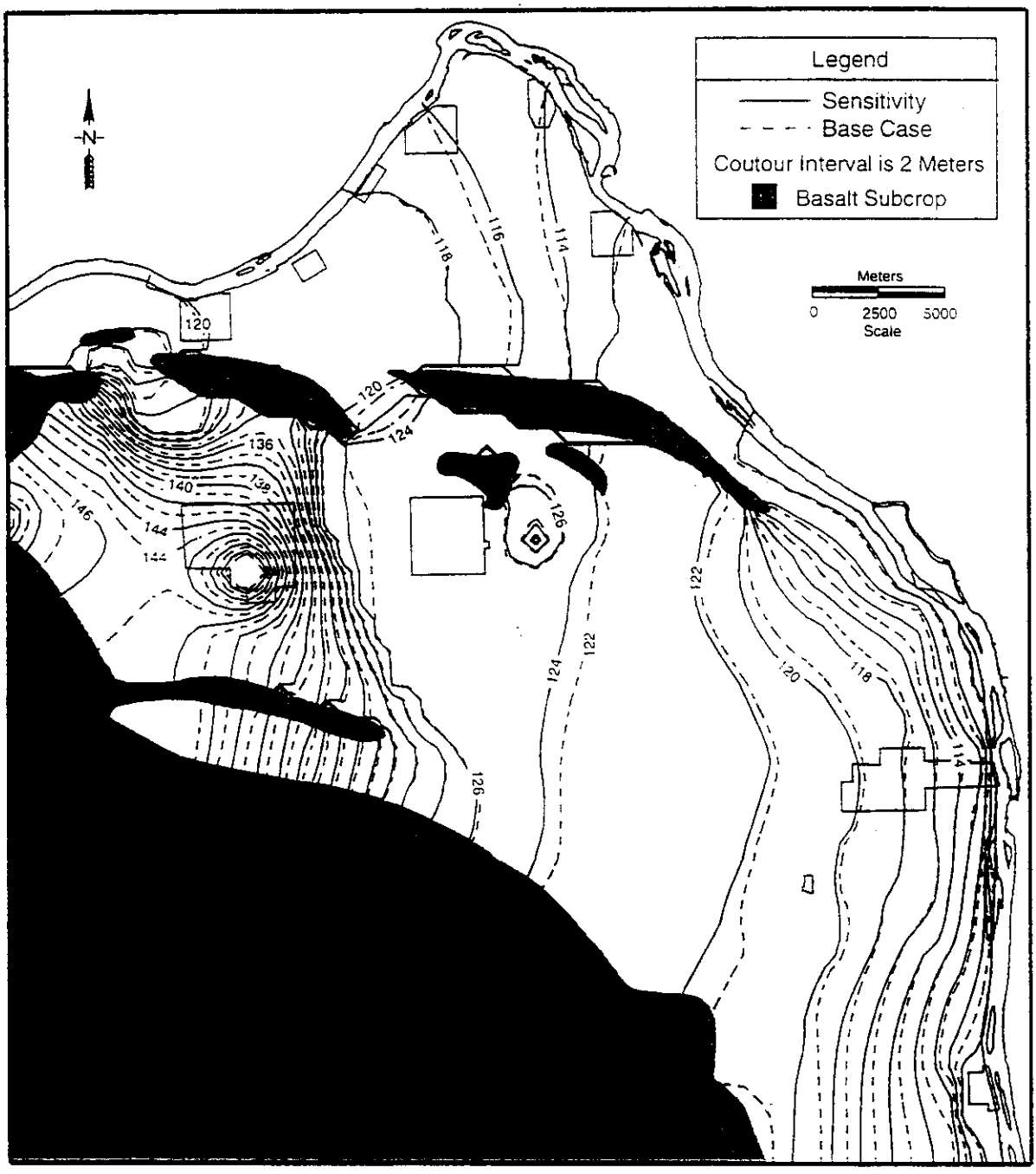

Figure B-12. Comparison of Water Table for Hydrogeologic Unit Contact Position Sensitivity Case with Base Case - 1988.

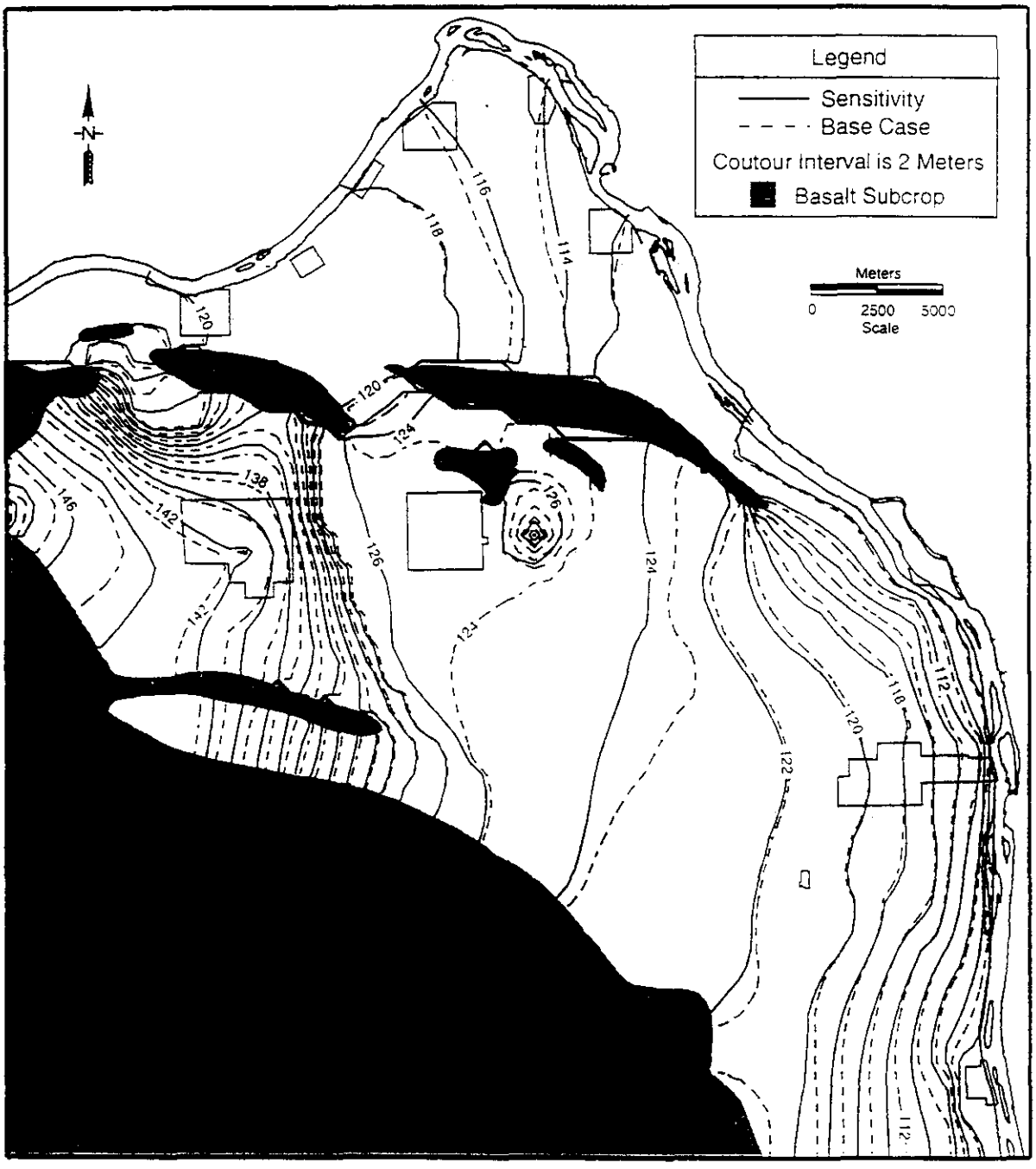

Figure B-13. Comparison of Water Table for Hydrogeologic Unit Contact Position Sensitivity Case with Base Case - 1993.

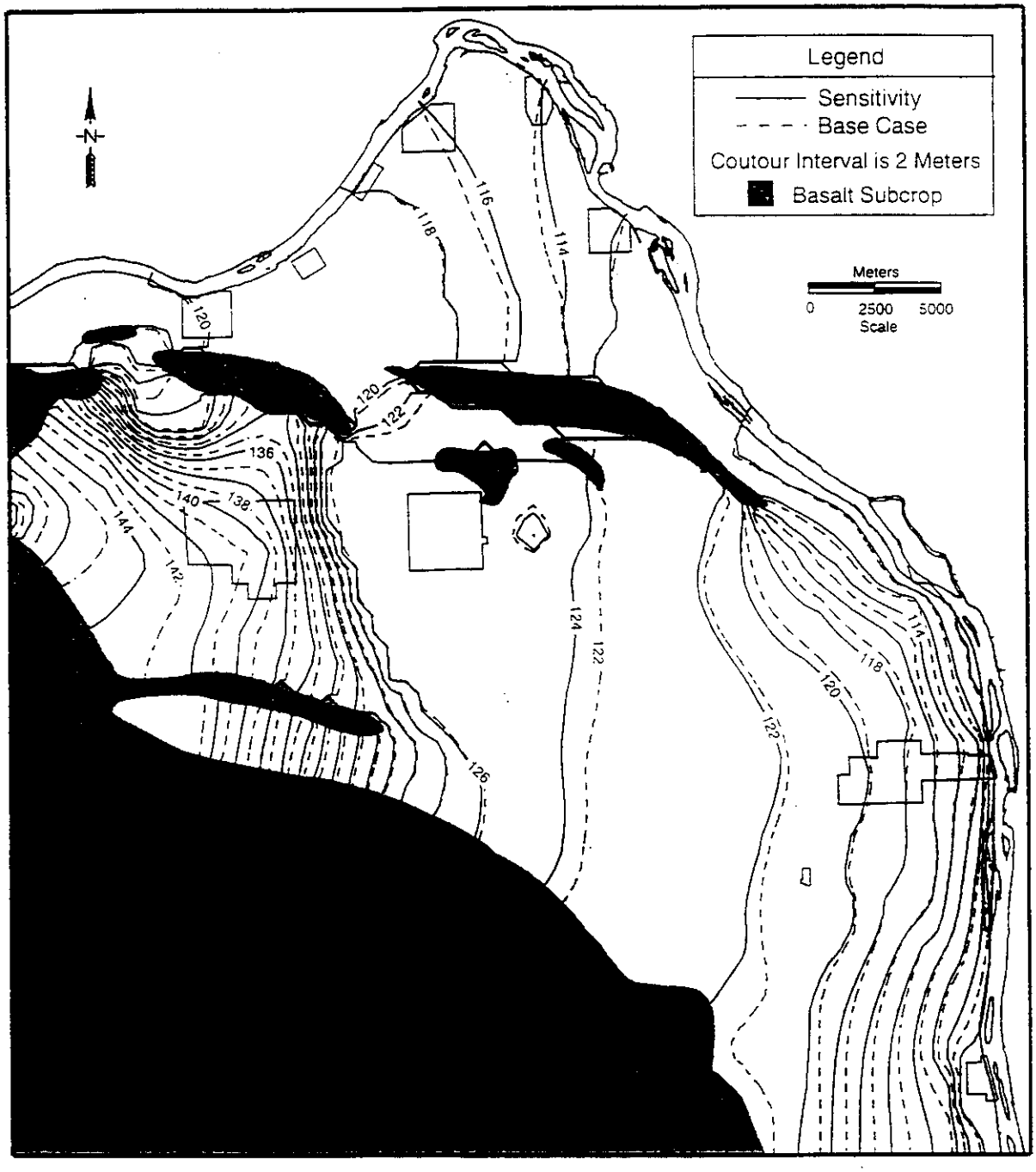

Figure B-14. Comparison of Tritium Concentrations for Hydrogeologic Unit Contact Position Sensitivity Case with Base Case - 1988.

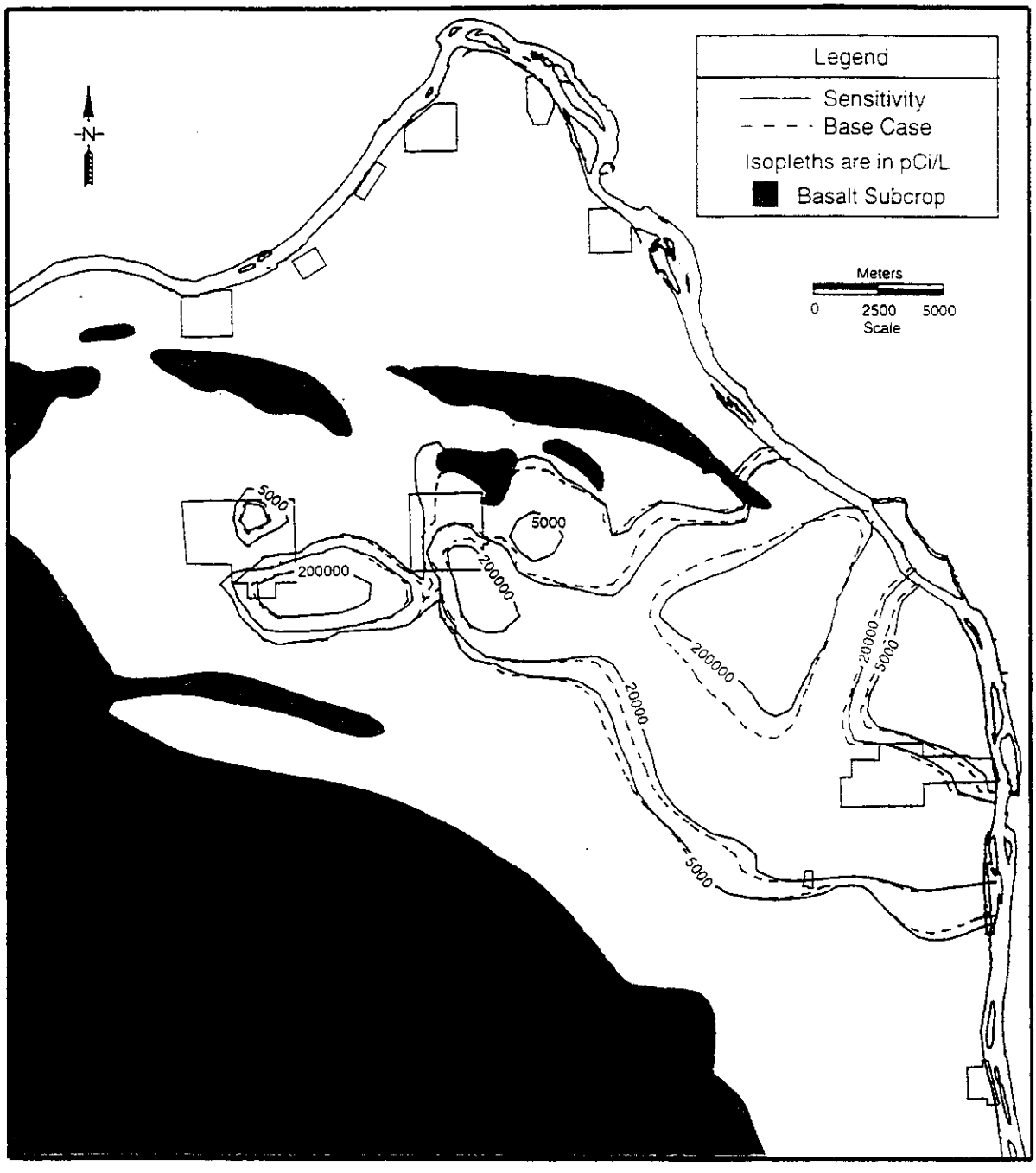

Figure B-15. Comparison of Tritium Concentrations for Hydrogeologic Unit Contact Position Sensitivity Case with Base Case - 1993.

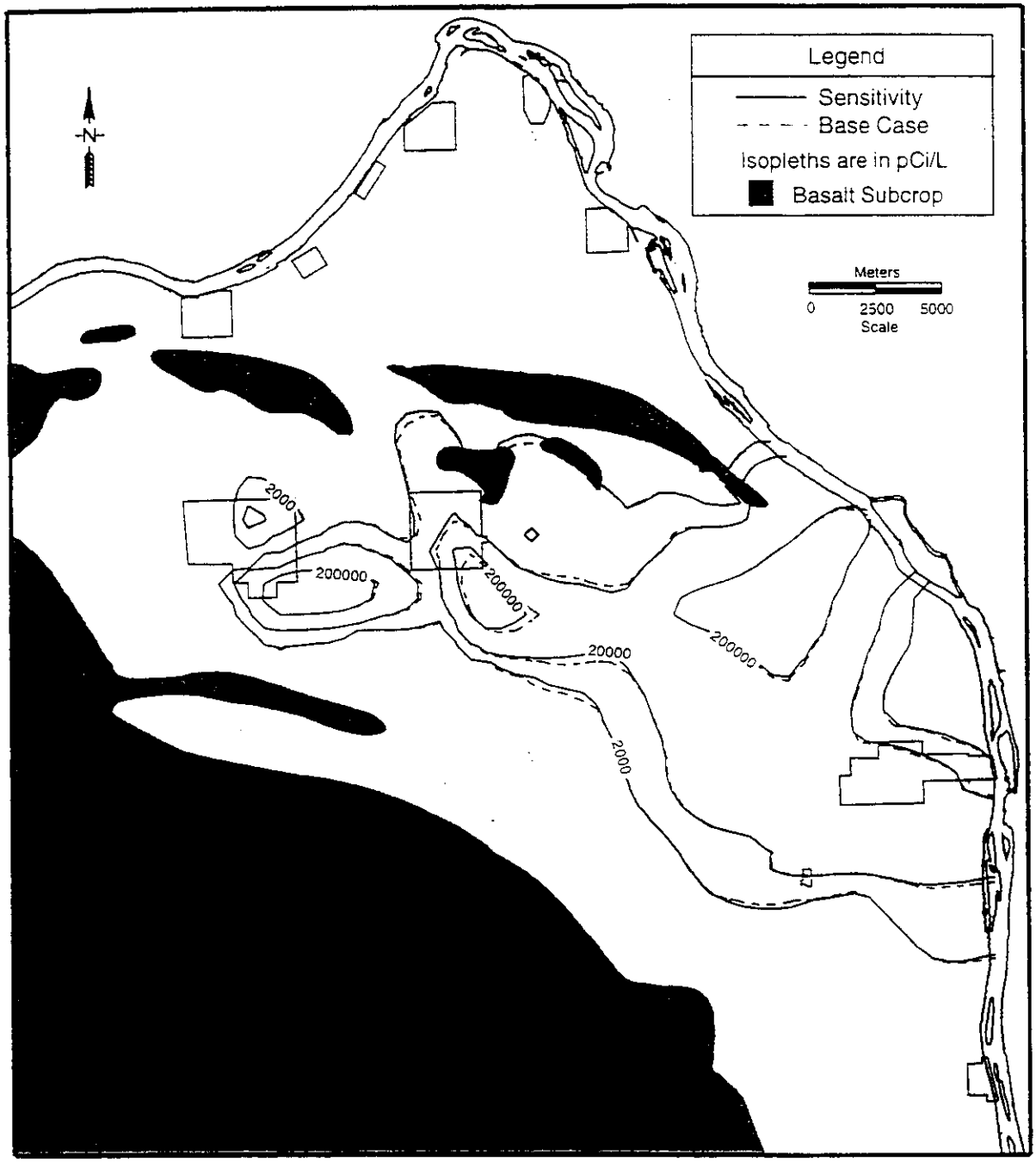

Figure B-16. Comparison of Tritium Concentrations for Sensitivity to Tritium Decay Case with Base Case - 1988.

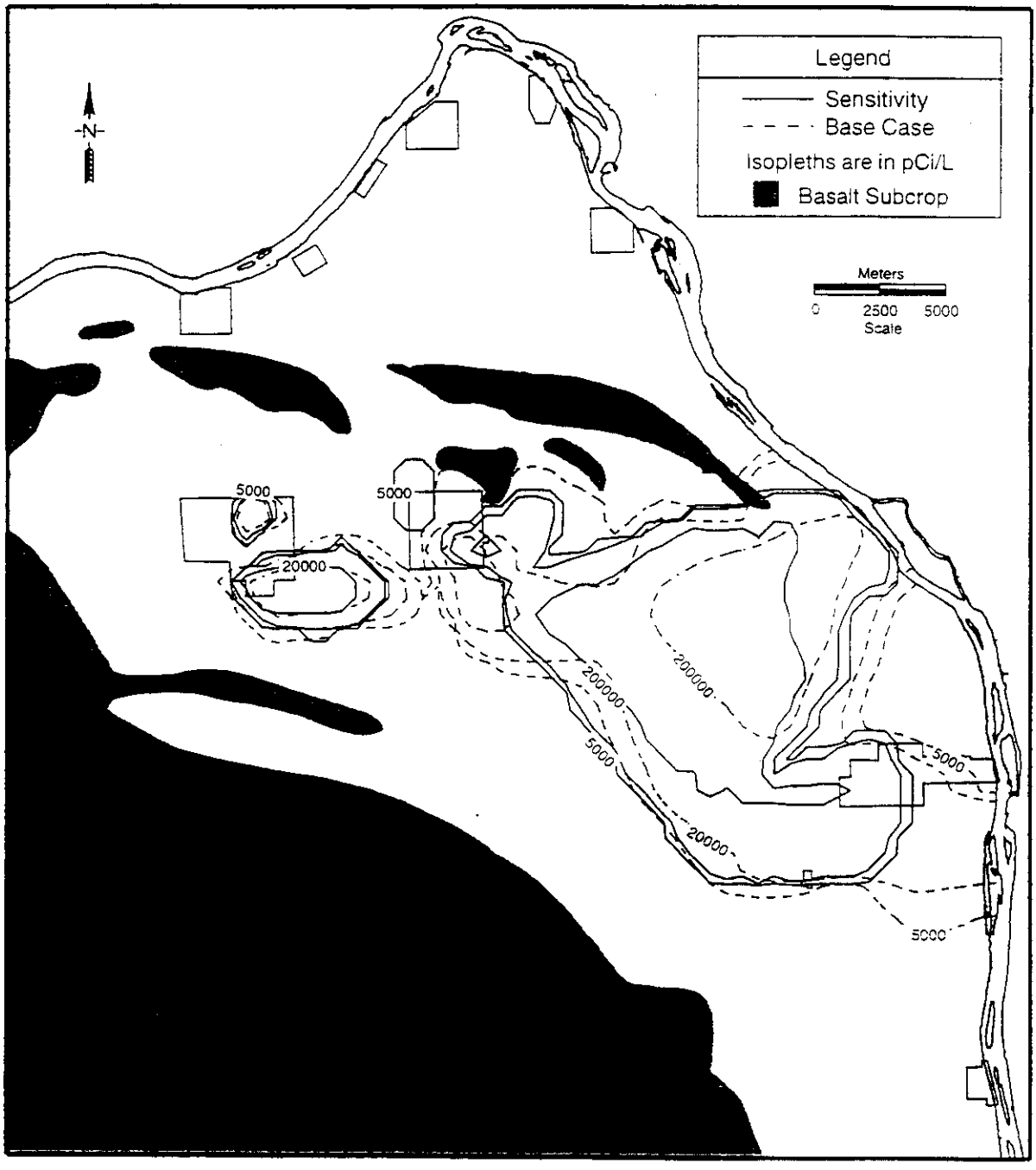

Figure B-17. Comparison of Tritium Concentrations for Sensitivity to Tritium Decay Case with Base Case - 1993.

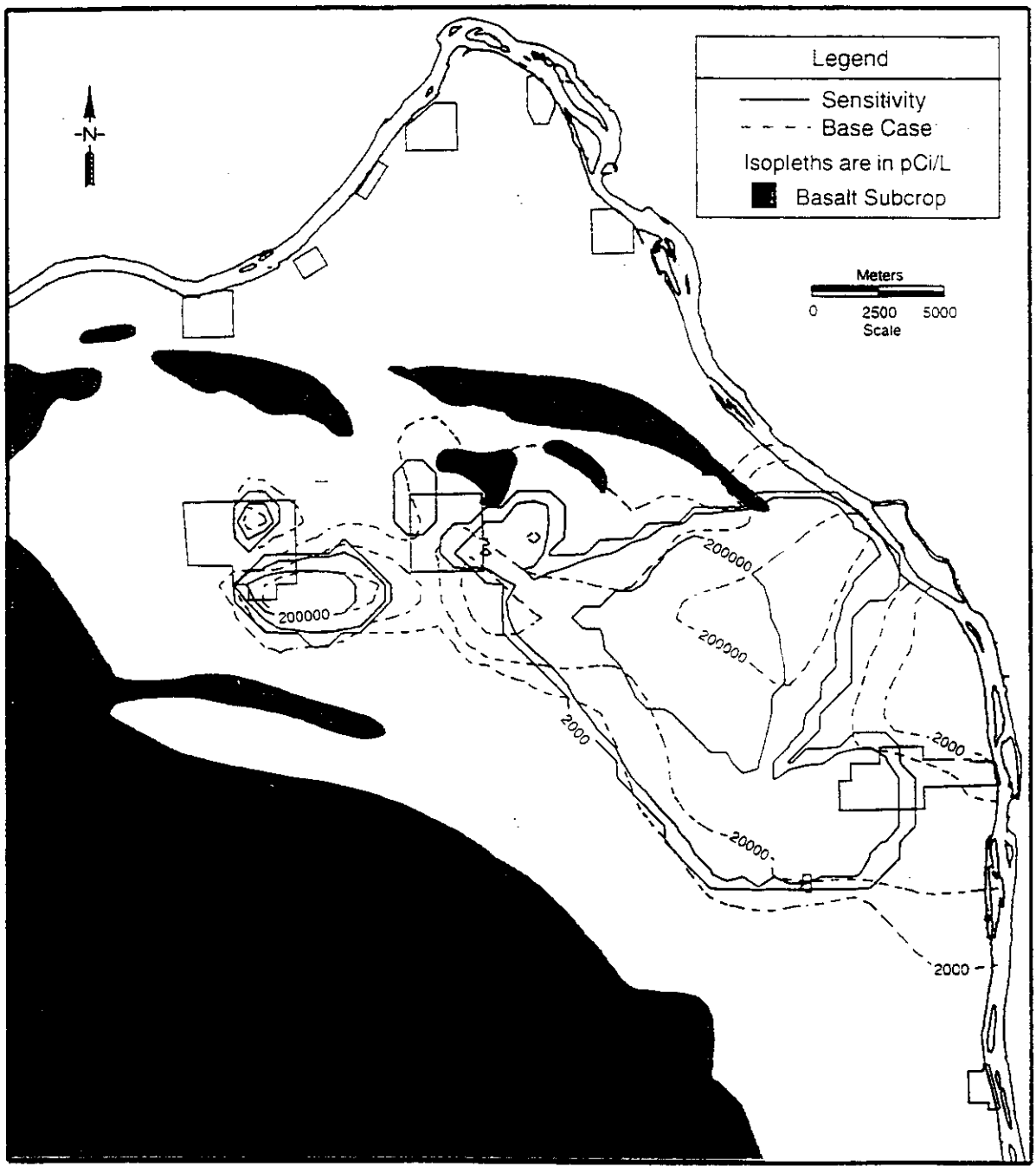

Figure B-18. Comparison of Tritium Concentrations for Advective and Dispersive Flow Sensitivity Case with Base Case - 1988.

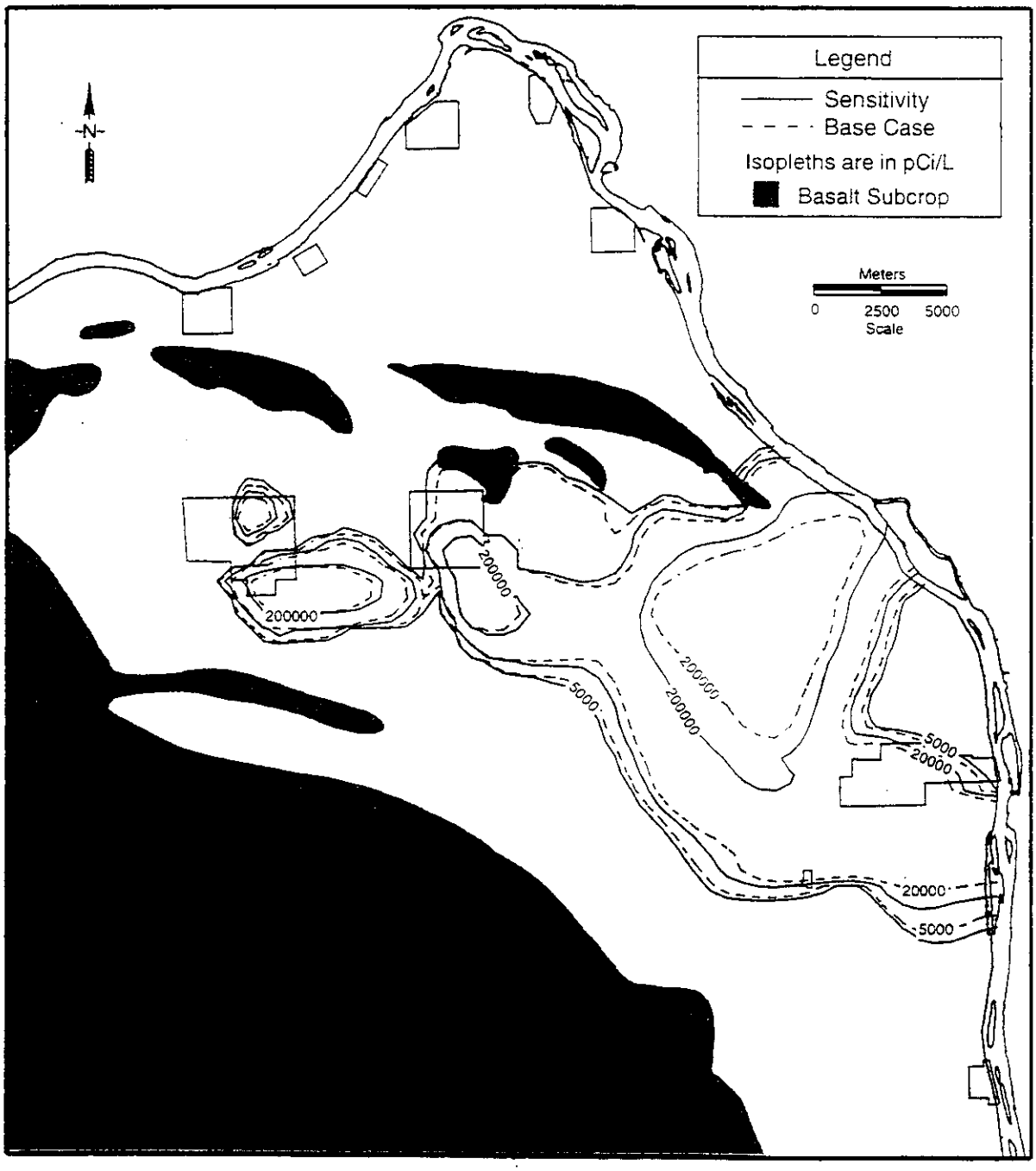

Figure B-19. Comparison of Tritium Concentrations for Advective and Dispersive Flow Sensitivity Case with Base Case - 1993.

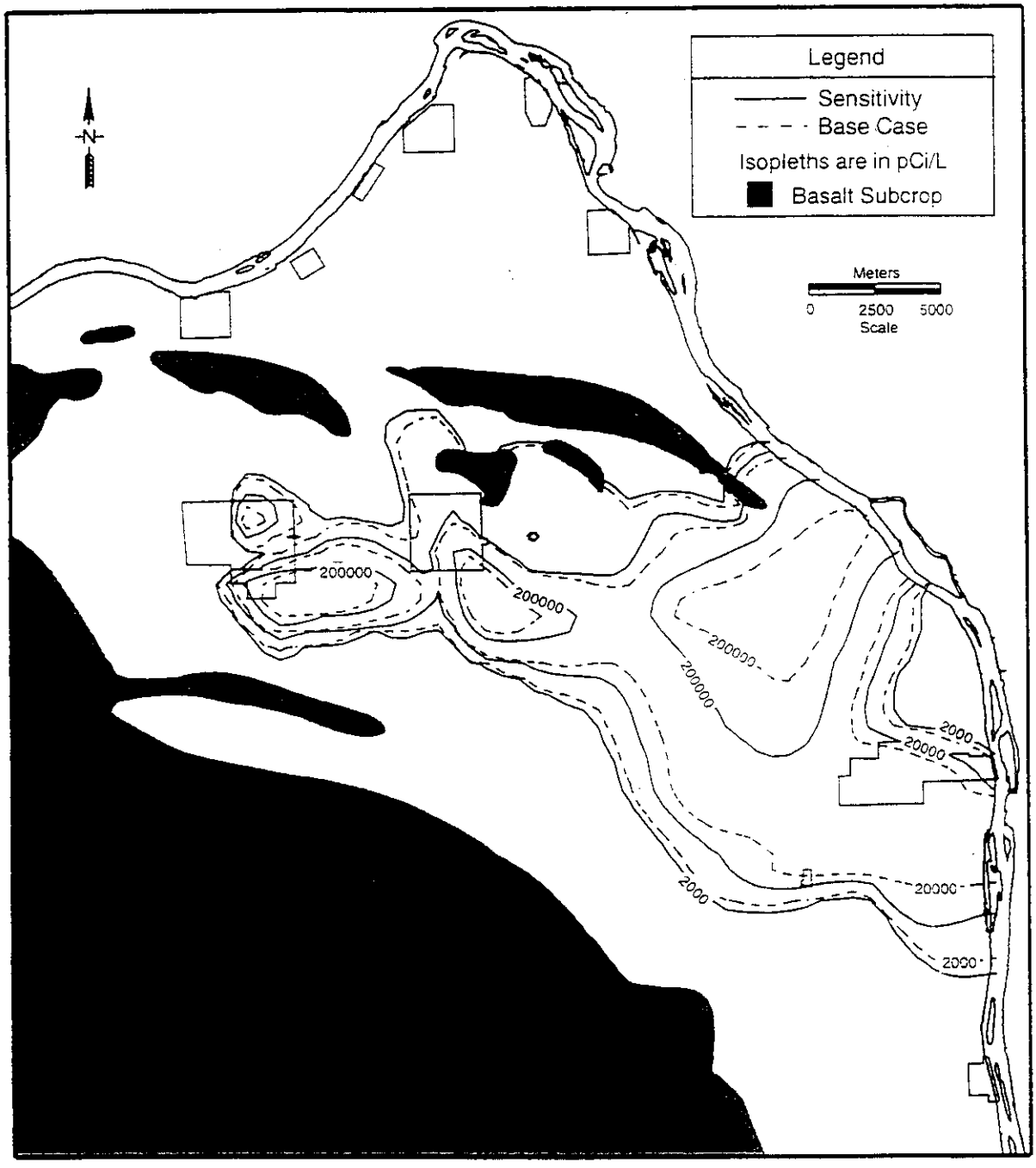

APPENDIX C

STATISTICAL EVALUATION OF MODEL CALIBRATION

An evaluation of the groundwater flow calibration was conducted by comparing 1979, 1988, and 1993 observed water table elevations with interpolated values from the model. By statistically comparing the observed and simulated values, an assessment of the model calibration can be done. The following discussion presents the methodology used and the results of the evaluation.

The evaluation can be divided into three parts:

- Determination of wells used in the analysis
- Calculation of model water table elevations at well locations
- Statistical analysis of the results.

To ensure a consistent well set for the analysis, only wells with water level measurements during each of the three calibration periods (1979, 1988, and 1993) were used. Water level data, obtained from the Hanford Environmental Information System (HEIS), indicate that 196 wells fit this criteria. Seven of these wells were eliminated from the sample set because they were located within a basalt subcrop area used in the model area. These wells were further screened to exclude those wells that were screened greater than 15 m across the unconfined aquifer or the top of the screened interval was below the water table. This resulted in 124 wells that were included in the statistical analysis. The location of the wells used in the analysis is shown in Figure C-1.

Because the well locations do not correspond to grid nodes in the sitewide model, an interpolation of model water level elevations was required to obtain a value at the exact location of the observation well. The first step to accomplish this was to construct a grid of the model output using EarthVision from Dynamic Graphics. The model output for each of the calibration timesteps was input into EarthVision as scattered data and then gridded. Gridding was restricted within basalt subcrop areas and along the bank of the Columbia River to obtain an accurate physical representation of the site. Creating a grid allowed easy calculation of water level elevations at each well point with EarthVision's built in formula processor. The interpolated model values were used to determine the difference, or residual, between the observed and simulated water table elevation for each well in the data set. Table C-1 lists the wells used in the analysis and the observed and model simulated value for the three timesteps used in the calibration effort.

Summary statistics were then performed on these residuals and are presented in Table C-2. In all three simulation timesteps, the mean difference between the observed and simulated water table elevations is below -0.72 m (-2.36 ft). This is reasonable considering the range of values and high gradients observed in some portions of the modeled area.

Figure C-1. Location of Wells Used in Statistical Analysis.

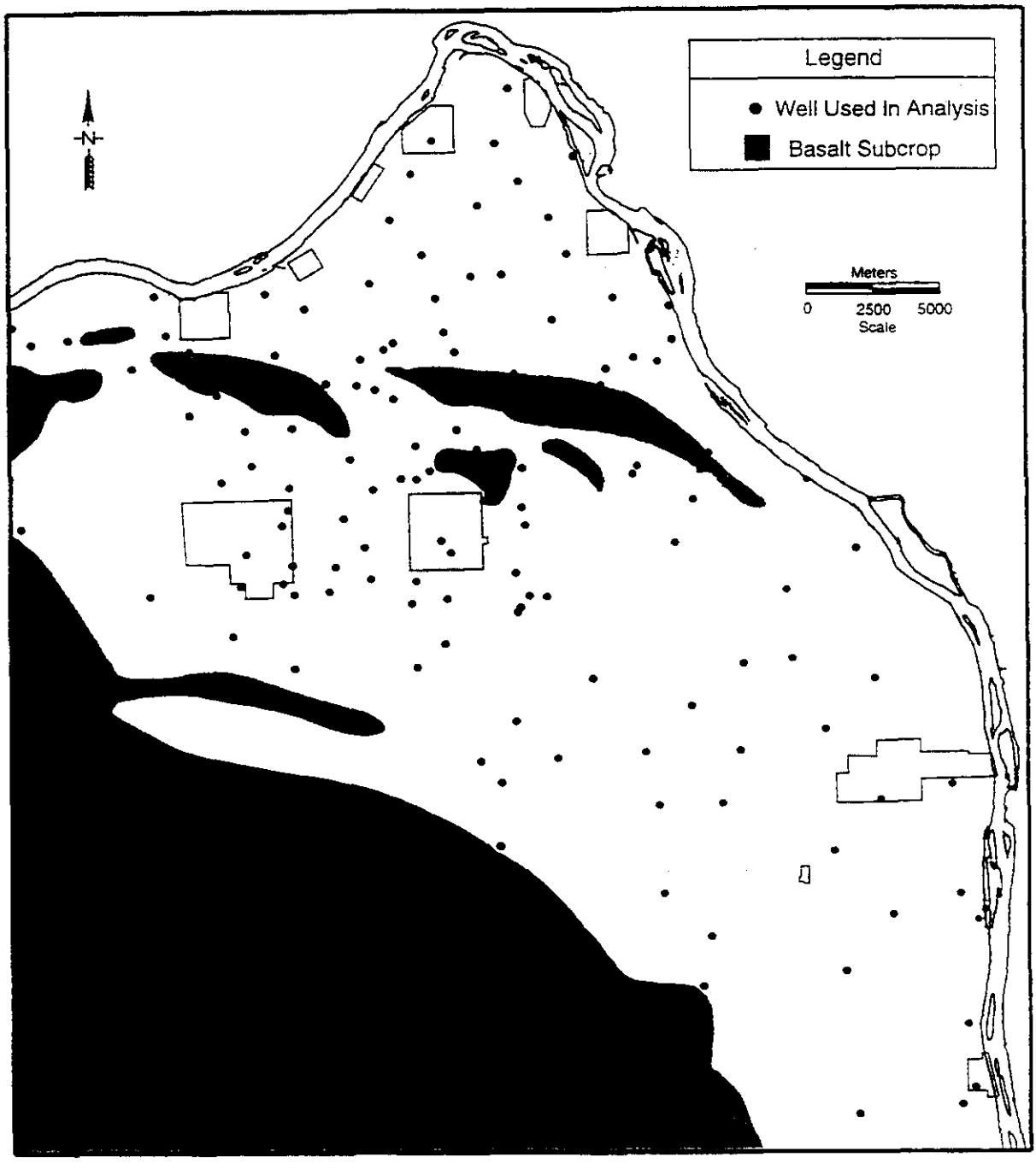

Table C-1. Comparison of Observed versus Simulated Water Table Elevations at 124 Selected Wells. (Page 1 of 3)

Well	1979 Simulated Elevation (m)	1979 Observed Elevation (m)	1979 Residual (m)	1988 Simulated Elevation (m)	1988 Observed Elevation (m)	1988 Residual (m)	1993 Simulated Elevation (m)	1993 Observed Elevation (m)	1993 Residual (m)	Root Mean Square for 1993 Residuals
199-D2-5	116.13	118.19	-2.06	116.14	117.53	-1.39	116.13	117.45	-1.32	2.12
299-E13-14	123.61	122.94	0.67	124.55	123.63	0.92	123.37	122.64	0.73	
299-E23-1	123.62	122.76	0.85	124.68	123.65	1.04	123.20	122.59	0.62	
299-E24-7	123.56	122.76	0.80	124.65	123.58	1.08	123.19	122.47	0.73	
299-W11-10	139.82	139.88	-0.07	137.75	139.79	-2.04	136.07	138.34	-2.27	
299-W12-1	137.39	138.12	-0.73	136.20	138.19	-1.99	134.83	136.93	-2.10	
299-W15-5	151.72	146.36	5.36	142.31	143.78	-1.46	139.99	141.92	-1.93	
299-W21-1	142.48	140.45	2.03	138.59	139.50	-0.91	136.95	137.77	-0.82	
299-W23-11	149.96	146.17	3.79	141.68	142.60	-0.92	139.73	140.56	-0.83	
699-10-E12	112.37	108.47	3.90	112.39	108.96	3.43	112.58	108.88	3.71	
699-11-45A	123.12	124.81	-1.69	123.58	125.33	-1.75	123.37	125.59	-2.22	
699-14-38	121.99	122.76	-0.77	122.58	123.17	-0.59	122.23	123.37	-1.14	
699-14-47	123.33	124.93	-1.60	123.85	125.41	-1.56	123.54	125.58	-2.04	
699-15-15A	120.73	120.84	-0.11	121.16	121.58	-0.42	121.03	121.24	-0.21	
699-15-26	121.41	121.72	-0.31	121.95	122.69	-0.74	121.68	121.91	-0.23	
699-17-5	118.78	117.43	1.35	118.98	118.33	0.65	119.14	118.17	0.97	
699-19-43	122.45	122.64	-0.19	123.09	123.41	-0.32	122.61	122.85	-0.24	
699-2-3	118.09	118.05	0.03	118.29	118.88	-0.59	118.42	118.92	-0.50	
699-20-20	121.29	121.75	-0.46	121.84	122.67	-0.84	121.54	121.94	-0.40	
699-24-1T	116.83	114.11	2.72	116.90	114.75	2.15	117.18	113.87	3.31	
699-24-33	121.84	122.33	-0.49	122.51	123.30	-0.79	122.04	122.36	-0.32	
699-25-55	123.55	125.59	-2.04	124.26	126.04	-1.78	123.57	125.72	-2.15	
699-25-70	136.75	137.72	-0.97	136.06	136.99	-0.93	135.37	136.01	-0.64	
699-26-15A	119.56	120.96	-1.40	119.93	121.82	-1.89	119.87	121.15	-1.28	
699-27-8	118.26	119.56	-1.30	118.51	120.45	-1.94	118.60	119.83	-1.24	
699-28-52A	123.29	124.65	-1.37	124.06	123.99	0.07	123.30	123.01	0.29	
699-29-78	140.93	143.49	-2.56	139.87	141.84	-1.97	138.99	140.32	-1.33	
699-3-45	123.05	124.74	-1.69	123.44	125.42	-1.98	123.35	115.44	7.91	
699-32-43	122.67	122.56	0.11	123.63	123.72	-0.09	122.67	122.50	0.18	
699-33-42	122.67	123.20	-0.53	123.66	123.75	-0.09	122.66	122.55	0.11	
699-33-56	123.65	123.02	0.63	124.49	123.95	0.54	123.52	122.85	0.67	
699-34-39A	122.45	122.53	-0.09	123.45	123.55	-0.10	122.46	122.50	-0.05	
699-34-41B	122.64	122.59	0.05	123.68	123.78	-0.10	122.61	122.56	0.05	
699-34-51	123.30	122.80	0.50	124.27	123.89	0.38	123.15	122.63	0.52	
699-34-88	143.98	144.29	-0.30	143.31	143.45	-0.14	142.54	142.64	-0.10	
699-35-66A	132.51	134.50	-1.99	131.89	134.16	-2.27	131.00	133.37	-2.37	
699-35-70	139.47	138.89	0.57	137.10	138.00	-0.90	135.78	136.80	-1.03	
699-35-9	116.42	116.91	-0.49	116.64	117.83	-1.19	116.70	117.37	-0.67	
699-36-61A	123.88	124.39	-0.51	124.72	124.81	-0.09	123.66	124.13	-0.47	
699-37-43	123.15	122.71	0.44	124.47	125.05	-0.58	122.93	122.82	0.11	
699-38-65	129.62	131.79	-2.16	129.44	131.33	-1.89	128.44	130.79	-2.35	
699-38-70	140.62	139.35	1.28	137.44	138.59	-1.15	135.78	139.49	-3.73	
699-40-1	110.87	110.11	0.76	110.92	110.75	0.17	110.98	110.63	0.35	
699-40-62	123.97	123.52	0.45	124.82	124.25	0.58	123.60	123.36	0.24	
699-41-23	121.09	120.83	0.27	121.85	121.68	0.17	121.27	120.97	0.30	
699-43-104	148.78	149.44	-0.66	148.56	153.20	-4.64	148.02	150.85	-2.82	
699-43-42	126.84	127.56	-0.72	133.16	128.62	4.54	124.88	128.25	-3.37	
699-44-64	124.16	123.76	0.40	124.97	124.41	0.57	123.75	123.71	0.05	
699-45-42	125.18	126.03	-0.85	129.01	127.74	1.27	123.95	126.74	-2.79	
699-46-21B	120.68	118.81	1.87	121.35	119.36	1.99	120.89	119.04	1.86	
699-47-60	123.81	122.68	1.13	124.59	123.89	0.70	123.31	122.44	0.87	

Table C-1. Comparison of Observed versus Simulated Water Table Elevations at 124 Selected Wells. (Page 2 of 3)

Well	1979 Simulated Elevation (m)	1979 Observed Elevation (m)	1979 Residual (m)	1988 Simulated Elevation (m)	1988 Observed Elevation (m)	1988 Residual (m)	1993 Simulated Elevation (m)	1993 Observed Elevation (m)	1993 Residual (m)	Root Mean Square for 1993 Residuals
699-48-71	135.72	136.07	-0.35	135.17	136.31	-1.13	134.22	135.46	-1.24	
699-49-28	121.71	119.53	2.18	122.59	120.14	2.45	121.79	119.97	1.82	
699-49-55A	123.57	122.68	0.89	124.37	123.75	0.62	122.91	122.50	0.41	
699-49-57A	123.53	122.68	0.85	124.29	123.72	0.57	122.87	122.40	0.47	
699-49-79	139.10	139.63	-0.54	138.15	139.58	-1.43	137.18	138.75	-1.57	
699-50-28B	121.68	119.45	2.23	122.52	120.02	2.50	121.76	119.97	1.79	
699-50-42	123.94	124.32	-0.38	125.21	125.41	-0.20	122.88	125.10	-2.22	
699-50-53A	123.58	122.69	0.89	124.34	123.67	0.67	122.86	122.47	0.38	
699-51-63	123.72	123.38	0.34	124.47	124.00	0.47	123.33	123.24	0.10	
699-51-75	137.35	137.08	0.27	136.76	137.34	-0.58	135.95	136.71	-0.76	
699-52-19	110.12	110.01	0.10	110.12	110.15	-0.03	110.12	110.12	0.00	
699-53-47A	123.68	125.37	-1.69	123.99	123.90	0.09	122.55	123.64	-1.09	
699-53-55B	123.48	122.80	0.68	124.02	123.35	0.67	122.57	122.20	0.37	
699-55-50C	123.62	122.82	0.80	123.99	123.11	0.87	122.54	122.27	0.27	
699-55-70	132.68	131.22	1.46	132.67	131.90	0.77	132.57	131.49	1.08	
699-55-76	133.88	135.13	-1.25	133.73	135.64	-1.91	133.38	135.20	-1.82	
699-57-83A	126.72	131.56	-4.84	126.69	131.96	-5.27	126.56	131.71	-5.15	
699-59-58	121.03	122.64	-1.61	121.32	123.02	-1.70	120.58	122.26	-1.69	
699-59-80B	129.41	128.72	0.69	129.38	130.39	-1.01	129.21	130.92	-1.71	
699-60-32	111.51	110.10	1.42	111.52	110.25	1.27	111.51	110.17	1.34	
699-60-60	119.75	122.55	-2.80	119.90	123.14	-3.24	119.56	122.25	-2.69	
699-61-62	119.45	122.53	-3.08	119.56	122.80	-3.24	119.31	122.25	-2.94	
699-61-66	119.27	122.19	-2.93	119.35	122.77	-3.42	119.17	122.04	-2.87	
699-62-31	111.63	110.08	1.54	111.64	110.22	1.42	111.62	110.17	1.45	
699-62-43A	115.80	120.68	-4.89	115.83	120.93	-5.10	115.79	120.65	-4.86	
699-63-25A	111.12	110.02	1.10	111.12	110.15	0.97	111.12	110.09	1.04	
699-63-90	124.24	120.99	3.25	124.23	121.10	3.13	124.13	120.95	3.17	
699-64-27	111.44	110.07	1.37	111.44	110.21	1.23	111.44	110.10	1.33	
699-64-62	119.20	122.00	-2.81	119.27	122.50	-3.23	119.10	121.86	-2.76	
699-65-50	118.28	121.71	-3.43	118.32	122.13	-3.81	118.25	121.62	-3.37	
699-65-59A	119.00	121.97	-2.97	119.06	122.47	-3.41	118.94	121.81	-2.87	
699-65-72	119.13	121.27	-2.14	119.15	121.90	-2.74	119.10	121.34	-2.23	
699-65-83	120.51	120.97	-0.46	120.52	121.43	-0.91	120.46	121.07	-0.61	
699-66-103	121.17	121.06	0.10	121.17	121.36	-0.19	121.16	121.45	-0.28	
699-66-23	111.06	110.19	0.87	111.06	110.11	0.95	111.05	110.22	0.84	
699-66-58	118.88	121.93	-3.05	118.92	122.41	-3.49	118.83	121.69	-2.86	
699-67-51	118.99	121.71	-2.72	119.02	122.17	-3.15	118.94	121.67	-2.72	
699-67-86	121.86	120.92	0.95	121.86	121.34	0.52	121.79	121.72	0.06	
699-67-98	121.22	120.91	0.31	121.23	121.54	-0.31	121.21	121.46	-0.25	
699-68-105	121.14	120.62	0.52	121.14	120.96	0.18	121.14	119.92	1.22	
699-69-38	114.97	122.67	-7.70	115.00	122.40	-7.40	114.97	122.68	-7.71	
699-70-23	111.26	110.34	0.92	111.26	110.66	0.60	111.26	110.64	0.62	
699-70-68	118.92	121.41	-2.49	118.94	120.60	-1.66	118.89	121.40	-2.50	
699-71-30	111.97	113.33	-1.36	111.98	112.99	-1.01	111.98	112.85	-0.87	
699-71-52	118.62	121.47	-2.85	118.66	121.97	-3.31	118.59	121.41	-2.81	
699-72-73	119.04	120.63	-1.60	119.05	121.20	-2.15	119.03	120.73	-1.70	
699-72-88	120.16	121.57	-1.41	120.16	121.94	-1.78	120.15	121.70	-1.55	
699-73-61	118.73	121.51	-2.78	118.76	121.94	-3.17	118.71	121.42	-2.70	
699-74-44	115.86	120.83	-4.97	115.89	121.04	-5.14	115.86	120.84	-4.98	
699-74-48	116.82	121.18	-4.36	116.86	121.59	-4.73	116.81	121.12	-4.31	
699-77-36	113.24	114.80	-1.56	113.25	114.76	-1.51	113.24	114.54	-1.30	

Table C-1. Comparison of Observed versus Simulated Water Table Elevations at 124 Selected Wells. (Page 3 of 3)

Well	1979 Simulated Elevation (m)	1979 Observed Elevation (m)	1979 Residual (m)	1988 Simulated Elevation (m)	1988 Observed Elevation (m)	1988 Residual (m)	1993 Simulated Elevation (m)	1993 Observed Elevation (m)	1993 Residual (m)	Root Mean Square for 1993 Residuals
699-77-54	118.59	121.03	-2.44	118.62	121.37	-2.75	118.57	120.89	-2.32	
699-8-17	120.70	120.84	-0.15	121.10	121.60	-0.50	121.01	121.21	-0.20	
699-8-25	121.15	121.26	-0.11	121.62	122.08	-0.46	121.45	121.60	-0.14	
699-81-38	113.71	115.66	-1.96	113.71	115.64	-1.93	113.71	115.54	-1.83	
699-81-58	118.41	120.90	-2.49	118.42	121.09	-2.67	118.40	119.76	-1.36	
699-83-47	115.55	118.55	-3.00	115.56	118.74	-3.17	115.55	118.42	-2.87	
699-86-42	114.41	117.25	-2.84	114.41	117.29	-2.88	114.41	117.20	-2.79	
699-87-55	117.21	118.48	-1.27	117.22	118.17	-0.95	117.21	117.69	-0.47	
699-89-35	113.19	113.09	0.10	113.19	112.98	0.21	113.19	112.93	0.26	
699-9-E2	117.19	113.04	4.15	117.35	113.34	4.01	117.52	113.46	4.06	
699-90-45	114.65	117.22	-2.57	114.66	117.12	-2.46	114.66	117.05	-2.39	
699-97-43	114.48	115.40	-0.92	114.48	115.44	-0.97	114.48	115.44	-0.97	
699-S12-3	116.75	115.21	1.54	116.85	115.73	1.12	117.07	116.10	0.97	
699-S14-20A	120.10	122.00	-1.90	120.31	122.13	-1.82	120.51	122.14	-1.63	
699-S19-E13	106.68	104.67	2.01	106.03	104.75	1.28	106.03	104.74	1.30	
699-S27-E14	106.68	104.02	2.66	106.00	103.98	2.02	106.00	104.00	2.00	
699-S29-E12	106.66	105.39	1.27	105.96	105.24	0.72	105.96	105.36	0.61	
699-S3-25	120.74	121.15	-0.42	121.07	121.75	-0.68	121.10	121.54	-0.44	
699-S3-E12	109.95	107.61	2.33	109.99	107.94	2.05	110.09	107.94	2.15	
699-S31-1	114.80	114.24	0.56	114.80	114.93	-0.13	114.93	114.06	0.86	
699-S6-E4D	114.93	112.88	2.05	115.02	113.42	1.60	115.19	113.52	1.67	
699-S8-19	120.23	120.20	0.04	120.49	120.79	-0.30	120.62	120.91	-0.29	

Table C-2. Model Summary Statistics.

Statistic	1979 Data	1988 Data	1993 Data
Residual Mean	-0.41 m (-1.34 ft)	-0.72 m (-2.36 ft)	-0.68 m (-2.23 ft)
Residual Standard Deviation[a]	2.00 m (6.57 ft)	1.96 m (6.43 ft)	2.01 m (6.59 ft)
Residual Range	13.06 m (42.85 ft)	11.94 m (39.17 ft)	15.61 m (51.21 ft)

[a] The standard deviation was calculated relative to the residual mean.

DISTRIBUTION

Number of Copies

ONSITE

70

U.S. Department of Energy
Richland Operations Office

R. D. Hildebrand (50)	H0-12
K. M. Thompson	H0-12
DOE-RL Public Reading Room	H2-53

ERC Team

G. R. Chiaramonte	H9-12
M. P. Connelly	H9-03
C. W. Denslow	H9-03
K. R. Fecht	H0-02
G. C. Henckel	H0-19
M. C. Kelly	H9-01
A. J. Knepp	H0-19
R. D. Landon	H0-02
M. H. Sturges	H9-01
L. C. Swanson	H9-02
Document and Information Services (4)	H0-09

Pacific Northwest National Laboratory

C. R. Cole	K9-36
M. D. Freshley	K9-36
Hanford Technical Library	P8-55